frontiers | Research Topics

Emerging topics in human physiology

Edited by
Luis Monteiro Rodrigues, Antigone Lazou, Adelino Leite-Moreira, Joaquin Garcia-Estañ and Ginés Viscor

Published in
Frontiers in Physiology

ISSN 1664-8714
ISBN 978-2-8325-6227-7
DOI 10.3389/978-2-8325-6227-7

About Frontiers

Frontiers is more than just an open access publisher of scholarly articles: it is a pioneering approach to the world of academia, radically improving the way scholarly research is managed. The grand vision of Frontiers is a world where all people have an equal opportunity to seek, share and generate knowledge. Frontiers provides immediate and permanent online open access to all its publications, but this alone is not enough to realize our grand goals.

Frontiers journal series

The Frontiers journal series is a multi-tier and interdisciplinary set of open-access, online journals, promising a paradigm shift from the current review, selection and dissemination processes in academic publishing. All Frontiers journals are driven by researchers for researchers; therefore, they constitute a service to the scholarly community. At the same time, the *Frontiers journal series* operates on a revolutionary invention, the tiered publishing system, initially addressing specific communities of scholars, and gradually climbing up to broader public understanding, thus serving the interests of the lay society, too.

Dedication to quality

Each Frontiers article is a landmark of the highest quality, thanks to genuinely collaborative interactions between authors and review editors, who include some of the world's best academicians. Research must be certified by peers before entering a stream of knowledge that may eventually reach the public - and shape society; therefore, Frontiers only applies the most rigorous and unbiased reviews. Frontiers revolutionizes research publishing by freely delivering the most outstanding research, evaluated with no bias from both the academic and social point of view. By applying the most advanced information technologies, Frontiers is catapulting scholarly publishing into a new generation.

What are Frontiers Research Topics?

Frontiers Research Topics are very popular trademarks of the *Frontiers journals series*: they are collections of at least ten articles, all centered on a particular subject. With their unique mix of varied contributions from Original Research to Review Articles, Frontiers Research Topics unify the most influential researchers, the latest key findings and historical advances in a hot research area.

Find out more on how to host your own Frontiers Research Topic or contribute to one as an author by contacting the Frontiers editorial office: frontiersin.org/about/contact

Emerging topics in human physiology

Topic editors

Luis Monteiro Rodrigues — Lusofona University, Portugal
Antigone Lazou — Aristotle University of Thessaloniki, Greece
Adelino Leite-Moreira — University of Porto, Portugal
Joaquin Garcia-Estañ — University of Murcia, Spain
Ginés Viscor — University of Barcelona, Spain

Citation

Monteiro Rodrigues, L., Lazou, A., Leite-Moreira, A., Garcia-Estañ, J., Viscor, G., eds. (2025). *Emerging topics in human physiology*. Lausanne: Frontiers Media SA. doi: 10.3389/978-2-8325-6227-7

Table of contents

frontiers | Frontiers in Physiology

TYPE Editorial
PUBLISHED 25 March 2025
DOI 10.3389/fphys.2025.1594305

OPEN ACCESS

EDITED AND REVIEWED BY
Geoffrey A. Head,
Baker Heart and Diabetes Institute, Australia

*CORRESPONDENCE
Luis Monteiro Rodrigues,
monteirorodrigues@sapo.pt

RECEIVED 15 March 2025
ACCEPTED 19 March 2025
PUBLISHED 25 March 2025

CITATION
García-Estañ López J, Viscor G and Monteiro Rodrigues L (2025) Editorial: Emerging topics in human physiology.
Front. Physiol. 16:1594305.
doi: 10.3389/fphys.2025.1594305

Editorial: Emerging topics in human physiology

Joaquín García-Estañ López[1], Ginés Viscor[2] and Luis Monteiro Rodrigues[3]*

[1]Centro de Estudios en Educación Médica, School of Medicine, University Murcia, Murcia, Spain, [2]Cell Biology, Physiology and Immunology Dep., School of Biology, University Barcelona, Barcelona, Spain, [3]School of Health Sciences, Universidade Lusófona, Lisboa, Portugal

KEYWORDS

human physiology, special issue, emerging topics, big data, cutting edge research

Editorial on the Research Topic
Emerging topics in human physiology

The present Frontiers Emerging Topic in Human Physiology was launched by the end of 2022 with the 2nd International Meeting of the Portuguese Physiological Society marking a significant moment in the post-pandemic landscape. This endeavor underscored the importance of preserving and disseminating research and knowledge as we navigate such troubled waters, facing unprecedented challenges, highlighting our resilience and adaptability in the face of adversity. By fostering collaboration and innovation, this Research Topic addressed emerging health issues and promoted cutting-edge research. More important, it served as a platform for physiologists to share insights, drive discussions, and inspire new ideas, ultimately contributing to the advancement of physiology and related fields.

Eight groundbreaking articles have been compiled, demonstrating that Physiology is thriving. Together, these studies enhance our understanding of human physiological adaptation across clinical, athletic, and technological spheres. Prominent themes include personalized medicine, adaptive training protocols, and innovations in diagnostics. Notably, the integration of wearable technologies with physiological insights holds significant promise for advancing clinical management and optimizing performance.

The first article (Kochanowicz et al.) discusses the acute inflammatory response in elite gymnasts by comparing inflammatory responses in elite male gymnasts (EAG) versus physically active men (PAM) after upper- and lower-body Wingate anaerobic tests. The key findings were that EAG showed superior performance in upper-body power output, and that upper-body exercise caused greater IL-6 increases in EAG, while lower-body exercise induced higher IL-6 in PAM. Finally, the anti-inflammatory IL-10 levels remained elevated in EAG post-exercise, correlating with baseline iron status in PAM. The results suggest that gymnastic training modulates iron-dependent anti-inflammatory responses during intense exercise.

The second article in this series (McLaughlin et al.) deals with caffeine bioavailability during exercise. Researchers examined how exercise-induced physiological changes affect caffeine's unbound fraction (f_u) and found that high-intensity cycling caused significant core temperature rise (+1.37°C) and blood acidification (pH −0.12), but neither f_u (0.86 → 0.75) nor paraxanthine (0.59 → 0.70) changed significantly and the metabolic ratio ([paraxanthine]/[caffeine]) remained stable under exercise conditions. The results indicate that the pharmacological activity of caffeine is not substantially altered by acute exercise stressors.

In the third article by Liu et al., renal pelvis pressure dynamics was studied in a murine model in order to identify factors influencing renal pressure measurements. The main findings were that perfusion rates (15–120 mL/h) directly correlated with pelvic pressure, the ureter obstruction sites: ureteropelvic junction (UPJ) vs. ureterovesical junction (UVJ) caused differential pressure increases and the bladder emptying protocols significantly affected pressure readings. A good precision regression model is proposed to provide a reference for evaluating renal pelvis pressure. These findings have important implications for obstructive uropathy diagnosis.

In an interesting paper, performed on elite divers (Kjeld et al.), hemoglobin concentration changes and blood shifts during dry static apnea in elite breath-hold divers were observed revealing unique physiological adaptations. Thus, 162% greater blood shift from extremities than from spleen during apnea, elevated hemoglobin concentrations compared to controls ($p < 0.05$) and no significant left ventricular myocardial mass changes during 4-min apneas, which are interesting responses since these findings demonstrate that blood shift is not towards the heart during dry apnea in humans.

Advanced physiological data acquisition was also applied to through wearable devices for seizure monitoring in the PreEpiSeizures project (Abreu et al.). The authors achieved 2,721 h of multimodal biosensor data from 59 epilepsy patients, matching ECG, high-quality video and EEG systems which allow the identification of 18 technical challenges in wearable epilepsy monitoring in home and clinical settings. The authors state, and we agree, that this work establishes a new and promising framework for daily life seizure detection technologies.

Leite-Moreira et al. studied myocardial compliance in *ex vivo* rabbit right ventricular papillary muscles under ischemic and non-ischemic conditions. Pressure-volume hemodynamics was also evaluated in an experimental *in vivo* acute myocardial infarction (MI) induced by left anterior descending artery ligation in rats. Results showed that ischemia abolishes stretch-induced myocardial compliance and that PKG activation restored 68% of compliance in ischemic tissue. Interestingly, sildenafil-enhanced compliance improved cardiac output by 22% post-MI. These findings suggest that PDE5 inhibitors could optimize volume management in acute MI, An interesting work by Monteiro Rodrigues et al. reported the role of central control of microcirculation through cutaneous perfusion changes induced by two different maneuvers by simultaneous monitoring of both feet by laser Doppler flowmetry and photoplethysmography. They demonstrated systemic hemodynamic responses to local stimuli (venoarteriolar reflex and reactive hyperemia), and blood redistribution between vascular plexuses via central mechanisms while showing age-independent response patterns across cohorts previously studied. The authors state that their findings challenge traditional local reflex models of microcirculatory regulation, highlighting the role of a centrally mediated reflex, documented in real-time through functional imaging, and with pending identification of its sensors and efectors.

Finally, an opinion piece by Li et al. proposed an automatic heart rate clamp, a practical tool to control internal and external training loads during aerobic exercise. They compared automatic versus manual control methods to maintain a target HR by monitoring internal/external load proportionality thus allowing real-time adjustments for cardiovascular drift compensation. AutoHR clamp method allows more precise control of the HR response compared to manual adjustment of external load. However, as the study was a pilot test with only five participants, further investigations are required to confirm these results. The authors conclude that the internal load of exercise can be easily controlled through the adjustment of external workload via an automatic HR clamp. Such a method allows for relative exercise intensity to be maintained constant both within and between exercise sessions, notably when training with additional environmental stress.

In conclusion, this Research Topic contributes to underscore the evolving significance of physiology at present. Clearly, the growing utility of wearable devices and advanced big data collection methods suggest new understandings and research directions within modern human physiology. In any case, this deliverable, only possible by this combined initiative and effort from Topic Editors, emphasizes the crucial role of researchers in the dissemination of knowledge. Such efforts are essential to foster a healthier and more informed society as we progress together into the future, paving the way for improved health outcomes and a deeper comprehension of the physiological factors that influence our daily lives.

Author contributions

JG-E: Writing – review and editing. GV: Writing – review and editing. LM: Writing – review and editing.

Funding

The author(s) declare that no financial support was received for the research and/or publication of this article.

Conflict of interest

The authors declare that the research was conducted in the absence of any commercial or financial relationships that could be construed as a potential conflict of interest.

The author(s) declared that they were an editorial board member of Frontiers, at the time of submission. This had no impact on the peer review process and the final decision.

Generative AI statement

The author(s) declare that no Generative AI was used in the creation of this manuscript.

Publisher's note

frontiers | Frontiers in Physiology

TYPE Opinion
PUBLISHED 07 April 2023
DOI 10.3389/fphys.2023.1170105

OPEN ACCESS

EDITED BY
Ginés Viscor,
University of Barcelona, Spain

REVIEWED BY
Camilo Povea,
National University of Colombia, Colombia
Morin Lang,
University of Antofagasta, Chile

*CORRESPONDENCE
Siu Nam Li,
casper.li@research.uwa.edu.au
Olivier Girard,
oliv.girard@gmail.com

SPECIALTY SECTION
This article was submitted to Exercise Physiology, a section of the journal Frontiers in Physiology

RECEIVED 20 February 2023
ACCEPTED 29 March 2023
PUBLISHED 07 April 2023

CITATION
Li SN, Peeling P, Scott BR, Peiffer JJ, Shaykevich A and Girard O (2023), Automatic heart rate clamp: A practical tool to control internal and external training loads during aerobic exercise. *Front. Physiol.* 14:1170105. doi: 10.3389/fphys.2023.1170105

Automatic heart rate clamp: A practical tool to control internal and external training loads during aerobic exercise

Siu Nam Li [1]*, Peter Peeling [1,2], Brendan R. Scott [3,4], Jeremiah J. Peiffer [3,4], Alex Shaykevich [1,5] and Olivier Girard [1]*

[1]School of Human Sciences (Exercise and Sports Science), The University of Western Australia, Perth, WA, Australia, [2]Department of Sport Science, Western Australian Institute of Sport, Mount Claremont, WA, Australia, [3]Murdoch Applied Sport Science Laboratory, Discipline of Exercise Science, Murdoch University, Perth, WA, Australia, [4]Centre for Healthy Ageing, Murdoch University, Perth, WA, Australia, [5]Perron Institute for Neurological and Translational Science, Perth, WA, Australia

KEYWORDS

training loads, clamped heart rate, environmental stress, hypoxia, exercise prescription

Background

Prescribing and monitoring exercise intensity is a fundamental competency for exercise physiologists and sport scientists working across a range of populations to achieve desired clinical and/or performance outcomes (Impellizzeri et al., 2019). A variety of external and internal load metrics can be considered for this purpose. External load refers to the objective measures of the work performed (i.e., sustained mechanical output), whereas internal load represents the physiological and perceptual responses to that external load (Foster et al., 2017). Said differently, external load answers the question "*How was training implemented?*" (i.e., what happens on the 'outside'), while internal loads determine "*Did the individual respond to the training as planned?*" (i.e., what happens on the 'inside'). Although internal load during exercise relates closely to the psycho-physiological adaptations elicited (Impellizzeri et al., 2019), exercise intensity is often controlled from external load metrics. To sustain cycling exercise intensity at lactate threshold, power output (PO) corresponding to lactate threshold is commonly used as a surrogate measure, resulting in external load as a proxy to elicit a given internal load. However, when exercise intensity is prescribed from an external load metric, a dissociation may occur between external and internal loads. For instance, cardiovascular drift can manifest 10 min after the onset of moderate-intensity exercise, which reflects a progressive increase in internal load for a constant external load (Ekelund, 1967). Internal load could therefore be disproportionally increased beyond the required stimulus (i.e., above threshold), such that an expected physiological adaptation may not be elicited. As a result, internal load metrics are more commonly used to prescribe exercise stimulus in order to achieve the desired training outcomes. This article will explore the use of alternative strategies to prescribe and monitor exercise intensity during aerobic exercise.

Internal load metrics

In order to carefully control internal load during an aerobic exercise bout, it is possible to continually adjust external load so that a pre-planned internal load is reached and

maintained. For example, in a laboratory setting, external load can be altered by increasing or decreasing belt speed on a treadmill or resistance on a cycle-ergometer. A variety of physiological variables (i.e., heart rate, blood lactate concentration, muscle oxygenation and activation, and oxygen consumption) can be considered to reflect internal load. Any selected variable would then need to be measured relatively easily and continuously, and be relevant to the sporting context, for their adoption by a large number of end-users in real-world training scenarios. For example, although blood lactate can be measured continuously (Cass and Sharma, 2017), its response time to changes in exercise intensity is relatively long compared to other physiological measures (Bentley et al., 2007). While oxygen consumption has a quick response time to changes in exercise intensity, collecting gas exchange requires an expensive metabolic cart with participants also constrained to wear a face mask that likely restricted fluid intake during exercise. Alternatively, HR is an easy-to-measure, non-invasive, and inexpensive physiological variable to represent internal load. By wearing a chest or watch strap monitor, continuous HR measurements can be readily obtained to inform exercise prescription for a wide range of active populations (sedentary to elite athletes). Of note, the simplicity of this measure also enables simultaneously tracking a large number of individuals training together. Therefore, for most exercise bouts performed on an ergometer, HR is considered a suitable indicator of internal load to monitor and control aerobic exercise intensity.

Current practices to control heart rate during exercise

Controlling for internal load derived from HR metrics is achieved *via* manual adjustment of external load. To guide training delivery, HR zones defined according to noticeable physiological landmarks, such as ventilatory thresholds (VT), are often considered. By using HR zones relative to VT (i.e., 10–15 bpm below VT1, 10–20 bpm above VT1, and below VT2, 10–15 bpm above VT2), improvements in maximal oxygen uptake following a 12-week protocol have been reported (Wolpern et al., 2015). To successfully maintain HR within the prescribed zones, investigators had to regularly adjust treadmill speed and gradient. However, the actual HR response during sessions is unknown because intra-session HR data was not reported. Therefore, the accuracy of manual adjustment to maintain internal load is undetermined. A potential limitation of manual adjustment of external workload is that HR is prescribed in zones, while this approach may not be valid when the maintenance of HR needs to be more accurate (i.e., a specific HR value). For example, given large differences in inter-individual responses to standardized exercise training (prescribing HR in zones), the approach of prescribing exercise intensity must be tailored and carefully controlled to achieve the desired outcomes (Mann et al., 2014). Consequently, the inter-individual variability of exercise responses may be reduced when HR is controlled to a fixed value when compared to HR controlled to zones. Another limitation of this method is that the adjustment to external load relies on the discretion of the investigators, which may introduce inter-rater reliability issues. For example, different experimenters may adjust external workload at different magnitudes to maintain the target HR (i.e., increasing/decreasing treadmill speed by 0.1 versus 0.5 km h^{-1} or resistance by 1 versus 5 W). Other drawbacks of manual adjustment include the frequency of when external workloads are modified and the HR averaging period. For instance, Racinais et al. (2021) altered cycling PO every 30 s to maintain a HR corresponding to 60% of maximal oxygen uptake during a study requiring fixed HR across various environmental conditions. Because HR may have changed with each 30-s epoch, the fluctuations in HR may be higher than if HR was adjusted continuously. As such continuous and immediate adjustments of external workload are needed if HR is to be precisely controlled.

Automatic heart rate clamp

A possible solution to solve some of the aforementioned issues associated with controlling HR is the use of an automatic HR clamp. When using this method, after a target HR is first set, a computer program would instantaneously adjust external workload (e.g., cycling PO) so that participants may reach and maintain this pre-planned HR response. An initial attempt to achieve this was made by Kawada et al. (1999), who used a servo-controller to clamp HR in healthy individuals cycling an ergometer. In this study, the time taken to reach 90% of target HR corresponding to 60% and 75% HR_{max} was ~136 s, and the difference between target and actual HR was ~3 bpm. These findings suggest that an automatic HR clamp likely allows HR to be precisely regulated. An advantage of this approach is also that the difference between target and actual HR is calculated almost instantaneously at each timepoint (0.1 Hz), so that reactive adjustments to cycling PO can be implemented immediately. Additionally, the control of HR dictated by an algorithm removes any inter-rater reliability issues. When exercise is prescribed at a constant sub-maximal exercise intensity, an automatic HR clamp likely represents a suitable method to tightly regulate internal load.

In addition to continuous exercise, the HR clamp approach has successfully been implemented to control intermittent exercise intensity (i.e., interval training sessions). For instance, through the use of an automatic HR clamp tool Hunt and Hurni (2019) had participants perform four intervals alternating between active (~140 bpm) and passive (~120 bpm) phases. The reported mean tracking error of ~3.1 bpm would suggest that HR can be closely controlled even when the target HR fluctuates during exercise. Overall, an automatic HR clamp approach can be successfully implemented for different modes of aerobic training.

Comparing automatic and manual control of power output to reach a pre-planned HR

Previously, direct comparisons have not been made between manual and automatic control methods of external workload to maintain a target HR. Here, we present pilot data from five participants comparing an automatic and manual control of PO to reach a pre-planned HR (Figure 1). We specifically compared an automatic HR clamp (AutoHR) installed on an iPod Touch (Apple Incs., Cupertino, CA, United States) against manual adjustments to

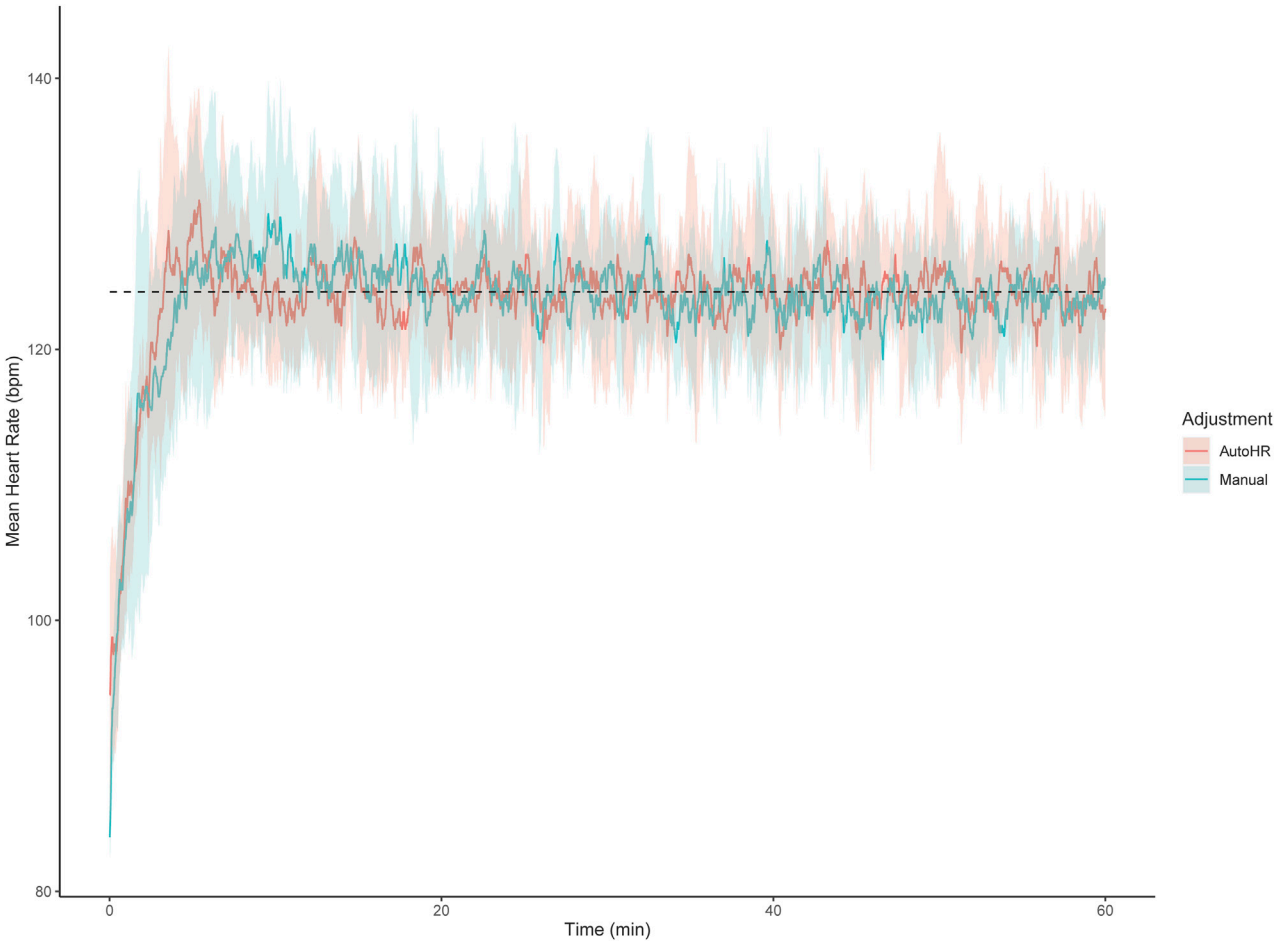

FIGURE 1
Pilot data depicting average heart rate across 60 min of heart rate clamped cycling between automatic (AutoHR) and manual control of power output. Dashed line represents average target heart rate (124 bpm). The shaded areas represent the standard deviation of mean actual heart rate.

external workload by the same experimenter during 60 min of cycling at individual HR corresponding to 80% VT (~40% peak oxygen consumption) in trained males. The AutoHR app uses a standard Bluetooth low energy profile to control the resistance of the ergometer, which is supported by many off-the-shelf cycling ergometers (e.g., Wahoo kickR, Tacx Neo). To maintain HR, the AutoHR application calculates the HR error (difference between current and target HR), computes target wattage, and sets the ergometer's resistance accordingly at 5-s intervals by implementing a proportional-integral controlled based on the principles of Kawada et al. (1999). Furthermore, the proportional integral controller is defined by the equation: $u(t) = Kpe(t) + Ki\int e(t)\,dt$, where Kp and Ki are the proportional and integral gains, respectively; $e(t)$ is the error at time t defined as the difference between the measured (HR from the chest strap monitor) and target (target HR set on the app) values of the observed variable at time t, and $\int e(t)d$ is the integral of the error term with respect to time (Aström and Hägglund, 2001). From the equation, the app calculates the adjustments in ergometer resistance required to match measured and target HR. The increase in PO during the first 3 min of exercise from a resting state with this HR clamp procedure was strictly replicated for manual adjustment trials. Interestingly, after the initial 3 min, root mean square error for the automatic HR clamp and manual adjustment methods were ~2 ± 2.0 and ~4 ± 2.0 bpm, respectively. These observations suggest that the AutoHR clamp method allows a more precise control of the HR response compared to manual adjustment of external load. However, as the study was a pilot test with only five participants, further investigations are required to confirm these results.

Practical applications

For a given external workload, many factors can affect internal load and subsequently the training outcomes. For instance, individuals' training status, psychological status, health, nutrition, environment, and genetics can all affect the internal load response to training (Impellizzeri et al., 2019). Consequently, suggested practical applications of the automatic HR clamp include automatically controlling the internal load of exercise across various environmental conditions during both acute and chronic interventions.

Acute interventions

Environmental stressors (i.e., cold, hot, hypoxia, pollution) can affect the relationship between internal and external loads during exercise (Impellizzeri et al., 2019). When compared to ambient near sea-level conditions, exposure to either hot or hypoxic environments induce a disproportionate elevation of the internal load response to exercise for a given external load in a dose-response manner (Buchheit et al., 2013). In this context, a HR clamp approach may be useful to monitor and reduce the external workload in response to these challenging environments, eliciting a comparable cardiometabolic response in reference to controls (Girard et al., 2021). Therefore, by using a HR clamp, the desired physiological responses from exercise can be achieved, regardless of the severity of the environmental stress.

Chronic interventions

By taking advantage of the *higher-than-normal* stress of exercising in challenging environmental conditions, a HR clamp approach may allow similar (or eventually better) post-intervention physiological and/or functional benefits, despite a lower overall mechanical stress during actual training sessions (Girard et al., 2021). To date, there is no published evidence of the chronic effects of exercise that uses a HR clamp across different environmental conditions. Nonetheless, similar maximal oxygen uptake improvements were achieved in overweight-to-obese individuals after training at HR corresponding to 65% maximal oxygen uptake (albeit *via* manual adjustment of external load) between sea-level and moderate hypoxia (Wiesner et al., 2010). Remarkably, the hypoxia group had greater body composition improvements (i.e., % fat free mass, waist circumference) when compared to the sea-level group despite a 17.5% reduction in external load. An automatic HR clamp approach may therefore become advantageous to more carefully control HR to maintain internal load across a range of environmental conditions during chronic interventions.

In clinical populations (e.g., cardiometabolic pathologies, pulmonary, and cardiac rehabilitation), the automatic HR clamp can be very useful for a strict control of exercise intensity, which is pertinent given the risk associated with exceeding prescribed intensities in such populations (Warburton et al., 2011). Additionally, the algorithm within the AutoHR app may be further improved by taking into account any known chronic abnormalities in HR during exercise and adjust external load accordingly. Therefore, the automatic HR clamp can help to tightly control exercise intensity in clinical populations.

Logistically, the automatic HR clamp is relatively easy to implement during group training sessions compared to manual adjustment to external load. For example, for a group of participants exercising simultaneously, no additional practitioners would need to be present to adjust external load for each individual when the automatic HR clamp is used. Comparatively, manual adjustment likely requires one practitioner for each person, which may not be feasible (or even possible) for large groups. One advantage of the automatic HR clamp is chronic interventions is therefore to control exercise intensities in large cohorts training together.

Conclusion

We argue that internal load of exercise can be easily controlled through the adjustment of external workload *via* automatic HR clamps. Such method allows for relative exercise intensity to be maintain constant both within and between exercise sessions, notably when training with additional environmental stress. Moving forward, it is our hope that automatic HR clamp approaches will be more commonly considered as a means of prescribing exercise intensities in research and practical settings when ergometer-based exercises are performed.

Author contributions

SNL wrote the first draft of the manuscript. All authors wrote sections of the manuscript, and contributed to manuscript revision, read, and approved the submitted version.

Conflict of interest

The authors declare that the research was conducted in the absence of any commercial or financial relationships that could be construed as a potential conflict of interest.

Publisher's note

References

Åström, K. J., and Hägglund, T. (2001). The future of PID control. *Control Eng. Pract.* 9 (11), 1163–1175. doi:10.1016/s0967-0661(01)00062-4

Bentley, D. J., Newell, J., and Bishop, D. (2007). Incremental exercise test design and analysis: Implications for performance diagnostics in endurance athletes. *Sports Med.* 37, 575–586. doi:10.2165/00007256-200737070-00002

Buchheit, M., Racinais, S., Bilsborough, J., Hocking, J., Mendez-Villanueva, A., Bourdon, P. C., et al. (2013). Adding heat to the live-high train-low altitude model: A practical insight from professional football. *Br. J. Sports Med.* 47 (1), 59–69. doi:10.1136/bjsports-2013-092559

Cass, A. E., and Sharma, S. (2017). Microneedle enzyme sensor arrays for continuous *in vivo* monitoring. *Methods Enzym.* 589, 413–427. doi:10.1016/bs.mie.2017.02.002

Ekelund, L. G. (1967). Circulatory and respiratory adaptation during prolonged exercise. *Acta Physiol. Scand. Suppl.* 292, 1–38.

Foster, C., Rodriguez-Marrovo, J. A., and De Koning, J. J. (2017). Monitoring training loads: The past, the present, and the future. *Int. J. Sports Physiology Perform.* 12 (2), S22–S28. doi:10.1123/ijspp.2016-0388

Girard, O., Girard, I. M., and Peeling, P. (2021). Hypoxic conditioning: A novel therapeutic solution for load-compromised individuals to achieve similar exercise

benefits by doing less mechanical work!. *Br. J. Sports Med.* 55 (17), 944–945. doi:10.1136/bjsports-2020-103186

Hunt, K. J., and Hurni, C. C. (2019). Robust control of heart rate for cycle ergometer exercise. *Med. Biol. Eng. Comput.* 57 (11), 2471–2482. doi:10.1007/s11517-019-02034-6

Impellizzeri, F. M., Marcora, S. M., and Coutts, A. J. (2019). Internal and external training load: 15 years on. *Int. J. Sports Physiology Perform.* 14 (2), 270–273. doi:10.1123/ijspp.2018-0935

Kawada, T., Ikeda, Y., Takaki, H., Sugimachi, M., Kawaguchi, O., Shishido, T., et al. (1999). Development of a servo-controller of heart rate using a cycle ergometer. *Heart Vessels* 14 (4), 177–184. doi:10.1007/BF02482304

Mann, T. N., Lamberts, R. P., and Lambert, M. I. (2014). High responders and low responders: Factors associated with individual variation in response to standardized training. *Sports Med.* 44, 1113–1124. doi:10.1007/s40279-014-0197-3

Racinais, S., Périard, J. D., Piscione, J., Bourdon, P. C., Cocking, S., Ihsan, M., et al. (2021). Intensified training supersedes the impact of heat and/or altitude for increasing performance in elite Rugby Union players. *Int. J. Sports Physiology Perform.* 16 (10), 1416–1423. doi:10.1123/ijspp.2020-0630

Warburton, D. E., Bredin, S. S., Charlsworth, S. A., Foulds, H. J., McKenzie, D. C., and Shephard, R., J. (2011). Evidence-based risk recommendations for best practices in the training of qualified exercise professionals working with clinical populations. *Appl. Physiology, Nutr. Metabolism* 36 (S1), S232–S265. doi:10.1139/h11-054

Wiesner, S., Haufe, S., Engeli, S., Mutchler, H., Haas, U., Luft, F. C., et al. (2010). Influences of normobaric hypoxia training on physical fitness and metabolic risk markers in overweight to obese subjects. *Obesity* 18 (1), 116–120. doi:10.1038/oby.2009.193

Wolpern, A. E., Burgos, D. J., Janot, J. M., and Dalleck, L. C. (2015). Is a threshold-based model a superior method to the relative percent concept for establishing individual exercise intensity? A randomized controlled trial. *BMC Sports Sci. Med. Rehabilitation* 7 (1), 16–19. doi:10.1186/s13102-015-0011-z

frontiers | Frontiers in Physiology

TYPE Original Research
PUBLISHED 04 May 2023
DOI 10.3389/fphys.2023.1177583

OPEN ACCESS

EDITED BY
Eduardo Colombari,
Departamento de Fisiologia e Patologia da Faculdade de Odontologia da Universidade Estadual Paulista, Brazil

REVIEWED BY
Roland Pittman,
Virginia Commonwealth University, United States
Daniel Bottino,
Rio de Janeiro State University, Brazil

*CORRESPONDENCE
Luís Monteiro Rodrigues,
monteiro.rodrigues@ulusofona.pt

RECEIVED 01 March 2023
ACCEPTED 17 April 2023
PUBLISHED 04 May 2023

CITATION
Monteiro Rodrigues L, Rocha C, Andrade S, Granja T and Gregório J (2023), The acute adaptation of skin microcirculatory perfusion *in vivo* does not involve a local response but rather a centrally mediated adaptive reflex. *Front. Physiol.* 14:1177583. doi: 10.3389/fphys.2023.1177583

The acute adaptation of skin microcirculatory perfusion *in vivo* does not involve a local response but rather a centrally mediated adaptive reflex

Luís Monteiro Rodrigues*, Clemente Rocha, Sérgio Andrade, Tiago Granja and João Gregório

CBIOS—Universidade Lusofona's Research Center for Biosciences and Health Technologies, Universidade Lusófona (Lisbon's University Campus), Lisbon, Portugal

Introduction: Cardiovascular homeostasis involves the interaction of multiple players to ensure a permanent adaptation to each organ's needs. Our previous research suggested that changes in skin microcirculation—even if slight and distal—always evoke an immediate global rather than "local" response affecting hemodynamic homeostasis. These observations question our understanding of known reflexes used to explore vascular physiology, such as reactive hyperemia and the venoarteriolar reflex (VAR). Thus, our study was designed to further explore these responses in older healthy adults of both sexes and to potentially provide objective evidence of a centrally mediated mechanism governing each of these adaptive processes.

Methods: Participants (n = 22, 52.5 $\pm$ 6.2 years old) of both sexes were previously selected. Perfusion was recorded in both feet by laser Doppler flowmetry (LDF) and photoplethysmography (PPG). Two different maneuvers with opposite impacts on perfusion were applied as challengers to single limb reactive hyperemia evoked by massage and a single leg pending to generate a VAR. Measurements were taken at baseline (Phase I), during challenge (Phase II), and recovery (Phase III). A 95% confidence level was adopted. As proof of concept, six additional young healthy women were selected to provide video imaging by using optoacoustic tomography (OAT) of suprasystolic post-occlusive reactive hyperemia (PORH) in the upper limb.

Results: Modified perfusion was detected by LDF and PPG in both limbs with both hyperemia and VAR, with clear systemic hemodynamic changes in all participants. Comparison with data obtained under the same conditions in a younger cohort, previously published by our group, revealed that results were not statistically different between the groups.

Discussion: The OAT documentary and analysis showed that the suprasystolic pressure in the arm changed vasomotion in the forearm, displacing blood from the superficial to the deeper plexus vessels. Deflation allowed the blood to return and to be distributed in both plexuses. These responses were present in all individuals independent of their age. They appeared to be determined by the need to re-establish hemodynamics acutely modified by the challenger, which means that they were centrally mediated. Therefore, a new mechanistic interpretation of these exploratory maneuvers is required to better characterize in vivo cardiovascular physiology in humans.

KEYWORDS

venoarteriolar reflex, reactive hyperemia, acute perfusion adaptation, cardiovascular homeostasis, skin microcirculation, local and central reflexes

1 Introduction

Cardio-circulatory adaptation is essential in managing acute physiological challenges (e.g., posture change) as in chronic pathological processes (e.g., hypertension or heart failure) to continuously harmonize hemodynamics with cell needs. A permanent crosstalk between microcirculation and higher circulatory structures involving different sensors and effectors, central and peripheral, is part of these complex mechanisms (Mazzoni & Schmid-Schonbein, 1996; Mei et al., 2018; Cracowski & Roustit, 2020; Guven et al., 2020). However, the details of these interactions remain largely unknown.

In normal physiology, acute perfusion adaptations, such as those originating from sudden changes in venous and capillary flow and pressure are believed to be mostly determined by tissue-related intervenients (neuro-humoral, metabolic, and endocrine) converging to a "local reflex" thought to protect the microcirculatory unit (Rowell et al., 2011; Masashi et al., 2013). The venoarteriolar reflex (VAR) (Cracowski & Roustit 2020; Low 2004; Silva et al., 2018) is one well-known example. In the opposite direction, sudden perfusion changes due to imposed suprasystolic pressure applied to a main artery's post-occlusive reactive hyperemia (PORH) have also been explained on the basis of local endothelial vasodilators' sensory nerves and myogenic activities (Cracowski & Roustit 2020; Rosenberry & Nelson MD 2020). No matter their limitations, non-agreement regarding the character of the mechanisms involved, VAR and PORH have been long used in experimental physiology to provide a functional window to assess vascular physiology in human (Cracowski & Roustit 2020; Low 2004; Silva et al., 2018; Rosenberry & Nelson MD 2020; Crandall et al., 2002). Nevertheless, recent studies on these cardio-circulatory responses suggest a different view.

This localized reactive hyperemia evoked by short-term low-intensity massage in one of the lower limbs produced a statistically significant observable perfusion increase in the contralateral non-massaged limb in humans (Rocha C et al., 2018a; Rocha C et al., 2018b; Rodrigues et al., 2020). Similar observations were recorded in the upper limb with a suprasystolic pressure cuff maneuver (Florindo et al., 2021; Monteiro Rodrigues et al., 2022). In addition, the classical VAR evoked a perfusion reduction in the contralateral resting limb (Cracowski & Roustit 2020; Silva et al., 2018; Crandall et al., 2002). All these observations strongly suggested that any modification of local perfusion produced an immediate integrative parallel response that was proportional to the challenge intensity to restore hemodynamics. We named it a prompt adaptive hemodynamic response (PAHR) and considered its potential utility as a global marker with clinical relevance to further characterize *in vivo* cardiovascular physiology. Apart from these observations, we recognized that this potential endpoint is insufficiently characterized, especially regarding common determinants such as age, and that further evidence of the existence of this supposed centrally mediated reflex is still required.

To these purposes, the present study was designed to extend some previously published results (Silva et al., 2015; 2018; Rodrigues et al., 2020) to study these responses to two challengers—superficial hyperemia (massage) and the venoarteriolar reflex in an older group of healthy participants. In complement and as a part of the "proof of concept," the study included the use of functional imaging to create a mechanistic documentary of a PORH maneuver in the upper limb during a suprasystolic pressure cuff experiment.

2 Materials and methods

For the present study, a convenience sample of 22 healthy individuals (52.5 ± 6.2 years old) of both sexes (n = 11 each) was selected after informed written consent (Group A). Specific inclusion/non-inclusion criteria that were previously defined for a similar research (Rodrigues et al., 2020) were applied. All participants were normotensive with no signs of vascular impairment, confirmed by the ankle–brachial index (ABI, 1.1 ± 0.1) (Aboyans et al., 2013), normal body mass index (BMI, 24.8 ± 2.1), and (self-reported) equivalent levels of physical activity. Furthermore, participants were non-smokers and free of any regular medication or food supplementation. All female participants were menopausal without hormone-replacement therapy. Study participants were asked to refrain from consuming caffeinated and/or any other vasoactive beverages for 24 h prior to the experiments. Table 1 summarizes the general characteristics of these participants.

An additional group of six young healthy women (mean age, 23.0 ± 2.19 years) using similar health selection criteria was chosen to document the circulatory mechanisms involved in the PORH maneuver using functional imaging (Group B).

All procedures were previously approved by the institutional ethical commission and carried out in accordance with the Declaration of Helsinki and its respective amendments, observing good clinical practices for medical research involving human participants (WMA 2013).

2.1 Experimental

Experiments took place with controlled temperature, humidity (21°C ± 1°C; 40%–60%), and light. Participants were acclimatized to room conditions for approximately 20 min while lying comfortably in the supine position.

2.1.1 Hyperemia

Participants in Group A (n = 22) had one randomly chosen leg massaged, while the contralateral leg (in the same position) served as the control. This procedure, applied by a licensed, experienced therapist, involved the application of short, rhythmic, light repetitive strokes in the ascending direction from the ankle to the knee, with the palms of both hands gliding along one (challenged) leg's longitudinal axis (Rocha et al., 2016). The protocol included three phases—a 10-min baseline resting register (Phase I), a 5-min massage challenge (Phase II), and a 10-min recovery (Phase III).

TABLE 1 Participants' characterization. Results are presented as medians and Q1–Q3 (25th empirical quartile to 75th empirical quartile). Statistical comparison between sexes within the age group using the Mann–Whitney test (*$p < 0.05$).

	Men	Women	*p*
N (%)	11 (50)	11 (50)	—
Smokers (%)	No (100)	No (100)	—
Age, years (Q1–Q3)	53.0 (46.0–58.0)	51.0 (48.5–54.5)	0.921
Body mass, kg (Q1–Q3)	76.0 (74.5–81.5)	65.0 (60.0–68.3)	0.002*
Height, m (Q1–Q3)	1.75 (1.72–1.81)	1.60 (1.56–1.64)	<0.001*
BMI, kg/m^2 (Q1–Q3)	25.4 (24.4–25.8)	24.8 (22.8–26.3)	0.949
SYSTP, mmHg (Q1–Q3)	124.7 (117.8–127.0)	114.0 (112.3–131.8)	0.606
DIASP, mmHg (Q1–Q3)	84.0 (76.6–88.0)	77.5 (76.0–78.2)	0.743
ABI (Q1–Q3)	1.17 (1.06–1.17)	1.14 (1.06–1.16)	0.148
PR, bpm (Q1–Q3)	57.0 (52.0–63.8)	64.0 (59.7–68.3)	0.094

BMI, body mass index; SYSTP, systolic pressure; DIASP, diastolic pressure; ABI, ankle–brachial index; PR, pulse rate; bpm, beats per minute.

2.1.2 Venoarteriolar reflex

From the participant pool of Group A, five men and five women (mean age, 50.3 ± 5.64 years; ABI, 1.1 ± 0.1; and BMI, 24.9 ± 2.2) volunteered to participate in a standard VAR procedure (Low 2004; Rathbun et al., 2008). The experimental procedure likewise involved a baseline recording in the supine position with both legs lying parallel to the body axis (Phase I), the challenge with one randomly chosen leg pending approximately 50 cm below the heart level (Phase II), and recovery (Phase III), resuming the initial position.

2.1.3 Functional imaging: proof of concept

To document the perfusion changes in these conditions, a classical post-occlusive reactive hyperemia (PORH) maneuver was applied to Group B participants ($n = 6$) and videos were recorded by optoacoustic tomography (OAT) for further analysis. A pressure cuff was applied in the middle of the upper arm. After stabilization (Phase I), the cuff was rapidly inflated to 200 mmHg to occlude the brachial artery for approximately 1 min to ensure hemodynamical stabilization in the area (Phase II). The cuff was then deflated for recovery (Phase III).

2.2 Measurement technologies and signal processing

For the massage and VAR protocols, blood perfusion was continuously assessed through laser Doppler flowmetry (LDF) and photoplethysmography (PPG), two optical technologies based on related principles but with different skin depth capacities (Ash et al., 2017; Bergstrand et al., 2009; Rodrigues et al., 2019). LDF and PPG sensors were applied in the plantar aspects of the second and first toes, respectively, in both feet. This strategy substantially reduces variability when measuring in the distal inferior limb (Silva et al., 2018; Rodrigues et al., 2020; Rodrigues et al., 2018). The LDF signal, expressed in arbitrary blood perfusion units (BPUs), was obtained with a Perimed PF 5010 (Perimed, Sweden) system with a pair of P457 probes secured with a PF 105-3 tape. The skin surface temperature was also continuously monitored by the system. The PPG signal, expressed in BPUs, was obtained by a BITalino Plugged Kit (PLUX Biosignals, Portugal), which also recorded the blood volume pulse (BVP) and heart rate. The blood pressure (systolic and diastolic) was measured in the arm (Tensoval Comfort, Hartman, Germany) in each procedural phase.

For functional imaging, we used an optoacoustic system from iThera Medical GmbH (Munich, Germany) MSOT for multi-spectral optoacoustic tomography. This technology detects sound waves generated by molecules previously excited by light from a wave laser beam. In consequence, a transitory thermoelastic expansion occurs that characterizes the specific (excited) chromophores. The signal pattern across the measured wavelengths serves as an exclusive absorption feature for each (chromophore) molecule (Daiwei et al., 2021; Hu and Wang 2010; Wang 2008). Recent specifications and operation details of this technology are available elsewhere (Daiwei et al., 2021; Granja et al., 2022; Hu and Wang 2010; Monteiro Rodrigues et al., 2022; Wang 2008).

OAT measurements were taken in the same limb, in the volar forearm, with the measurement probe held in contact with the skin surface using a flexible metal arm (Granja et al., 2022). The system allows the visualization of the chromophores from oxyhemoglobin HbO2 and deoxyhemoglobin Hb in real time during the acquisition. Recorded videos were post-processed for image reconstruction by the viewMSOT software (iThera Medical, version 4.0), which allows the quantification of HbO2, Hb, total hemoglobin (HbT as the sum of HbO_2 and Hb), and the mean saturation of oxygen (mSO2). The ImageJ software (National Institutes of Health, version 1.53k14) was also used in the image reconstruction process.

2.3 Statistical analysis

Descriptive and comparative statistics were applied to LDF and PPG signals using the IBM SPSS v 22.0 software (IBM Corporation, NY, United States) and jamovi software version 2.2 (jamovi project,

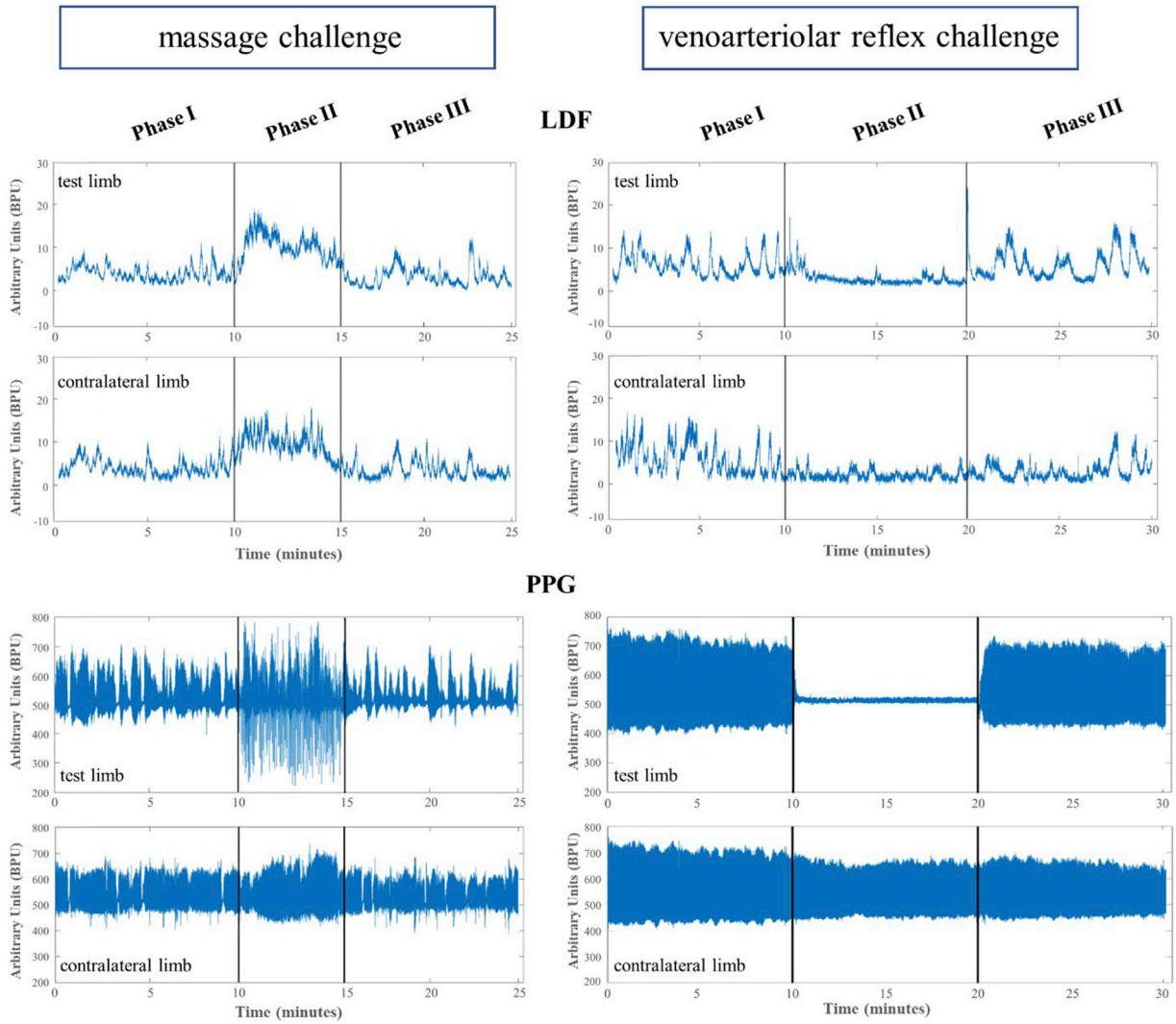

FIGURE 1
Illustrative example of the mean lower limb perfusion changes expressed in arbitrary blood perfusion units obtained by laser Doppler flowmetry (LDF) and reflection photoplethysmography (PPG) in participants' test and contralateral lower limbs after evoking a massage hyperemia (left panels) and the venoarteriolar reflex responses (right panels).

Sydney, AU). Perfusion changes were calculated as the mean value of the LDF area under the curve and as the mean amplitude of the PPG signal. Upon confirmation of normal data distribution by the Shapiro–Wilk test, parametric (repeated measures ANOVA with the Tukey test for *post hoc* correction) or non-parametric tests (Kruskal–Wallis and Friedman test with paired comparison corrections) were chosen. For the functional imaging analysis, we applied one-way ANOVA with Tukey's multiple comparison test with a single pooled variance distribution. A confidence level of 95% ($p < 0.05$) was assumed.

3 Results

Illustrative records of our observations are shown in Figure 1. Perfusion changes were recorded with LDF and PPG systems in both limbs during all phases of both the procedures.

The application of massage to a single limb produced a reactive hyperemia with perfusion elevation in both limbs (Table 2). This increase was statistically significant in the challenged limb foot (Phase II–Phase I), disappearing in recovery (Phase III–Phase I). The blood pressure and pulse clearly changed throughout the experimental procedure; however, the reduction in Phase II was statistically significant only for the diastolic pressure (Table 2).

A comparison of LDF and PPG data obtained from all participants for each phase of the experimental procedures (Table 2) revealed perfusion differences between limb pairs in Phase II, but not in Phases I and III. These perfusion differences, detected with both LDF and PPG, could only be attributed to the challenge.

The VAR procedure evoked a significant reduction in perfusion in Phase II with both LDF and PPG in the pending limb and in the contralateral (resting) limb (Table 3). Changes in blood pressure were also detected, but significant differences could not be found. After

TABLE 2 Mean perfusion changes expressed in arbitrary blood perfusion units (BPUs) obtained by laser Doppler flowmetry (LDF) and reflection photoplethysmography (PPG) in aged adult participants' test and contralateral feet after application of the massage procedure (see text). Blood pressure (systolic and diastolic, mm Hg) and pulse (bpm) are also shown. Data are expressed as means + SD. Statistical comparison with the Friedman test with paired comparison correction (Durbin–Conover) between lower limbs across phases. The blood pressure and pulse rate comparison assessed with repeated measures ANOVA with the Tukey test for *post hoc* correction. *$p < 0.05$.

	Phase I		Phase II		Phase III		Phase II–Phase I (*p*-value)		Phase III–Phase I (*p*-value)		All phases
	Test limb	Contralateral limb	Test limb	Contralateral limb	Test limb	Contralateral limb	Test limb	Contralateral limb	Test limb	Contralateral limb	
LDF (BPUs)	19.6 + 27.2	25.8 + 45.8	35.2 + 43.3	30.6 + 49.0	23.3 + 31.7	23.4 + 37.2					
p-value	0.079		0.049*		0.518		<0.001*	0.518	0.145	0.344	0.002*
PPG (BPUs)	148.7 + 141.3	138.5 + 129.9	208.8 + 152.8	156.8 + 137.3	147.8 + 128.6	129.6 + 131.7					
p-value	0.554		0.054		0.612		0.036*	0.447	0.272	0.311	0.009*
	Phase I		Phase II		Phase III		Phase II–Phase I (*p*-value)		Phase III–Phase I (*p*-value)		All phases
Systolic pressure (mmHg)	121.5 + 12.5		119.5 + 12.8		123.0 + 12.1		0.116		0.332		0.034*
Diastolic pressure (mmHg)	80.3 + 7.4		77.2 + 5.3		81.0 + 7.1		0.002*		0.679		<0.001*
Pulse rate (bpm)	62.0 + 10.7		60.4 + 10.8		61.9 + 11.7		0.185		0.992		0.098

10.3389/fphys.2023.1177583

TABLE 3 Mean perfusion changes expressed in arbitrary blood perfusion units (BPUs) obtained by laser Doppler flowmetry (LDF) and reflection photoplethysmography (PPG) in aged adults participants' test and contralateral feet after the single leg dropping procedure to evoke the venoarteriolar reflex (see text). Data are expressed as means + SD. Statistical comparison with the Friedman test with paired comparison correction (Durbin–Conover) between feet across phases. *$p < 0.05$.

	Phase I		Phase II		Phase III		Phase II–Phase I (p-value)		Phase III–Phase I (p-value)		All phases
	Test limb	Control limb	Test limb	Control limb	Test limb	Control limb	Test limb	Control limb	Test limb	Control limb	
LDF (BPUs)	49.1 ± 52.9	46.4 ± 49.3	24.1 ± 36.7	38.3 ± 48.0	39.4 ± 43.4	41.4 ± 51.2					
p-value	0.294		0.004		0.294		<0.001	0.028	0.547	0.547	<0.001
PPG (BPUs)	231.3 ± 194.5	167.4 ± 123.5	172,4 ± 69.3	128.8 ± 97.3	205.1 ± 199.2	140.0 ± 103.8					
p-value	0.521		0.019		0.630		<0.001	0.006	0.059	0.082	<0.001
	Phase I		Phase II		Phase III		Phase II–Phase I (p-value)		Phase III–Phase I (p-value)		All phases
Systolic pressure (mmHg)	119,2 + 9.6		123.6 + 11.0		125.0 + 10.4		0.086		0.422		0.078
Diastolic pressure (mmHg)	82.1 + 4.3		83,4 + 6.4		84.0 + 6.3		0.222		0.739		0.734
Pulse rate (bpm)	61.8 + 6.9		63,2 + 10.7		69.3 + 7.2		0.185		0.919		0.083

resuming the initial position, perfusion recovered in both limbs, although at the end of Phase III, perfusion remained lower than at baseline, indicating a slower establishment of a new homeostatic state.

To further disclose the potential effect of age on the evoked perfusion adaptive mechanisms, the evolution of these perfusion variables was compared to data from identical experimental conditions applied to a group of young participants recently published involving massage (Rodrigues et al., 2020) and VAR (Silva et al., 2018) interventions. Figures 2, 3 display the perfusion evolution obtained in these young and aged individuals with massage–hyperemia and with the pending leg VAR procedures, respectively. Aged participants have shown significantly higher perfusions in both limbs than the younger group (both in LDF and PPG perfusion data (Figure 2). Regarding VAR, differences between age groups were not statistically significant in any protocol, with the exception of LDF perfusion data in the control limb in Phase III ($p = 0.041$). Nevertheless, the evolution profiles in both groups were similar for each protocol. Comparing the extent of these interventions, measured as the difference in percentage between each phase, we found no significant differences in the magnitude of the effect between age groups, as shown in Tables 4, 5.

The functional imaging obtained with the MSOT system during PORH revealed the skin vascular plexus parallel to the skin surface with larger deep plexus vessels, located 2–6 mm below the skin surface, and the smaller vessels and superficial plexus located 0.6–2 mm below the skin (Figure 4). Thus, we could follow in real time and full extension the effects of PORH in skin vasculature. As recently published (Monteiro Rodrigues et al., 2022), HbO2 and Hb, as quantitatively monitored by our chromophores of interest, significantly changed during the suprasystolic pressure challenge (Figures 4, 5) as a consequence of the transitory movement of blood from superficial to deep structures and back from occlusion to cuff deflation and recovery.

4 Discussion

Reactive hyperemia and VAR, although still poorly understood and characterized, have been widely used to explore cardiovascular physiology and pathophysiology. Our findings on the adaptive responses following reactive hyperemia and VAR in human distal limbs question earlier local mechanistic views behind their interpretation, as the effects of both maneuvers occur simultaneously in the test limb as in the contralateral limb. In other words, the intervention in one limb acutely alters perfusion in the same direction in both limbs. Once the intervention ceases, adaptive responses restore hemodynamics as part of homeostasis.

Previous studies on PORH and VAR used a variety of technologies, typically optically measuring perfusion, although in most cases, measurements were made in a single limb, at a single (contact) point. PORH and VAR observations were perceived as "local"—the hypothesis of a centrally mediated response could not be experimentally explored without the simultaneous contralateral limb measurements. In fact, these analogous responses in blood perfusion in the contralateral non-challenged limb strongly suggest that the adaptive response is centrally mediated, signifying it could be used as a marker of cardiovascular adaptation with clinical interest (Silva et al., 2018; Rodrigues et al., 2020). Therefore, recognizing that to date no clear evidence of this central mechanism had been presented and aware of the potential bias introduced by obtaining results only from young healthy populations, the present study was meant to provide further data to address these issues. For this purpose, we used the same challengers as in recent publications—the (mild) reactive hyperemia produced by massage (Rocha C et al., 2018a; Rocha C et al., 2018b; Rodrigues et al., 2020) and the intense perfusion reduction evoked by one leg pending in dorsal decubitus (Silva et al., 2018) in a group of aged participants.

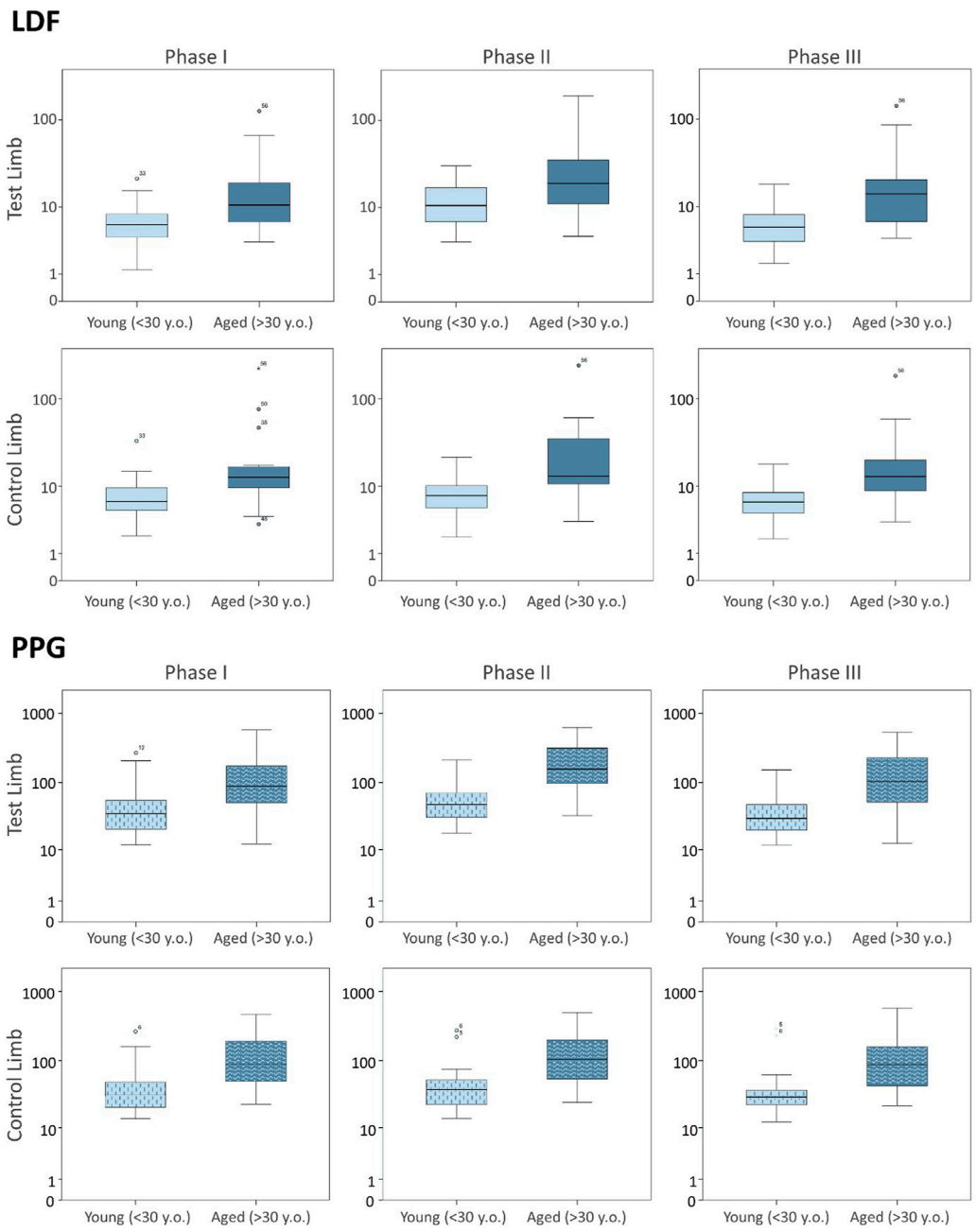

FIGURE 2
Blood perfusion changes registered as a consequence of massage hyperemia applied to one leg measured simultaneously by LDF (upper panel) and PPG (lower panel) in the test and contralateral feet in two different age groups. Data from the current age group (A) study is compared with data from a younger cohort previously published (Rodrigues et al., 2020), which is reproduced under the same protocol conditions (see section 3). The log scale is only applied to better visualize data distribution.

As shown (Figure 1; Table 2), the superficial, light intensity massage of one lower limb evoked a reactive hyperemia visibly detected in both limbs, although perfusion differences were statistically significant only in the massaged limb. Significant reductions ($p < 0.05$) in diastolic pressure were also noted in this aged group (Table 2). To look deeper into the effect of age on the evolution of these perfusion profiles, we further compared these values with those of the younger participants obtained under the same conditions (Figure 2) (Rodrigues et al., 2020). A similar perfusion evolution could be seen in both groups, in both legs, as detected with LDF and PPG (Figure 2). Therefore, these responses were similar to the ones previously published in younger volunteers (Table 4) and consistently asymmetric, as hyperemia was always more pronounced in the massaged (test) limb than in the non-massaged (contralateral) limb. Nevertheless, a similar reflex was equally present in both age groups, as we observed no significant differences in the magnitude of these effects between age groups. In Phase III, a perfusion reduction in both age groups in both limbs was noted (Table 4), but in the aged group a significant difference persisted ($p = 0.029$).

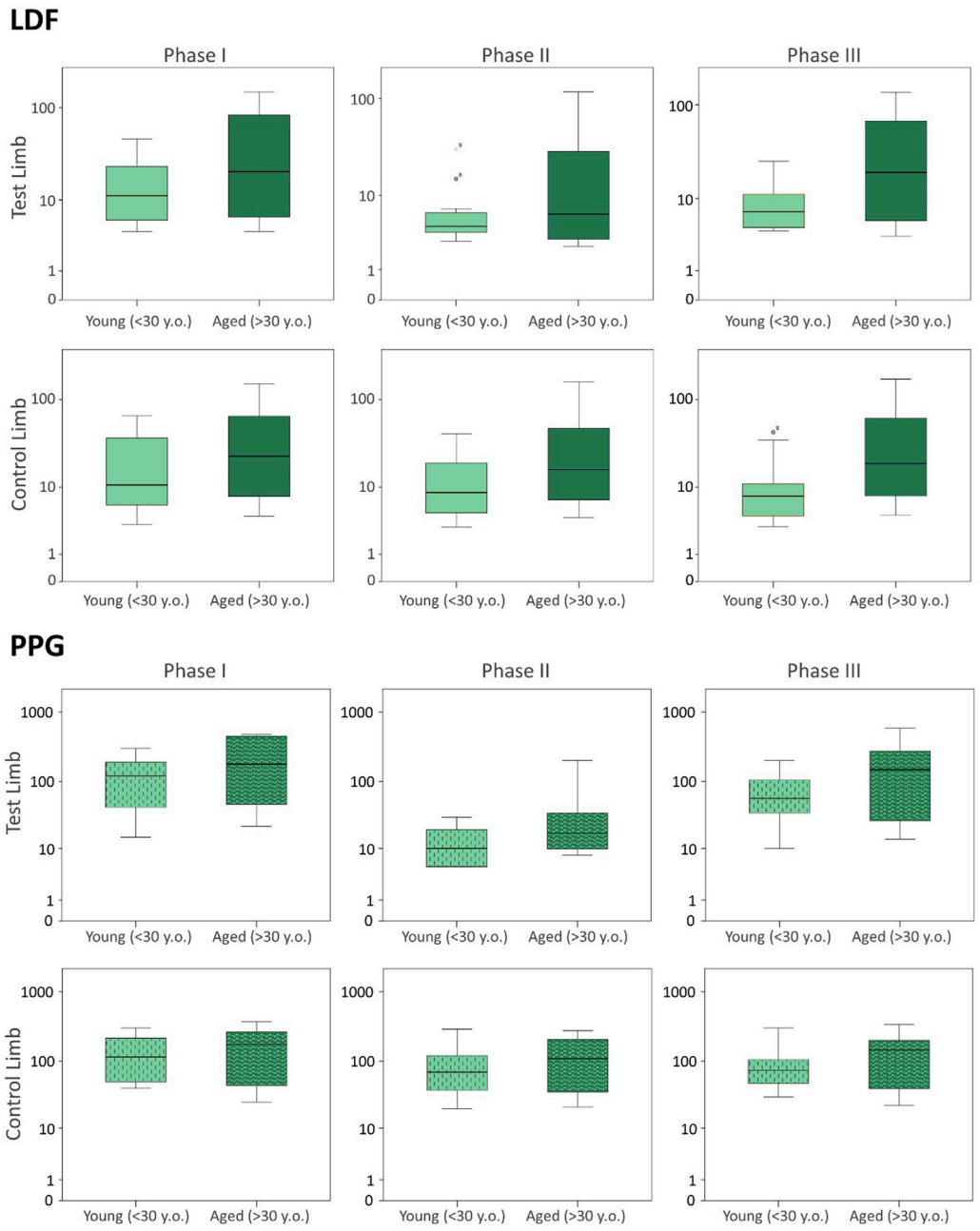

FIGURE 3
Blood perfusion changes registered as a consequence of a venoarteriolar reflex evoked in a single leg measured simultaneously by LDF (upper panel) and PPG (lower panel) in the test and contralateral feet of two different age groups. Data from the current age group (A) study is compared with data from a younger cohort previously published (Silva et al., 2018), which is reproduced under the same protocol conditions (see section 3). The log scale is applied to better visualize data distribution.

The pending leg VAR maneuver evoked the expected significant decrease of perfusion in both legs as detected with LDF and PPG. We further compared these data with the younger participants' values obtained under the same conditions (Figure 3) (Silva et al., 2018) and concluded that both groups' responses were not significantly different (Table 3; Figure 3). As shown in the previous example, the response was asymmetric, being more visible in the pending (test) limb than in the contralateral limb (Table 5). Recovery also seemed to follow a similar evolution in both groups since differences between the magnitudes of these effects were not found (Table 5). Again, this procedure evoked a proportional reflex in both groups, indicating that this reflex is independent of age.

The effect of age on microcirculatory physiology remains poorly characterized, with contradictory reports on capillary density, endothelium structural modifications, and flow (Bigler et al., 2016; Groen et al., 2014). Some authors have reported a reduction of the lower leg flow with (increased) age as a consequence of less effective muscular activity and reduced

TABLE 4 Perfusion differences (%) between Phase II and Phase I, and Phase III and Phase I, for both limbs by the age group in the massage protocol. As the assumption of normality was not met, non-parametric tests were performed. ¥—Statistical comparison between lower limbs with the Friedman test with paired comparison correction (Durbin–Conover) statistical comparison between participants of two different age groups with the Kruskal–Wallis test and the Dwass–Steel–Critchlow–Fligner procedure for pairwise comparisons of perfusion changes obtained in the same experimental conditions.

LDF	Median % Δ Phase II–Phase I (Q1–Q3)			Median % Δ Phase III–Phase I (Q1–Q3)		
	Test limb	Contralateral limb	*p*-value¥	Test limb	Contralateral limb	*p*-value¥
Young	83.6 (47.6–117.3)	7.1 (−3.3–34.0)	<0.001	−2.1 (−13.1–14.4)	−5.3 (−9.5–0.2)	0.501
Age	59.6 (23.1–88.0)	7.83 (−8.5–14.7)	<0.001	9.4 (−3.8–22.2)	−9.4 (−20.3–16.3)	0.029
p-value↓	0.174	0.374		0.067	0.568	
PPG	Median % Δ Phase II–Phase I (Q1–Q3)			Median % Δ Phase III–Phase I (Q1–Q3)		
	Test limb	Contralateral limb	*p*-value¥	Test limb	Contralateral limb	*p*-value¥
Young	32.9 (2.9–69.0)	1.4 (−17.2–23.2)	<0.001	−5.9 (−22.0–8.0)	−12.3 (−21.7–1.1)	0.606
Age	26.9 (−3.7–109.1)	3.8 (−5.6–9.6)	0.028	−7.4 (−19.5–11.4)	−12.9 (−21.5–0.6)	0.403
p-value↓	0.960	0.592		0.763	0.712	

TABLE 5 Percentage difference between Phase II and Phase I, and Phase III and Phase I, for both limbs by the age group in the VAR protocol. As the assumption of normality was met and the homogeneity of variances was also verified, repeated measures ANOVA with the post hoc Tukey test for pairwise comparisons were performed.

LDF	Median % Δ Phase II–Phase I (Q1–Q3)			Median % Δ Phase III–Phase I (Q1–Q3)		
	Mean % Δ Phase II–Phase I (SD)			Mean % Δ Phase III–Phase I (SD)		
	Test limb	Contralateral limb	*p*-value¥	Test limb	Contralateral limb	*p*-value¥
Young	−50.4 (20.1)	−26.3 (14.9)	0.002	−36.3 (23.0)	−32.5 (24.2)	0.997
Age	−51.3 (21.8)	−18.6 (18.3)	<0.001	−5.5 (37.7)	−8.2 (25.3)	1.000
p-value↓	1.000	0.952		0.312	0.345	
PPG	Median % Δ Phase II–Phase I (Q1–Q3)			Median % Δ Phase III–Phase I (Q1–Q3)		
	Test limb	Contralateral limb	*p*-value¥	Test limb	Contralateral limb	*p*-value¥
Young	−84.9 (13.7)	−29.6 (17.3)	<0.001	−36.2 (19.5)	−24.2 (22.0)	0.248
Age	−77.9 (18.0)	−21.1 (14.7)	<0.001	−16.5 (23.3)	−11.4 (21.6)	0.975
p-value↓	0.960	0.913		0.414	0.862	

oxygen demand (Bentov & Reed 2015; Dinenno et al., 1999; Donato et al., 2006; Seals 2003). Other studies assessing the influence of age during a post-occlusive response and matched-intensity leg exercise could not find differences between young and older healthy adults (Meneses et al., 2020). Recent data seem to indicate that aging impacts the entire circulatory system, as the same risk factors affect the macrocirculatory structures, reducing their buffering capacity, which in turn increases the pulsatile stress on microcirculation (Climie et al., 2019; Groenwagen et al., 2016; Huang et al., 2020; Laurent & Boutouyrie 2015). Our findings consistently identified a significant increase in peripheral perfusion in the older healthy participants. Endothelial and myogenic responsiveness could be expected in this group, even if less effective than in younger individuals. However, our results have shown that this massage hyperemia and the pending leg procedure evoked proportional reflexes that appear independent of age.

Finally, to better document and illustrate these involved mechanisms, we applied a classical PORH procedure in a group of young healthy participants, all women, and followed the circulatory responses by functional imaging (OAT-MSOT). In brief, suprasystolic occlusion (200 mmHg) was applied in the middle upper arm, on the brachial artery. After stabilization, MSOT images and videos were collected in the volar forearm for baseline. Occlusion followed (1 min) and further imaging was acquired through cuff deflation in the recovery period. The results obtained were in line with other preliminary results recently published by our group (Monteiro Rodrigues et al., 2022). As shown in Figure 4, the MSOT system allows us to visualize the two skin vascular plexuses parallel to the skin surface at different depths—larger vessels located 2–6 mm below the skin surface corresponding to the deep plexus and smaller vessels located 0.6–2 mm below the epidermis with

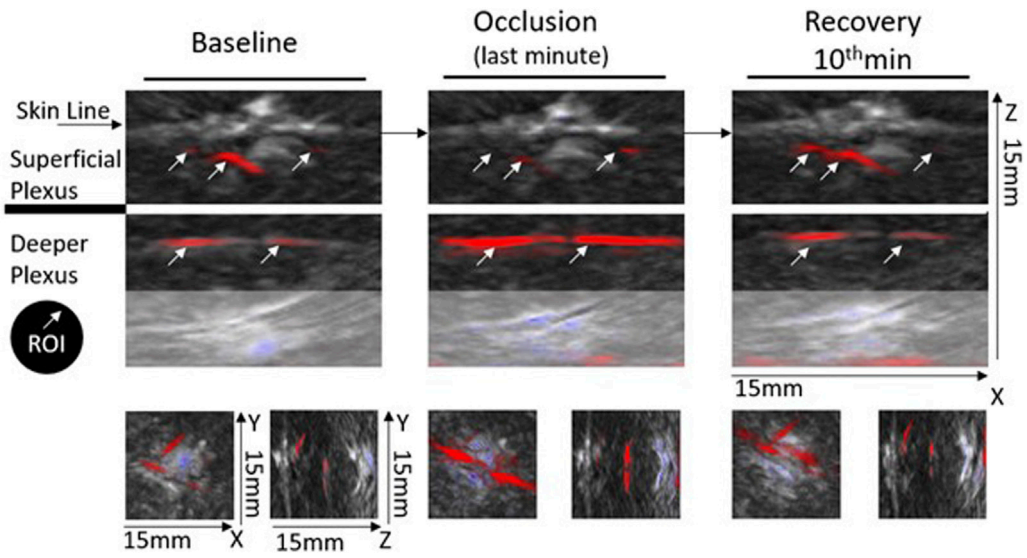

FIGURE 4
Representative optoacoustic images of a PORH maneuver in the human forearm—images were selected from continuous acquisition and displayed according to the progression of the experimental protocol. Each image section, e.g., baseline (Phase I), occlusion (Phase II), and recovery (Phase III) are depicted with a depth of 15 mm in the XYZ axis. Each image section (orthogonal view XZ) includes a frame from the first baseline minute, from the final second of occlusion (held for 1 min at 200 mmHg), and a frame from the final minute of recovery. Selected ROIs for analysis are indicated (white arrows) in the main XZ frame. For proper inter-individual calibration, ROIs must be identified at the deeper and superficial plexus during each acquisition. The XY and YZ axes highlight the 3D impact of the PORH maneuver across the protocol.

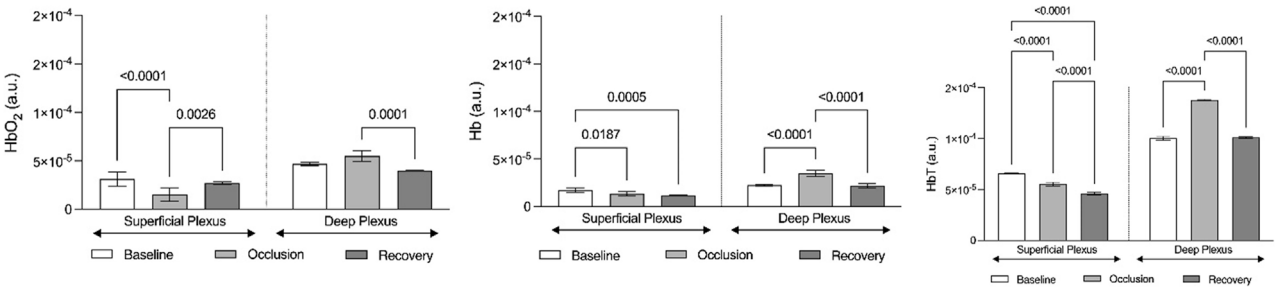

FIGURE 5
Graphic representation of the evolution of hemoglobin chromophores (HbO2, HbO, and HbT) as registered by optoacoustic tomography in the volar forearm during the course of the suprasystolic post-occlusion maneuver in the arm (n = 6). Hemoglobin chromophores are represented as means (+SD) at baseline (before occlusion), during occlusion, and in the recovery phase after cuff deflation. These evolutions depict the centrally mediated adaptive movement of blood between skin vascular plexus as illustrated in Figure 4 (see section 3).

perpendicular structures connecting both plexuses. Real-time images show (color coded) HbO2 and Hb moving from the superficial to the deeper plexus with occlusion and backward with deflation. The ROI analysis and signal post-processing provide the quantification of several variables. As shown in Figure 5, the main markers, HbO2 and Hb, change in the same direction with PORH. During occlusion, these markers practically disappear in the superficial plexus. Contraction of these vessels necessarily ensured by somatic and autonomous outflow seems to push down the blood to deeper structures. Thus, with occlusion, HbO_2 and Hb practically disappear from the superficial plexus, increasing in the deep plexus in a similar proportion. After cuff deflation, a rapid recovery is seen in the superficial vessels. The blood pressure and pulse rate were consistently reduced along the protocol but significant differences were not detected.

These findings provide considerable evidence that sudden *in vivo* changes in local skin circulation immediately trigger this centrally mediated response to re-establish hemodynamic homeostasis. Although interventions occurred in single limb, identical responses (e.g., hyperemia increasing perfusion and VAR reducing perfusion) were noticeable in both limbs during the intervention phases. Responses seem to be proportional to the magnitude of the intervention, as shown with moderate local

massage hyperemia or with the intense reduction affecting larger deep vessels evoked by the pending leg VAR or by PORH. Perfusion recovered once the intervention ceased, restoring hemodynamics. Furthermore, we have confirmed that, under these conditions, responses were similarly present independent of age and might be expected to be modified in the presence of pathological processes. Our ongoing research explores this direction further evaluating the applicability of this response as a cardiovascular marker with clinical diagnostic interest.

Our study has some limitations, such as (i) the use of a convenience sample with a reduced number of participants limits the extrapolation for the general population; (ii) the single point measurement technology chosen (LDF and PPG), although widely referenced, have recognized resolution limitations; (iii) our studies are strictly physiological, developed exclusively with healthy participants, which means that impact on these responses within specific groups of cardiovascular patients still must be established. Nevertheless, independent of the circulatory challenger or age of the participant involved, an identical adaptive response was fully reproducible. Therefore, we believe these exploratory maneuvers cannot be explained without considering a centrally mediated reflex as we have observed and documented in real time through functional imaging. Further identification of the sensors and effectors, here involved, will improve understanding of these adaptive mechanisms, potentially leading to markers with practical utility.

Data availability statement

The raw data supporting the conclusion of this article will be made available by the authors, without undue reservation.

Ethics statement

The studies involving human participants were reviewed and approved by the Ethics Commission for Health Sciences—ULusófona Lisboa. The patients/participants provided their written informed consent to participate in this study.

Author contributions

MR, CR and JG were responsible for the concept and design of the study. CR, SA, and TG performed the experimental investigation. CR, TG and JG organised data bases and performed the statistical analysis. MR wrote the final version of the manuscript. All authors contributed to manuscript revision and approved the submitted version.

Funding

This research is funded by the national Foundation for Science and Technology (FCT) through grant UIDB/04567/2020 to CBIOS. JG is supported by FCT through the Scientific Employment Stimulus contract with the reference number CEEC/CBIOS/EPH/2018. COFAC and ALIES financed the optoacoustic instrument and analysis.

Conflict of interest

The authors declare that the research was conducted in the absence of any commercial or financial relationships that could be construed as a potential conflict of interest.

Publisher's note

All claims expressed in this article are solely those of the authors and do not necessarily represent those of their affiliated organizations, or those of the publisher, editors, and reviewers. Any product that may be evaluated in this article, or claim that may be made by its manufacturer, is not guaranteed or endorsed by the publisher.

References

Aboyans, V., Criqui, M. H., Abraham, P., Allison, M. A., Creager, M. A., Diehm, C., et al. (2013). Measurement and interpretation of the ankle-brachial index: A scientific statement from the American heart association. *Circulation* 126 (24), 2890–2909. doi:10.1161/CIR.0b013e318276fbcb

Ash, C., Dubec, M., Donne, K., and Bashford, T. (2017). Effect of wavelength and beam width on penetration in light-tissue interaction using computational methods. *Lasers Med. Sci.* 32 (8), 1909–1918. doi:10.1007/s10103-017-2317-4

Bentov, I., and Reed, M. J. (2015). The effect of aging on the cutaneous microvasculature. *Microvasc. Res.* 100, 25–31. doi:10.1016/j.mvr.2015.04.004

Bergstrand, S., Lindberg, L. G., Ek, A. C., Lindén, M., and Lindgren, M. (2009). Blood flow measurements at different depths using photoplethysmography and laser Doppler techniques. *Res. Technol.* 15, 139–147. doi:10.1111/j.1600-0846.2008.00337.x

Bigler, M., Koutsantonis, D., Odriozola, A., Halm, S., Tschanz, S. A., Zakrzewicz, A., et al. (2016). Morphometry of skeletal muscle capillaries: The relationship between capillary ultrastructure and ageing in humans. *Acta Physiol. (Oxf)* 218 (2), 98–111. doi:10.1111/apha.12709

Climie, R. E., Gallo, A., Picone, D. S., Di Lascio, N., van Sloten, T. T., Guala, A., et al. (2019). Measuring the interaction between the macro- and micro-vasculature. *Front. Cardiovasc Med.* 6, 169. doi:10.3389/fcvm.2019.00169

Cracowski, J. L., and Roustit, M. (2020). Human skin microcirculation. *Compr. Physiol.* 10 (3), 1105–1154. doi:10.1002/cphy.c190008

Crandall, C. G., Shibasaki, M., and Yen, T. C. (2002). Evidence that the human cutaneous venoarteriolar response is not mediated by adrenergic mechanisms. *J. Physiol.* 538, 599–605. doi:10.1113/jphysiol.2001.013060

Daiwei, L., Lucas, H., Emelina, V., Tri, V., and Junjie, Y. (2021). Seeing through the skin: Photoacoustic tomography of skin vasculature and beyond. *JID Innov.* 1, 100039. doi:10.1016/j.xjidi.2021.100039

Dinenno, F. A., Jones, P. P., Seals, D. R., and Tanaka, H. (1999). Limb blood flow and vascular conductance are reduced with age in healthy humans: Relation to elevations in sympathetic nerve activity and declines in oxygen demand. *Circulation* 100, 164–170. doi:10.1161/01.cir.100.2.164

Donato, A. J., Uberoi, A., Wray, D. W., Nishiyama, S., Lawrenson, L., and Richardson, R. S. (2006). Differential effects of aging on limb blood flow in humans. *Am. J. Physiol. Heart Circ. Physiol.* 290 (1), H272–H278. doi:10.1152/ajpheart.00405.2005

Florindo, M., Nuno, S., Andrade, S., Rocha, C., and Rodrigues, L. M. (2021). The acute modification of the upper-limb perfusion *in vivo* evokes a Prompt adaptive hemodynamic response to reestablish cardiovascular homeostasis. Physiology21 Annual Conference Abstract Book 2021. Available online: https://static.physoc.org/app/uploads/2021/06/10115155/Physiology-2021-Abstract-Book.pdf.

Granja, T., Faloni de Andrade, S., and Rodrigues, L. M. (2022). Multi-spectral optoacoustic tomography for functional imaging in vascular research. *J. Vis. Exp.* 184, e63883. doi:10.3791/63883

Groen, B. B., Hamer, H. M., Snijders, T., van Kranenburg, J., Frijns, D., Vink, H., et al. (2014). Skeletal muscle capillary density and microvascular function are compromised with aging and type 2 diabetes. *J. Appl. Physiol. (1985)* 116 (8), 998–1005. doi:10.1152/japplphysiol.00919.2013

Groenwagen, K. A., den Ruijter, H. M., Pasterkamp, D. R., Polak, J. F., Bots, M. L., and Peters Sanne, A. E. (2016). Vascular age to determine cardiovascular disease risk: A systematic review of its concepts, definitions, and clinical applications. *Eur. J. Prev. Cardiol.* 23, 264–274. doi:10.1177/2047487314566999

Guven, G., Hilty, M. P., and Ince, C. (2020). Microcirculation: Physiology, pathophysiology, and clinical application. *Blood Purif.* 49 (1-2), 143–150. doi:10.1159/000503775

Hu, S., and Wang, L. V. (2010). Photoacoustic imaging and characterization of the microvasculature. *J. Biomed. Opt.* 15 (1), 011101. doi:10.1117/1.3281673

Huang, Q. F., Aparicio, L. S., Thijs, L., Wei, F. F., Melgarejo, F. D., Cheng, Y. B., et al. (2020). Cardiovascular end points and mortality are not closer associated with central than peripheral pulsatile blood pressure components. *Hypertension* 76, 350–358. doi:10.1161/HYPERTENSIONAHA.120.14787

Laurent, S., and Boutouyrie, P. (2015). The structural factor of hypertension: Large and small artery alterations. *Circ. Res.* 116, 1007–1021. doi:10.1161/CIRCRESAHA.116.303596

Low, P. A. (2004). "Venoarteriolar reflex," in *Primer on the autonomic nervous system*. Second Edition (Netherlands: Elsevier Inc).

Masashi, L., Seiji, M., Narihiko, K., and Takeshi, N. (2013). Blood pressure regulation II: What happens when one system must serve two masters—oxygen delivery and pressure regulation? *Eur. J. Appl. Physiology* 114 (3), 451–465. doi:10.1007/s00421-013-2691-y

Mazzoni, M. C., and Schmid-Schonbein, G. W. (1996). Mechanisms and consequences of cell activation in the microcirculation. *Cardiovasc Res.* 32, 709–719. PMID: 8915189. doi:10.1016/s0008-6363(96)00146-0

Mei, C. C., Zhang, J., and Jing, H. X. (2018). Fluid mechanics of Windkessel effect. *Med. Biol. Eng. Comput.* 56 (8), 1357–1366. doi:10.1007/s11517-017-1775-y

Meneses, A. L., Nam, M. C. Y., Bailey, T. G., Anstey, C., Golledge, J., Keske, M. A., et al. (2020). Skeletal muscle microvascular perfusion responses to cuff occlusion and submaximal exercise assessed by contrast-enhanced ultrasound: The effect of age. *Physiol. Rep.* 8, e14580. doi:10.14814/phy2.14580

Monteiro Rodrigues, L., Granja, T. F., and de Andrade, S. F. (2022). Optoacoustic imaging offers new insights into *in vivo* human skin vascular physiology. *Life* 12 (10), 1628. doi:10.3390/life12101628

Rathbun, S., Heath, P. J., and Whitsett, T. (2008). Images in vascular medicine. The venoarterial reflex. *Vasc. Med.* 13 (4), 315–316. doi:10.1177/1358863X08092101

Rocha, C., Macedo, A., Nuno, S., Silva, H., Ferreira, H., and Rodrigues, L. M. (2018a). Exploring the perfusion modifications occurring with massage in the human lower limbs by non contact polarized spectroscopy. *Biomed. Biopharm. Res.* 15 (2), 196–204. doi:10.19277/bbr.15.2.186

Rocha, C., Silva, H., Ferreira, H., and Rodrigues, L. M. (2018b). Comparing the effects of human hind limb massage by analysis of Laser Doppler flowmetry and Photoplethysmography signal components using the wavelet transform. *Biomed. Biopharm. Res.* 15 (1), 70–81. doi:10.19277/bbr.15.1.176

Rocha, C., Silva, H., Frazão, I., and Rodrigues, L. M. (2016). Assessing the effect of manual massage on the lower limb microcirculation. *Biomed. Biopharm. Res.* 13 (2), 2273–2290. doi:10.19277/bbr.13.2.144

Rodrigues, L. M., Rocha, C., Ferreira, H., and Silva, H. (2019). Different lasers reveal different skin microcirculatory flowmotion - data from the wavelet transform analysis of human hindlimb perfusion. *Sci. Rep.* 9 (1), 16951. doi:10.1038/s41598-019-53213-2

Rodrigues, L. M., Rocha, C., Ferreira, H. A., and Silva, H. N. (2020). Lower limb massage in humans increases local perfusion and impacts systemic hemodynamics. *J. Appl. Physiol.* 128, 1217–1226. doi:10.1152/japplphysiol.00437.2019

Rodrigues, L. M., Silva, H., Ferreira, H., Renault, M. A., and Gadeau, A. P. (2018). Observations on the perfusion recovery of regenerative angiogenesis in an ischemic limb model under hyperoxia. *Physiol. Rep.* 6 (12), e13736. doi:10.14814/phy2.13736

Rosenberry, R., and Nelson, M. D. (2020). Reactive hyperemia: A review of methods, mechanisms, and considerations. *Am. J. Physiol. Regul. Integr. Comp. Physiol.* 318 (3), R605–R618. doi:10.1152/ajpregu.00339.2019

Rowell, L. B., O'Leary, D. S., and Kellogg, D. L., Jr. (2011). "Integration of cardiovascular control systems in dynamic exercise," in *Comprehensive physiology*. Editor R. Terjung (New York: Wiley).

Seals, D. (2003). Habitual exercise and the age-associated decline in large artery compliance. *Exerc Sport Sci. Rev.* 31, 68–72. doi:10.1097/00003677-200304000-00003

Silva, H., Ferreira, H., Bujan, M. J., and Rodrigues, L. M. (2015). Regarding the quantification of peripheral microcirculation - comparing responses evoked in the *in vivo* human lower limb by postural changes, suprasystolic occlusion and oxygen breathing. *Microvasc. Res.* 99, 110–117. doi:10.1016/j.mvr.2015.04.001

Silva, H., Ferreira, H., Renault, M. A., Silva, H. P., and Rodrigues, L. M. (2018). The venoarteriolar reflex significantly reduces contralateral perfusion as part of the lower limb circulatory homeostasis *in vivo*. *Front. Physiol.* 9, 1123. doi:10.3389/fphys.2018.01123

Wang, L. V. (2008). Prospects of photoacoustic tomography. *Med. Phys.* 35 (12), 5758–5767. doi:10.1118/1.3013698

World Medical Association (2013). World medical association declaration of Helsinki: Ethical principles for medical research involving human subjects. *JAMA* 310, 2191–2194. doi:10.1001/jama.2013.281053

frontiers | Frontiers in Physiology

TYPE Original Research
PUBLISHED 02 October 2023
DOI 10.3389/fphys.2023.1271698

OPEN ACCESS

EDITED BY
Antigone Lazou,
Aristotle University of Thessaloniki, Greece

REVIEWED BY
Peter Pokreisz,
Medical University of Vienna, Austria
Francisco O. Silva,
University of Texas Southwestern Medical Center, United States

*CORRESPONDENCE
André P. Lourenço,
aplourenco@yahoo.com

†These authors have contributed equally to this work and share first authorship

‡These authors share last authorship

RECEIVED 02 August 2023
ACCEPTED 18 September 2023
PUBLISHED 02 October 2023

CITATION
Leite-Moreira AM, Almeida-Coelho J, Neves JS, Castro-Ferreira R, Ladeiras-Lopes R, Leite-Moreira AF and Lourenço AP (2023), Myocardial stretch-induced compliance is abrogated under ischemic conditions and restored by cGMP/PKG-related pathways. *Front. Physiol.* 14:1271698. doi: 10.3389/fphys.2023.1271698

Myocardial stretch-induced compliance is abrogated under ischemic conditions and restored by cGMP/PKG-related pathways

André M. Leite-Moreira[1,2†], João Almeida-Coelho[1†], João S. Neves[1,3], Ricardo Castro-Ferreira[1,4], Ricardo Ladeiras-Lopes[1], Adelino F. Leite-Moreira[1,5‡] and André P. Lourenço[1,2‡*]

[1]Cardiovascular R&D Centre—UnIC@RISE, Department of Surgery and Physiology, Faculty of Medicine of the University of Porto, Porto, Portugal, [2]Department of Anesthesiology, Centro Hospitalar Universitário São João, Porto, Portugal, [3]Department of Endocrinology, Metabolism and Diabetes, Centro Hospitalar Universitário São João, Porto, Portugal, [4]Department of Vascular Surgery, Centro Hospitalar de Vila Nova de Gaia/Espinho, Vila Nova de Gaia, Portugal, [5]Department of Cardiothoracic Surgery, Centro Hospitalar Universitário São João, Porto, Portugal

Introduction: Management of acute myocardial infarction (MI) mandates careful optimization of volemia, which can be challenging due to the inherent risk of congestion. Increased myocardial compliance in response to stretching, known as stretch-induced compliance (SIC), has been recently characterized and partly ascribed to cGMP/cGMP-dependent protein kinase (PKG)-related pathways. We hypothesized that SIC would be impaired in MI but restored by activation of PKG, thereby enabling a better response to volume loading in MI.

Methods: We conducted experiments in *ex vivo* rabbit right ventricular papillary muscles under ischemic and non-ischemic conditions as well as pressure–volume hemodynamic evaluations in experimental *in vivo* MI induced by left anterior descending artery ligation in rats.

Results: Acutely stretching muscles *ex vivo* yielded increased compliance over the next 15 min, but not under ischemic conditions. PKG agonists, but not PKC agonists, were able to partially restore SIC in ischemic muscles. A similar effect was observed with phosphodiesterase-5 inhibitor ($PDE5_i$) sildenafil, which was amplified by joint B-type natriuretic peptide or nitric oxide donor administration. *In vivo* translation revealed that volume loading after MI only increased cardiac output in rats infused with $PDE5_i$. Contrarily to vehicle, sildenafil-treated rats showed a clear increase in myocardial compliance upon volume loading.

Discussion: Our results suggest that ischemia impairs the adaptive myocardial response to acute stretching and that this may be partly prevented by pharmacological manipulation of the cGMP/PKG pathway, namely, with $PDE5_i$. Further studies are warranted to further elucidate the potential of this intervention in the clinical setting of acute myocardial ischemia.

KEYWORDS

myocardial ischemia, myocardial infarction, cardiac stretch, volume loading, myocardial compliance, diastolic function, phosphodiesterase-5 inhibitors, cGMP-dependent protein kinase

1 Introduction

In acute myocardial infarction (MI) and coronary syndromes, ischemia impairs both systolic and diastolic function (Ratshin et al., 1972). Early revascularization is critical and should not be delayed. Nevertheless, many patients develop cardiogenic shock, and their hemodynamics must be supported (Gowda et al., 2008). Current medical focus has shifted toward mechanical circulatory support, inotropic or vasopressor therapy, and advanced hemodynamic monitoring (Kirigaya et al., 2023), but the first support measure remains fluid resuscitation. Optimization of filling pressures by volume loading increases the cardiac output and allows downtitration of inotropes, thereby preventing side effects (Gowda et al., 2008). Still, the therapeutic margin may be narrow since the acutely ischemic heart already faces elevated filling pressures and there is an impending risk of lung congestion. A deeper understanding of the mechanisms of adjustment to volume loading in physiology and disease becomes crucial.

In its healthy state, the heart swiftly adapts to acute bouts of stretching or overload throughout life. While the mechanisms of systolic function adaptation to stretch have been widely investigated (Neves et al., 2016), diastolic adaptation under physiological conditions has only recently been described in multiple mammalian species and experimental conditions by our group (Leite-Moreira et al., 2018). This adaptive stretch-induced compliance (SIC) response was partly ascribed to titin phosphorylation by cyclic guanosine monophosphate (cGMP)/cGMP-dependent protein kinase (PKG)-related pathways and shown to be decreased in the hypertrophic heart of rats with transverse aortic constriction. We had also previously observed impaired slow force response after stretching rabbit papillary muscles *ex vivo* under ischemic conditions, which could be partly mitigated by the cGMP-specific type 5 phosphodiesterase inhibitors ($PDE5_i$) (Castro-Ferreira et al., 2014). Together, these findings led us to hypothesize that SIC might be impaired under ischemic conditions and that pinpointing and targeting the underlying mechanisms might enable broadening the therapeutic margin for volume loading in acute MI.

In this study, we aimed to dissect the effects of stretching myocardial compliance under ischemic conditions *ex vivo*, to elucidate the underlying signaling pathways, and then modulate them *in vivo* during volume loading in experimental acute MI.

2 Materials and methods

2.1 Ethics and animal care

Animal experiments were approved by the competent authorities (016531) and complied with the Guide for the Care and Use of Laboratory Animals (NIH Publication no. 85–23, revised 2011) and the guidelines from Directive 2010/63/EU of the European Parliament on the protection of animals used for scientific purposes. Male 11-week-old Wistar Han rats (n = 14; Charles River, Spain) and 10- to 12-week-old New Zealand white rabbits (n = 42) were housed in groups of 3 and 1 per cage, respectively, in a controlled environment at 22°C under a 12:12-h light–dark cycle and with free access to food and water.

2.2 Papillary muscle preparations

Male New Zealand white rabbits were anesthetized with intravenous sodium pentobarbital (25 mg kg^{-1}) injected through a superficial ear vein. After confirming the loss of toe pinch and ear prick reflexes, a left thoracotomy was performed, and the beating hearts were quickly excised and immersed in modified Krebs–Ringer buffer (KRB; in mM: 98 NaCl, 4.7 KCl, 2.4 $MgSO_4$, 1.2 KH_2PO_4, 4.5 glucose, 1.8 $CaCl_2$, 17 $NaHCO_3$, 15 sodium pyruvate, 5 CH_3COONa, and 30 2,3-butanedione monoxime—BDM) at 30°C with 5% newborn calf serum. Right ventricle (RV) papillary muscles were dissected and vertically mounted in a 10-mL plexiglass organ bath. One or two papillary muscles were used from each animal. The lower muscular end was fixed in a phosphor-bronze clip, the upper tendinous end was attached to an electromagnetic length–tension transducer (University of Antwerp, Belgium), and preload was initially set to 3 mN. After replacement with KRB without calf serum or BDM, the preparations were stimulated at 0.2 Hz with square 5-ms pulses, with the voltage set 10% above the stimulation threshold. The length for maximum active force development was determined (L_{max}), and the muscles were allowed to stabilize at 92% of L_{max}. The pH was set at 7.4 with 5% CO_2. The experimental protocol consisted of serial evaluation of passive tension in isometric twitches for 15 min after sudden stretch from 92% to 100% of L_{max}. Papillary muscles were randomized to undergo either evaluation under oxidative conditions with 95% O_2 (n = 9) or under conditions mimicking myocardial ischemia (glucose was removed from the bathing solution and O_2 was interrupted, n = 7). Under oxidative (non-ischemic) conditions, further randomization was carried out between no pharmacological manipulation or previous addition of a PKA inhibitor (KT-5720; Sigma-Aldrich; 10^{-5} M; n = 7), a PKG inhibitor (Rp-8-Br-PET-cGMPS; Sigma-Aldrich; 10^{-6} M; n = 7), or a PKC inhibitor (chelerythrine; Sigma-Aldrich; 10^{-5} M; n = 7). Likewise, under ischemic conditions, muscles were randomized to no pharmacological modulation or previous incubation with a PKG agonist (8-bromo-cGMP; Sigma-Aldrich; 10^{-5} M; n = 7) or a PKC agonist (phorbol 12-myristate 13-acetate; Sigma-Aldrich; 5×10^{-6} M; n = 7). Based on the modification of response under ischemic conditions with PKG agonists, new experiments were conducted by randomly assigning muscles to incubation with either B-type natriuretic peptide-32 (BNP; Sigma-Aldrich; 10^{-6} M; n = 7), a nitric oxide (NO) donor (S-nitroso-N-acetylpenicillamine (SNAP; Sigma-Aldrich; 10^{-5} M; n = 7), or a phosphodiesterase-5 inhibitor (PDE_i; sildenafil; Pfizer; 10^{-6} M; n = 7), and later also with the combinations sildenafil + BNP (n = 7) and sildenafil + SNAP (n = 6). The doses of inhibitor and agonist drugs were based on supramaximal effects, as reported in previous studies, and following the manufacturers' recommendations. Drug efficacy was confirmed in previous experiments carried out at the department. Recording and analysis were performed with dedicated software (University of Antwerp, Belgium).

2.3 Volume loading after myocardial infarction *in vivo*

Eleven-week-old male Wistar Han rats weighing 416 ± 110 g (n = 14) were anesthetized by inhalation of 8% sevoflurane and 100 µg/kg subcutaneous injection of fentanyl. Upon orotracheal intubation with a 14G intravenous catheter, anesthesia was maintained with 2.5%–3% sevoflurane, and animals were mechanically ventilated (PhysioSuite®, Kent Scientific) with 100% O_2 in a volume-controlled mode with end-expiratory pressure held at 4 cmH_2O. The respiratory rate and tidal volume were adjusted to achieve normocapnia. Body temperature was kept at 37–38°C with a heating pad. Peripheral venous access (24G) was placed in the dorsal foot vein, and warm Ringer lactate solution was infused at a rate of 20 mL/kg/h. Surface electrocardiogram (ECG), peripheral oximetry, and body temperature were monitored throughout the procedure. In the position of a slight right lateral decubitus and upon wide left thoracotomy, a pressure–volume catheter was placed along the left ventricular long axis through an apical puncture (SPR-869, Millar), a pressure catheter was placed in the pulmonary artery through a puncture in the RV outflow tract (PVR-1045, Millar), and a transit-time flow probe (MA-2.5PSB, Transonic) was placed in the ascending aorta. When the preparation was deemed stable, rats were subjected to acute MI by left anterior descending artery ligation with a 5-0 polypropylene suture 2–3 mm distal to the anterior–inferior edge of the left auricle following a line connecting the intersection between the RV outflow tract and the right border of the left auricle and the left ventricular apex (Hou et al., 2011). MI was confirmed by ST segment changes and arrhythmia development on the ECG, hemodynamic changes, and by visual confirmation of dyskinesia and pallor of the left ventricular anterior wall (illustrative video and ECG changes are presented in Supplementary Material). When rhythm and hemodynamics were deemed stable, rats were randomized to either sildenafil 42.5 µg/kg/min or an equal volume of infused vehicle (groups Sil and Veh, n = 7 each, respectively), and after at least 20 min of infusion, upon stabilization, Veh and Sil were then subjected to acute volume loading. Volume loading consisted of an infusion of 10% estimated extracellular fluid volume for 15 min. Extracellular water was estimated as 24% of body weight (Cornish et al., 1992). The solution infused was a 50% mixture of 20% mannitol and Ringer lactate, with one-fourth of the volume infused in 2 min and maintenance and the remaining three-fourths for the next 13 min.

There was no mortality, and ventricular fibrillation episodes were resolved by transient cardiac massage and defibrillation by a sudden flick of the myocardium with the back of a metal forceps. All signals were continuously recorded at 2000 Hz (MPVS ultra, LabChart Pro, ADInstruments). Inferior vena cava occlusions with ventilation suspended at end-expiration were carried out at baseline, after MI, upon drug/vehicle infusion and, finally, after volume loading. Pressure–volume signals were calibrated by aortic flow (slope factor α calibration) and repeated injection of 40 µL 10% hypertonic saline (parallel conductance). End-systolic and end-diastolic pressure–volume relationships were fitted as end-systolic elastance (E_{es})*(end-systolic volume—zero volume (v0)) and $\alpha^{*}e^{\text{end-diastolic volume}^{*}\beta}$ upon confirmation that the non-linear component and pressure decay asymptote were neglectable, respectively.

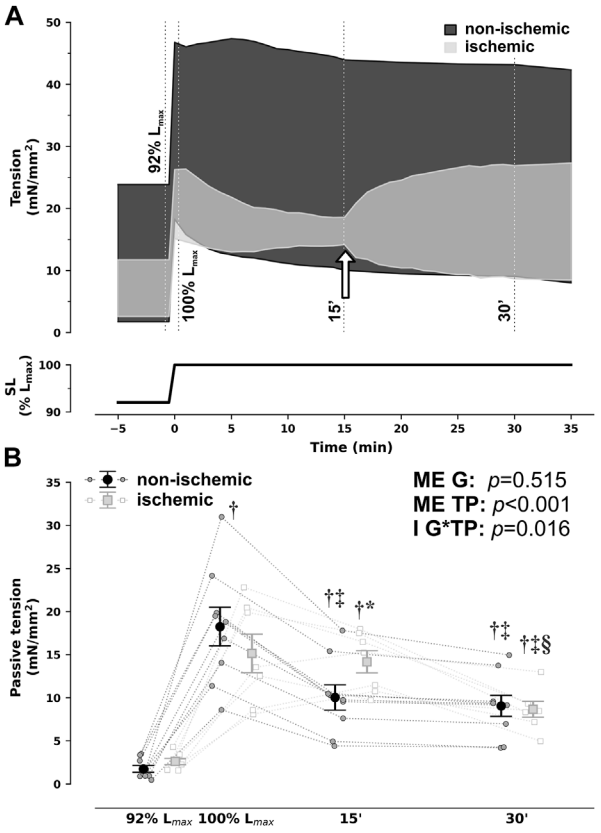

FIGURE 1
Group-averaged tracings of developed tension in isometric contractions of right ventricular rabbit papillary muscles under non-ischemic and ischemic conditions when sudden and sustained stretch from 92% to 100% of optimal maximum muscle and sarcomere length (SL, L_{max}) was applied **(A)** and passive tension comparisons at selected timepoints **(B)**. For illustration purposes, the timepoints of evaluation from **(B)** are depicted by dotted lines in **(A)**. In addition, in **(A)**, the white arrow signals denote changing perfusion conditions from ischemic back to non-ischemic in the ischemic group. Ischemic and non-ischemic muscles showed a comparable increase in passive tension upon stretch, but while non-ischemic muscles developed the expected Frank–Starling and slow-force response and a steady decrease in passive tensions throughout the next 15 min (stretch-induced compliance), ischemic muscles did not. Nonetheless, passive tension did decrease after restoration of non-ischemic conditions from 15 to 30 min *$p < 0.05$ *vs* non-ischemic (same timepoint), †$p < 0.05$ vs. 92% L_{max}, ‡$p < 0.05$ vs. 100% L_{max}, §$p < 0.05$ *vs* 15′ by two-way repeated measures analysis of variance; n = 9 and 7 for non-ischemic and ischemic, respectively. G, group; I, interaction; ME, main effect, TP, timepoint.

2.4 Statistical analysis

Pressure–volume signal analysis was performed by Python scripts developed in-house, and statistical analysis was carried out with statsmodels and pingouin mixed_anova Python packages for two-way repeated measures analysis of variance, except for the end-systolic and end-diastolic pressure–volume

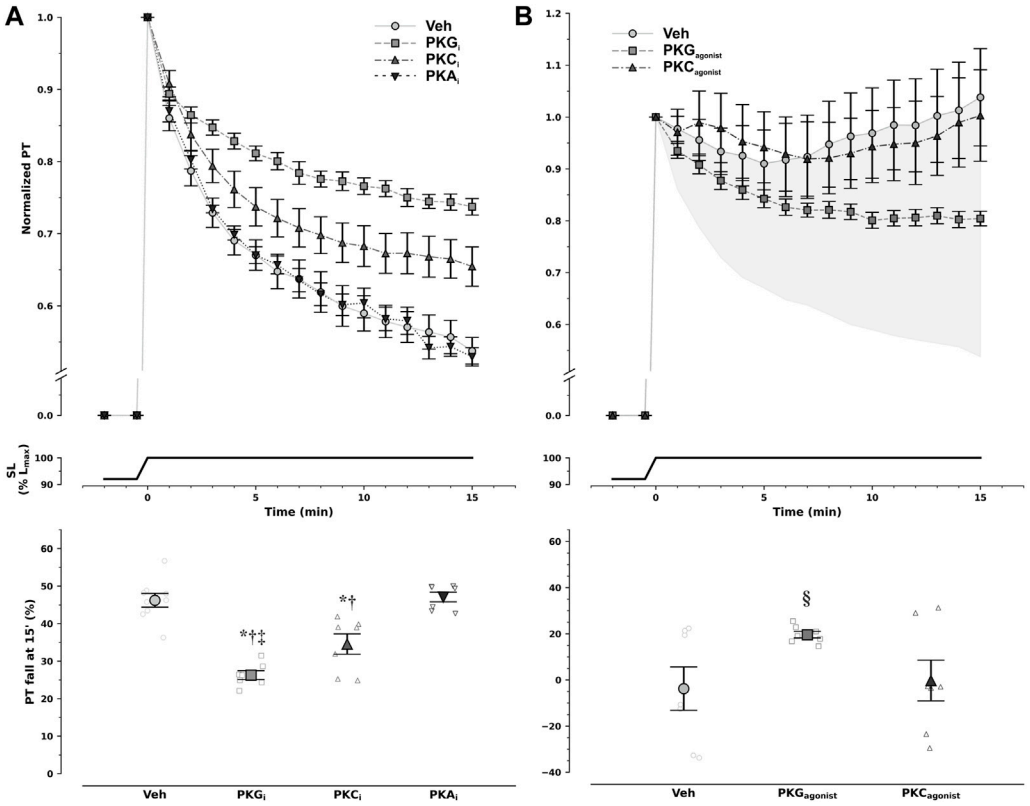

FIGURE 2
Modulation of diastolic response to stretch by protein kinase (PK) pathways. Non-ischemic muscles were incubated with either vehicle (Veh) or PK inhibitors **(A),** whereas ischemic muscles were incubated with either vehicle (Veh) or PK agonists **(B)**. Decay of normalized passive tension (PT) during the 15 min that followed stretch from 92% to 100% of optimal maximum muscle and sarcomere length (Lmax, SL) is presented at the top, while overall magnitude of PT decrease is shown at the bottom. Inhibition of PKA (PKAi) had no effect on passive tension decrease, whereas PKC inhibition (PKCi) slightly reduced it, and PKG inhibition (PKGi) attenuated it by approximately 50% in non-ischemic muscles. Under ischemic conditions only PKG, and not PKC, activation was able to partly restore passive tension decrease with stretch ($^{\S}p = 0.029$ vs. Veh and PKC by least-squares contrasts). In panel B, the shaded area represents the difference in magnitude of response between ischemic and non-ischemic myocardium. Remarkably, PKG agonism restored nearly 50% of pressure decay in the ischemic myocardium. PKA agonists were not tested. Comparisons were performed with one-way analysis of variance: $^{*}p < 0.001$ *vs* Veh, $^{\dagger}p < 0.001$ vs. PKA_i, and $^{\ddagger}p = 0.026$ vs. PKC_i; $n = 9, 7, 7$, and 7 for Veh, PKGi, PKCi, and PKAi in non-ischemic muscles, respectively, and 7, 7, and 7 for Veh, PKG agonism, and PKC agonism in ischemic muscles, respectively.

relationships, which were analyzed with tydiverse and rstatix R packages for two-way repeated measures analysis of covariance. Plots were generated with the matplotlib Python package. Experiments conducted on papillary muscles were analyzed with two-way repeated measures (passive tension evolution in ischemic and non-ischemic myocardium) or one-way analysis of variance (comparisons of percent passive tension decay between experimental groups). Assumptions were checked by visual inspection of model residuals and Shapiro–Wilk's test, Levene's test for homogeneity of variances, Mauchly's test for sphericity assumption, and Box-M test for homogeneity of covariates. There were no major deviations from assumptions: when sphericity assumption was not met, the Greenhouse–Geisser correction was applied. Multiple groups' pairwise comparisons were performed with Sidak's adjustment. Data are expressed as mean ± standard error of mean. The significance value ascertained by the two-tailed test was set at 0.05.

3 Results

3.1 Response to stretch in non-ischemic and ischemic myocardium

As previously reported, rabbit RV papillary muscles steadily decreased passive tension from 92% to 100% of Lmax under non-ischemic conditions, in the 15 min that followed sudden stretch, denoting SIC (Figure 1). This response was entirely abrogated in ischemia but fully restored upon return to aerobic conditions, as can be clearly visualized in Figure 1A.

To dissect the underlying intracellular pathways, we probed the contributions of protein kinases PKA, PKC, and PKG by previous incubation with direct inhibitors in non-ischemic muscles. PKG inhibition substantially reduced PT to approximately half. PKC inhibition also slightly blunted PT decrease, while inhibition of PKA had no effect (Figure 2A).

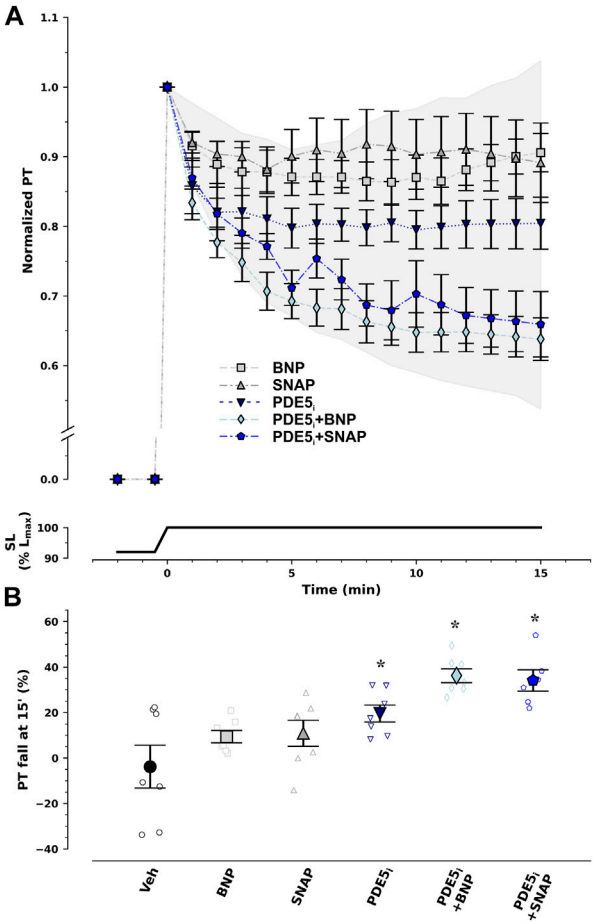

FIGURE 3
Recovery of response to stretch ex vivo under ischemic conditions by pharmacological modulation of the protein kinase G/cyclic guanosine monophosphate pathway. Normalized passive tension (PT) decay after stretch from 92% to 100% of optimal maximum muscle and sarcomere length (SL, L_{max}) is presented in **(A)**, while final percentage of PT decrease at 15 min is summarized in **(B)**. Type-B natriuretic peptide (BNP) and nitric oxide (NO) donor S-nitroso-N-acetylpenicillamine (SNAP) had no effect. On the other hand, type 5 phosphodiesterase inhibitor ($PDE5_i$) sildenafil restored PT decay by 50% and combination therapy with $PDE5_i$ + BNP or $PDE5_i$ + SNAP almost completely reestablished PT decay with stretch. The extent of the effect can be appraised from the shaded area which represents the difference in response between ischemic and non-ischemic myocardium. *$p < 0.05$ *vs* Veh by one-way analysis of variance; $n = 7$ in each group, except for $PDE5_i$ + SNAP ($n = 6$).

3.2 Restoring stretch-induced compliance in ischemic myocardium *ex vivo*

PKC activation had no effect on PT decay after stretching under ischemic conditions, whereas PKG inhibition partly restored the response (Figure 2B). Noticeably, inhibition and stimulation of PKG in non-ischemia and ischemia, respectively, had symmetric effects, implying not only PKG pathway involvement in SIC but also the potential to restore the healthy response in ischemia. Of note, given the previous results, stimulation of PKA in ischemia was not further pursued.

To further exploit the PKG pathway, we undertook incubation with several modulators of this pathway, namely, natriuretic peptides, NO donors, and the $PDE5_i$ sildenafil (Figure 3). In isolation, neither BNP nor SNAP restored response to stretch under ischemic conditions. Contrastingly, $PDE5_i$ recovered it by nearly half. Nevertheless, only the combination of $PDE5_i$ with either natriuretic peptide or an NO donor enabled almost full restitution of the effect.

3.3 Translation to *in vivo*: restoring stretch-induced compliance with PDE5i in acute myocardial infarction

The summary of hemodynamic data is presented in Table 1. Despite randomization, rats that underwent sildenafil infusion showed a trend toward higher heart rates and faster relaxation, as appraised by the time-constant of isovolumetric relaxation, τ, and higher peak pressure derivative values at baseline. Nevertheless, there were no differences between groups regarding cardiac output, end-diastolic volume, and load-independent indexes of left ventricular contractility or compliance.

Upon MI, both Veh and Sil showed decreased left ventricular maximum pressure (P_{max}) and elevated end-diastolic volumes and pressures, as well as a drop in ejection fraction and preload recruitable stroke work (PRSW). No remarkable changes in hemodynamics were observed after vehicle or sildenafil infusion, at least for the duration of the stabilization period. After myocardial stretch by volume loading, as expected, both Veh and Sil exhibited increased end-diastolic volumes. There were remarkable differences between groups, however, in terms of left ventricular function. Compared with Veh, Sil showed not only increased cardiac output and improved systolic function, as appraised by both ejection fraction and load-independent PRSW, but also enhanced myocardial compliance, denoted by a minor increase in end-diastolic pressures and by a decrease in chamber stiffness constant, β. For simplicity, representative pressure–volume loops and end-systolic and end-diastolic regressions before and after volume loading are shown in Figure 4A. In Figure 4B, we depict predicted end-diastolic pressures derived according to the fitting parameters per animal and timepoint for a common volume of 350 μL at all timepoints (Panel B). Higher compliance after volume loading in Sil is clearly visualized both by the gentler slope of the end-diastolic pressure–volume relationships (panel A) and by the consistent decrease in predicted end-diastolic pressures (panel B).

4 Discussion

In this study, we demonstrate that SIC, the increase in myocardial compliance upon stretching, is abrogated under ischemic conditions. PKG-related pathways not only contribute to this adaptive response in the non-ischemic myocardium but are also able to partly restore it in ischemia *ex vivo*. These findings were translated to *in vivo* experimental MI. Type 5 phosphodiesterase (PDE5) inhibition with sildenafil after MI enhanced myocardial performance, enabling lower filling pressures during volume loading.

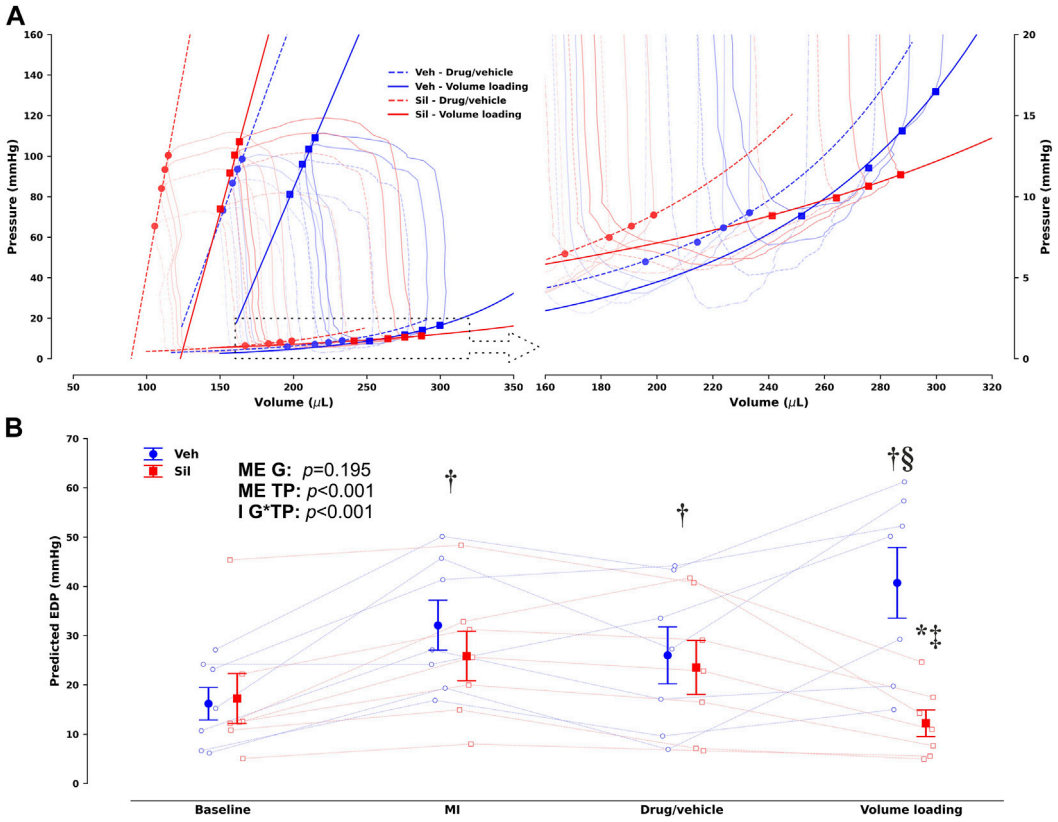

FIGURE 4
Group- and timepoint-averaged pressure–volume (PV) loops and corresponding end-systolic and end-diastolic PV relationships (EDPVR) before and after volume loading in vehicle-treated (Veh) and sildenafil-treated (Sil) rats upon myocardial infarction induction [**(A)**, with the EDPVR highlighted on the right] and corresponding predicted end-diastolic pressures for a common volume of 350 μL based on the EDPVR fits **(B)**. Unlike **(B),** not all timepoints are presented in **(A)** to avoid image clutter; the timepoint before volume loading is marked by circles and dashed lines, whereas squares and solid lines mark the timepoint after volume loading (drug/vehicle and volume loading, respectively, to retain compatibility with Table 1). A clearly different response to volume loading is evident in Sil, which increases compliance. This difference is easily appraised and quantified in **(B)**, where the main effects (ME) of the group (G) and timepoint (TP) are presented along with the interaction effect (I). *$p < 0.05$ *vs* other group at the same timepoint, †$p < 0.05$ *vs* baseline, ‡$p < 0.05$ *vs* MI, §$p < 0.05$ *vs* drug/vehicle by two-way repeated-measures analysis of variance; $n = 7$ for each group.

4.1 The diastolic response to stretching is impaired by myocardial ischemia

Systolic function is enhanced by myocardial stretch through intricate mechanisms that have been extensively investigated in physiology, from the Frank–Starling mechanism to slow-force response (Neves et al., 2016). Given the strong interlinks between systolic and diastolic physiology, it comes as no surprise that diastolic adaptations are also at play. Indeed, we have described SIC (Leite-Moreira et al., 2018), a physiological mechanism that enables the heart to cope with overload by increasing compliance in several experimental preparations, as well as in human volunteers. Like any other physiological response, disturbances are expected in disease conditions. In fact, our preliminary reports suggested impaired SIC in the hypertrophic heart of rats with transverse aortic constriction.

Myocardial ischemia has a strong effect on both systolic and diastolic function. Deprivation of energy stores will not only lead to disturbances in calcium handling and impaired crossbridge cycles but also to abnormal cell-signaling mechanisms (Zhang et al., 2022). Furthermore, an increased ADP/ATP ratio can independently increase myocardial stiffness by increasing the proportion of crossbridges in the bound state (Sequeira et al., 2015). Classic experiments showed increased left ventricular end-diastolic pressure after MI in animals and humans (Hood et al., 1970; Ratshin et al., 1972).

This suggests that the physiological response to loading will most likely be compromised as well. Indeed, early clinical experiments with MI patients in cardiogenic shock revealed that the capacity to respond favorably to fluid challenges strongly predicts better prognosis (Russell et al., 1970; Loeb et al., 1973) while, more recently, abnormal exercise tolerance shortly after acute MI has also been associated with poorer outcomes (Andersen et al., 2012). Our results in *ex vivo* simulated hypoxic conditions clearly demonstrate that SIC is blunted in ischemia.

4.2 Stimulation of cGMP/PKG activity restores stretch-induced compliance under ischemic conditions

In our past mechanistic studies of SIC, we have partly ascribed the effects on compliance to titin phosphorylation mediated by upstream cell-signaling pathways, pinpointing PKG-related pathways as the most

TABLE 1 Summary of pressure–volume data.

	Baseline		MI		Drug/vehicle		Volume loading		ME	ME	Interaction
	Veh	Sil	Veh	Sil	Veh	Sil	Veh	Sil	G	TP	G * TP
HR, bpm	349 ± 12	376 ± 14	354 ± 14	383 ± 16	348 ± 12	408 ± 12*†‡	325 ± 10‡	381 ± 9$^{*\$}$	0.025	0.011	0.040
CO, mL/min	39 ± 1	42 ± 2	39 ± 2	41 ± 2	41 ± 3	42 ± 1	44 ± 4	57 ± 2$^{*\dagger\ddagger\$}$	0.200	<0.001	0.004
mPAP, mmHg	15 ± 1	14 ± 2	14 ± 1	13 ± 1	15 ± 1	15 ± 1	17 ± 2†‡	14 ± 2*	0.564	0.045	0.269
EF, %	66 ± 3	58 ± 1	56 ± 2	47 ± 2*†	49 ± 1	54 ± 3	45 ± 3†	55 ± 2*	0.817	<0.001	0.003
P_{max}, mmHg	115 ± 2	124 ± 3	104 ± 2†	117 ± 4†	101 ± 1†	109 ± 3†	112 ± 6	114 ± 3	0.058	0.002	0.291
EDP, mmHg	6 ± 1	5 ± 0	10 ± 1†	10 ± 1†	9 ± 1	8 ± 1†‡	16 ± 2$^{\dagger\ddagger\$}$	11 ± 1†	0.437	<0.001	0.021
EDV, μL	174 ± 13	190 ± 7	201 ± 13†	209 ± 5†	232 ± 16†	200 ± 12	300 ± 22$^{\dagger\ddagger\$}$	288 ± 17$^{\dagger\ddagger\$}$	0.758	<0.001	0.103
dP/dt_{max}, mmHg/s	6,470 ± 183	7,380 ± 191*	5,950 ± 220†	6,910 ± 221*†	5,800 ± 156†	6,940 ± 176*†	6,270 ± 304	7,380 ± 179*	<0.001	0.004	0.842
$\tau_{logistic}$, ms	7.2 ± 0.5	6.0 ± 0.2	8.0 ± 0.6	6.2 ± 0.3*	7.8 ± 0.6	5.3 ± 0.3*	8.0 ± 0.7	5.5 ± 0.2*	0.004	0.275	0.161
β,/mL	10.3 ± 2.91	12.6 ± 0.77	11.7 ± 2.68	10.7 ± 1.89	13.1 ± 3.34	10.7 ± 1.52	13.9 ± 2.19	5.65 ± 1.31*	0.001	0.192	0.77
e_{es}, mmHg/μL	3.1 ± 0.6	4.6 ± 0.7	2.9 ± 0.7	4.3 ± 0.5	2.0 ± 0.3	4.4 ± 0.6*	1.8 ± 0.3	2.8 ± 0.4	<0.001	0.030	0.729
PRSW, mmHg	105 ± 9	95 ± 7	48 ± 3†	58 ± 6†	57 ± 4†	61 ± 4†	50 ± 4†	64 ± 4*†	0.376	<0.001	0.127

Summary of *in vivo* hemodynamic pressure–volume data recorded sequentially at baseline, after myocardial infarction (MI) induction, after vehicle (Veh) or drug (sildenafil) administration (Sil), and, finally, after subsequent volume loading. HR, heart rate; CO, cardiac output; mPAP, mean pulmonary artery pressure; EF, ejection fraction; P_{max}, maximum pressure; EDP, end-diastolic pressure; EDV, end-diastolic volume; dP/dt_{max}, peak (maximum) pressure derivative; $\tau_{logistic}$, time constant of isovolumetric relaxation by the logistic method; β, chamber stiffness constant derived from the end-diastolic pressure–volume relationship; e_{es}, end-systolic elastance; PRSW, preload recruitable stroke work; $^{*}p < 0.05$ *vs* other group at the same timepoint, $^{\dagger}p < 0.05$ *vs* baseline, $^{\ddagger}p < 0.05$ *vs* MI, $^{\$}p < 0.05$ *vs* drug/vehicle with two-way repeated-measures analysis of variance; $n = 7$ for each group. For β and e_{es} analysis, we included α and v0 as covariates, respectively (analysis of covariance). The main effect (ME) for group (G), timepoint (TP), and their interaction are presented in the three rightmost columns.

likely responsible (Leite-Moreira et al., 2018). However, other stretch-activated protein kinases such as PKA and PKC can also target titin in domains that influence its elastic properties, including PKA and PKC (Linke and Hamdani, 2014). By direct pharmacological inhibition, a potential role for PKC, but not PKA, was also unveiled. Still, the most relevant effect could be attributed to PKG. Indeed, in contrast to PKG activation, pharmacological activation of PKC under ischemic conditions had no appreciable effect on myocardial compliance after stretch, something that we had also reported for the slow-force response (Neves et al., 2013). Given the effects of PKG agonism on stretch response in ischemia, we pursued further elucidation of the ability of its upstream activators BNP and NO (as direct stimulators of particulate and soluble guanylyl cyclase, respectively) as well as of $PDE5_i$ that prevent degradation of cGMP. Only $PDE5_i$ was able to recover SIC, suggesting that preventing degradation of cGMP is a key step to restore PKG activation under ischemic conditions. Moreover, despite the differential subcellular localization of nitric oxide and natriuretic soluble peptide and particulate guanylyl cyclase receptors, along with their pathways being modulated by diversely localized phosphodiesterases (Fischmeister et al., 2006), the addition of BNP or NO donors to $PDE5_i$ enhanced the response to the point of near restoration of SIC by the synergistic effect.

4.3 Phosphodiesterase-5 inhibition improves load tolerance during acute myocardial infarction

As a final step, we attempted to translate our findings *ex vivo* to the *in vivo* scenario. This translation is of course fraught with many limitations. Although we employed a reproducible model of MI (Hou et al., 2011), we acknowledge that there might have been some heterogeneity in the extent of ischemic areas between groups and that non-uniformity and systemic and neurohumoral responses to MI and sildenafil add another layer of complexity to the issue. Moreover, although restoration of SIC in ischemia was optimal under combination therapy *ex vivo*, for practical purposes and to avoid a marked decrease in systemic vascular resistance, only $PDE5_i$ was administered *in vivo*.

$PDE5_i$ has well-recognized beneficial effects in MI, namely, a reduction in infarct size (Reffelmann and Kloner, 2003), mitigation of reperfusion injury (Ebner et al., 2013; Andersen et al., 2016), and overall cardioprotection (Botha et al., 2010). Indeed, $PDE5_i$'s cardioprotective effects include inhibition of Na^+/H^+ exchanger-1, modulation of Ca^{2+} handling, and mitochondrial permeability transition, and many of these may even be independent of PKG (Elrod et al., 2007; Perez et al., 2007; Das et al., , 2008; Inserte and Garcia-Dorado, 2015) or related to cGMP signaling in distinct subcellular compartments of non-cardiomyocytes (Cuello and Nikolaev, 2020). On clinical grounds, in the SIDAM trial (Andersen et al., 2013), sildenafil therapy for 9 weeks increased LV end-diastolic volume and cardiac index after MI, with further enhancement during exercise, and despite the negative results in the primary outcome measure, a drop in pulmonary capillary wedge pressure was shown. Many of these multifarious actions of $PDE5_i$ might be at play and partly explain our results.

Nevertheless, we did observe a sharp increase in myocardial compliance after volume loading in MI rats upon sildenafil infusion. This response was clearly different from that of the vehicle group. Together with our *ex vivo* findings, this strongly suggests that $PDE5_i$ enhances myocardial compliance in ischemia and thus might

broaden the therapeutic margin for volume loading in acute MI. By restoring SIC, $PDE5_i$ might enable a more favorable hemodynamic response to volume loading in acute MI, while reducing the risk of lung congestion.

4.4 Study limitations

Our results are preclinical and purely experimental. The MI model did not entail cardiogenic shock, and there was no need for inotropic or vasopressor support. There was also no reperfusion, and therefore ischemia–reperfusion injury was not studied. The effects of sildenafil in cardiogenic shock and ischemia–reperfusion injury may be substantially different. Infarct size was also not formally measured. The *ex vivo* experimental protocol emulated ischemia by glucose and O_2 deprivation, which is a poor substitute for MI. Though invaluable for pharmacological studies at the cellular and tissue level, these preparations significantly deviate from physiology, due to the absence of blood perfusion. Interrupting the O_2/CO_2 supply entails not only anaerobic metabolism and acidosis due to hypoxia but also opposite changes in acid–base balance due to the lack of CO_2 supply. Experiments were carried out in right, and not in the bulkier left, ventricular papillary muscles to avoid core hypoxia. Sympathetic denervation intrinsic to the *ex vivo* setup limits upstream activation of signaling pathways that enhance PKA activity and therefore may influence the apparent absence of the effect of inhibiting this protein kinase on SIC.

5 Conclusion

We were able to demonstrate that ischemia impairs the adaptive myocardial response to stretching or volume loading and that this may be partly prevented by pharmacological manipulation of the PKG pathway, namely, with $PDE5_i$. Translation to the clinical scenario will require well-designed randomized trials where cautious use of $PDE5_i$ and volume loading should be tested in terms of outcomes in acute MI.

Data availability statement

The raw data supporting the conclusion of this article will be made available by the authors, without undue reservation.

Ethics statement

The animal study was approved by the Direção Geral de Animais e Veterinária—Órgãos Responsáveis pelo Bem Estar Animal. The study was conducted in accordance with the local legislation and institutional requirements.

Author contributions

AL-M: conceptualization, data curation, formal analysis, investigation, methodology, project administration, software, validation, writing–original draft, and writing–review and editing. JA-C: conceptualization, formal analysis, investigation, methodology, project administration, validation, writing–original draft, and writing–review and editing. JN: conceptualization, data curation, formal analysis, investigation, methodology, project administration, supervision, validation, and writing–review and editing. RC-F: conceptualization, formal analysis, investigation, methodology, project administration, supervision, validation, and writing–review and editing. RL-L: conceptualization, data curation, formal analysis, investigation, methodology, project administration, validation, and writing–review and editing. AL-M: conceptualization, funding acquisition, methodology, project administration, resources, supervision, validation, and writing–review and editing. AL: conceptualization, data curation, formal analysis, funding acquisition, investigation, methodology, project administration, resources, software, supervision, validation, writing–original draft, and writing–review and editing.

Funding

The author(s) declare financial support was received for the research, authorship, and/or publication of this article. This work was supported by grants from the Portuguese Foundation for Science and Technology to the Cardiovascular Research Center of the Faculty of Medicine of Porto (PTDC/DTP-PIC/4104/2014); partially supported by Fundo Europeu de Desenvolvimento Regional (FEDER) through COMPETE 2020—Programa Operacional Competitividade e Internacionalização (POCI); the project DOCnet (NORTE-01-0145-FEDER-000003), supported by Norte Portugal Regional Operational Programme (NORTE 2020), under the PORTUGAL 2020 Partnership Agreement, through the European Regional Development Fund (ERDF); the project NETDIAMOND (POCI-01-0145-FEDER-016385), supported by European Structural and Investment Funds, Lisbon's Regional Operational Programme 2020 and national funds from the Portuguese Foundation for Science and Technology, and the European Commission (FP7-Health-2010; MEDIA-261409).

Conflict of interest

The authors declare that the research was conducted in the absence of any commercial or financial relationships that could be construed as a potential conflict of interest.

Publisher's note

Supplementary material

The Supplementary Material for this article can be found online at: https://www.frontiersin.org/articles/10.3389/fphys.2023.1271698/full#supplementary-material

References

Andersen, A., Povlsen, J. A., Johnsen, J., Jespersen, N. R., Botker, H. E., and Nielsen-Kudsk, J. E. (2016). sGC-cGMP-PKG pathway stimulation protects the healthy but not the failing right ventricle of rats against ischemia and reperfusion injury. *Int. J. Cardiol.* 223, 674–680. doi:10.1016/j.ijcard.2016.08.264

Andersen, M. J., Ersboll, M., Axelsson, A., Gustafsson, F., Hassager, C., Kober, L., et al. (2013). Sildenafil and diastolic dysfunction after acute myocardial infarction in patients with preserved ejection fraction: the sildenafil and diastolic dysfunction after acute myocardial infarction (SIDAMI) trial. *Circulation* 127 (11), 1200–1208. doi:10.1161/CIRCULATIONAHA.112.000056

Andersen, M. J., Ersboll, M., Bro-Jeppesen, J., Gustafsson, F., Hassager, C., Kober, L., et al. (2012). Exercise hemodynamics in patients with and without diastolic dysfunction and preserved ejection fraction after myocardial infarction. *Circ. Heart Fail* 5 (4), 444–451. doi:10.1161/CIRCHEARTFAILURE.112.967919

Botha, P., MacGowan, G. A., and Dark, J. H. (2010). Sildenafil citrate augments myocardial protection in heart transplantation. *Transplantation* 89 (2), 169–177. doi:10.1097/TP.0b013e3181c42b22

Castro-Ferreira, R., Neves, J. S., Ladeiras-Lopes, R., Leite-Moreira, A. M., Neiva-Sousa, M., Almeida-Coelho, J., et al. (2014). Revisiting the slow force response: the role of the PKG signaling pathway in the normal and the ischemic heart. *Rev. Port. De. Cardiol.* 33 (9), 493–499. doi:10.1016/j.repc.2014.03.006

Cornish, B. H., Ward, L. C., and Thomas, B. J. (1992). Measurement of extracellular and total body water of rats using multiple frequency bioelectrical impedance analysis. *Nutr. Res.* 12 (4), 657–666. doi:10.1016/S0271-5317(05)80035-1

Cuello, F., and Nikolaev, V. O. (2020). Cardiac cGMP signaling in health and disease: location, location, location. *J. Cardiovasc Pharmacol.* 75 (5), 399–409. doi:10.1097/FJC.0000000000000802

Das, A., Xi, L., and Kukreja, R. C. (2008). Protein kinase G-dependent cardioprotective mechanism of phosphodiesterase-5 inhibition involves phosphorylation of ERK and GSK3beta. *J. Biol. Chem.* 283 (43), 29572–29585. doi:10.1074/jbc.M801547200

Ebner, B., Ebner, A., Reetz, A., Bohme, S., Schauer, A., Strasser, R. H., et al. (2013). Pharmacological postconditioning by bolus injection of phosphodiesterase-5 inhibitors vardenafil and sildenafil. *Mol. Cell Biochem.* 379 (1-2), 43–49. doi:10.1007/s11010-013-1625-7

Elrod, J. W., Greer, J. J., and Lefer, D. J. (2007). Sildenafil-mediated acute cardioprotection is independent of the NO/cGMP pathway. *Am. J. Physiol. Heart Circ. Physiol.* 292 (1), H342–H347. doi:10.1152/ajpheart.00306.2006

Fischmeister, R., Castro, L. R., Abi-Gerges, A., Rochais, F., Jurevicius, J., Leroy, J., et al. (2006). Compartmentation of cyclic nucleotide signaling in the heart: the role of cyclic nucleotide phosphodiesterases. *Circ. Res.* 99 (8), 816–828. doi:10.1161/01.RES.0000246118.98832.04

Gowda, R. M., Fox, J. T., and Khan, I. A. (2008). Cardiogenic shock: basics and clinical considerations. *Int. J. Cardiol.* 123 (3), 221–228. doi:10.1016/j.ijcard.2006.03.099

Hood, W. B., Jr., Bianco, J. A., Kumar, R., and Whiting, R. B. (1970). Experimental myocardial infarction. IV. Reduction of left ventricular compliance in the healing phase. *J. Clin. Invest.* 49 (7), 1316–1323. doi:10.1172/JCI106347

Hou, Y., Huang, C., Cai, X., Zhao, J., and Guo, W. (2011). Improvements in the establishment of a rat myocardial infarction model. *J. Int. Med. Res.* 39 (4), 1284–1292. doi:10.1177/147323001103900416

Inserte, J., and Garcia-Dorado, D. (2015). The cGMP/PKG pathway as a common mediator of cardioprotection: translatability and mechanism. *Br. J. Pharmacol.* 172 (8), 1996–2009. doi:10.1111/bph.12959

Kirigaya, J., Iwahashi, N., Terasaka, K., and Takeuchi, I. (2023). Prevention and management of critical care complications in cardiogenic shock: A narrative review. *J. Intensive Care* 11 (1), 31. doi:10.1186/s40560-023-00675-2

Leite-Moreira, A. M., Almeida-Coelho, J., Neves, J. S., Pires, A. L., Ferreira-Martins, J., Castro-Ferreira, R., et al. (2018). Stretch-induced compliance: A novel adaptive biological mechanism following acute cardiac load. *Cardiovasc Res.* 114 (5), 656–667. doi:10.1093/cvr/cvy026

Linke, W. A., and Hamdani, N. (2014). Gigantic business: titin properties and function through thick and thin. *Circ. Res.* 114 (6), 1052–1068. doi:10.1161/CIRCRESAHA.114.301286

Loeb, H. S., Rahimtoola, S. H., Rosen, K. M., Sinno, M. Z., Chuquimia, R., and Gunnar, R. M. (1973). Assessment of ventricular function after acute myocardial infarction by plasma volume expansion. *Circulation* 47 (4), 720–728. doi:10.1161/01.cir.47.4.720

Neves, J. S., Castro-Ferreira, R., Ladeiras-Lopes, R., Neiva-Sousa, M., Leite-Moreira, A. M., Almeida-Coelho, J., et al. (2013). The effects of angiotensin II signaling pathway in the systolic response to acute stretch in the normal and ischemic myocardium. *Peptides* 47, 77–84. doi:10.1016/j.peptides.2013.07.004

Neves, J. S., Leite-Moreira, A. M., Neiva-Sousa, M., Almeida-Coelho, J., Castro-Ferreira, R., and Leite-Moreira, A. F. (2016). Acute myocardial response to stretch: what we (don't) know. *Front. Physiology* 6, 408. doi:10.3389/fphys.2015.00408

Perez, N. G., Piaggio, M. R., Ennis, I. L., Garciarena, C. D., Morales, C., Escudero, E. M., et al. (2007). Phosphodiesterase 5A inhibition induces Na+/H+ exchanger blockade and protection against myocardial infarction. *Hypertension* 49 (5), 1095–1103. doi:10.1161/HYPERTENSIONAHA.107.087759

Ratshin, R. A., Rackley, C. E., and Russell, R. O., Jr. (1972). Hemodynamic evaluation of left ventricular function in shock complicating myocardial infarction. *Circulation* 45 (1), 127–139. doi:10.1161/01.cir.45.1.127

Reffelmann, T., and Kloner, R. A. (2003). Effects of sildenafil on myocardial infarct size, microvascular function, and acute ischemic left ventricular dilation. *Cardiovasc Res.* 59 (2), 441–449. doi:10.1016/s0008-6363(03)00435-8

Russell, R. O., Jr., Rackley, C. E., Pombo, J., Hunt, D., Potanin, C., and Dodge, H. T. (1970). Effects of increasing left ventricular filling. Pressure in patients with acute myocardial infarction. *J. Clin. Invest.* 49 (8), 1539–1550. doi:10.1172/JCI106371

Sequeira, V., Najafi, A., McConnell, M., Fowler, E. D., Bollen, I. A., Wust, R. C., et al. (2015). Synergistic role of ADP and Ca(2+) in diastolic myocardial stiffness. *J. Physiol.* 593, 3899–3916. doi:10.1113/JP270354

Zhang, Q., Wang, L., Wang, S., Cheng, H., Xu, L., Pei, G., et al. (2022). Signaling pathways and targeted therapy for myocardial infarction. *Signal Transduct. Target Ther.* 7 (1), 78. doi:10.1038/s41392-022-00925-z

frontiers | Frontiers in Physiology

TYPE Original Research
PUBLISHED 10 October 2023
DOI 10.3389/fphys.2023.1248899

OPEN ACCESS

EDITED BY
Ginés Viscor,
University of Barcelona, Spain

REVIEWED BY
Petroula Laiou,
King's College London, United Kingdom
Cesar Alexandre Teixeira,
University of Coimbra, Portugal

*CORRESPONDENCE
Mariana Abreu,
mariana.abreu@tecnico.ulisboa.pt

RECEIVED 27 June 2023
ACCEPTED 04 September 2023
PUBLISHED 10 October 2023

CITATION
Abreu M, Carmo AS, Peralta AR, Sá F, Plácido da Silva H, Bentes C and Fred AL (2023), PreEpiSeizures: description and outcomes of physiological data acquisition using wearable devices during video-EEG monitoring in people with epilepsy.
Front. Physiol. 14:1248899.
doi: 10.3389/fphys.2023.1248899

PreEpiSeizures: description and outcomes of physiological data acquisition using wearable devices during video-EEG monitoring in people with epilepsy

Mariana Abreu[1,2]*, Ana Sofia Carmo[1,2], Ana Rita Peralta[3], Francisca Sá[4], Hugo Plácido da Silva[1,2,5], Carla Bentes[3] and Ana Luísa Fred[1,2]

[1]Instituto de Telecomunicações, Lisboa, Portugal, [2]Departamento de Bioengenharia, Instituto Superior Técnico, Universidade de Lisboa, Lisboa, Portugal, [3]Lab EEG-Sono, Centro Hospitalar Universitário Lisboa Norte, Hospital de Santa Maria, Lisboa, Portugal, [4]Departamento Neurologia, Centro Hospitalar Lisboa Ocidental, Hospital Egas Moniz, Lisboa, Portugal, [5]Lisbon Unit for Learning and Intelligent Systems (LUMLIS), A Unit of the European Laboratory for Learning and Intelligent Systems (ELLIS), Lisboa, Portugal

The PreEpiSeizures project was created to better understand epilepsy and seizures through wearable technologies. The motivation was to capture physiological information related to epileptic seizures, besides Electroencephalography (EEG) during video-EEG monitorings. If other physiological signals have reliable information of epileptic seizures, unobtrusive wearable technology could be used to monitor epilepsy in daily life. The development of wearable solutions for epilepsy is limited by the nonexistence of datasets which could validate these solutions. Three different form factors were developed and deployed, and the signal quality was assessed for all acquired biosignals. The wearable data acquisition was performed during the video-EEG of patients with epilepsy. The results achieved so far include 59 patients from 2 hospitals totaling 2,721 h of wearable data and 348 seizures. Besides the wearable data, the Electrocardiogram of the hospital is also useable, totalling 5,838 h of hospital data. The quality ECG signals collected with the proposed wearable is equated with the hospital system, and all other biosignals also achieved state-of-the-art quality. During the data acquisition, 18 challenges were identified, and are presented alongside their possible solutions. Though this is an ongoing work, there were many lessons learned which could help to predict possible problems in wearable data collections and also contribute to the epilepsy community with new physiological information. This work contributes with original wearable data and results relevant to epilepsy research, and discusses relevant challenges that impact wearable health monitoring.

KEYWORDS

wearable devices, physiological signals, protocol design, epilepsy dataset, epilepsy monitoring, cardiorespiratory function, physiological data acquisition

1 Introduction

Over the past years, research in epilepsy has been integrating more physiological information (i.e. biosignals) besides the electrical brain activity, captured by the Electroencephalography (EEG) (Ranjan et al., 2019). In fact, some devices with non-EEG biosignals have already been approved as medical devices by the Federal Drugs Administration (FDA), for their ability to detect of Generalised Tonic-clonic Seizures (GTCS) (Bruno et al., 2020). Examples include the Embrace Smartwatch by Empatica (McCarthy et al., 2016; Regalia et al., 2019), or the SPEAC device by Brain Sentinel (Whitmire et al., 2019). Additionally, non-EEG biosignals are also being used in epilepsy research for ambulatory daily monitoring of people with epilepsy (PWE), and for the development of seizure forecast and prediction models, where the most frequently mentioned device is the smartwatch E4 by Empatica (Meisel et al., 2020; Brinkmann et al., 2021; Vieluf et al., 2022). One essential aspect for the development of end-user solutions is the access to large datasets of multimodal quality data. This has been the focus of multiple international initiatives, such as the Remote Assessment of Disease and Relapse-Central Nervous System (RADAR-CNS), an initiative focused on ambulatory data collection is based on an open-source platform (RADAR-Base) to integrate data from different sources including smartphone and wearables (Ranjan et al., 2019).

The use of biosignals in epilepsy is especially relevant for the prevention of Sudden Unexpected Death in Epilepsy (SUDEP) (Van de Vel et al., 2013), which is thought to be a consequence of severe cardio-respiratory dysfunctions (Sivathamboo et al., 2020; 2021). With this in mind, our research group has given special focus to peripheral physiological signals which have shown to be of interest for these pathological changes, such as Electrocardiography (ECG), Respiration (RESP) and Chest Motion.

The PreEpiSeizures project was motivated by the collection of multimodal non-EEG data from PWE through wearables, in order to be leveraged towards the development of methods for early seizure detection, as well as expanding the understanding of epilepsy in different lenses. Although the use of biosignals in epilepsy is common, their contribution to different epilepsy types is still yet to prove, thus motivating the collection of comprehensive data to sustain and improve non-EEG based solutions. The rest of this document is structured as follows: Section 2 provides the current landscape of epilepsy-related data collection as well as commercial wearables which serve that purpose; Section 3 describes the experimental protocol employed in this project, along with the characteristics of the wearable devices used, together with the data quality assessment metrics; Section 4 details the main findings extracted from the data collected so far, including the analysis of the signal quality and patients' metadata; Section 5 overviews several challenges faced in the context of wearable data collection, possible solutions, and presents a discussion of the results achieved. Lastly, Section 6 summarises the main outcomes and conclusions, followed by some future work directions for the PreEpiSeizures project.

2 Background

2.1 Datasets in epilepsy

Throughout the years, the epilepsy research community has been working in multi-centre collaborations. The joint efforts of stakeholders from different backgrounds, such as industry, healthcare and academia, as well as different countries, is essential to provide better and faster solutions to epilepsy. Some of the collaborations found were iEEG.org, SeizeIT, Epilepsy Ecosystem and EPILEPSIAE. Additionally, other publicly available datasets were found in the literature, which also comprise data from epileptic patients. The description of these datasets is summarised in Table 1 alongside the one proposed in this project. This includes the number of patients, their age, the modalities acquired, the number of seizures, the seizure types, the total duration and the setting.

The *iEEG.org* online platform[1], supported by the National Institutes of Neurological Disorders and Stroke, provides access to over 900 datasets on human and animal epilepsy, as well as analytic and visualisation tools to aid data exploration. By inserting the corresponding keywords, the datasets are filtered to a desired EEG montage, population and seizure types, just to name a few. Nonetheless, the source of the signal is always assumed to be EEG and other physiological signals are not an option when filtering.

SeizeIT[2] is another collaborative project within epilepsy, which is supported by the European Institute of Innovation and Technology (EIT Health). This consortium aims to tackle the continuous ambulatory monitoring of epilepsy, in order to accurately register seizures, thereby enabling the optimisation of treatment plans.

The Epilepsy Ecosystem[3] (Kuhlmann et al., 2018) is a crowd-sourcing environment supported through the My Seizure Gauge project, supported by the Epilepsy Foundation of America, the Aikenhead Centre for Medical Discovery at St. Vincent's Hospital Melbourne, the University of Melbourne, Monash University and Seer Medical. Its goal is to improve the performance of seizure prediction algorithms with the purpose of making them a viable option for PWE. They are responsible for gathering and maintaining two public datasets: NeuroVista Trial (Cook et al., 2013) and My Seizure Gauge Wearable[4]. Both datasets are available in the Seer platform requiring only a login setup. The NeuroVista trial (Cook et al., 2013) contains 15 patients that were submitted to an ambulatory intracranial EEG (iEEG) monitoring for more than 80 days. This dataset consists of a set of carefully selected patients whom experienced 2 to 12 monthly seizures, while still having a level of independence compatible with using the device for daily management. Another dataset made available in the Seer platform is the My Seizure Gauge Wearable, which is a collection of wearable data using 3 wearable

1 https://www.ieeg.org/

2 https://eithealth.eu/spotlight-story/seizeit/

3 https://www.epilepsyecosystem.org/

4 https://www.epilepsyecosystem.org/my-seizure-gauge-1

TABLE 1 Comparison of public datasets with PreEpiSeizures, regarding number of patients, age, signal modalities, number of seizures, seizure types and total number of recording hours, and monitoring settings. If the number of seizures also includes subclinical, the number of subclinical seizures is specified in brackets. The numbers in brackets in the patients and total hours for the PreEpiSeizures are related to the wearable data, where the leftside numbers correspond to the hospital data. (* The 8 seizure types in the TUH EEG Corpus are: focal non specific seizure, generalised non-specific seizure, FAS, FIAS, absence, myoclonic, tonic and tonic-clonic seizures.)

Dataset name	# Patients	Age	Modalities	# Seizures	Seizure types	Total hours	Setting
PreEpiSeizures	59 (37)	[16,60]	ECG, Resp, ACC, EDA, PPG, EMG	348 (89)	FAS, FIAS, FUAS, FBTCS, E	5,838 (2,721)	Video-EEG
My Seizure Gauge Wearable (footnote 4)	27	-	EDA, PPG, ACC, EMG, GYR, EEG	226 (85)	GTCS, FIAS, FUAS, FAS, E	2640	Unclear
Siena Scalp EEG Detti (2020)	14	44 ± 14	EEG, ECG	47	FAS, FIAS and FBTCS	128	Hospital long-term
EPILEPSIAE Klatt et al. (2012)	30	41 ± 14	EEG, ECG	276	-	2881	Hospital long-term
NeuroVista Trial Cook et al. (2013)	15	44 ± 13	iEEG	2–12 monthly	Focal	>1*y*	Ambulatory
Bern-Barcelona Andrzejak et al. (2012)	5	-	EEG and iEEG	-	-	100 × 23.6s	Hospital
Bonn-Barcelona micro-, and macro- EEG database Martínez et al. (2020)	3	[20,39,47]	iEEG	0	-	66	Hospital long-term
TUH EEG Corpus Obeid and Picone (2016)	>10*k*	51 ± 56	EEG	≥3050	8 seizure types*	29.1*y*	Hospital long and short-term
New Delhi EEG Swami et al. (2016)	10	-	EEG	-	-	10 × 50 × 5.12s	Hospital
Epilepsy Seizure Recognition Andrzejak et al. (2001)	500	-	EEG	-	-	500 × 23.6s	Hospital short-term
CHB MIT Shoeb (2009)	23	10 ± 5.6	EEG	198	Not mentioned	969	Hospital long-term

10.3389/fphys.2023.1248899

devices: Empatica E4, Epilog (Frankel et al., 2021) and Byteflies (Swinnen et al., 2021). It comprises 27 patients that were monitored for approximately 4.4 ± 2.4 days. Although this dataset provides unprecedented wearable data in the context of epilepsy, it does not provide any information regarding the positioning of the devices nor some relevant clinical symptoms such as sleep/vigilance state and loss of awareness during the seizure events. Since no information was found regarding the acquisition conditions, we could not assume whether this dataset was acquired during video-EEG or in ambulatory.

The EPILEPSIAE database (Klatt et al., 2012) was created under a joint European project between Epilepsy Center, University Hospital of Freiburg; Center for Informatics and Systems, University of Coimbra; and Epilepsy Unit, CHU Pitie-Salpetriere, Paris. This database contains more than 275 patients that performed Video-EEG monitoring, focusing on the EEG signal. Still, since the ECG is also acquired by the hospital system, it is also present in this database. Several works have used this database both for EEG and ECG analysis (Truong et al., 2019; Gómez et al., 2020; Leal et al., 2021). However, EPILEPSIAE only makes available 30 patients for external researchers, which is always the same subset, without disclosing the type of seizures, or the clinical semiology. Moreover, it does not provide wearable data, only hospital data.

The Siena Scalp EEG Epilepsy Database (Detti et al., 2020) contains the data of 14 patients that performed the video-EEG monitoring in the Unit of Neurology and Neurophysiology of the University of Siena. This dataset is curated to the seizure episodes, hence for some patients, only the peri-ictal period is available to the public. The signal sources present in this database include EEG and ECG, both acquired by the hospital system.

Other epilepsy datasets also available in the literature were included in Table 1 for dimensionality comparison, however, they are out of the scope of this research, since they provide neither non-EEG data or wearable data. For more information in EEG datasets (Wong et al., 2023), provides a comprehensive review.

The majority of available datasets is focused on EEG analysis, and only a few also include the ECG signal acquired by the hospital system. Regarding the acquisition settings, four datasets contain data from long-term or video-EEG monitorings, and four datasets contain short-term EEG acquisitions. The EEG was intracranial in three datasets (indicated with iEEG), and the NeuroVista Trial is the only ambulatory dataset, to the best of our knowledge. The only multimodal wearable dataset found was My Seizure Gauge Wearable data, however it does not provide clear information on seizure types, the acquisition conditions, or the clinical manifestations of seizures. Most events annotated in this dataset have little seizure information, and for some of them it is unclear if they are even seizures or not. Larger datasets are needed to sustain the use of non-EEG data as lens for epileptic activity. Recently, projects such as My Seizure Gauge and Radar-CNS started to create multicenter datasets with hundreds of patients acquired in ambulatory scenarios (Böttcher et al., 2022). However, it was not yet proven the ability of these devices to capture pathophysiological manifestations in non-EEG modalities related to non-convulsive seizures. Hence more evidence based on data collected in a semi-controlled scenario (e.g. as the video-EEG monitoring), is essential towards the use of non-EEG physiological modalities in the prediction and forecast of epileptic seizures, and in the detection of non-convulsive epileptic seizures.

2.2 Peripheral multimodal devices

The ever-decreasing size of devices with built-in sensors, internal battery and powerful processors, allow continuous wearable long-term monitoring of movement patterns and physiological variables. A wearable device similar to a smartwatch can be decomposed in four main layers: top cover, electronics board, lithium battery and bottom cover[5]. The top cover serves as a protective shield for the other components; the electronics board contains sensors, communication antenna (Bluetooth or WiFi), memory, and MCU; the lithium battery provides a power supply; finally the bottom cover often contains the interface with the patient when necessary (e.g., dry electrodes). This example of a wearable device unfolds the physical constraint associated with each layer: on the one hand, multiple embedded sensors lead to more information, and larger battery sizes lead to longer continuous acquisitions; on the other hand, devices should be small and unobtrusive. Thus, there is a trade-off between the device's size and its modus operandi.

The devices that can simultaneously record data from multiple sensors are more interesting for epilepsy monitoring since they can increase the chances of capturing manifestations from different seizure types, thus enhancing the performance of detection or early prediction algorithms (Verdru and Van Paesschen, 2020). Some devices are commercially available for the purpose of physiological signal acquisition, which could be used for research purposes. In Table 2, relevant devices found in the literature are described, which were validated and can record multimodal physiological signals. In this table, the devices are compared based on their target use, validation, modalities available, body location, battery duration, sampling frequency (FS) and data accessibility. For comparison, the bottom part of Table 2, contains the characteristics of the devices used in this project.

Table 2 illustrates the characteristics that prove to be the most relevant in wearable devices applied to epilepsy. However, it also uncovers some limitations of current options: from restrictive form factors, to short battery life, lack of validation, limited storage options, or insufficient physiological information. In fact, this last point accurately illustrates one pressing issue in epilepsy research: the extent of the applicability of seizure detection devices is inherently related to their location/signals they acquire, for example, an ACC- or EMG-based device will not be able to detect non-motor seizures. Even though the research community's intention is in detecting all seizure types, there is an imbalance, in both research and evidence, towards an overrepresentation of convulsive motor seizures (Bruno et al., 2020). Therefore, research efforts should be endorsed for other seizure types. Moreover, additional research is needed towards the applicability of multimodal wearables in epilepsy in ambulatory scenarios, especially combined with seizure risk forecasting.

The benchmark device for epilepsy research is the Empatica E4 smartwatch, since it is discreet, it captures four biosignals and its

5 https://www.empatica.com/en-eu/research/e4/

TABLE 2 Devices with multiple sensors, characterised with respect to their applicability to research, validation status, form factor or body positioning, battery duration, method to access the data, measured signals and sampling frequency.

Product	Research use	Validation	Modalities	Site	Battery	FS(Hz)	Data accessibility
EQ02[9]	Ambulatory Orphanidou and Drobnjak (2017), Athletes Kenny et al. (2017)	With Holter Akintola et al. (2016)	ECG, Resp, Temp, ACC	Vest	48 h	256	BT transmission
E4 footnote 5	Migraines Koskimäki et al. (2017), Stress Ollander et al. (2016)	CE Regalia et al. (2019)	EDA, PPG, Temp, ACC	Bracelet	+32 h	128	BLE to Cloud Storage
VisiMobile[10]	Ambulatory Weenk et al. (2017)	FDA	ECG, Resp, SpO_2, Temp	Wristband	+12 h	-	WiFi transmission
Bioharness3 Johnstone et al. (2012)	Sports	HR validation Nepi et al. (2016)	ECG, Resp, Temp, ACC	Chest Strap	12–24 h	-	BLE transmission
Hexoskin[11]	Remote	With gold-standard Smith et al. (2019)	ECG, Resp, ACC	Smart Shirt	12 h	256	Cloud Storage or BLE
Vivosmart4[12]	Stress	With gold-standard Tedesco et al. (2019)	Optical HRV, SpO_2, Light, ACC	Smartwatch	5 days	-	BLE transmission
Byteflies[13]	Epilepsy	CE	EEG, ACC, Resp, HR	Behind Ear	24 h	250	Cloud Storage
ArmBIT + ForearmBIT			ECG, EDA, EMG, PPG, ACC	Arm + Wrist	12 h	1,000	BT transmission
WristBIT			EDA, PPG, ACC	Wrist	24 h	1,000	BT transmission
ChestBIT			ECG, PZT, ACC	Chest	24 h	1,000	BLE transmission

[9]https://equivital.com/
[10]https://soteradigitalhealth.com/
[11]https://www.hexoskin.com/
[12]https://www.garmin.com/en-US/p/605739
[13]https://byteflies.com/

10.3389/fphys.2023.1248899

battery lasts for 32 h. However, the data management is performed in a cloud-based platform, which compromises our privacy protection clauses. Moreover, (Vandecasteele et al., 2017), have reported the higher reliability of ECG, comparatively to PPG, to obtain the heart rate and heart rate variability, which are considered significant autonomic change predictors. These two factors motivated the development of our own devices, designed to ensure the privacy preservation and the recording of relevant physiological modalities, such as the ECG, PZT, PPG, EDA and ACC (for chest motion).

3 Methodology

Data collection within the PreEpiSeizures project started as a collaboration from Instituto Superior Técnico (IST) with the EEG-Sleep Lab of Hospital de Santa Maria - Centro Hospitalar Universitário Lisboa Norte (CHULN), that is responsible for supervising video-EEG monitorings. This project was approved in 2015 by the ethics committee of CHULN. This collaboration was later extended to Centro de Epilepsia Refratária of Hospital Egas Moniz—Centro Hospitalar Lisboa Ocidental towards continuous monitoring in the scope of the PreEpiSeizures project underwent multiple iterations with the purpose of achieving a friendlier and more autonomous solution for patients. The approach is divided into the development of the wearable device and in the acquisition system for data collection and storage.

3.1 Wearable devices

The devices developed in this scope are based on BITalino (Da Silva et al., 2014), which allowed for the experimentation around form-factors and sensors modalities. The BITalino device consists of a core block with a microprocessor (MCU) and a Bluetooth (BT) module for communication, sensors for each physiological modality, and a lithium-ion polymer (LiPo) battery. BITalino has the ability of recording simultaneously up to 6 analog channels (with a FS up to 1000Hz). When all channels are being acquired, the first four channels also allow for 10-bit resolution, while the last two only record with 6-bit resolution.

The first prototypes developed within the PreEpiSeizures project were ArmBIT and ForearmBIT (shown in Figure 1), both consisting of one BITalino core block (with MCU and BT module), and respective sensors, all enclosed within a 3D printed case with an adjustable strap. The ArmBIT, which is displayed in left side of Figure 1, collected the equivalent of lead I ECG and the triaxial ACC of the upper arm. The ForearmBIT, represented in right side of Figure 1, was design to record the bicep's EMG, EDA on the palm of the hand, fingertip's PPG, and forearm's triaxial ACC. Interface with the patient was performed with the use of pre-gelled Ag/AgCl electrodes. These two devices were used simultaneously and were connected by a cable, to enable synchronisation (not shown in Figure 1). Although this montage is acceptable for short-term data acquisitions, it becomes impractical for longer sessions. This is due to the prolonged use of pre-gelled electrodes and connection cables, which can cause discomfort, associated with the fact that wearables are secured to the arm, inhibiting patients from adopting certain sleeping positions. Since these two devices are both on the arm and physically connected by a cable, the remainder of this work uses ArmBIT to refer to the ensemble with both devices.

Given the higher resolution in the first four channels, these were usually used for the more relevant physiological signals (e.g., ECG, EEG, EMG and PPG). Since the ACC possesses three axis, and the human motion has frequencies lower than 5 Hz (Korohoda et al., 2013), two of its axis were usually acquired in the channels with lower resolution.

The second iteration of the PreEpiSeizures wearable devices, consisted on rejecting gel electrodes and finding other ways to collect the same signals. The ForearmBIT was replaced by a BITalino assembled in a wristband (WristBIT), whereas the ArmBIT was replaced by a BITalino mounted in a chestband (ChestBIT). The WristBIT device (shown in Figure 2), is composed of an elastic wristband with a pocket to enclose the BITalino core block, as well as EDA and ACC sensors. The EDA signal was being recorded on the wrist, using two metallic electrodes encapsulated in the strechable fabric. Additionally, the finger strap enclosing the PPG sensor was connected to the wristband.

The ChestBIT is shown in Figure 3, and it was previously applied in other contexts within the research group (Manso et al., 2018). The chestband used was a Polar chest strap[6], with the ECG sensor connected to the metal buttons of the chest strap. The BITalino MCU was glued to the chest strap, alongside the ACC, the Bluetooth module, and a piezoelectric PZT sensor used to record the RESP signal. The entire electronics was protected with a soft sponge and covered with a synthetic leather textile, to improve endurance. The battery remained outside, in a pocket, and a small opening allowed the battery connector to reach the BITalino power module; this enabled easier natter charging and replacement to ensure near-continuous operation. The on/off button was accessible through the side, since the left side of the textile was not fully closed.

To ensure greater battery life, the batteries used in ArmBIT and ForearmBIT were LiPo with 750 mAh and lasted for 12 h, which required a bi-diary battery exchange. However, the new wearables ChestBIT and WristBIT reduce the physical constrain of battery size, reason for which LiPo batteries of 1,600 mAh were used, requiring a single daily battery change.

3.2 Data quality assessment

The quality of all data recorded was assessed both for the hospital system and for the wearable devices, following the approach found in (Böttcher et al., 2022) for data quality evaluation. In this approach, the quality of the acquired data is assessed globally for each dataset, through statistical metrics (mean, median, standard deviation, minimum value and maximum value). These metrics are applied to the patient data variables, namely: duration, data completeness, and each biosignal quality.

The duration variable consists on the time span from the first timestamp marking the beginning of the acquisition until the last timestamp. It is presented in hours, minutes and seconds (H:M:S). The percentage of usable data (i.e., not loss) is measured by the data completeness. This variable is the ratio between the recorded

6 https://www.polar.com/us-en/products/accessories/polar-soft-strap

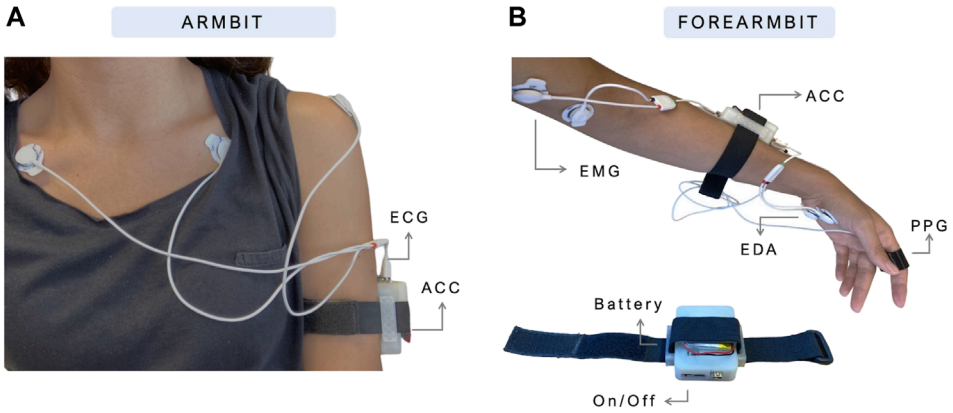

FIGURE 1
Prototypes of ArmBIT **(A)** and ForearmBIT **(B)**, the first wearable devices used to record multimodal data during video-EEG acquisitions.

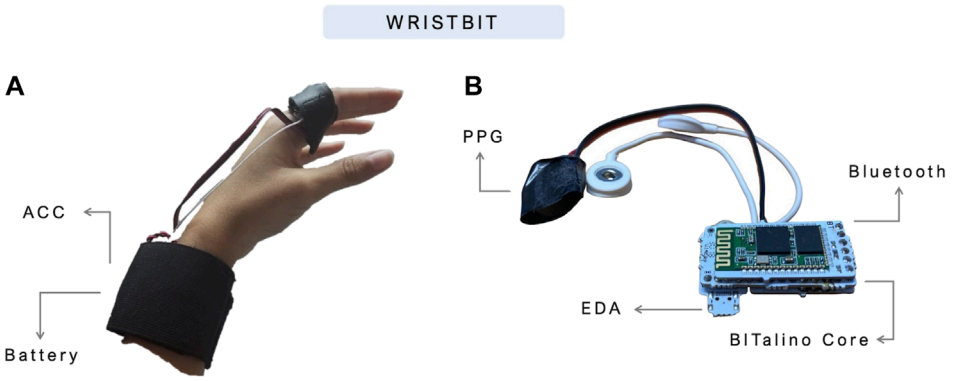

FIGURE 2
WristBIT prototype used in the PreEpiSeizures project. In the **(A)**, the WristBIT is being worn in the left hand, where the EDA and ACC are recorded in the wrist and the PPG in the finger. The **(B)** shows the interior of the wristband, with the BITalino main unit attached to the Bluetooth module and sensors.

duration and aforementioned duration variable. The recorded duration is given by all the timestamps associated to a data value between the first and last data points.

The ECG quality was evaluated in segments of 10 s and in three levels: low, medium and high. Low quality corresponds to an unusable segment, whether due to the presence of an artifact, or due to the loss of connection with the body. Medium quality (ECG MQ) corresponds to a segment where it is possible to extract rhythm information, in particular the heart rate and heart rate variability. In this scenario, the R peak detection is reliable, but the rest of the ECG waveform can be indistinguishable. Lastly, the high quality (ECG HQ) corresponds to a reliable and consistent depiction of the ECG wave throughout the segment. This qualitative stratification was also described in previous works and gives a perception of possible applications of the acquired data. To reach these levels, each segment is processed according to the following method: the R peaks locations are found and the instantaneous heart rate is calculated. If the heart rate is between 40 and 200 beats per minute, the low quality level is discarded (the low quality is chosen otherwise). Then, the ECG wave cycles are cross-correlated through Pearson correlation (between 0 and 1). If the cross correlation is above 0.8, then the segment is classified as high quality (and medium quality if below the threshold).

For the ACC, (Nasseri et al., 2020), evaluated the quality of Empatica E4 in the context of video EEG-monitoring, proposing as SQI the ratio between human motion activity frequency and the entire frequency range, as given by Eq. 1, where p refers to the power's spectrum in the indicated frequency band and FN is the Nyquist frequency (half of the sampling frequency). In this paper, the metric was calculated for 4-s non-overlapping segments and averaged across 10-min intervals.

$$SQI_{ACC} = \frac{P_{[0.5,8]}}{P_{[0.8,F_N]}} \tag{1}$$

The signal quality analysis of the RESP signal was calculated following the metric proposed by (Charlton et al., 2021) for a respiratory signal acquired through impedance pneumography. This metric consists on the analysis of valid breaths from segments with 32 s of length. For each segment, the peaks are extracted and used to find breath cycles. The segment is valid if the breaths respect some

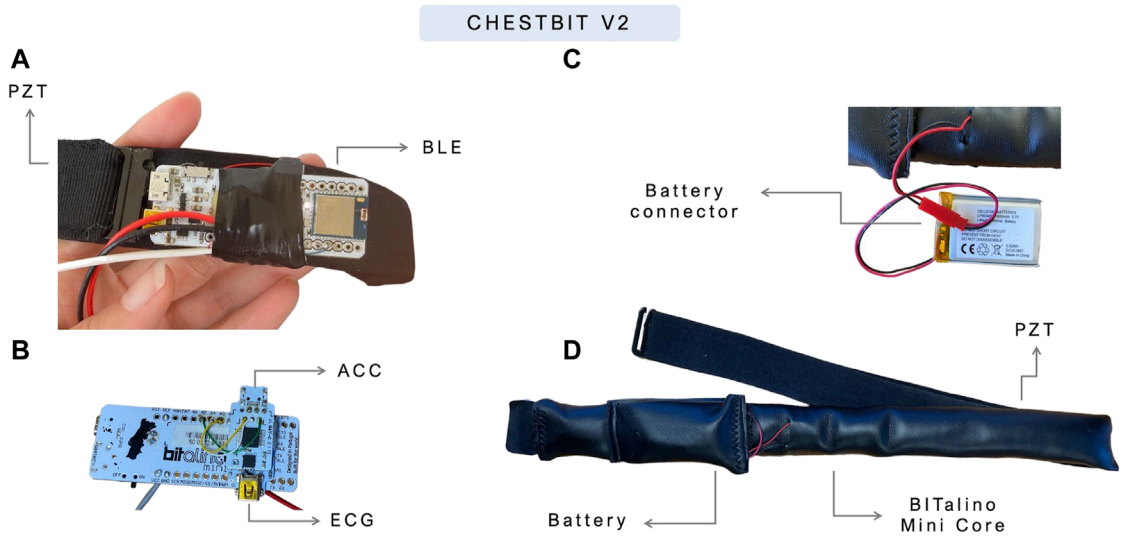

FIGURE 3
Current prototype of ChestBIT in the PreEpiSeizures project. On the **(A,B)** the ChestBIT components are shown, namely, the BItalino mini, and the mounted sensors ECG and ACC. On the **(C)** the connection between the battery and the BITalino Mini is shown, and in the **(D)**, the components are covered by a comfortable textile.

predefined conditions proposed by the authors. This metric results in a binary separation between high quality and low quality.

The EDA quality was retrieved from (Böttcher et al., 2022), where the binary decision high/low quality is based on two factors. The first is the signal amplitude, which has to be above 0.05 μS; then, the signal amplitude change rate is calculated as the ratio between the min-max amplitude and the first of these two extremes to appear. This rate should be below 0.2 in the assessment of EDA for windows with 2 s.

The aforementioned work, evaluates the quality of the PPG also in a binary low/high quality distinction, using the spectral entropy in windows of 4 s. A spectral entropy value should be below 0.8 for the segment to be considered high quality.

The decision to follow the quality assessment approaches taken by (Nasseri et al., 2020; Böttcher et al., 2022) enabled the comparison between our wearable devices and other datasets and data acquired in similar conditions. Both these works acquired wearable data using the Empatica E4.

3.3 Experimental protocol

When a patient is admitted to the hospital stay, they sign an informed consent from the hospital so that their data can be analysed and used for research purposes. After the hospital system setup, the patient is approached to participate in the wearable data collection as well. If accepted, a new informed consent is given for the use of wearable devices during the hospital stay. The proposed acquisition system collects data unobtrusively and only requires a daily short-time interruption for battery replacement. This section describes the process of accessing the wearable and the hospital data, the structure of the dataset, as well as the several formats in which each data source was saved.

3.3.1 Hospital data extraction

The hospital data of the video-EEG monitoring consisted on the patient's reports and hospital admission notes, along with the data recorded by the monitoring unit. The physiological data is always reviewed by an EEG technician and a neurologist resulting in a video-EEG monitoring report with all the relevant events annotated. This is usually saved as Word and PDF documents. The reports were only consulted with the purpose of retrieving the seizures' onsets and details, being dissociated from the biosignals' records, which are anonymised thus preserving patients' and data privacy. The physiological data is stored in the hospital servers and accessed through a secure computer in the hospital's facility. All physiological data files are retrieved with all acquired channels, varying from 24 (22 EEG channels and 2 ECG channels) up to 77 (72 EEG channels, 2 ECG, 1 SpO2, 1 EMG, and 1 EOG). However, most of the time, EOG and SpO2 are disconnected, and EMG is only connected in some motor seizures, usually on the deltoid or tibia.

Concerning the data extraction, we came across different systems in the two hospitals included in this study, which led to different extraction processes and file formats. The HSM video-EEG data is managed by the Nihon Kohden DMS system[7]; all HSM files are extracted in the European Data Format (EDF), resulting in files with 2 h of data, sampled at 1,000 Hz. Through the mne python package, it is also possible to use the raw Nihon Kohden files (.EEG format) (Gramfort et al., 2013). The HEM video-EEG data is managed by Micromed software[8]. All HEM files are extracted in the micromed raw file format (TRC), resulting in files with 2 h of data, sampled at 256 Hz.

7 https://us.nihonkohden.com/
8 https://micromedgroup.com/

In both hospital systems, two ECG channels are recorded, corresponding to the positive and negative channels. The difference between these channels results in the approximation of the Lead I derivation, sometimes requiring inversion of the signal (i.e., when the positive and negative electrodes are placed on the wrong side).

3.3.2 Wearable data extraction

The acquisition setup relied on a processing unit to receive BITalino data in real-time and store it appropriately. This was initially performed using a laptop and Python script, but was later replaced by a more user-friendly acquisition system developed within our research group, named EpiBOX (Carmo et al., 2022). Nonetheless, both systems stored the data in the same structure.

The data collected by the wearables was saved every time the system disconnected, or after 1 h in a stabilised connection. These files are in the TXT format, comprising the data of one or two devices (if they are acquired simultaneously), with a list-like header (with one dictionary per device, where the key corresponds to the device MAC address) on the first few rows and the values over the next rows, in a table-like structure. All the header fields are detailed with examples in the Supplementary Material. Besides the header, each subsequent row corresponds to a new time instant ($1/FS$), where FS corresponds to the sampling frequency of 1,000 Hz. Each TXT file is named after its starting time (e.g., 2021-04-02 18-09-05.TXT). The table produced with two devices is equal to one device with the only difference being the addition of the second device's columns. The order of first and second is known by the order in which they appear in the header. When retrieving data from the second device, it is necessary to recognise the presence of the first, and use its number of columns as an offset. This structure is easily scalable to additional devices.

4 Results

The results detailed in this section are divided into the signal quality analysis and the characteristics of the dataset acquired so far.

4.1 PreEpiSeizures data quality

The quality of biosignals was studied for all data acquired by the hospital system, the ChestBIT, the WristBIT and the ArmBIT and these results are summarised in Table 3. The hospital data was acquired for 59 patients totalling almost 6 k hours of ECG data. Data completeness is fairly high with a median of 99.21%. The majority of the signal was classified, on average, as high quality (around 70%), however, on average, 15% of the data was of poor quality. Regarding the ChestBIT, 37 patients used this device, with some sessions being more successful than others (this is observable by the minimum and maximum metrics). The data completeness is lower (in mean and median) when compared to the hospital system, which is expected since the system communicates through Bluetooth, hence being more susceptible to connection losses. Nonetheless, the discrepancy between the mean and the median indicates that the majority of acquisitions was mostly successful in terms of data completeness. In ChestBIT, more segments were discarded as poor quality, however, the median of low quality segments is also around 15% (100 - (ECG HQ + ECG MQ)). Interestingly, the median percentage of ECG HQ is higher in the ChestBIT than in the hospital system, and very few segments were classified as medium quality. The quality of RESP signals is on average 60%, which is reasonable.

The WristBIT was only acquired in 9 patients, still, it comprises 500 h of data, with data completeness percentage comparable to the ChestBIT. The quality of the EDA signal was significantly high, however the PPG quality was significantly lower, since on average, only half of the segments have high quality. This was expected, since the PPG is highly susceptible to noise. Moreover, this is comparable to the results reported by (Böttcher et al., 2022) with the Empatica E4, where the mean and median quality of PPG data was in the range [51.5, 63.3]% for the datasets acquired in hospital settings. The SQI_{ACC} values of the WristBIT are in agreement with those reported by the study of (Nasseri et al., 2020).

4.2 PreEpiSeizures dataset

The total number of patients in this dataset is 59. From this cohort, 36 performed the video-EEG in Hospital de Santa Maria (HSM), while 23 performed the video-EEG in Hospital Egas Moniz (HEM). This dataset includes biosignals recorded by our wearable devices, as well as records from the hospital. The classification of seizure types follows the guidelines of the 2017 ILAE's instruction manual (Fisher et al., 2017a; b). Focal seizures were classified as FUAS, whenever the awareness was not registered or tested. The ictal semiology described in this dataset, follows the 2022 ILAE's glossary of terms (Beniczky et al., 2022).

4.2.1 Hospital de Santa Maria

Figure 4 provides a visual depiction of the wearable data acquired so far in HSM. The horizontal axis represents the days of the week, whereas the vertical axis represents the different patients enrolled. The label of vertical axis contain the information of the wearable device and the acquisition system. The blue lines represent the wearable data, while the pink shade corresponds to the missing data. The red and grey diamonds represent clinical and subclinical seizures, respectively.

The first 4 patients enrolled in this study used the wearables ArmBIT and ForearmBIT during their video-EEG monitoring: in Figure 4, these are represented in the four bottom rows. These acquisitions lasted for 5 days and 19 h, 13 h, and 1 h and 30 min for the remaining two, respectively. However, only one of these acquisitions captured a seizure event (the patient with the longest acquisition did not experienced any seizure during their hospital stay, whilst the other patients' seizures occurred outside the wearables' recorded time spans). There were 10 patients that used the ChestBIT and WristBIT during their video-EEG monitoring, recording over 102 seizures. Their distribution according to seizure type is: subclinical = 63; FBTCS = 8; FAS = 5; FIAS = 17, and unknown focus = 9. The percentage of recorded data by these wearable devices was on average 53{%} ± 18{%} of the entire video-EEG monitoring stay (4 full days = 96 h). The number of actual recorded seizures by the wearable device is 19, from a total of 39 clinical seizures, which occurred during the monitorings.

The EpiBOX deployment as the acquisition system was mostly successful, with only 4 out of 13 patients having less than a day

TABLE 3 Signal quality analysis for the data acquired by the hospital system and the devices ChestBIT and WristBIT. The N indicates the number of patients and the total duration is in H:M:S. The first column indicates the statistical metric, followed by the data completeness (in %), the quality of the biosignals, where the ECG is divided in high and medium quality (in %) and the acquisition duration (in H:M:S).

Hospital data, *N* = 59				Total duration: 5,838:19:12
p	Data Completeness (%)	ECG HQ (%)	ECG MQ (%)	Duration
Mean	92.33	68.58	17.15	98:57:16
Median	99.21	71.83	16.11	94:33:40
SD	15.09	20.29	11.33	33:51:50
Min	43.40	4.10	0.88	10:43
Max	100	96.60	52.23	165:47:15

WristBIT, *N* = 9				Total Duration: 510:04:07	
p	Data Completeness (%)	EDA (%)	BVP (%)	ACC	Duration
Mean	70.64	92.84	64.33	0.44	56:39:46
Median	69.95	98.23	71.72	0.39	60:33:25
SD	21.11	13.73	25.31	0.19	15:21:54
Min	31.82	57.55	20.39	0.22	26:31:28
Max	93.38	99.86	89.72	0.80	76:25:50

ChestBIT, *N* = 37					Total Duration: 2,211:53:29	
p	Data Completeness (%)	ECG HQ (%)	ECG MQ (%)	PZT (%)	ACC	Duration
Mean	69.64	67.33	4.44	58.52	0.35	59:46:51
Median	85.98	82.03	3.02	61.63	0.34	61:20:44
SD	31.84	34.59	6.07	21.16	0.22	34:18:16
Min	1.15	0.0	0.0	1.81	0.0	10:20
Max	100	98.65	30.89	89.47	0.82	192:38:58

ArmBIT, *N* = 4					Total Duration: 156:14:54	
p	Data Completeness (%)	ECG HQ (%)	ECG MQ (%)	EDA (%)	BVP (%)	Duration
Mean	60.09	$8.18*10^{-3}$	0.84	15.50	58.52	39:03:43
Median	59.19	0.0	0.64	$2.03*10^{-2}$	61.63	7:27:19
SD	28.56	$1.64*10^{-2}$	0.97	30.97	21.16	67:27:35
Min	26.35	0.0	0.0	0.0	1.81	1:26
Max	95.65	$3.27*10^{-2}$	2.05	61.95	89.47	139:54:13

recorded (their recorded duration was: 13 h; 3 h; 12 min and 9 min). The ChestBIT enabled the recording of 30 out of 60 clinical seizures. Besides the mentioned patients so far, there was the case of patients who were enrolled in the study and only have hospital data. Since the hospital monitoring equipment provides ECG recordings, they were still included in the dataset, despite the lack of wearable data. 9 patients are included in this group with a total of 47 clinical seizures, with a distribution in seizure types of FBTCS = 6; FAS = 19; FIAS = 16 and subclinical = 6.

4.2.2 Hospital Egas Moniz

The expansion of the data acquisition to another centre was possible due to the reproducibility of EpiBOX. Figure 5 shows the time domain analysis of wearable data recorded for all patients enrolled in this hospital. This set is composed of 15 patients, who performed the wearable acquisition with the EpiBOX setup, along with the ChestBIT device. From this group, one patient did not register any data during the acquisition, hence being excluded from this plot. The time domain analysis of the remaining 14 patients ranges from 10 min up to 3 days and 9 h. The average percentage of actual recorded time domain is 64.2%, with a standard deviation of 34.0%. Nonetheless, the median recorded time percentage rises to 83.6% (the median of time loss is only 16.4%). The total of seizures in this cohort is 45 clinical seizures (FIAS = 11, FAS = 34) and 20 subclinical seizures. As it is observed in Figures 5, 6 patients do not have reports on clinical seizures: 2 only experienced subclinical seizures; and 4 did not experienced any seizure during the exam. Nonetheless, the wearable device was able to capture 15 clinical seizures in this cohort.

Besides the data acquired in the scope of our project, the hospital also provided additional retrospective data, from other patients with temporal lobe epilepsy, who underwent the same monitoring exam.

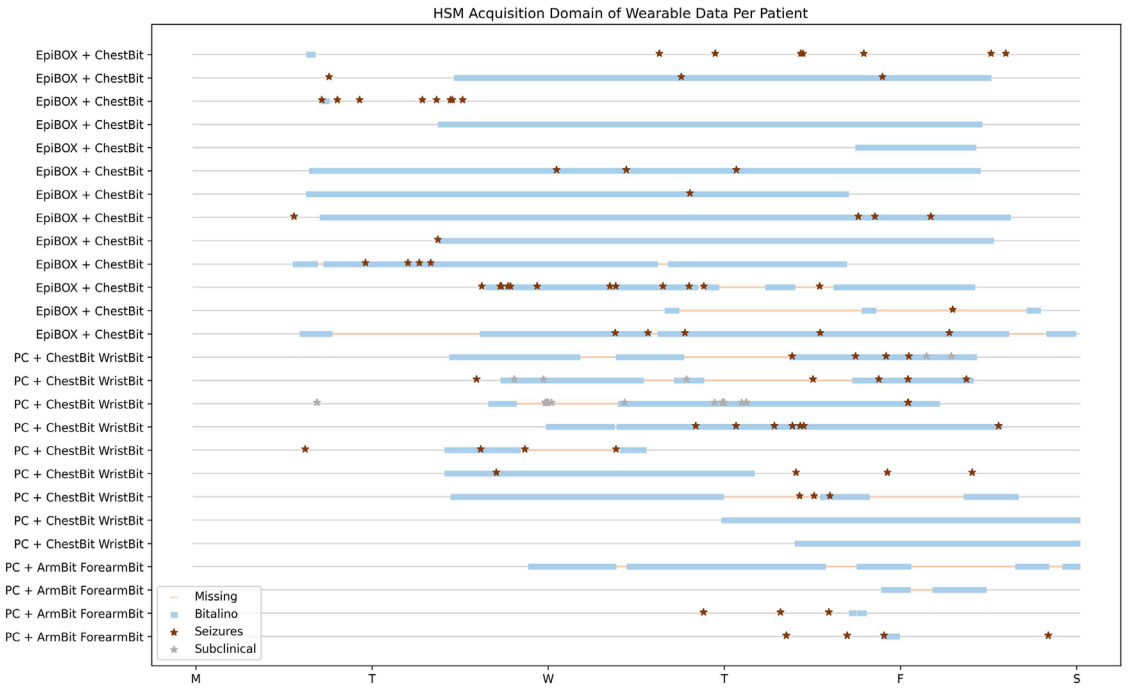

FIGURE 4
HSM Data Acquisition Temporal Overview. Patients with wearable and hospital data. The horizontal axis represents the temporal domain, from the beginning of the video-EEG monitoring, until its end. Each row consists in a single patient.

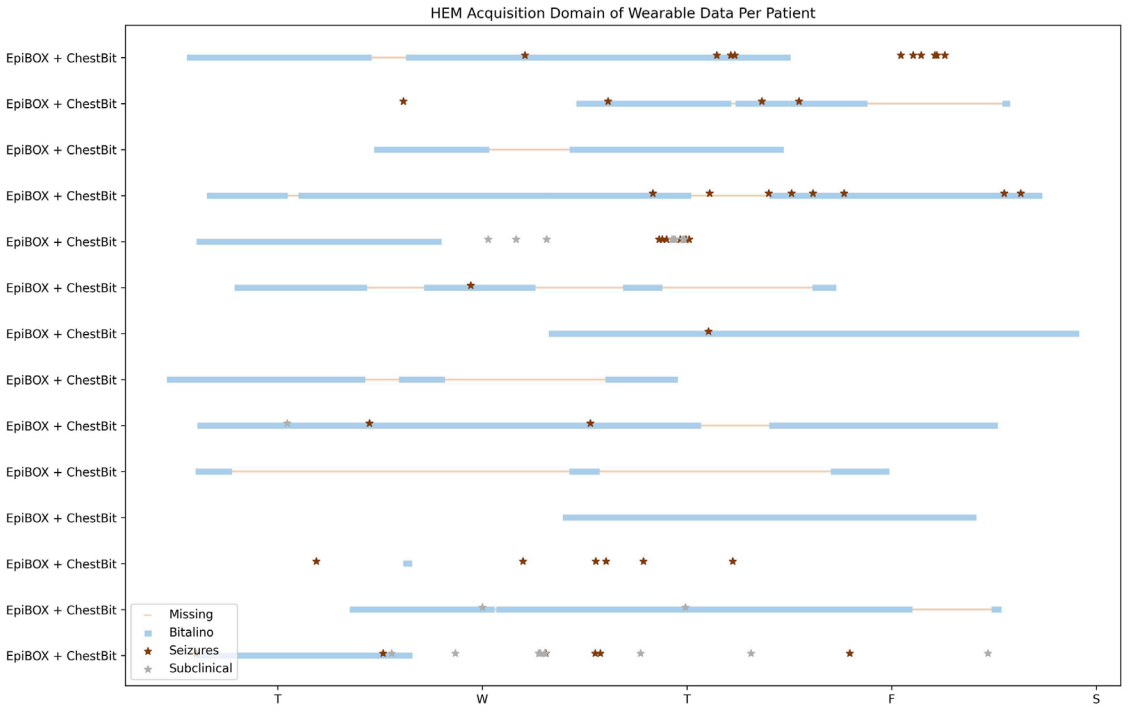

FIGURE 5
HEM Data Acquisition Temporal Overview. Patients with wearable and hospital data. The *X*-axis represents the temporal domain, from the beginning of the video-EEG monitoring, until its end. Each row consists in a single patient.

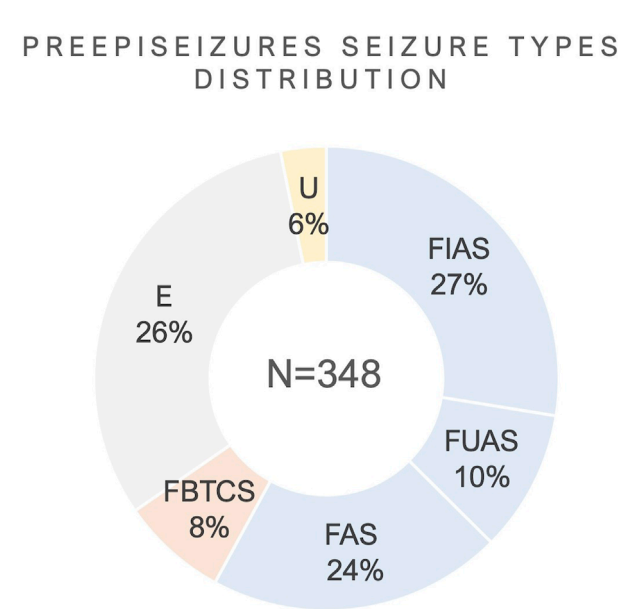

FIGURE 6
Distribution of seizure types from the cohort. *E*: Subclinical; *U*: Unknown; FIAS, Focal Impaired Awareness Seizure; FBTCS, Focal to Bilateral Tonic-Clonic Seizure; FAS, Focal Aware Seizure; FUAS, Focal Unknown Awareness Seizures.

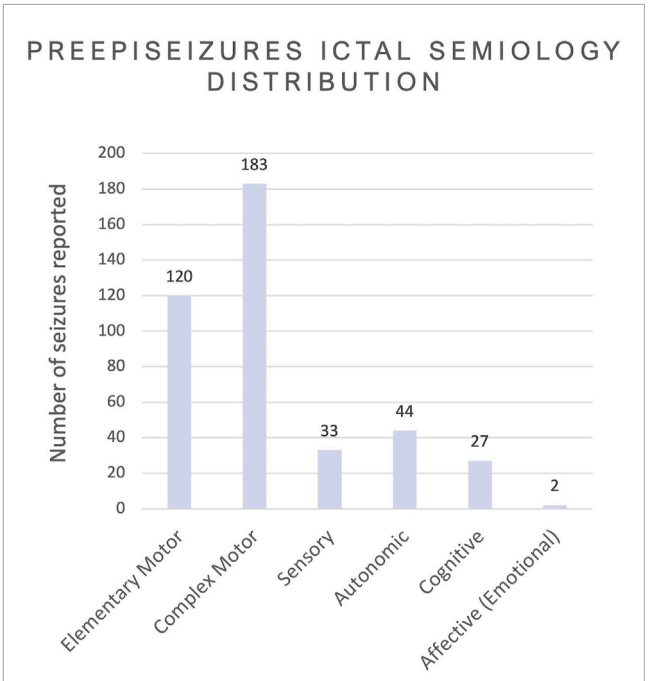

FIGURE 7
Overview of all ictal semiology phenomena reported in the video-EEG, grouped according to the nature of the phenomena following the 2022 ILAE's glossary (Beniczky et al., 2022).

This set consisted on 9 patients, who experienced 61 clinical seizures (FBTCS = 1, FIAS = 36, FAS = 20 and FUAS = 4). This retrospective data contains the hospital system's measurements, which includes the ECG. This cohort was used to initiate the ECG analysis and assess the validation of ECG-based seizure manifestations.

4.3 Overview

The patients collected in this database were performing the video-EEG monitoring for presurgical assessment. This section will detail the distribution of onset localisation and lateralisation, seizure types and ictal semiology reported by the clinical team.

In this cohort (59 patients), 64.41% (N = 38) showed temporal lobe activation during the onset of ictal period. The frontal lobe ictal onset activation showed a prevalence of 25.42% (N = 15), closely followed by the parietal lobe with 18.64% (N = 11). Lastly, the occipital lobe ictal onset was reported in 6.78% (N = 4). The ictal onset activation reported in more than one lobe region (e.g., fronto-temporal) was included in both categories. Concerning lateralisation, 38% had a left hemisphere onset seizure, whereas the epileptogenic zone was in the right hemisphere for 44% of patients. Bilateral ictal onsets were described in 4% of patients from the cohort.

In Figure 6, the distribution of seizures per seizure types is shown, regarding the seizure types which were reported in the video-EEG reports. The total number of seizures in the PreEpiSeizures dataset is 348, distributed a across six seizure types (FBTCS = 27, FIAS = 95, FUAS = 35, FAS = 82, subclinical = 89 and unknown = 20). These values are illustrated as a percentage in Figure 6, where the predominance of focal seizures is notable. The classification of seizures as Unknown was chosen when there was no information regarding the type of seizure, whereas FUAS correspond to focal seizures, in which only the awareness was not tested.

Besides the classification of seizure types, the video-EEG reports also contained some details regarding the events occurring during the seizure. In Figure 7, the reported ictal semiology from the dataset is displayed in 6 categories. The Elementary Motor Behaviour was found in 120 seizures and includes Dystonic (N = 23), head version or head orientation (N = 45), eye blinking (N = 12), myoclonic/clonic (N = 14), tonic (N = 6) and tonic-clonic (N = 27). The Complex Motor Behaviour (N = 183) included automatisms and hyperkinetic behaviour (N = 3). The most common automatisms were distal (N = 67) followed by oroalimentary (N = 59) and proximal (N = 16). Other reported automatisms were: verbal (N = 11); vocal (N = 6); mimic (N = 7); nose-wiping (N = 9) and Rinch (N = 5). Sensory phenomena (N = 33) was mostly populated by the somatosensory symptoms (N = 15), followed by cephalic aura (N = 5). Other reported sensory phenomena was gustatory (N = 1) and olfactory (N = 2). The most reported autonomic semiology was epigastric aura (N = 20), followed by hyperventilation (N = 12), tachycardia (N = 11) and piloerection (N = 1). Few seizures reported cognitive ictal phenomena (N = 27), where the most common symptom was autoscopy (N = 12), followed by dejá vu (N = 9), ictal aphasia (N = 3) and dysarthria (N = 3). Only 2 seizures reported emotional phenomena and the symptom was fear.

In Table 3, the total duration of ArmBIT, ChestBIT and WristBIT is shown separately. Figure 8 gives a visual depiction of the number of recorded hours by each modality. The different colours represent the device responsible for each measurement. The least represented modality is EMG with 156 h, 14 min and 54 s of data. Since

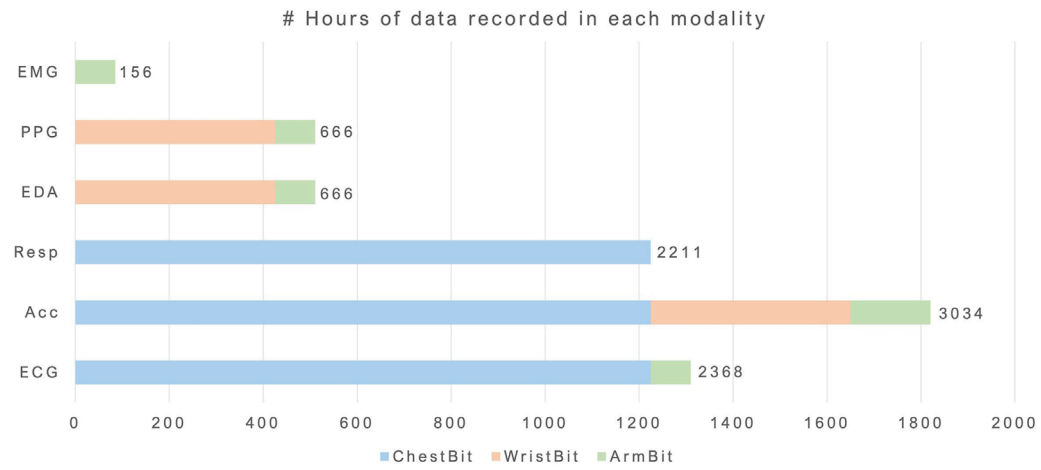

FIGURE 8
Number of hours acquired per modality. Each colour represents one form factor.

this measurement required gel electrodes, it was discarded in the new devices. The EDA totals 666 h, 19 min and 2 s of data, which is decomposed in 156 h of using pre-gelled electrodes (with ForearmBIT) and 510 h, 4 min and 7 s of metallic electrodes in the WristBIT. The chest-ACC corresponds to 2,211 h of data, whereas the wrist-ACC totals 510 h. Additionally, the ArmBIT and ForearmBIT add more 312 h to the ACC data. Regarding RESP, 2,211 h were recorded so far, using only the ChestBIT. The ECG was captured using pre-gelled electrodes in 156 h (ArmBIT) and the ChestBIT has so far recorded 2,211 h. The total number of recorded hours by all wearables is 2,721 h, 57 min and 36 s. The broader use of ChestBIT instead of WristBIT was based on three arguments: an easier reproducibility; a higher reliability of ECG instead of PPG to record cardiac activity; and being more discreet, since it is placed under the clothes. This last point is aligned with previously surveyed preferences of PWE (Simblett et al., 2020).

To conclude the overview of the PreEpiSeizures dataset, the aforementioned Table 1 provides a side-by-side characterisation of this dataset with those available within the state-of-the-art. Three of the public databases (Bern-Barcelona (Andrzejak et al., 2012), New Delhi EEG (Swami et al., 2016) and Epilepsy Seizure Recognition (Andrzejak et al., 2001)) only presented segments of a few seconds duration. Bonn-Barcelona micro- and macro-EEG database (Martínez et al., 2020), comprises data from epileptic patients without epileptic seizures.

The comparison of our dataset with EPILEPSIAE (Klatt et al., 2012) and Siena Scalp EEG (Detti, 2020) is performed with regards to the ECG recorded by the hospital system (this is the number in the left side of columns patient and total hours). Our dataset size, both in terms of patients, and in total recorded hours, surpasses its peers.

Regarding wearable data, the only other dataset found with wearable data was the My Seizure Gauge Wearable, which does not contain ECG, PZT or Chest Motion data. Both datasets duration is quite similar (our wearable duration is the right number of column Total Hours in Table 1). Concerning the number of seizures and the variety of seizure types, PreEpiSeizures is similar to EPILEPSIAE and My Seizure Gauge Wearable. Regarding the number of recorded hours, the proposed dataset also closely follows those of the literature.

5 Discussion

The patients which are admitted for video-EEG monitoring are usually patients that either have refractory epilepsy and require a differential diagnosis, or are included in the presurgical evaluation program. In HSM, a new patient comes every 2 weeks, with some exceptions like vacations or other unforeseen events, which can change this schedule. Then, the patient stays for a work week (Monday to Friday) and sometimes also spends the weekend if the hospital team finds it necessary, for example, if no seizure occurred until Friday. Although this is a very good pace, allowing for up to 26 patients per year, not all these patients meet the eligibility criteria: patients need to have at least 16 years old; the EEG monitoring should be performed with scalp electrodes, instead of intracranial; patients also require a high level of independence, compatible with using an extra device continuously throughout the hospital stay. In HEM, the EEG technicians are all day with the patients (from 8AM to 11PM), hence the majority does not need accompaniment. The cadence in this ward is of 1–2 patients per week, however only one is asked to participate in the study. This is related also to the duration of the monitoring, since one patients stays in the hospital for the work week, whereas the other only stays for 48 h (the case of differential diagnosis) or less (in the case of other exams).

Despite having a great number of seizures, the proposed dataset suffers from one core issue also found in its peers: the great variability of seizure types. In both hospitals, many types of seizures are monitored (from tonic-clonic and myoclonic to subclinical seizures), and often the epileptogenic zone is not even known prior to the monitoring. As a result, it is difficult to predict what will be the outcome of the data collection. So far, the majority of seizures encountered have a focal onset, nevertheless they vary in duration, awareness or semiology. Even the broader classifications of seizure types (such as FAS and FIAS) enclose seizures that have motor and non-motor manifestations. Although patients in video-EEG

10.3389/fphys.2023.1248899

TABLE 4 Common concerns of wearable data acquisition.

Name	Description	Nature	Solution
Forget battery exchange	Uncontrolled scenarios can lead to forgetting battery exchanges	Real-world acquisition	Mobile app
User Compliance	The acceptance to participate and the proper realisation of the experiment	Real-world acquisition	Reward system
Incorrect placement	Uncontrolled scenarios can lead to incorrect device placement by non-experts	Real-world acquisition	Mobile app
Cohort's variability	Real-world settings might translate into an unexpected variability to the cohort	Real-world acquisition	Multi-centre
Battery size	Battery shortage could cause more connection losses	Wearable design	Reduce FS
Design constraints	The signals to record are restricted by the sensors' requirements	Wearable design	Adaptative factor
Device resistance	Resistance to sweat and to the continuous use over multiple acquisitions	Wearable design	Detachable electronics
Materials Hygienisation	Materials properly clean before and after each new acquisition, cleanable materials	Wearable design	Resistant materials
Signal quality	Uncontrolled scenarios can lead to noise presence in the signals of a variety of natures	Processing	Multimodal denoising
Temporal synchronisation	Signals acquired in different sources may present a relative temporal shift	Processing	HR synchronisation
Big data	High sampling frequencies and long hours leads to great amounts of data	Processing	Batch processing
Fragmented files	File fragmentation can lead to contiguous files with different signal offsets or amplitudes, sometimes time loss is unknown	Processing	Discrete analysis
Device drift	Devices can drift and originate signals with slightly different characteristics	Processing	Constant calibration
Motion artifacts	The presence of motion artifacts affects the proper measurements of other signals	Noise Interference	ACC denoising
Sensor interference	The continuous use of a device might degrade its sensors, and contamination can occur	Noise interference	Automatic check
Contact loss	Contact with the body can be lost during acquisition	Noise interference	Automatic check
Network interference	The surroundings can cause electrical disturbances in the physiological signal	Noise interference	Low-pass filtering
Baseline wander	Fluctuations on the ECG signal are common and might result in incorrect measurements	Noise interference	Baseline removal techniques

monitoring have refractory epilepsy, their seizure occurrence is often highly reduced in daily life by ASM. During the monitoring, the ASM is slowly suspended to allow for resurgence of epileptic activity. For some patients, the complete withdraw of ASM could result in bilateral tonic-clonic seizures, which would hamper the identification of seizure onset. The goal in video-EEG monitoring is to achieve the balance that allows to clearly identify the ictal onset of seizures, with the minimum number of seizures. However, for some patients, no seizure occurs during the hospital admission, despite their frequent seizure rate outside the hospital.

The wearable data acquisition itself was an eventful process, filled with a great variety of challenges. Hereinafter, this section is divided into an overview of the problems faced and proposed solutions, followed by a discussion of the quality between the wearable device and the hospital system, and finally the quality assessment of the current acquisition setup and its comparison with the previous setup.

In Table 4, the various issues faced during the wearable data acquisition process are described, being divided into four categories according to their nature: real-world acquisition; wearable design; processing; and noise interference. Though this data collection was specific to a singular disease and a strict protocol, the challenges herein faced are general to wearable and even some non-wearable data collection experiments.

Four challenges were identified in relation to real-world acquisition: forget battery exchange (1.1); user compliance (1.2); incorrect placement (1.3) and cohort's variability (1.4). Although all data was collected in the hospital ward, there was no constant supervision by an expert, leading to several challenges, that can also be expected in an ambulatory scenario (hence their "real-world" nature). (1.1) Most wearable devices require a quasi-daily change of battery, as seen in Table 2. Hence, it could be expected that users forget to charge the device or to have a charged battery at-hand. To help in this process, the proposed solution is a mobile application with reminders to charge the device or change the battery. (1.2) User compliance is important for any experiment, especially those in which the patient plays a major role in the acquisition control. Mental and emotional availability is required to perform a rigorous experiment control; despite the relative good rate of potential patients, not all will meet the inclusion criteria to participate in the data collection. Moreover, this is amplified in ambulatory data collection, and strategies should be established to increase patient's compliance. As a suggestion, a more immediate reward system could be added to the protocol, such as their data overview, or daily statistics. (1.3) Unsupervised experiments such as this, could lead to incorrect placement of the devices, especially if more than one device is used simultaneously. For example, the ChestBIT could be inverted from its original orientation, or shifted to one side or the other. Moreover, the ChestBIT could fall during the night or even detach itself. In order to solve these issues, the device should be reinforced especially in the attachment area. Moreover, in an ambulatory setting, the mobile application could aid the patient to properly adjust the device, for example, via a signal quality assessment algorithm. (1.4) The variability of the cohort is something to account for when dealing with such specific diseases. Potential patients could have different ages, unique

disease characteristics, or even specific comorbidities. In this case it could be useful to design the protocol upfront as a multi-centre data collection. The increase of potential patients could enable the encounter of similar cases and better deal with the great cohort's variability.

The category of wearable design included four challenges: battery size (2.1); design constraints (2.2); device's resistance (2.3); and materials hygienisation (2.4). The nature of these challenges comprises issues which conditioned the wearable design, and should be accounted for when proposing new designs for continuous wearable data collection. (2.1) The battery size is a constraint on wearable devices, especially in preliminary versions, based on lithium ion polymer batteries, hence their energy consumption should be reduced to the minimum, to ensure the maximum operability. In the proposed devices, the FS is 1,000 Hz, which corresponds to a battery drain rate of approximately 62 mAh (i.e., milliamp hour). As a result, 1,500 mAh are required for lasting 24 h. One solution could be to decrease the FS to 100 Hz for the ChestBIT (or less in the case of the WristBIT), to enable a slower rate of battery drain, while still capturing the major physiological manifestations. (2.2) The design of a wearable device is conditioned to its embedded sensors. For example, the ECG sensor requires at least two contact points with the body, one in each side of the heart, whereas the EDA has better quality in places with more eccrine glands (Nagai et al., 2019). Thus, when designing a new wearable it is necessary to understand which modalities are more relevant to the task, since not all are possible to acquire with the same form factor. (2.3) The device should be resistant to ensure long-term use without quality loss. This could be achieved by choosing appropriate materials, by attaching securely the electronics to the textiles, or even by adopting bendable electronics. (2.4) The materials disinfection is important to remove bacteria and fluids, especially during patient exchange. The choice of materials could also play an important part, not only comfort-wise but also for proper hygienisation.

The next category of challenges is processing, and it includes: signal quality (3.1); temporal synchronisation (3.2); big data (3.3), fragmented files (3.4); and device drift (3.5). Processing concerns the first steps towards the extraction of meaningful information from the acquired data. The challenges herein described could be detrimental and lead to misinformation, thus they should be carefully addressed, preferably during the actual data collection. (3.1) As it was previously mentioned, the device could be incorrectly placed due to various reasons. Moreover, other factors (which will be addressed in the next category) could contribute to poor quality signals. Quality control should be assured automatically through an algorithm, specific for each modality acquired. (3.2) When acquiring data from more than one device simultaneously, or when comparing two signals acquired simultaneously (such as the hospital's ECG against the device's ECG), or even when using the hospital's annotations with the wearables, it is relevant to confirm whether the temporal line is properly defined. It could be the case that the wearable does not save data with the correct time. To solve this issue, it should be implemented a temporal synchronisation. The temporal synchronisation between the same modality time series is possible using cross-correlation (e.g., in ECG/PPG, one can use the instantaneous heart rate from both sources). This could be used between the hospital's signal and the device's signal, and the devices time should be adjusted according to this temporal offset. In our case the EpiBOX smartphone's application allows to save the device's time alongside the real time (fetched by the smartphone). This time difference could also be used to adjust the time to a better estimation prior to signal synchronisation.

(3.3) The FS of 1,000 Hz, associated to several days of acquisition, originates several gigabytes of data per patient. This poses a problem for opening such files during the processing phase. One solution could be batch processing; through this technique, the time is divided into intervals of a few hours (or even less than 1 h), and the signals are extracted from the TXT format to a more compressed format, such as parquet (a columnar file optimized for processing big data). This could allow to save space and time in future operations. (3.4) There is always the case of ending one file and starting another in the middle of the acquisition. This also occurs for hospital files. While it is expected that the next file will be in the same conditions as the previous, changes can occur in both signal's amplitude and/or offset. Moreover, battery exchange can lead to a slight change in the devices position. During processing, the timeseries should be considered discontiguous if they come from fragmented files, and processing should occur separately for each fragment. (3.5) As it was previously mentioned, a drift in device position during the course of the acquisition is inevitable, due to several reasons. The timeseries should be seen as an evolving signal, and not static according to an initial defined baseline. The normalisation or even signal shape correctedness should be assessed with nearby points and not the entire signal. This does not invalidate standard references of quality for the entire signal, but simply whether signal changes are a result of drifts or they contain meaningful information towards the final purpose.

Noise interference in timeseries is especially prominent in wearable acquisitions, with a multitude of noise types (Vijayan et al., 2021). Noises can be difficult to remove when they fall into the frequency bands of the acquired signal. The following noises found in the data acquisition were: motion artifacts (4.1); sensor interference (4.2); contact loss (4.3); network interference (4.4); and baseline wander (4.5). The proper identification of each noise type, could be the first step for their automatic removal during the processing phase. (4.1) Motion artifacts fall into most signals frequencies of interest, thus their removal is not trivial. Since acceleration is acquired in most wearable devices, one solution could be to use the ACC signal to remove motion from the other signal modalities. This would mostly work when the sensors are placed in proximity. For example, the ACC from WristBIT could have common motion with the EDA, however motion captured in the PPG acquired at the finger might not have been captured by the ACC. (4.2) The continuous long-term use of the device could deteriorate the electronic board contacts and originate improper signals, which should be tested regularly. (4.3) Loss of contact between the device and the skin is something to account for, since the connection is still maintained but the desired signal is no longer there. This should also be assessed automatically by identifying the types of signal shapes induced by such issue, and seeking them in the original signal prior to meaningful extraction. (4.4) The presence of other electronic devices in the surrounding space can influence the quantity of noise in the signal. The video-EEG room contains a great amount of electrical devices acquiring simultaneously and constantly, and one should be prepared for a small signal-to-noise ratio. (4.5) The presence of baseline wander, especially in the ECG

signal, is common in both the wearable device and the hospital's system. Similarly to motion artifacts, baseline wander can also fall in the signal frequency range and affect meaningful information extraction. There are several baseline wander techniques proposed in the literature which could be implemented during the processing step.

Given this last set of challenges, one potentially valuable addition to the PreEpiSeizures dataset would be to provide the quality assessment within the metadata of each file. The developed approach should be based on the assessment of quality against the physiological basis in an agnostic manner. This will be addressed in the future work.

6 Conclusion

The PreEpiSeizures project was motivated by the limited number of available wearable data in epilepsy; this collaboration has enabled the collection of data from 59 patients over the past few years (where 37 patients also wore a chest device, nine wore a wrist device, and four wore an arm device). The data collection resulted in 5,838 h of hospital data and 2,721 h of wearable data.

So far, three different form factors of wearable devices were worn by the patients: ArmBIT, WristBIT and ChestBIT. The ChestBIT's ability to record the ECG signal using non-gelled conductive materials, is an advantage compared with the ArmBIT. The quality assessment of ChestBIT was at the level of the hospital system (in the case of the ECG), and WristBIT quality was comparable to the quality of Empatica E4 used in similar conditions, reported in previous works. The advantage of using our own devices, allowed to have the liberty to experiment with form-factors and physiological modalities. Although not all patients have used the wearable devices, the availability of the hospital's ECG signal allows to draw similar conclusions regarding the physiological manifestations of epilepsy in cardiac activity, which is also aligned with the literature.

The video-EEG monitoring in the hospital significantly reduces the variability of the real-world while allowing the access of ground truth annotations. The ambulatory setting may reveal additional challenges which are not being considered yet, nevertheless it was possible to identify 18 challenges that impacted the wearable data collection and may also appear in real-world scenarios. Further research on these challenges should be a priority to avoid data and time losses. Moreover, the concerns and challenges raised in the discussion affect overall continuous health monitoring studies and are not exclusively epilepsy monitoring.

The future of the PreEpiSeizures project will include the maintenance of the data collection process, as well as the curation of the dataset and the expansion to ambulatory monitoring is also envisioned. Additionally, the project will address some of the acquisition challenges mentioned, such as: the battery size, the real-time signal quality assessment, and noise reduction.

Data availability statement

The raw data supporting the conclusion of this article will be made available by the authors, without undue reservation.

Ethics statement

The studies involving humans were approved by the Comissão de Ética do Centro Académico de Medicina de Lisboa—CAML. The studies were conducted in accordance with the local legislation and institutional requirements. The participants provided their written informed consent to participate in this study.

Author contributions

HP, AF, MA, and AC were responsible for the wearable design and function. MA performed the data quality analysis. MA, CB, and FS were responsible for the data collection and availability. MA wrote the article. AC, AP, FS, CB, HP, and AF reviewed the article. All authors contributed to the article and approved the submitted version.

Funding

This work was partially supported by the Fundação para a Ciência e (FCT), Portugal, under the grants 2021.08297.BD and 2022.12369.BD, under the Scientific Employment Stimulus—Individual Call—2022.04901.CEECIND, and project PCIF/SSO/0163/2019 "SafeFire". The work has also been partially supported by Centro Hospitalar Universitário Lisboa Norte, EPE, under the project "Pre_EpiSeizures", by the FCT/Ministério da Ciência, Tecnologia e Ensino Superior (MCTES) through national funds and when applicable co-funded by EU funds under the project UIDB/50008/2020, and by the Instituto de Telecomunicações (IT).

Acknowledgments

The authors would like to thank Instituto de Telecomunicações for the materials and help with the acquisition setup, namely, the technical engineer José Gouveia. In Hospital de Santa Maria, the authors thank the EEG technician Rosa Santos and their team for clinical support and supervision. In Hospital Egas Moniz, the authors acknowledge the contribution of the EEG technician Octávia Brás and their team for their involvement during the acquisitions and annotations. The authors would also like to express their gratitude to all the volunteers that participated in the study.

Conflict of interest

The authors declare that the research was conducted in the absence of any commercial or financial relationships that could be construed as a potential conflict of interest.

Publisher's note

All claims expressed in this article are solely those of the authors and do not necessarily represent those of their affiliated

organizations, or those of the publisher, the editors and the reviewers. Any product that may be evaluated in this article, or claim that may be made by its manufacturer, is not guaranteed or endorsed by the publisher.

Supplementary Material

The Supplementary Material for this article can be found online at: https://www.frontiersin.org/articles/10.3389/fphys.2023.1248899/full#supplementary-material

References

Akintola, A. A., van de Pol, V., Bimmel, D., Maan, A. C., and van Heemst, D. (2016). Comparative analysis of the equivital EQ02 lifemonitor with holter ambulatory ECG device for continuous measurement of ECG, heart rate, and heart rate variability: A validation study for precision and accuracy. *Front. Physiology* 7, 391. doi:10.3389/fphys.2016.00391

Andrzejak, R. G., Lehnertz, K., Mormann, F., Rieke, C., David, P., and Elger, C. E. (2001). Indications of nonlinear deterministic and finite-dimensional structures in time series of brain electrical activity: dependence on recording region and brain state. *Phys. Rev. E* 64, 061907. doi:10.1103/PhysRevE.64.061907

Andrzejak, R. G., Schindler, K., and Rummel, C. (2012). Nonrandomness, nonlinear dependence, and nonstationarity of electroencephalographic recordings from epilepsy patients. *Phys. Rev. E* 86, 046206. doi:10.1103/PhysRevE.86.046206

Beniczky, S., Tatum, W. O., Blumenfeld, H., Stefan, H., Mani, J., Maillard, L., et al. (2022). Seizure semiology: ILAE glossary of terms and their significance. *Epileptic Disord.* 24, 447–495. doi:10.1684/epd.2022.1430

Böttcher, S., Vieluf, S., Bruno, E., Joseph, B., Epitashvili, N., Biondi, A., et al. (2022). Data quality evaluation in wearable monitoring. *Sci. Rep.* 12, 21412. doi:10.1038/s41598-022-25949-x

Brinkmann, B. H., Karoly, P. J., Nurse, E. S., Dumanis, S. B., Nasseri, M., Viana, P. F., et al. (2021). Seizure diaries and forecasting with wearables: epilepsy monitoring outside the clinic. *Front. Neurology* 12, 690404. doi:10.3389/fneur.2021.690404

Bruno, E., Viana, P. F., Sperling, M. R., and Richardson, M. P. (2020). Seizure detection at home: do devices on the market match the needs of people living with epilepsy and their caregivers? *Epilepsia* 61, S11–S24. doi:10.1111/epi.16521

Carmo, A. S., Abreu, M., Fred, A. L. N., and da Silva, H. P. (2022). EpiBOX: an automated platform for long-term biosignal collection. *Front. Neuroinformatics* 16, 837278. doi:10.3389/fninf.2022.837278

Charlton, P. H., Bonnici, T., Tarassenko, L., Clifton, D. A., Beale, R., Watkinson, P. J., et al. (2021). An impedance pneumography signal quality index: design, assessment and application to respiratory rate monitoring. *Biomed. Signal Process. Control* 65, 102339. doi:10.1016/j.bspc.2020.102339

Cook, M. J., O'Brien, T. J., Berkovic, S. F., Murphy, M., Morokoff, A., Fabinyi, G., et al. (2013). Prediction of seizure likelihood with a long-term, implanted seizure advisory system in patients with drug-resistant epilepsy: a first-in-man study. *Lancet Neurology* 12, 563–571. doi:10.1016/S1474-4422(13)70075-9

Da Silva, H. P., Guerreiro, J., Lourenço, A., Fred, A. L., and Martins, R. (2014). "BITalino: A novel hardware framework for physiological computing," in International Conference on Physiological Computing Systems, Lisbon, Portugal, January 7-9, 2014, 246–253.

Detti, P. (2020). Siena scalp EEG database. Version Number: 1.0.0 Type: dataset. doi:10.13026/5D4A-J060

Detti, P., Vatti, G., and Zabalo Manrique de Lara, G. (2020). EEG synchronization analysis for seizure prediction: A study on data of noninvasive recordings. *Processes* 8, 846. doi:10.3390/pr8070846

Fisher, R. S., Cross, J. H., D'Souza, C., French, J. A., Haut, S. R., Higurashi, N., et al. (2017a). Instruction manual for the ILAE 2017 operational classification of seizure types. *Epilepsia* 58, 531–542. doi:10.1111/epi.13671

Fisher, R. S., Cross, J. H., French, J. A., Higurashi, N., Hirsch, E., Jansen, F. E., et al. (2017b). Operational classification of seizure types by the international league against epilepsy: position paper of the ILAE commission for classification and terminology. *Epilepsia* 58, 522–530. doi:10.1111/epi.13670

Frankel, M. A., Lehmkuhle, M. J., Watson, M., Fetrow, K., Frey, L., Drees, C., et al. (2021). Electrographic seizure monitoring with a novel, wireless, single-channel EEG sensor. *Clin. Neurophysiol. Pract.* 6, 172–178. doi:10.1016/j.cnp.2021.04.003

Gramfort, A., Luessi, M., Larson, E., Engemann, D. A., Strohmeier, D., Brodbeck, C., et al. (2013). MEG and EEG data analysis with MNE-Python. *Front. Neurosci.* 7, 267. doi:10.3389/fnins.2013.00267

Gómez, C., Arbeláez, P., Navarrete, M., Alvarado-Rojas, C., Le Van Quyen, M., and Valderrama, M. (2020). Automatic seizure detection based on imaged-EEG signals through fully convolutional networks. *Sci. Rep.* 10, 21833. doi:10.1038/s41598-020-78784-3

Johnstone, J. A., Ford, P. A., Hughes, G., Watson, T., and Garrett, A. T. (2012). Bioharness(TM) multivariable monitoring device: part. I: validity. *J. Sports Sci. Med.* 11, 400–408.

Kenny, J., Cullen, S., and Warrington, G. D. (2017). The "ice-mile": case study of 2 swimmers' selected physiological responses and performance. *Int. J. Sports Physiology Perform.* 12, 711–714. doi:10.1123/ijspp.2016-0323

Klatt, J., Feldwisch-Drentrup, H., Ihle, M., Navarro, V., Neufang, M., Teixeira, C., et al. (2012). The epilepsiae database: an extensive electroencephalography database of epilepsy patients. *Epilepsia* 53, 1669–1676. doi:10.1111/j.1528-1167.2012.03564.x

Korohoda, P., Kolodziej, J., and Stepien, J. (2013). Time-frequency analysis of accelerometry data for seizure detection. *Bio-Algorithms Med-Systems* 9, 65–71. doi:10.1515/bams-2013-0010

Koskimäki, H., Mönttinen, H., Siirtola, P., Huttunen, H.-L., Halonen, R., and Röning, J. (2017). "Early detection of migraine attacks based on wearable sensors: experiences of data collection using Empatica E4," in Proceedings of the 2017 ACM International Joint Conference on Pervasive and Ubiquitous Computing and Proceedings of the 2017 ACM International Symposium on Wearable Computers, Maui Hawaii, September 11 - 15, 2017 (ACM), 506–511. doi:10.1145/3123024.3124434

Kuhlmann, L., Karoly, P., Freestone, D. R., Brinkmann, B. H., Temko, A., Barachant, A., et al. (2018). Epilepsyecosystem.org: crowd-sourcing reproducible seizure prediction with long-term human intracranial EEG. *Brain* 141, 2619–2630. doi:10.1093/brain/awy210

Leal, A., Pinto, M. F., Lopes, F., Bianchi, A. M., Henriques, J., Ruano, M. G., et al. (2021). Heart rate variability analysis for the identification of the preictal interval in patients with drug-resistant epilepsy. *Sci. Rep.* 11, 5987. doi:10.1038/s41598-021-85350-y

Manso, A. F., Fred, A. L. N., Neves, R. C., and Ferreira, R. C. (2018). "Smart-wearables and heart-rate assessment accuracy," in *2018 IEEE international symposium on medical measurements and applications (MeMeA)* (Rome: IEEE), 1–5. doi:10.1109/MeMeA.2018.8438812

Martínez, C. G. B., Niediek, J., Mormann, F., and Andrzejak, R. G. (2020). Seizure onset zone lateralization using a non-linear analysis of micro vs. Macro electroencephalographic recordings during seizure-free stages of the sleep-wake cycle from epilepsy patients. *Front. Neurology* 11, 553885. doi:10.3389/fneur.2020.553885

McCarthy, C., Pradhan, N., Redpath, C., and Adler, A. (2016). "Validation of the Empatica E4 wristband," in *2016 IEEE EMBS international student conference (ISC)* (Ottawa, ON, Canada: IEEE), 1–4. doi:10.1109/EMBSISC.2016.7508621

Meisel, C., El Atrache, R., Jackson, M., Schubach, S., Ufongene, C., and Loddenkemper, T. (2020). Machine learning from wristband sensor data for wearable, noninvasive seizure forecasting. *Epilepsia* 61, 2653–2666. doi:10.1111/epi.16719

Nagai, Y., Jones, C. I., and Sen, A. (2019). Galvanic skin response (GSR)/Electrodermal/Skin conductance biofeedback on epilepsy: A systematic review and meta-analysis. *Front. Neurology* 10, 377. doi:10.3389/fneur.2019.00377

Nasseri, M., Nurse, E., Glasstetter, M., Böttcher, S., Gregg, N. M., Laks Nandakumar, A., et al. (2020). Signal quality and patient experience with wearable devices for epilepsy management. *Epilepsia* 61, S25–S35. doi:10.1111/epi.16527

Nepi, D., Sbrollini, A., Agostinelli, A., Maranesi, E., Di Nardo, F., Fioretti, S., et al. (2016). "Validation of the heart:rate signal provided by the zephyr BioHarness 3.0," in Proc. of the 43rd Computing in Cardiology Conference (CINC), Vancouver, BC, Canada, 11-14 September 2016 (IEEE), 361–364. doi:10.22489/CinC.2016.106-358

Obeid, I., and Picone, J. (2016). The temple university hospital EEG data Corpus. *Front. Neurosci.* 10, 196. doi:10.3389/fnins.2016.00196

Ollander, S., Godin, C., Campagne, A., and Charbonnier, S. (2016). "A comparison of wearable and stationary sensors for stress detection," in 2016 IEEE International Conference on Systems, Man, and Cybernetics (SMC), Budapest, Hungary, 09-12 October 2016 (IEEE), 004362–004366. doi:10.1109/SMC.2016.7844917

Orphanidou, C., and Drobnjak, I. (2017). Quality assessment of ambulatory ECG using wavelet entropy of the HRV signal. *IEEE J. Biomed. Health Inf.* 21, 1216–1223. doi:10.1109/JBHI.2016.2615316

Ranjan, Y., Rashid, Z., Stewart, C., Conde, P., Begale, M., Verbeeck, D., et al. (2019). RADAR-Base: open source mobile health platform for collecting, monitoring, and analyzing data using sensors, wearables, and mobile devices. *JMIR mHealth uHealth* 7, e11734. doi:10.2196/11734

Regalia, G., Onorati, F., Lai, M., Caborni, C., and Picard, R. W. (2019). Multimodal wrist-worn devices for seizure detection and advancing research: focus on the Empatica wristbands. *Epilepsy Res.* 153, 79–82. doi:10.1016/j.eplepsyres.2019.02.007

Shoeb, A. H. (2009). "Application of machine learning to epilepsy seizure onset detection and treatment,". Doutoramento, Harvard (MIT).

Sivathamboo, S., Friedman, D., Laze, J., Nightscales, R., Chen, Z., Kuhlmann, L., et al. (2021). Association of short-term heart rate variability and sudden unexpected Death in epilepsy. *Neurology* 97, e2357–e2367. doi:10.1212/WNL.0000000000012946

Simblett, S. K., Biondi, A., Bruno, E., Ballard, D., Stoneman, A., Lees, S., et al. (2020). Patients' experience of wearing multimodal sensor devices intended to detect epileptic seizures: A qualitative analysis. *Epilepsy & Behav.* 102, 106717. doi:10.1016/j.yebeh.2019.106717

Sivathamboo, S., Constantino, T. N., Chen, Z., Sparks, P. B., Goldin, J., Velakoulis, D., et al. (2020). Cardiorespiratory and autonomic function in epileptic seizures: A video-EEG monitoring study. *Epilepsy & Behav.* 111, 107271. doi:10.1016/j.yebeh.2020.107271

Smith, C. M., Chillrud, S. N., Jack, D. W., Kinney, P., Yang, Q., and Layton, A. M. (2019). Laboratory validation of hexoskin biometric shirt at rest, submaximal exercise, and maximal exercise while riding a stationary bicycle. *J. Occup. Environ. Med.* 61, e104–e111. doi:10.1097/JOM.0000000000001537

Swami, P., Panigrahi, B. K., Nara, S., Bhatia, M., and Gandhi, T. (2016). *EEG epilepsy datasets*. Publisher: Unpublished. doi:10.13140/RG.2.2.14280.32006

Swinnen, L., Chatzichristos, C., Jansen, K., Lagae, L., Depondt, C., Seynaeve, L., et al. (2021). Accurate detection of typical absence seizures in adults and children using a two-channel electroencephalographic wearable behind the ears. *Epilepsia* 62, 2741–2752. doi:10.1111/epi.17061

Tedesco, S., Sica, M., Ancillao, A., Timmons, S., Barton, J., and O'Flynn, B. (2019). Validity evaluation of the fitbit Charge2 and the garmin vivosmart HR+ in free-living environments in an older adult cohort. *JMIR mHealth uHealth* 7, e13084. doi:10.2196/13084

Truong, N. D., Kuhlmann, L., Bonyadi, M. R., Querlioz, D., Zhou, L., and Kavehei, O. (2019). Epileptic seizure forecasting with generative adversarial networks. *IEEE Access* 7, 143999–144009. doi:10.1109/ACCESS.2019.2944691

Van de Vel, A., Cuppens, K., Bonroy, B., Milosevic, M., Jansen, K., Van Huffel, S., et al. (2013). Non-EEG seizure-detection systems and potential SUDEP prevention: state of the art. *Seizure* 22, 345–355. doi:10.1016/j.seizure.2013.02.012

Vandecasteele, K., De Cooman, T., Gu, Y., Cleeren, E., Claes, K., Paesschen, W., et al. (2017). Automated epileptic seizure detection based on wearable ECG and PPG in a hospital environment. *Sensors* 17, 2338. doi:10.3390/s1710-2338

Verdru, J., and Van Paesschen, W. (2020). Wearable seizure detection devices in refractory epilepsy. *Acta Neurol. Belg.* 120, 1271–1281. doi:10.1007/s13760-020-01417-z

Vieluf, S., El Atrache, R., Cantley, S., Jackson, M., Clark, J., Sheehan, T., et al. (2022). Seizure-related differences in biosignal 24-h modulation patterns. *Sci. Rep.* 12, 15070. doi:10.1038/s41598-022-18271-z

Vijayan, V., Connolly, J. P., Condell, J., McKelvey, N., and Gardiner, P. (2021). Review of wearable devices and data collection considerations for connected health. *Sensors* 21, 5589. doi:10.3390/s21165589

Weenk, M., van Goor, H., Frietman, B., Engelen, L. J., van Laarhoven, C. J., Smit, J., et al. (2017). Continuous monitoring of vital signs using wearable devices on the general ward: pilot study. *JMIR mHealth uHealth* 5, e91. doi:10.2196/mhealth.7208

Whitmire, L., Voyles, S., Cardenas, D., and Cavazos, J. (2019). Diagnostic utility of continuous sEMG monitoring in a home setting-real-world use of the speac® system (p4. 5-012). *Neurology* 92.

Wong, S., Simmons, A., Rivera-Villicana, J., Barnett, S., Sivathamboo, S., Perucca, P., et al. (2023). Eeg datasets for seizure detection and prediction—A review. *Epilepsia Open* 8, 252–267. doi:10.1002/epi4.12704

frontiers | Frontiers in Physiology

TYPE Original Research
PUBLISHED 30 April 2024
DOI 10.3389/fphys.2024.1305171

OPEN ACCESS

EDITED BY
Ginés Viscor,
University of Barcelona, Spain

REVIEWED BY
Angelica Lodin-Sundström,
Mid Sweden University, Sweden
Dieter Böning,
Charité Medical University of Berlin, Germany
Pierre Louge,
Hôpitaux Universitaires de Genève (HUG), Switzerland

*CORRESPONDENCE
Thomas Kjeld,
thomaskjeld@hotmail.com

RECEIVED 30 September 2023
ACCEPTED 23 January 2024
PUBLISHED 30 April 2024

CITATION
Kjeld T, Krag TO, Brenøe A, Møller AM, Arendrup HC, Højberg J, Fuglø D, Hancke S, Tolbod LP, Gormsen LC, Vissing J and Hansen EG (2024), Hemoglobin concentration and blood shift during dry static apnea in elite breath hold divers.
Front. Physiol. 15:1305171.
doi: 10.3389/fphys.2024.1305171

Hemoglobin concentration and blood shift during dry static apnea in elite breath hold divers

Thomas Kjeld[1]*, Thomas O. Krag[1], Anders Brenøe[2], Ann Merete Møller[3], Henrik Christian Arendrup[2], Jens Højberg[4], Dan Fuglø[5], Søren Hancke[2], Lars Poulsen Tolbod[6], Lars Christian Gormsen[6], John Vissing[1] and Egon Godthaab Hansen[3]

[1]Copenhagen Neuromuscular Center, Rigshospitalet, University of Copenhagen, Copenhagen, Denmark, [2]Department of Clinical Medicine, Panum Institute, University of Copenhagen, Copenhagen, Denmark, [3]Department of Anesthesiology, Herlev Hospital, University of Copenhagen, Copenhagen, Denmark, [4]Department of Cardiothoracic Anesthesiology, Rigshospitalet, University of Copenhagen, Copenhagen, Denmark, [5]Department of Nuclear Medicine, Herlev Hospital, University of Copenhagen, Copenhagen, Denmark, [6]Department of Nuclear Medicine and PET Centre, Aarhus University Hospital, Aarhus, Denmark

Introduction: Elite breath-hold divers (BHD) enduring apneas of more than 5 min are characterized by tolerance to arterial blood oxygen levels of 4.3 kPa and low oxygen-consumption in their hearts and skeletal muscles, similar to adult seals. Adult seals possess an adaptive higher hemoglobin-concentration and Bohr effect than pups, and when sedated, adult seals demonstrate a blood shift from the spleen towards the brain, lungs, and heart during apnea. We hypothesized these observations to be similar in human BHD. Therefore, we measured hemoglobin- and 2,3-biphosphoglycerate-concentrations in BHD (n = 11) and matched controls (n = 11) at rest, while myocardial mass, spleen and lower extremity volumes were assessed at rest and during apnea in BHD.

Methods and results: After 4 min of apnea, left ventricular myocardial mass (LVMM) determined by ^{15}O-H_2O-PET/CT (n = 6) and cardiac MRI (n = 6), was unaltered compared to rest. During maximum apnea (~6 min), lower extremity volume assessed by DXA-scan revealed a ~268 mL decrease, and spleen volume, assessed by ultrasonography, decreased ~102 mL. Compared to age, BMI and VO_2max matched controls (n = 11), BHD had similar spleen sizes and 2,3-biphosphoglycerate-concentrations, but higher total hemoglobin-concentrations.

Conclusion: Our results indicate: 1) Apnea training in BHD may increase hemoglobin concentration as an oxygen conserving adaptation similar to adult diving mammals. 2) The blood shift during dry apnea in BHD is 162% more from the lower extremities than from the spleen. 3) In contrast to the previous theory of the blood shift demonstrated in sedated adult seals, blood shift is not towards the heart during dry apnea in humans.

KEYWORDS

cardiac PET/CT, cardiac MR (CMR), spleen ultrasound examination, dual x-ray absorptiometry (DXA), Bohr effect, free diving, myocardial mass, lower extremity blood volume

In memoriam Poul-Erik Paulev, 1935 - 2017

Introduction

Diving mammals like the adult Weddell seals (WS) possess an adaptive higher hemoglobin concentration and Bohr effect than pups and during simulated dives, sedated adult seals have been demonstrated to direct blood from the spleen to the heart, lungs and brain to meet metabolic requirements during dives, when partial pressures of oxygen (PaO_2) decrease to 3.2 kPa (Zapol et al., 1979; Kjekshus et al., 1982; Kjekshus et al., 1982; Qvist et al., 1986). Elite breath-hold divers (BHD) are adapted to tolerate PaO_2 to similar levels as demonstrated in the diving and foraging adult seals (Kjeld et al., 2018; Kjeld et al., 2021a; Kjeld et al., 2021c). However, in contrast to sedated seals, BHD decrease all internal cardiac chamber volumes ~40% during apnea, whereas left ventricle wall thickness increases (Kjeld et al., 2021c), and the question is, whether the left ventricle wall thickness increase could be due to myocardial contraction or increased internal myocardial wall blood volume and hence a blood shift, as demonstrated in the adult seal? The adult hooded seals also have large spleens constituting 4% of their body volume and are capable of expanding the total circulating blood volume by up to 13% during dives as part of the mammalian diving response, and hereby increasing erythrocyte gas exchange capability (Hurford et al., 1996; Foster and Sheel, 2005; Kjeld et al., 2009; Kjeld et al., 2021a). These findings in diving mammals have led to studies of human apnea diving, which demonstrated splenic volume reductions of up to 170 mL and conclude that the spleen is an important reservoir of erythrocytes (Schagatay et al., 2001; Schagatay et al., 2005; Prommer et al., 2007; Schagatay et al., 2012; Ilardo et al., 2018; Bouten et al., 2019; Persson et al., 2023). However, considering that an average 70 kg man has a spleen size ~200 mL, a blood volume of 5.5 L, of which 20% is in the musculoskeletal system and the lower extremities alone contain volumes of ~ 2.2 L of blood (Karpeles and Huff, 1955; Adams and Albert, 1962), the question is whether lower extremity blood volume would be at least equally as important as the spleen to direct blood to the vital organs during apnea diving in humans?

As an adaptive response to chronic hypoxia, high-altitude species may also have higher concentrations of hemoglobin, changed standard half saturation pressures and a different Bohr effect than those of their lowland relatives (Vargas and Spielvogel, 2006) although this has been debated (Lenfant et al., 1968a; Winslow, 2007). The Bohr effect is a physiological phenomenon first described in 1904 by the Danish physiologist Christian Bohr: the binding affinity of the hemoglobin to oxygen is inversely related both to acidity and to the concentration of carbon dioxide (CO_2) (Benner et al., 2023). Hence, the Bohr effect refers to the shift in the oxygen dissociation curve caused by changes in the concentration of CO_2 or the pH of the environment. Since CO_2 reacts with water to form carbonic acid, an increase in CO_2 – like during apnea diving – results in a decrease in blood pH, resulting in release of oxygen by hemoglobin. Harbour seals also have a large fixed-acid Bohr coefficient at 37°C and increasing with temperature (Willford et al., 1990) – in contrast to humans (Boning et al., 1978). This relatively large value for the Bohr coefficient is similar to those reported for the Northern Elephant seals, Bladdernose seals, and Weddell Seals, and may facilitate oxygen off-loading as acidosis develops during a dive (Willford et al., 1990).

In competitive BHD, bouts of static and dynamic apnea increase plasma erythropoietin (Richardson et al., 2005; Kjeld et al., 2015). Hence, it may be that also the human elite BHD, that endure apneas of up to 11 mins and swimming more than 300 m, or going beyond 200 m in depth, all on a single breath of air (www.aida-international.org), would possess increased hemoglobin concentrations and oxygen offloading as an adaptation to (diving) hypoxia similar to diving mammals and high-altitude species.

Therefore, this study quantified 1) the oxygen binding properties of hemoglobin and 2,3 biphosphoglycerate (2,3-BPG) at rest in BHD as compared to matched controls, and 2) the left ventricle myocardial mass, spleen volume and lower extremity volume during apnea in elite BHD. BHD and controls were matched for age, body mass index (BMI), VO_2max and spleen size (Chow et al., 2016). To ensure similar adaptations in the BHD in this study towards diving hypoxia as diving mammals, we required as inclusion criteria for BHD that they could hold their breath for a minimum of 5 min (Kjeld et al., 2018; Kjeld et al., 2021c). Also, to ensure similar adaptations as diving mammals towards diving hypoxia, we instructed BHD to pause aerobic training for 4 weeks before blood sampling (Bennett et al., 2001; Kjeld et al., 2018). Likewise, controls were instructed to pause anaerobic training for 4 weeks before blood sampling. Hence, we hypothesised that BHD as compared to controls would possess similar adaptations including binding properties of the hemoglobin to diving hypoxia as adult diving mammals, and also a blood shift from the spleen and lower extremities during apnea.

Methods

22 healthy male, non-medicated, non-smoking participants were included in the study as approved by the Regional Ethics Committee of Copenhagen (H-1-2013-060). All clinical investigations have been conducted according to the principles expressed in the Declaration of Helsinki. Informed consent, written and orally, have been obtained from the participants.

Eleven participants were elite breath hold divers (BHD, age 44 ± 6 years), who were able to hold their breath for more than 5 min. For comparison we studied eleven judo athletes matched for morphometric variables (age, weight, body mass) and $\dot{V}O_2$max (Table 1; Figure 2) as described below. Judo athletes primarily train aerobic, and we have previously described judo athletes as controls in studies of BHD (Kjeld et al., 2018).

All BHD had ranked among national top 10, three of the participating free divers ranked among international top 10 and one was a 2016 outdoor free-diving World champion, one was a silver medalist at 2022 World Championships, and one was a World record holder.

All the matched controls were either judo or jiu-jitsu black belts, all were medalists at national championships, and all except one were active fighters.

This study included the following measurements of the BHD and matched controls (Figure 2; Table 2): Collection of blood samples for hemoglobin and 2,3-BPG at rest, a $\dot{V}O_2$ max test, ultrasonography of the spleen (US) at rest for both BHD and controls, whereas cardiac magnetic resonance imaging (cardiac MRI), positron emission tomography/computed tomography (PET-CT), ultrasonography of the spleen

TABLE 1 Participants characteristics (n = 11 BHD & 11 controls).

	Divers	Controls	p
No. participants	11 males	11 males	NS
Age (years)	44 ± 2	37 ± 2	NS
Static breath hold personal best (seconds)	381 ± 15	N/A	NS
Height (cm)	189 ± 2	183 ± 1	0.015
Weight (kg)	83 ± 2	82 ± 2	NS
Body Mass Index (kg/m^2)	23.3 ± 0.8	24.6 ± 0.6	NS
Spleen Volume/mL	230 ± 29	258 ± 30	NS
Maximal oxygen uptake (ml O_2/(min*kg)	51.1 ± 2.7	56.8 ± 2.5	NS

Basic morphometric data. Values are mean ± Standard error of mean. p: level of significance. NS: non-significant. BHD, breath hold divers.

TABLE 2 BHD (breath hold divers) participation in sub studies: Hb (hemoglobin), 2,3-BPG (2,3 biphosphoglycerate), CMRI (cardiac magnetic resonance imaging of left ventricle myocardial mass), PET-CT (positron emission tomography—computed tomography of left ventricle myocardial mass), US (ultrasound of the spleen volume), DXA (Dual Energy X-Ray Absorptiometry of the lower extremity volume).

BHD	Hb	2,3-BPG	CMRI	PET-CT	US	DXA
1	X	X	X	X		
2	X	X	X	X	X	X
3	X	X	X	X	X	X
4	X	X	X	X	X	X
5	X	X	X	X	X	X
6	X	X	X	X	X	X
7	X	X			X	X
8	X	X			X	X
9	X	X			X	X
10	X	X			X	X
11	X	X			X	X
Total	11	11	6	6	10	10

(US), and Dual Energy X-Ray Absorptiometry (DXA) measurements of the lower extremities during maximum apnea for BHD to ensure maximum cardiovascular response (Kjeld et al., 2021a).

2,3-BPG measurements

Before taking blood samples from participants, BHD were carefully instructed to refrain from aerobic exercise for 4 weeks, and controls to refrain from anaerobic exercise for 4 weeks: we assumed that this respectively would decrease and increase levels of 2,3-BPG in BHD and controls (Lenfant et al., 1968b; Willford et al., 1990). However, these instructions did overall not change any habits of the subjects in the study.

Blood samples were taken from an antecubital vein on the first day of the study at rest in a supine position.

To prepare samples for 2,3-BPG measurement, 2 mL of venous blood in heparinized tubes was collected, placed immediately on ice, deproteinized with 0.6 M perchloric acid (Sigma-Aldrich, Saint Louis, MO, United States) to lyse red blood cells, and neutralized with 2.5 M potassium carbonate (Sigma-Aldrich, Saint Louis, MO, United States). The supernatant was kept for at least 60 min in an ice bath and centrifuged at 3,000 × g for 10 min. The supernatant was stored at 28°C, and 2,3-DPG levels were measured using the either Roche diagnostic kit (n = 3 BHD & n = 4 controls; no. 10148334001, Basel, Switzerland) or Cusabio Human 2,3- BPG (n = 8 BDH & n = 7 controls) ELISA Kit (Houston, TX, United States).

The Roche 2,3-DPG assay is based on enzymatic cleavage of 2,3-BPG, and oxidation of nicotinamide adenine dinucleotide recorded by spectrophotometry. The 2,3-BPG assays were performed in three batches and in the range of 0.02–0.15 µmol (n = 3 BHD and 4 controls). Concentration of 2,3-BPG was calculated according to the procedure proposed by the manufacturer. The 2,3-BPG levels were normalized to the corresponding hematocrit value from the same sample. Since the concentration of 2,3-BPG rapidly decreases during storage (Hamasaki and Yamamoto, 2000), the procedure for determining the 2,3-BPG level was performed immediately after taking the blood samples. Determination of 2,3-BPG level was carried out in duplicate on each sample. The reliability of 2,3-BPG measurement was evaluated based on the coefficient of variation (CV) using the test–retest method (Atkinson and Nevill, 1998). CV for 2,3-BPG was between 0.30 and 0.76%, which indicates that these measurements are characterized by a high degree of reliability.

Production of the Roche assay had ceased when the remaining participants participated. Hence, for the remaining participants (n = 8 BHD and 7 controls), 100 µL plasma was analyzed in triplicate for each participant using a 2,3-BPG ELISA kit manufactured by Cusabio (Houston, TX). Briefly, analysis of samples were done according to manufacturer's instructions. All incubation was done at 37 degrees and absorbance was read at 450 nm, using wavelength correction by subtracting absorbance reading at 570 nm from absorbance read at 450 nm (Thermo Scientific Multiskan Go, Waltham, MA). Concentrations of 2,3-BPG were determined, using the average of the triplicate absorbances for each sample, from a four-parameter logistic curve of the absorbance of the standard at various concentrations.

The blood sample analyzes of two controls and one BHD failed and could not be repeated.

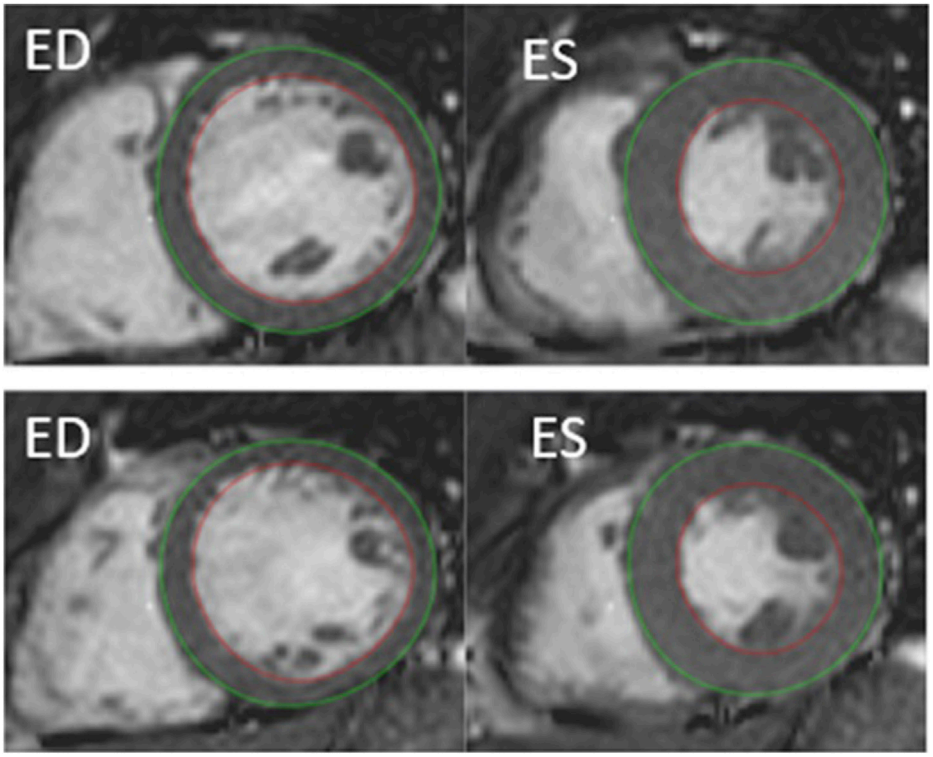

FIGURE 1
Example of cardiac MRI determined myocardial mass by semi-automatic segmentation of the left ventricle, short-axis view. Delineation of endocardial contour in red and epicardial contour in green. ED, end diastolic. ES, end systolic. Top: rest. Bottom: after 4 min of apnea.

Hb was determined on an ABL 90 Flex (Radiometer, Bronshoj, Denmark). Concentration of 2,3-BPG in mM was calculated per mM Hb, Analysis of samples from two controls and one BHD failed and could not be repeated.

$\dot{V}O_2$ max

After blood sampling, participants completed a standardized warm-up followed by an incremental cycle test (Lode®) starting at a workload of 50 W and increasing 50 W every minute until exhaustion (Astrand and Ryhming, 1954). The highest recorded 30 s average oxygen uptake ($\dot{V}O_2$) during the test was defined as $\dot{V}O_2$max. For recognition of true $\dot{V}O_2$max, three of five criteria had to be met: individual perception of exhaustion, respiratory exchange ratio >1.15, plateau of $\dot{V}O_2$ curve, heart rate approaching age-predicted maximum and inability to maintain a pedaling frequency above 70 rpm (Table 1).

Cardiac magnetic resonance imaging: image acquisition

On a separate day, the 6 participants with the longest breath holds refrained from physical exercise and consumption of alcohol or caffeine for 24 h before the following was performed: Imaging was performed in a 1.5 T cardiac MRI imaging system (Achieva, Philips Medical System, The Netherlands). Subjects warmed up by holding their breath three consecutive times with individual duration to maximize the diving response including the blood shift (Kjeld et al., 2009; Kjeld et al., 2021c). Cine images were acquired at 1) rest during a short (<20 s) apnea at end-expiration with open pharynx, 2) after 4 min of dry static apnea after glossopharyngeal insufflation (Seccombe et al., 2006). Images were collected shortly before end of apnea before breathing, and participants were instructed to stay as calm as possible during imaging to avoid imaging artefacts. Left ventricular myocardial mass was collected in the transversal and double-oblique short axis stacks with 8 mm thick slices and 25% gap. Cine imaging was performed with retrospectively ECG-gated steady-state free precession sequences (SSFP) reconstructed to 25 phases covering the entire cardiac cycle using the following settings: TR/TE 3.3/1.6 ms, flip angle 60°; and spatial resolution 1.3 × 1.3 × 8 mm^3 as previously described (Kjeld et al., 2021c).

Cardiac magnetic resonance imaging: image analysis

Left ventricular myocardial mass was determined in end-diastole (ED) and end-systole (ES, Figure 1). Data were analyzed

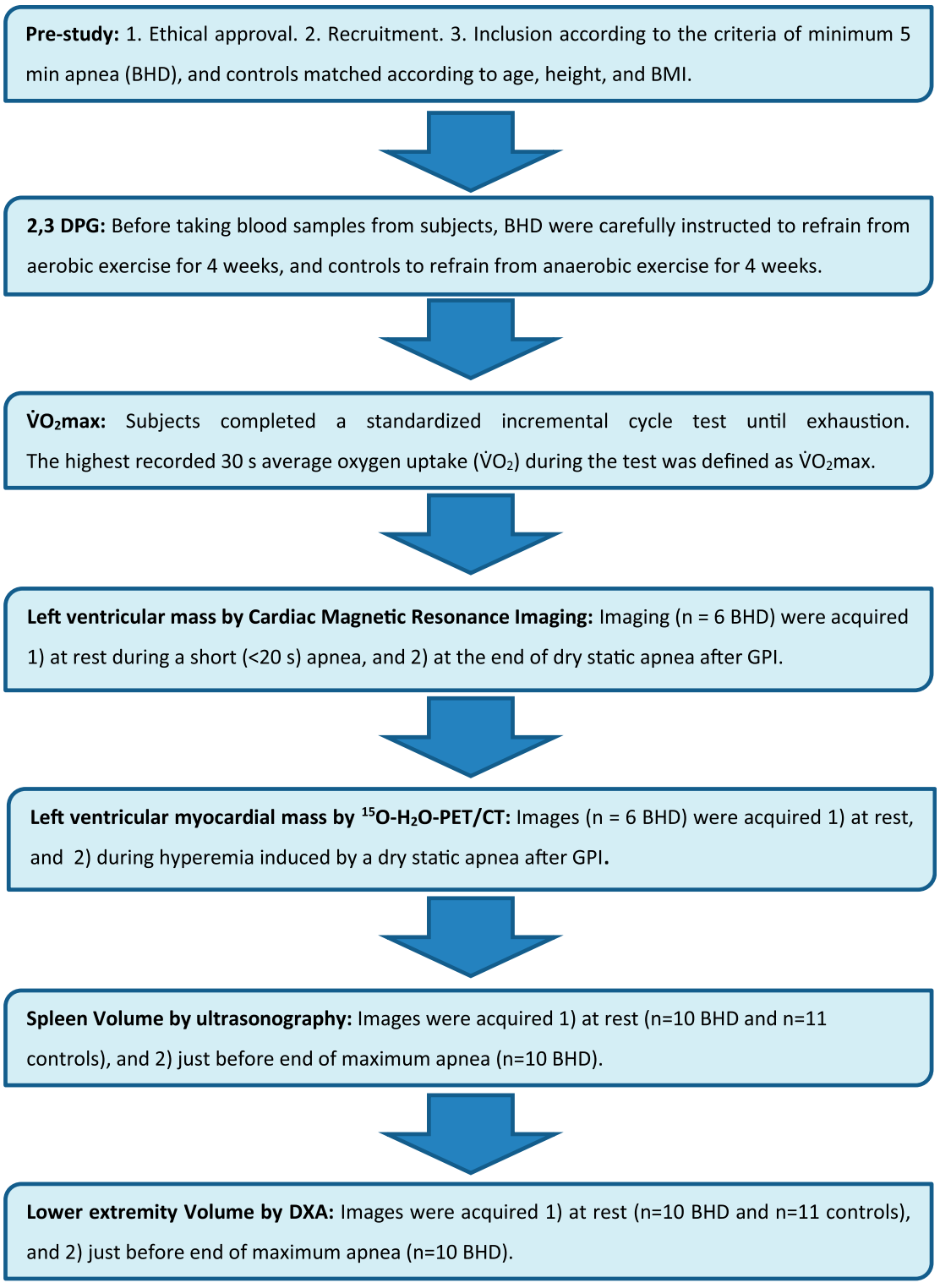

FIGURE 2
Flow chart.

by a level three nuclear physiologist and a level one Cardiac MRi cardiologist using dedicated software (Segment ® version 2.1, Lund, Sweden). Image artefacts were carefully avoided especially during involuntary breathing movements (Heiberg et al., 2010) and using a fitting algorithm in the Segment software ® as previously described (Bidhult et al., 2016; Kjeld et al., 2021c).

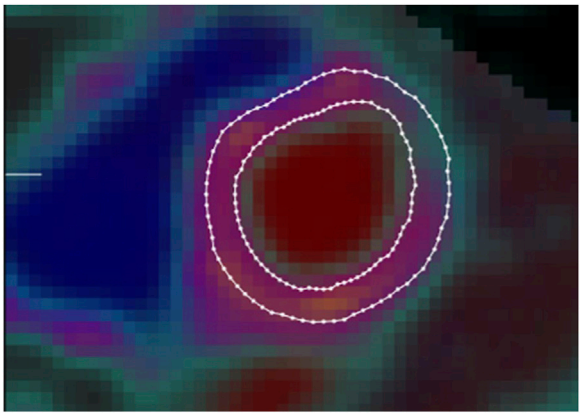

FIGURE 3
Example of left ventricular myocardial mass image as determined by ^{15}O-H_2O-PET/CT using semi-automatic segmentation of the left ventricular wall on parametric images of perfusable tissue fraction. Borders of endocardium (inner circle) and pericardium (outer circle) defined by delineated lines.

^{15}O-H_2O-PET/CT determined left ventricular myocardial mass: imaging protocol and image reconstruction

On a separate day, the same six participants who had cardiac MRI were recruited for an additional ^{15}O-H_2O-PET/CT study. The participants in the ^{15}O-H_2O-PET/CT sub-study were required to hold their breath for 5 min while lying in the PET/CT scanner in the supine position with arms raised above the head. They were instructed to refrain from intake of chocolate, to refrain from strenuous physical exercise for 1 day and to be fasting for at least 6 h before the study.

^{15}O-H_2O-PET/CT data were obtained in list mode on a GE Discovery MI Digital Ready PET/CT system (GE, Milwaukee, WI, United States) as described previously (Kjeld., et al., 2021a). In short, the participants were scanned using ^{15}O-H_2O cardiac perfusion PET/CT 1) at rest, 2) during hyperemia induced by a dry static apnea after glossopharyngeal insufflation (Seccombe et al., 2006) and after a warm-up of three individual consecutive apneas to maximize the diving response including the blood shift (Kjeld et al., 2009), and 3) in the recovery phase 4 min after the apnea.

^{15}O-H_2O-PET/CT determined left ventricular myocardial mass: image analysis

Left ventricular mass (LVM) was quantified by semi-automatic segmentation of the LV wall on parametric images of perfusable tissue fraction (PTF) as previously described (Sorensen et al., 2021). In short, parametric images were obtained by kinetic analysis of the dynamic ^{15}O-H_2O-PET/CT scan using a 1-tissue compartment model with image derived input from cluster analysis (Harms et al., 2011)In the model, PTF accounts for partial volume effects on the difference between myocardial blood flow estimated from ^{15}O-H_2O wash-in and wash-out. The PTF parameter is more robust for segmentation compared to myocardial blood flow since it is less affected by perfusion defects and segmentation has been shown to be highly reproducible (Sorensen et al., 2021) (Figure 3).

Spleen volume

On a separate day, the participants had ultrasonography (US) of the spleen using an Esaote ® scanner (Mylab, Omega, Genova, Italy, 2017) with a 3.5/5-MHz convex transducer probe. Spleen metrics were assessed by using defined standard algorithms according to Koga T. (1979). With the participants in the supine position after approximately 15 minutes of rest, the examination started in the posterior axillary line in the approximate area of the 10th rib through an intercostal space to identify the longitudinal view of the spleen with the hilus. In this position, maximum length, and width of the spleen was measured on a frozen high resolution ultrasound image.

During breath holds (BHD only), the diaphragm changes the position of the spleen, and to diminish measuring artefacts, we decided only to measure the spleen in transverse axis. Hence, the maximum length and the maximum width of the spleen was determined, and according to the formula by Koga T. (1979), the spleen volume calculates to

$$V = 7.53 \text{ x } 0,8 \text{ x } (\text{length x width}) - 77,56$$

The above was performed minimum three times in all participants at rest.

After a warm-up of three individual consecutive submaximal apneas with short pauses (minimum 4 and maximum 7 minutes pause) in between (Kjeld et al., 2014), BHD performed a following maximum apnea to maximize the diving response including the blood shift (Kjeld et al., 2009). Hence, the above-described measurements at rest were repeated after 4 min of maximum apnea and up to 4 additional measurements were made until just before termination of apnea in the BHD (Figure 4).

Lower extremity DXA scan

On a separate day, three consecutive whole body scans were performed, and data included total body weight bone mineral content, fat free mass and lean mass. The first and the third scans were routine whole-body scans at rest. After the first scan, the BHD then performed three sub-maximal apneas with short pauses (minimum 4 and maximum 7 minutes) in between to warm up (Kjeld et al., 2014), and BHD were instructed to do similar a warm-up as described above during the ultrasonography study. The second scan was following a short pause after the warm-up and during maximum apnea, of which the last part of the scan including the legs, was timed to be initiated 3 minutes and 30 seconds after initiation of apnea and

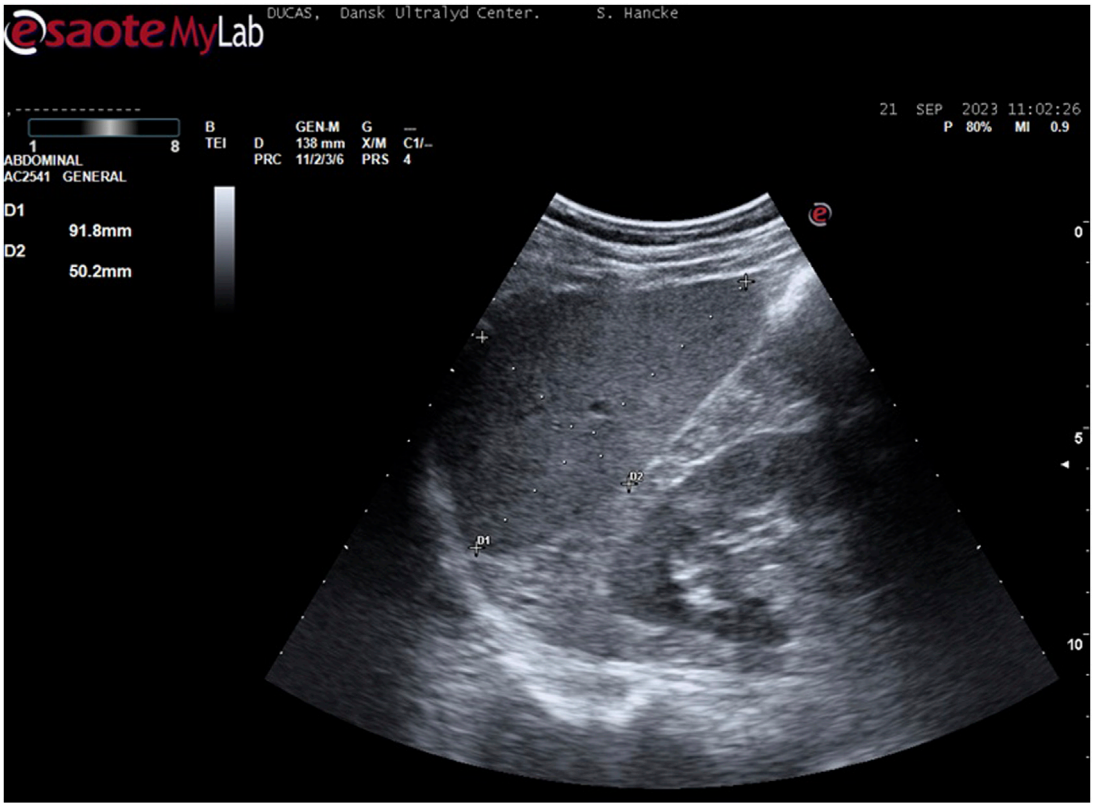

FIGURE 4
Example of spleen measurement (participant 6): With the participant in the supine position, the examination started in the posterior axillary line in the approximate area of the 10th rib through an intercostal space to identify the longitudinal view of the spleen with the hilus. In this position, maximum length and width were measured.

TABLE 3 ^{15}O-H_2O-PET/CT and cardiac MRi left ventricle myocardial mass (LVMM), ultrasonography assessed spleen volume and DXA lower extremities total mass and bone mineral content (BMC) of 11 breath hold divers.

	Rest	Apnea
^{15}O-H_2O-PET/CT assessed LVMM/g	149 ± 11	146 ± 12
Cardiac MRi assessed LVMM/g	116 ± 6	112 ± 5
Ultrasonography assessed spleen volume/mL	230 ± 29	128 ± 21 (*1, *2)
DXA assessed lower extremities total mass (g)	23,792 ± 1,084	23,546 ± 1,077 (*1, *2)
DXA assessed lower extremities BMC (g)	982 ± 37	984 ± 38

Basic morphometric data. Values are mean ± Standard error of mean. *1: $p < 0.001$ compared to rest. *2: $n = 10$: 1 subject moved abroad during the study.

finished after 4 minutes of apnea to ensure a maximum diving response (Kjeld et al., 2021a). There was no repositioning between scans except for movement of one arm in one case, where the diver needed to adjust the nose clip. The Table 3 shows changes in mass in tissue compartments of the lower extremities. Note that the total mass (including blood pool) changes whereas the bone mineral content remains unchanged indicating minimal movement of the participant. The change in mass of the lower extremities is attributed to a change in blood pool as other tissue compartments are not as volatile to change. All scans were performed on a GE Lunar iDXA scanner (GE Medical Systems, Madison, WI). Regions of interest over the legs were analyzed according to the method used by (Gjorup et al. (2017) (Figure 5).

Statistical analysis

To test for imbalances in the variables in our study with a limited number of participants, we performed a power calculation: The sample size of 6 participants in the ^{15}O-H_2O-PET/CT sub-study was calculated for the primary outcome (myocardial blood flow) of the study previously published by our group (Kjeld et al., 2021c). A power

10.3389/fphys.2024.1305171

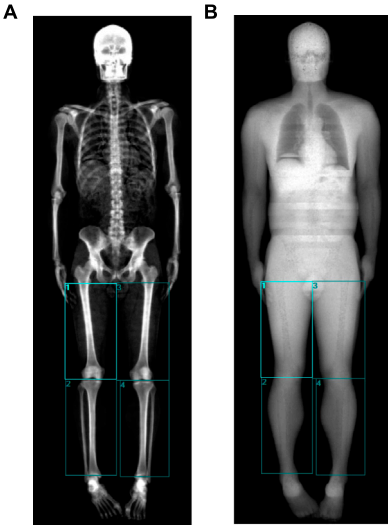

Participant 2	Baseline	End of 5:50 min apnea	6 min after apnea	Change
Total mass [g]	23875	23650	23538	337
BMC [g]	1129	1136	1135	-6

FIGURE 5
Example of DXA-scan (participant 2) with manually drawn regions in the lower extremities using bone tissues **(A)** and soft tissue **(B)** images to place regions. The table shows changes in mass of the lower extremities (sum of the four regions) before and after 5 min 50 s breath hold. Note that the bone mineral content (BMC) remains unchanged, indicating minimal movement of the participant (A image).

calculation was performed *post hoc* but based on the test-retest standard deviation of 19 g determined by Sorensen et al. (Sorensen et al., 2021). The current analysis had a power of 80% to detect a difference of at least 55 g. A p-value <0.05 was considered statistically significant. This was also the basis for the sample size of the sub study of cardiac MRI, and also the other sub-studies as the latter had more participants.

Variables are presented as mean ± standard error of the mean (SEM). Data were analyzed by Sigma-Plot ® using one-way repeated measures ANOVA. Holm-Sidaks method posthoc was used to evaluate differences between the collected data during rest, apnea, and recovery. A p-value <0.05 was considered statistically significant.

Results

BHD were higher (189 ± 2 cm) than controls (183 ± 1 cm, p = 0.015), but their spleen volumes were similar (Tables 1, 3).

Compared to the matched controls, the BHD had similar content of 2,3-BPG (BHD 0.138 ± 0.025 vs. controls 0.119 ± 0.009 mM, p = 0.534), but they had a higher concentration of hemoglobin (p = 0.038; Figure 6).

Subgroups of BHD who underwent cardiac PET-CT, cardiac MRI, ultrasonography of the spleen and DXA, respectively, were not significantly different when comparing their age, height, weight, BMI, $\dot{V}O_2$max and apnea duration (Table 1).

After 2 and 4 min of apnea, ^{15}O-H_2O-PET/CT determined left ventricular myocardial mass (149 ± 11 g) was unaltered as compared to rest (146 ± 12 g; n = 6). Images of one participant were of poor quality and could not be repeated. Therefore, results from only 5 participants could be obtained from this protocol.

After 4 min of apnea, cardiac MRI determined left ventricular myocardial mass (116 ± 6 g) was unaltered as compared to rest (112 ± 5 g; n = 6).

Spleen volumes at rest were not different between controls (n = 11) and BHD (n = 10: one participant moved abroad during the study; Table 1). During maximum apnea (370 ± 67 s) the spleen volumes of BHD decreased from 230 ± 29 to 128 ± 21 mL (p < 0.001; Table 3).

Whole-body DXA-scan of BHD revealed a total body weight of 81.2 ± 2.8 kg (n = 10: one participant moved abroad during the study).

During maximum apnea (343 ± 9 s) the lower extremity mass decreased from 23,792 ± 1,084 g at rest to 23,741 ± 1,081 g (p = 0.2) after 4 min of apnea and decreased further at the end of apnea to 23,546 ± 1,077 g (p < 0.001; Table 3). The bone mineral content in the regions remained unchanged indicating minimal movement of the participants (rest 982 ± 37 g, during apnea 984 ± 38 g, after apnea 984 ± 38 g).

Discussion

The main and novel findings of our study are as follows: After a warm-up of three consecutive apneas, BHD have 1) unaltered left ventricle myocardial mass after 2–4 min of apnea, 2) a decreased spleen volume by ~102 mL during maximum apnea, and 3) a decreased lower extremity weight by 268 g after maximum apnea, indicating 268 mL less blood volume. These results indicate that the blood shift during apnea in elite BHD– at least partly– comes from the lower extremities and from the spleen, but the blood shift is not towards the heart in contrast to observations in sedated adult diving mammals. The present study also demonstrated that BHD have a higher concentration of hemoglobin, but similar 2,3-BPG levels as compared to controls matched for BMI, age, spleen volume and $\dot{V}O_2$max.

Our results demonstrate for the first time in BHD, that the blood shift during maximum apnea after glossopharyngeal insufflation is only partly similar to the blood shift found in other diving mammals. Also, we suggest that the higher hemoglobin in BHD as compared to controls is an adaptation to sustain hypoxia during dives similar to adult diving mammals, that have higher hemoglobin mass and larger spleens relative to terrestrial mammals.

Relatively large Bohr effects are observed in adult Harbour seals, killer whales (Lenfant et al., 1968a) and Northern Elephant seals (Willford et al., 1990), especially in tissues with low oxygen content, for example, their skeletal muscles. Previously we have demonstrated a mitochondrial adaptation to hypoxia in the skeletal muscles of BHD similar to the adult northern elephant seal (Kjeld et al., 2018). As adult seals have a higher mitochondrial respiratory capacity and higher muscular myoglobin concentration than juvenile seals, which are not yet fully matured and adapted to long dives (Kanatous et al., 2008; Chicco et al., 2014), the above suggests that adaptations leading

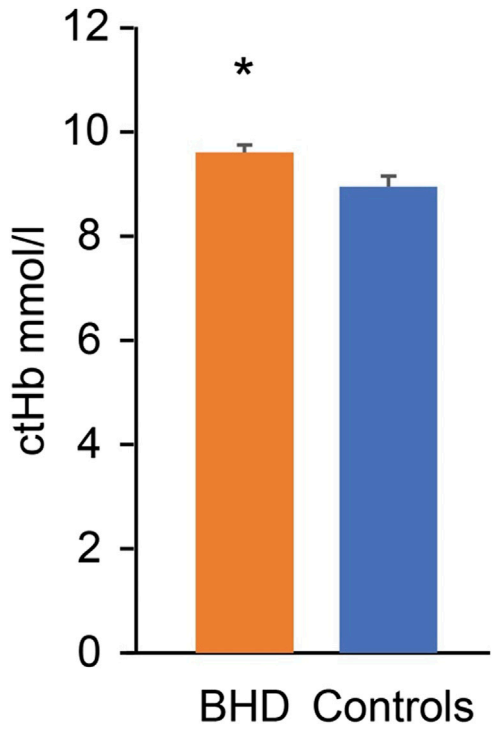

FIGURE 6
Hemoglobin concentration (ctHb) in breath hold divers (BHD, 9.7 ± 0.1 mmol/L) as compared to controls (9.1 ± 0.2 mmol/L). *: p = 0.038. Error bars: Standard error of the mean.

to increased skeletal muscle oxygen storage and diffusion capacity is associated with improved diving performance. Hence, a similar Bohr effect as demonstrated in diving mammals could be expected in the BHD in our study could be expected. However, Bohr effects in BHD and controls in our study were similar, whereas hemoglobin concentrations differed: Accordingly, no high altitude training studies have demonstrated permanent changes in Bohr effects or 2,3-BPG content nor permanently in hemoglobin concentration after returning from high altitude (Gore et al., 2006; Millet et al., 2010; Faiss et al., 2013): For example, Ploszczyca K. et al. demonstrated a decrease in 2,3-BPG just after exercise, likely due to changes in pH and CO_2 (Ploszczyca et al., 2021) and Elia et al., demonstrated higher hemoglobin levels, but lower mean cell volume and similar hematocrits in BHD compared to BMI matched controls, but not matched for $\dot{V}O_2$max (Elia et al., 2019). Our previous studies included BHD and controls with comparable levels of hemoglobin (Kjeld et al., 2018; Kjeld et al., 2021a; Kjeld et al., 2021c), but BHD in the previous studies were not instructed as in the present study to refrain from aerobic exercise 4 weeks before blood samples were taken and similarly for controls to refrain from anaerobic exercise for 4 weeks before blood samples were taken.

Hence, our results indicate that apnea training in BHD as compared to $\dot{V}O_2$max matched controls may increase hemoglobin concentration, however within normal reference values, but not 2,3-BPG.

Adult seals have increased hematocrits as compared to pups (Thomas and Ono, 2015). Also, South American natives living in high altitude with chronic hypoxic exposure have higher hemoglobin concentrations, than those of their lowland relatives (Boning et al., 1978; Vargas and Spielvogel, 2006; Storz and Moriyama, 2008; Böning, 2019). These natives are also demonstrated to decrease lactate concentrations during maximum exercise (Ge et al., 1994; Hochachka et al., 2002), similar to elite BHD during max apneas (Kjeld et al., 2021a; Kjeld et al., 2021a; Kjeld et al., 2021b; Kjeld et al., 2021c; Kjeld et al., 2021c). The increased hematocrits in high altitude natives due to hypobaric living are of interest in lowland living endurance athletes (Faiss et al., 2013), and hence hypobaric training has had focus to cause increased hematocrits in these athletes (Zelenkova et al., 2019), however, effects remain unproven (Hauser et al., 2016; Hauser et al., 2017). Accordingly, all the participants in our study had hemoglobin levels within normal range Hence, the explanation for an adequate oxygen supply to tissues under intermittent hypoxic conditions in BHD are not solely the oxygen carrier capacity in the blood, but also in the tissues, including the skeletal muscles similar to diving mammals, as demonstrated previously (Kjeld et al., 2018): relative to comparable terrestrial mammals– the skeletal muscles of seals and sea lions have higher mitochondrial volume densities and correspondingly higher citrate synthase activity, higher beta-hydroxyacyl CoA dehydrogenase activity and thus a higher capacity for fatty acid catabolism for aerobic ATP production (Kanatous et al., 2002). These adaptations may be speculated to result in higher mitochondrial respiratory capacity, but strikingly, the oxidative phosphorylation capacity of the northern elephant seal muscle is generally lower than in non-diving humans (Chicco et al., 2014). Interestingly, the skeletal muscles of BHD, compared to matched aerobic athletes, are also characterized by lower mitochondrial oxygen consumption both during low leak and high electron transfer system respiration indicating slow muscle oxygen consumption (Kjeld et al., 2018).

The movement pattern of the Northern Elephant Seal is impressive: they travel up to 13.000 miles per year, but swimming is slow: 1-2 m per second with less than 1 swimming stroke per second (Adachi et al., 2014). This swimming pattern is similar to elite BHD during their competitions and anaerobic exercise. Aerobic exercise increases blood flow 10-fold in the lower extremities of untrained individuals and up to 16 times in endurance cyclist and swimmers (~ 4,500 mL/min) (Walther et al., 2008). In comparison, the blood shift during apnea mediated by the contraction of the human spleen is ~ 102 mL in the present study. The human spleen contains 2-3% of total erythrocytes mass or 20–40 mL of erythrocytes (Wadenvik and Kutti, 1988), of which– if all can be assumed to be released– would increase blood volume in our study by ~ 256 mL. In our study we demonstrated that blood volume expelled from the lower extremities is 268 mL during dry apneas in BHD, and hence the legs are reservoir of blood volume of at least equal importance as compared to the spleen in humans (Schagatay et al., 2005; Schagatay et al., 2012; Ilardo et al., 2018): Diving mammals have short limbs with high content of myoglobin (Wright and Davis, 2006) in contrast to elite BHD (Kjeld et al., 2018), and the size of for example, the spleen of the hooded seals (Cystophora cristata, weighing ~ 250 kg) is up to 4% of the total body mass, and expels ~ 13% of the total blood volume during dives (Cabanac et al., 1997). Accordingly, the physiological characteristics observed in adult diving mammals during apnea and underwater

swimming are therefore not similar to terrestrial mammals during exercise: During aerobic exercise, terrestrial mammals increase ventilation, heart rate, cardiac output, and peripheral vasodilation, and the latter increases skeletal muscle perfusion (Wagner, 1991). By contrast, adult diving mammals during apnea and underwater swimming are characterized by bradycardia, decreased cardiac output and peripheral vasoconstriction including contraction of the spleen, which collectively is known as the dive response, and this physiological adaptive phenomenon has so far been interpretated as similar in elite BHD (Kjeld et al., 2009; Kjeld et al., 2014; Kjeld et al., 2015; Kjeld et al., 2018; Kjeld et al., 2021a; Kjeld et al., 2021c): A blood shift has been measured with ultrasonography and by injecting microspheres in anesthetized adult seals, placed with their heads downwards immersed in ice water, and it included centralization of blood to the brain, heart and lungs, and hence all peripheral tissue, including muscles and splanchnic organs, have reduced convective oxygen delivery resulting from both hypoxic hypoxia and ischemic hypoxia (Zapol et al., 1979; Hurford et al., 1996). However, studies of restrained and sedated seals during apnea, may demonstrate the physiological consequence of the sedation rather than the dive response, as the sedation depresses the cardiovascular system including the myocardial regional oxygen supply (Kanto, 1988), and cannot be compared to the foraging animal with an increased metabolic demand during their dives with concomitant hypoxia. Yet, our previous study demonstrated that left ventricle wall thickness increases during apnea in BHD, but that all internal cardiac chamber volumes decreases ~ 40% (Kjeld et al., 2021c). As the results of the present study indicates unaltered myocardial mass during apnea in BHD as compared to rest, we suggest that there is not a blood shift towards the heart in BHD as observed in sedated adult seals during apnea. Together these results indicates a remodeling of the myocardium during apnea and we suggest the remodeling to be similar as observed in a cardiac MRI animal study of cardiac arrest and as discussed previously (Berg et al., 2005; Kjeld et al., 2021c).

Conclusion

Our results indicate the following: 1) elite BHD compared to matched controls are adapted with increased hemoglobin concentrations to sustain extreme hypoxia, and 2) the blood shift in elite BHD during maximum apnea after glossopharyngeal insufflation is– at least partly– direction of blood from the lower extremities and with a smaller volume from the spleen, but 3) in contrast to previous studies of sedated diving mammals during apnea, our study of elite BHD do not demonstrate a blood shift towards the heart.

Perspectives

In our study BHD endured maximum apneas of 370 s on average. Previously we have demonstrated similar duration of apnea in BHD and similar tolerance for low PaO_2 during apnea as compared to diving mammals (Kjeld et al., 2021c). The BHD in the present study had unaltered left ventricular myocardial mass volumes after 2-4 min of apnea but decreased spleen volumes to 102 mL during maximum apnea, whereas extremities released 268 mL of blood, or ~162% more than the spleen. Mijacika et al. demonstrated a large decrease in pulmonary blood volume after glossopharyngeal insufflation following 4 min of apnea, and hence, we suggest that blood released from lungs, spleen and lower extremities are directed towards the abdomen. Accordingly, the intestine, the kidneys and the liver are highly sensitive to hypoxia in humans (Ebert, 2006; Fu et al., 2016; Mijacika et al., 2017a; Mijacika et al., 2017b; Singhal and Shah, 2020), whereas the heart, lungs and skeletal muscles seem resistant to hypoxic injury during maximum apnea in elite BHD (Kjeld et al., 2015; Kjeld et al., 2018; Kjeld et al., 2021c). Future studies may reveal whether blood is directed from the extremities towards the hypoxia sensitive abdominal organs as an oxygen conserving mechanism, which could explain the evolutionary development of short flat peripheral extremities in diving mammals (Goldbogen, 2018).

Limitations

The study population is small, because of the limitations in the inclusion criteria of minimum 5 min of apnea in different stressful environments. This limited the number of participants in the sub studies. In addition, measuring 2,3-BPG and hemoglobin concentrations compared to a control group instead of prospective measurement in BHD, is a limitation in our study. However, because we found no changes in the study of LVMM, and significant results in the rest of the sub studies, we assume this is of minor importance, although measurements of LVMM were after 4 min of apnea and not at end of maximum apnea (~6 min).

The study did not include measurements of the atrial and right ventricle mass as this was not possible due the thin walls of these structures. However, our previous studies indicated no changes in pro-atrial-natriuretic factor during maximum apnea in competitive BHD indicating no stretching of atrial muscle, and as the right ventricle is much less muscular than the left (Rodrigues et al., 2007), we assume that changes in these chambers may be of lesser importance (Kjeld et al., 2015; Kjeld et al., 2021c). Measurements were all done during dry apneas after glossopharyngeal insufflation, which limits venous return (Eichinger et al., 2010). As submersion during diving may cause 500-700 mL increase in circulating volume (Weston et al., 1987; Weenink and Wingelaar, 2021) future studies may reveal the most important reservoirs of blood and volume changes during human apnea diving.

Data availability statement

The data that support the findings of this study are saved encrypted at hospital servers, but restrictions apply to the availability of these data, which were used under license for the current study, and so data are not publicly available. Data are however available from the authors upon reasonable request and with permission from Region Hovedstaden, Herlev Hospital, Skejby Hospital and Rigshospitalet.

Author contributions

TKj: Conceptualization, Data curation, Formal Analysis, Investigation, Methodology, Project administration, Resources, Supervision, Validation, Visualization, Writing–original draft, Writing–review and editing. TKr: Data curation, Formal Analysis, Funding acquisition, Investigation, Methodology, Project administration, Resources, Software, Supervision, Validation, Visualization, Writing–original draft, Writing–review and editing. AB: Data curation, Formal Analysis, Investigation, Resources, Validation, Visualization, Writing–original draft, Writing–review and editing. AM: Data curation, Formal Analysis, Funding acquisition, Methodology, Resources, Supervision, Validation, Visualization, Writing–original draft, Writing–review and editing. HA: Conceptualization, Data curation, Formal Analysis, Funding acquisition, Investigation, Methodology, Project administration, Resources, Software, Supervision, Validation, Visualization, Writing–original draft, Writing–review and editing. JH: Supervision, Validation, Visualization, Writing–review and editing, Conceptualization, Data curation, Formal Analysis, Investigation, Resources, Software. DF: Conceptualization, Data curation, Formal Analysis, Funding acquisition, Investigation, Methodology, Project administration, Resources, Software, Supervision, Validation, Visualization, Writing–review and editing. SH: Conceptualization, Data curation, Formal Analysis, Funding acquisition, Investigation, Methodology, Project administration, Resources, Software, Supervision, Validation, Visualization, Writing–review and editing. LT: Conceptualization, Data curation, Formal Analysis, Funding acquisition, Investigation, Methodology, Project administration, Resources, Software, Supervision, Validation, Visualization, Writing–review and editing. LG: Conceptualization, Data curation, Formal Analysis, Funding acquisition, Investigation, Methodology, Project administration, Resources, Software, Supervision, Validation, Visualization, Writing–review and editing. JV: Conceptualization, Formal Analysis, Funding acquisition, Methodology, Project administration, Resources, Supervision, Validation, Visualization, Writing–review and editing. EH: Conceptualization, Data curation, Formal Analysis, Funding acquisition, Investigation, Methodology, Project administration, Resources, Software, Supervision, Validation, Visualization, Writing–original draft, Writing–review and editing.

Funding

The author(s) declare that no financial support was received for the research, authorship, and/or publication of this article.

Acknowledgements

Authors wish to thank Brian Møllgren for 2,3-BPG analyses. Marcus Carlsson, Jakob Møller, Kristian Fogh, and Professor DMSc. Henrik Thomsen are thanked for helping with cardiac MRI scans. Bo Zerahn and Lars Thorbjørn Jensen are thanked for helping with DXA scans. Isak Honerød Augestad is thanked for collecting and analyzing blood samples.

Conflict of interest

The authors declare that the research was conducted in the absence of any commercial or financial relationships that could be construed as a potential conflict of interest.

Publisher's note

References

Adachi, T., Maresh, J. L., Robinson, P. W., Peterson, S. H., Costa, D. P., Naito, Y., et al. (2014). The foraging benefits of being fat in a highly migratory marine mammal. *Proc. Biol. Sci.* 281, 20142120. doi:10.1098/rspb.2014.2120

Adams, J. P., and Albert, S. (1962). The blood volume in the lower extremities. A technique for its determination utilizing Cr-51 tagged red cells. *J.Bone Jt. Surg.Am.* 44-A, 489–493. doi:10.2106/00004623-196244030-00006

Astrand, P. O., and Ryhming, I. (1954). A nomogram for calculation of aerobic capacity (physical fitness) from pulse rate during sub-maximal work. *J. Appl. Physiol.* 7, 218–221. doi:10.1152/jappl.1954.7.2.218

Atkinson, G., and Nevill, A. M. (1998). Statistical methods for assessing measurement error (reliability) in variables relevant to sports medicine. *Sports Med.* 26, 217–238. doi:10.2165/00007256-199826040-00002

Benner, A., Patel, A. K., Singh, K., and Dua, A. (2023). "Physiology, Bohr effect," in *StatPearls* (Treasure Island (FL): StatPearls Publishing).

Bennett, K. A., McConnell, B. J., and Fedak, M. A. (2001). Diurnal and seasonal variations in the duration and depth of the longest dives in southern elephant seals (*Mirounga leonina*): possible physiological and behavioural constraints. *J. Exp. Biol.* 204, 649–662. doi:10.1242/jeb.204.4.649

Berg, R. A., Sorrell, V. L., Kern, K. B., Hilwig, R. W., Altbach, M. I., Hayes, M. M., et al. (2005). Magnetic resonance imaging during untreated ventricular fibrillation reveals prompt right ventricular overdistention without left ventricular volume loss. *Circulation* 111, 1136–1140. doi:10.1161/01.CIR.0000157147.26869.31

Bidhult, S., Xanthis, C. G., Liljekvist, L. L., Greil, G., Nagel, E., Aletras, A. H., et al. (2016). Validation of a new T2* algorithm and its uncertainty value for cardiac and liver iron load determination from MRI magnitude images. *Magn. Reson.Med* 75, 1717–1729. doi:10.1002/mrm.25767

Böning, D. (2019). Physical Exercise at Altitude - Acclimation and Adaptation Effects in Highlanders on Different Continents (Muskelarbeit in der Höhe - Akklimatisierung und Adaptation bei Hochlandbewohnern auf verschiedenen Erdteilen). *Dtsch. Z. fur Sportmed.* 70, 135–140. doi:10.5960/dzsm.2019.379

Boning, D., Draude, W., Trost, F., and Meier, U. (1978). Interrelation between Bohr and temperature effects on the oxygen dissociation curve in men and women. *Respir. Physiol.* 34, 195–207. doi:10.1016/0034-5687(78)90028-2

Bouten, J., Caen, K., Stautemas, J., Lefevere, F., Derave, W., Lootens, L., et al. (2019). Eight weeks of static apnea training increases spleen volume but not acute spleen contraction. *Respir.Physiol Neurobiol.* 266, 144–149. doi:10.1016/j.resp.2019.04.002

Cabanac, A., Folkow, L. P., and Blix, A. S. (1997). Volume capacity and contraction control of the seal spleen. *J. Appl. Physiol.* 82, 1989–1994. doi:10.1152/jappl.1997.82.6.1989

Chanutin, A., and Curnish, R. R. (1967). Effect of organic and inorganic phosphates on the oxygen equilibrium of human erythrocytes. *Arch. Biochem. Biophys.* 121, 96–102. doi:10.1016/0003-9861(67)90013-6

Chicco, A. J., Le, C. H., Schlater, A., Nguyen, A., Kaye, S., Beals, J. W., et al. (2014). High fatty acid oxidation capacity and phosphorylation control despite elevated leak and reduced respiratory capacity in northern elephant seal muscle mitochondria. *J. Exp. Biol.* 217, 2947–2955. doi:10.1242/jeb.105916

Chow, K. U., Luxembourg, B., Seifried, E., and Bonig, H. (2016). Spleen size is significantly influenced by body height and sex: establishment of normal values for spleen size at US with a cohort of 1200 healthy individuals. *Radiology* 279, 306–313. doi:10.1148/radiol.2015150887

Ebert, E. C. (2006). Hypoxic liver injury. *Mayo Clin.Proc.* 81, 1232–1236. doi:10.4065/81.9.1232

Eichinger, M., Walterspacher, S., Scholz, T., Tetzlaff, R., Puderbach, M., Tetzlaff, K., et al. (2010). Glossopharyngeal insufflation and pulmonary hemodynamics in elite breath hold divers. *Med.Sci.Sports Exerc.* 42, 1688–1695. doi:10.1249/MSS.0b013e3181d85dc3

Elia, A., Wilson, O. J., Lees, M., Parker, P. J., Barlow, M. J., Cocks, M., et al. (2019). Skeletal muscle, haematological and splenic volume characteristics of elite breath-hold divers. *Eur. J. Appl. Physiol.* 119, 2499–2511. doi:10.1007/s00421-019-04230-6

Faiss, R., Girard, O., and Millet, G. P. (2013). Advancing hypoxic training in team sports: from intermittent hypoxic training to repeated sprint training in hypoxia. *Br.J.Sports Med.* 47 (Suppl. 1), i45–i50. doi:10.1136/bjsports-2013-092741

Foster, G. E., and Sheel, A. W. (2005). The human diving response, its function, and its control. *Scand. J. Med. Sci. Sports* 15, 3–12. doi:10.1111/j.1600-0838.2005.00440.x

Fu, Q., Colgan, S. P., and Shelley, C. S. (2016). Hypoxia: the force that drives chronic kidney disease. *Clin. Med. Res.* 14, 15–39. doi:10.3121/cmr.2015.1282

Ge, R. L., Chen, Q. H., Wang, L. H., Gen, D., Yang, P., Kubo, K., et al. (1994). Higher exercise performance and lower VO2max in Tibetan than Han residents at 4,700 m altitude. *J.Appl.Physiol. (1985)* 77, 684–691. doi:10.1152/jappl.1994.77.2.684

Gjorup, C. A., Zerahn, B., Juul, S., Hendel, H. W., Christensen, K. B., and Holmich, L. R. (2017). Repeatability of volume and regional body composition measurements of the lower limb using dual-energy X-ray Absorptiometry. *J. Clin. Densitom.* 20, 82–96. doi:10.1016/j.jocd.2016.08.009

Goldbogen, J. A. (2018). Physiological constraints on marine mammal body size. *Proc. Natl. Acad. Sci. U.S.A* 115, 3995–3997. doi:10.1073/pnas.1804077115

Gore, C. J., Rodriguez, F. A., Truijens, M. J., Townsend, N. E., Stray-Gundersen, J., and Levine, B. D. (2006). Increased serum erythropoietin but not red cell production after 4 wk of intermittent hypobaric hypoxia (4,000-5,500 m). *J.Appl.Physiol. (1985)* 101, 1386–1393. doi:10.1152/japplphysiol.00342.2006

Hamasaki, N., and Yamamoto, M. (2000). Red blood cell function and blood storage. *Vox Sang.* 79, 191–197. doi:10.1159/000056729

Hardison, R. (1998). Hemoglobins from bacteria to man: evolution of different patterns of gene expression. *J. Exp. Biol.* 201, 1099–1117. doi:10.1242/jeb.201.8.1099

Hardison, R. C., Chui, D. H., Riemer, C. R., Miller, W., Carver, M. F., Molchanova, T. P., et al. (1998). Access to a syllabus of human hemoglobin variants (1996) via the World Wide Web. *Hemoglobin* 22, 113–127. doi:10.3109/03630269809092136

Harms, H. J., Knaapen, P., de, H. S., Halbmeijer, R., Lammertsma, A. A., and Lubberink, M. (2011). Automatic generation of absolute myocardial blood flow images using [15O]H2O and a clinical PET/CT scanner. *Eur. J. Nucl. Med. Mol. Imaging* 38, 930–939. doi:10.1007/s00259-011-1730-3

Hauser, A., Schmitt, L., Troesch, S., Saugy, J. J., Cejuela-Anta, R., Faiss, R., et al. (2016). Similar hemoglobin mass response in hypobaric and normobaric hypoxia in athletes. *Med.Sci.Sports Exerc.* 48, 734–741. doi:10.1249/MSS.0000000000000808

Hauser, A., Troesch, S., Saugy, J. J., Schmitt, L., Cejuela-Anta, R., Faiss, R., et al. (2017). Individual hemoglobin mass response to normobaric and hypobaric "live high-train low": a one-year crossover study. *A one-year crossover study* 123, 387–393. doi:10.1152/japplphysiol.00932.2016

Heiberg, E., Sjogren, J., Ugander, M., Carlsson, M., Engblom, H., and Arheden, H. (2010). Design and validation of Segment--freely available software for cardiovascular image analysis. *Bmc. Med. Imaging* 10, 1. doi:10.1186/1471-2342-10-1

Hochachka, P. W., Beatty, C. L., Burelle, Y., Trump, M. E., McKenzie, D. C., and Matheson, G. O. (2002). The lactate paradox in human high-altitude physiological performance. *News Physiol. Sci.* 17, 122–126. doi:10.1152/nips.01382.2001

Hurford, W. E., Hochachka, P. W., Schneider, R. C., Guyton, G. P., Stanek, K. S., Zapol, D. G., et al. (1996). Splenic contraction, catecholamine release, and blood volume redistribution during diving in the Weddell seal. *J.Appl.Physiol. (1985)* 80, 298–306. doi:10.1152/jappl.1996.80.1.298

Ilardo, M. A., Moltke, I., Korneliussen, T. S., Cheng, J., Stern, A. J., Racimo, F., et al. (2018). Physiological and genetic adaptations to diving in sea nomads. *Cell* 173, 569–580. doi:10.1016/j.cell.2018.03.054

Kanatous, S. B., Davis, R. W., Watson, R., Polasek, L., Williams, T. M., and Mathieu-Costello, O. (2002). Aerobic capacities in the skeletal muscles of Weddell seals: key to longer dive durations? *J. Exp. Biol.* 205, 3601–3608. doi:10.1242/jeb.205.23.3601

Kanatous, S. B., Hawke, T. J., Trumble, S. J., Pearson, L. E., Watson, R. R., Garry, D. J., et al. (2008). The ontogeny of aerobic and diving capacity in the skeletal muscles of Weddell seals. *J. Exp. Biol.* 211, 2559–2565. doi:10.1242/jeb.018119

Kanto, J. H. (1988). Propofol, the newest induction agent of anesthesia. *Int. J. Clin. Pharmacol. Ther. Toxicol.* 26, 41–57.

Karpeles, L. M., and Huff, R. L. (1955). Blood volume of representative portions of the musculoskeletal system in man. *Circ. Res.* 3, 483–489. doi:10.1161/01.res.3.5.483

Kjekshus, J. K., Blix, A. S., Elsner, R., Hol, R., and Amundsen, E. (1982). Myocardial blood flow and metabolism in the diving seal. *Am. J. Physiol.* 242, R97–R104. doi:10.1152/ajpregu.1982.242.1.R97

Kjeld, T., Isbrand, A. B., Linnet, K., Zerahn, B., Hojberg, J., Hansen, E. G., et al. (2021a). Extreme hypoxia causing brady-arrythmias during apnea in elite breath-hold divers. *Front. Physiol.* 12, 712573. doi:10.3389/fphys.2021.712573

Kjeld, T., Jattu, T., Nielsen, H. B., Goetze, J. P., Secher, N. H., and Olsen, N. V. (2015). Release of erythropoietin and neuron-specific enolase after breath holding in competing free divers. *Scand. J. Med. Sci. Sports* 25, e253–e257. doi:10.1111/sms.12309

Kjeld, T., Moller, J., Fogh, K., Hansen, E. G., Arendrup, H. C., Isbrand, A. B., et al. (2021b). Author Correction: cardiac hypoxic resistance and decreasing lactate during maximum apnea in elite breath hold divers. *Sci. Rep.* 11, 6138. doi:10.1038/s41598-021-85418-9

Kjeld, T., Moller, J., Fogh, K., Hansen, E. G., Arendrup, H. C., Isbrand, A. B., et al. (2021c). Cardiac hypoxic resistance and decreasing lactate during maximum apnea in elite breath hold divers. *Sci. Rep.* 11, 2545. doi:10.1038/s41598-021-81797-1

Kjeld, T., Pott, F. C., and Secher, N. H. (2009). Facial immersion in cold water enhances cerebral blood velocity during breathhold exercise in humans. *J. Appl. Physiol.* 106, 1243–1248. doi:10.1152/japplphysiol.90370.2008

Kjeld, T., Rasmussen, M. R., Jattu, T., Nielsen, H. B., and Secher, N. H. (2014). Ischemic preconditioning of one forearm enhances static and dynamic apnea. *Med.Sci.Sports Exerc.* 46, 151–155. doi:10.1249/MSS.0b013e3182a4090a

Kjeld, T., Stride, N., Gudiksen, A., Hansen, E. G., Arendrup, H. C., Horstmann, P. F., et al. (2018). Oxygen conserving mitochondrial adaptations in the skeletal muscles of breath hold divers. *PLoS.One.* 13, e0201401. doi:10.1371/journal.pone.0201401

Koga, T. (1979). Correlation between sectional area of the spleen by ultrasonic tomography and actual volume of the removed spleen. *J. Clin. Ultrasound* 7, 119–120. doi:10.1002/jcu.1870070208

Lenfant, C., Kenney, D. W., and Aucutt, C. (1968a). Respiratory function in the killer whale *Orcinus orca* (Linnaeus). *Am. J. Physiol.* 215, 1506–1511. doi:10.1152/ajplegacy.1968.215.6.1506

Lenfant, C., Torrance, J., English, E., Finch, C. A., Reynafarje, C., Ramos, J., et al. (1968b). Effect of altitude on oxygen binding by hemoglobin and on organic phosphate levels. *J. Clin. Invest.* 47, 2652–2656. doi:10.1172/JCI105948

Malte, H., Lykkeboe, G., and Wang, T. (2021). The magnitude of the Bohr effect profoundly influences the shape and position of the blood oxygen equilibrium curve. *Comp. Biochem.Physiol A Mol.Integr.Physiol* 254, 110880. doi:10.1016/j.cbpa.2020.110880

Mijacika, T., Frestad, D., Kyhl, K., Barak, O., Drvis, I., Secher, N. H., et al. (2017a). Blood pooling in extrathoracic veins after glossopharyngeal insufflation. *Eur. J. Appl. Physiol.* 117, 641–649. doi:10.1007/s00421-017-3545-9

Mijacika, T., Kyhl, K., Frestad, D., Otto, B. F., Drvis, I., Secher, N. H., et al. (2017b). Effect of pulmonary hyperinflation on central blood volume: an MRI study. *Respir.Physiol Neurobiol.* 243, 92–96. doi:10.1016/j.resp.2017.05.012

Millet, G. P., Roels, B., Schmitt, L., Woorons, X., and Richalet, J. P. (2010). Combining hypoxic methods for peak performance. *Sports Med.* 40, 1–25. doi:10.2165/11317920-000000000-00000

Persson, G., Lodin-Sundstrom, A., Liner, M. H., Andersson, S. H. A., Sjogreen, B., and Andersson, J. P. A. (2023). Splenic contraction and cardiovascular responses are augmented during apnea compared to rebreathing in humans. *Front. Physiol.* 14, 1109958. doi:10.3389/fphys.2023.1109958

Ploszczyca, K., Czuba, M., Chalimoniuk, M., Gajda, R., and Baranowski, M. (2021). Red blood cell 2,3-diphosphoglycerate decreases in response to a 30 km time trial under hypoxia in cyclists. *Front. Physiol.* 12, 670977. doi:10.3389/fphys.2021.670977

Prommer, N., Ehrmann, U., Schmidt, W., Steinacker, J. M., Radermacher, P., and Muth, C. M. (2007). Total haemoglobin mass and spleen contraction: a study on competitive apnea divers, non-diving athletes and untrained control subjects. *Eur. J. Appl. Physiol.* 101, 753–759. doi:10.1007/s00421-007-0556-y

Qvist, J., Hill, R. D., Schneider, R. C., Falke, K. J., Liggins, G. C., Guppy, M., et al. (1986). Hemoglobin concentrations and blood gas tensions of free-diving Weddell seals. *J.Appl.Physiol. (1985)* 61, 1560–1569. doi:10.1152/jappl.1986.61.4.1560

Richardson, M., de, B. R., Holmberg, H. C., Bjorklund, G., Haughey, H., and Schagatay, E. (2005). Increase of hemoglobin concentration after maximal apneas in divers, skiers, and untrained humans. *Can. J. Appl. Physiol.* 30, 276–281. doi:10.1139/h05-120

Rodrigues, S. L., Pimentel, E. B., and Mill, J. G. (2007). Cardiac ventricular weights recorded at the autopsy of healthy subjects who died of external causes. *Arq. Bras.Cardiol.* 89, 252–257. doi:10.1590/s0066-782x2007001700001

Schagatay, E., Andersson, J. P., Hallen, M., and Palsson, B. (2001). Selected contribution: role of spleen emptying in prolonging apneas in humans. *J.Appl.Physiol* 90, 1623–1629. doi:10.1152/jappl.2001.90.4.1623

Schagatay, E., Haughey, H., and Reimers, J. (2005). Speed of spleen volume changes evoked by serial apneas. *Eur. J. Appl. Physiol.* 93, 447–452. doi:10.1007/s00421-004-1224-0

Schagatay, E., Richardson, M. X., and Lodin-Sundstrom, A. (2012). Size matters: spleen and lung volumes predict performance in human apneic divers. *Front. Physiol.* 3, 173. doi:10.3389/fphys.2012.00173

Seccombe, L. M., Rogers, P. G., Mai, N., Wong, C. K., Kritharides, L., and Jenkins, C. R. (2006). Features of glossopharyngeal breathing in breath-hold divers. *J. Appl. Physiol.* 101, 799–801. doi:10.1152/japplphysiol.00075.2006

Singhal, R., and Shah, Y. M. (2020). Oxygen battle in the gut: hypoxia and hypoxia-inducible factors in metabolic and inflammatory responses in the intestine. *J. Biol. Chem.* 295, 10493–10505. doi:10.1074/jbc.REV120.011188

Sorensen, J., Nordstrom, J., Baron, T., Morner, S., Granstam, S. O., Lubberink, M., et al. (2021). Diagnosis of left ventricular hypertrophy using non-ECG-gated (15)O-water PET. *J. Nucl. Cardiol.* 29, 2361–2373. doi:10.1007/s12350-021-02734-3

Storz, J. F., and Moriyama, H. (2008). Mechanisms of hemoglobin adaptation to high altitude hypoxia. *High. Alt.Med.Biol.* 9, 148–157. doi:10.1089/ham.2007.1079

Thomas, A., and Ono, K. (2015). Diving related changes in the blood oxygen stores of rehabilitating harbor seal pups (*Phoca vitulina*). *PLoS.One.* 10, e0128930. doi:10.1371/journal.pone.0128930

Vargas, E., and Spielvogel, H. (2006). Chronic mountain sickness, optimal hemoglobin, and heart disease. *High. Alt.Med.Biol.* 7, 138–149. doi:10.1089/ham.2006.7.138

Wadenvik, H., and Kutti, J. (1988). The spleen and pooling of blood cells. *Eur. J. Haematol.* 41, 1–5. doi:10.1111/j.1600-0609.1988.tb00861.x

Wagner, P. D. (1991). Central and peripheral aspects of oxygen transport and adaptations with exercise. *Sports Med.* 11, 133–142. doi:10.2165/00007256-199111030-00001

Walther, G., Nottin, S., Karpoff, L., Perez-Martin, A., Dauzat, M., and Obert, P. (2008). Flow-mediated dilation and exercise-induced hyperaemia in highly trained athletes: comparison of the upper and lower limb vasculature. *Acta Physiol. (Oxf)* 193, 139–150. doi:10.1111/j.1748-1716.2008.01834.x

Weenink, R. P., and Wingelaar, T. T. (2021). The circulatory effects of increased hydrostatic pressure due to immersion and submersion. *Front. Physiol.* 12, 699493. doi:10.3389/fphys.2021.699493

Weston, C. F., O'Hare, J. P., Evans, J. M., and Corrall, R. J. (1987). Haemodynamic changes in man during immersion in water at different temperatures. *Clin. Sci. (Lond)* 73, 613–616. doi:10.1042/cs0730613

Willford, D. C., Gray, A. T., Hempleman, S. C., Davis, R. W., and Hill, E. P. (1990). Temperature and the oxygen-hemoglobin dissociation curve of the harbor seal, *Phoca vitulina*. *Respir. Physiol.* 79, 137–144. doi:10.1016/0034-5687(90)90013-o

Winslow, R. M. (2007). The role of hemoglobin oxygen affinity in oxygen transport at high altitude. *Respir.Physiol Neurobiol.* 158, 121–127. doi:10.1016/j.resp.2007.03.011

Wright, T. J., and Davis, R. W. (2006). The effect of myoglobin concentration on aerobic dive limit in a Weddell seal. *J. Exp. Biol.* 209, 2576–2585. doi:10.1242/jeb.02273

Zapol, W. M., Liggins, G. C., Schneider, R. C., Qvist, J., Snider, M. T., Creasy, R. K., et al. (1979). Regional blood flow during simulated diving in the conscious Weddell seal. *J.Appl.Physiol Respir.Environ.Exerc.Physiol* 47, 968–973. doi:10.1152/jappl.1979.47.5.968

Zelenkova, I., Zotkin, S., Korneev, P., Koprov, S., and Grushin, A. (2019). Comprehensive overview of hemoglobin mass and blood volume in elite athletes across a wide range of different sporting disciplines. *J.Sports Med.Phys.Fitness* 59, 179–186. doi:10.23736/S0022-4707.18.08018-0

frontiers | Frontiers in Physiology

TYPE Original Research
PUBLISHED 10 July 2024
DOI 10.3389/fphys.2024.1383141

OPEN ACCESS

EDITED BY
Luis Monteiro Rodrigues,
Lusofona University, Portugal

REVIEWED BY
Apostolos Theos,
Umeå University, Sweden
Łukasz Tota,
University School of Physical Education in Krakow, Poland

*CORRESPONDENCE
Andrzej Kochanowicz,
andrzej.kochanowicz@awf.gda.pl
Jan Mieszkowski,
mieszkowskijan@gmail.com

RECEIVED 06 February 2024
ACCEPTED 20 June 2024
PUBLISHED 10 July 2024

CITATION
Kochanowicz A, Waldziński T, Niespodziński B, Brzezińska P, Kochanowicz M, Antosiewicz J and Mieszkowski J (2024), Acute inflammatory response following lower-and upper-body Wingate anaerobic test in elite gymnasts in relation to iron status.
Front. Physiol. 15:1383141.
doi: 10.3389/fphys.2024.1383141

Acute inflammatory response following lower-and upper-body Wingate anaerobic test in elite gymnasts in relation to iron status

Andrzej Kochanowicz[1]*, Tomasz Waldziński[2], Bartłomiej Niespodziński[3], Paulina Brzezińska[1], Magdalena Kochanowicz[4], Jedrzej Antosiewicz[5] and Jan Mieszkowski[1]*

[1]Department of Gymnastics, Dance and Musical and Movement Exercises, Gdańsk University of Physical Education and Sport, Gdańsk, Poland, [2]Faculty of Health Sciences, University of Lomza, Łomża, Poland, [3]Faculty of Health Sciences and Physical Education, Kazimierz Wielki University, Bydgoszcz, Poland, [4]Department of Physical Therapy, Medical University of Gdansk, Gdańsk, Poland, [5]Department of Bioenergetics and Physiology of Exercise, Medical University of Gdansk, Gdańsk, Poland

Introduction: Artistic gymnastics is one of the most demanding sports disciplines, with the athletes demonstrating extremely high levels of explosive power and strength. Currently, knowledge of the effect of gymnastic training adaptation on exercise-induced inflammatory response is limited. The study aimed to evaluate inflammatory response following lower- and upper-body high-intensity exercise in relation to the iron status in gymnasts and non-athletes.

Methods: Fourteen elite male artistic gymnasts (EAG, 20.6 ± 3.3 years old) and 14 physically active men (PAM, 19.9 ± 1.0 years old) participated in the study. Venous blood samples were taken before and 5 min and 60 min after two variants of Wingate anaerobic test (WAnT), upper-body and lower-body WAnT. Basal iron metabolism (serum iron and ferritin) and acute responses of selected inflammatory response markers [interleukin (IL) 6, IL-10, and tumour necrosis factor α] were analysed.

Results: EAG performed significantly better during upper-body WAnT than PAM regarding relative mean and peak power. The increase in IL-6 levels after upper-body WAnT was higher in EAG than in PAM; the opposite was observed after lower-body WAnT. IL-10 levels were higher in EAG than in PAM, and tumour necrosis factor α levels were higher in PAM than those in EAG only after lower-body WAnT. The changes in IL-10 correlated with baseline serum iron and ferritin in PAM.

Discussion: Overall, gymnastic training is associated with the attenuation of iron-dependent post-exercise anti-inflammatory cytokine secretion.

KEYWORDS

muscle damage, inflammation, oxidative stress, anaerobic exercises, male athletes, iron status

Introduction

Artistic gymnastics is one of the most demanding sports disciplines. To stay competitive, the sports activity of elite professional gymnasts during the gymnastics season entails 5–6 h of gymnastic training per day, 6 days per week. The target training rigour starts at the early stages of the gymnast's career (5–6 years old), with the training volume increasing yearly. In this scenario, gymnastic training exerts great physiological stress associated with neuromuscular and central fatigue, affecting body homeostasis and function. Multiple physiological and biochemical changes are induced in response to training, as evidenced by the associated inflammatory adaptation, metabolic changes, and recovery process kinetics (Alshammari et al., 2010). This type of adaptation is critical for realising such a demanding physical activity and is directly related to post-exercise stress tolerance (Kochanowicz et al., 2017).

In sports physiology, several biomarkers reflect the biochemical and physiological mechanisms underlying the physical stress induced by professional training (Marqués-Jiménez et al., 2016; Waldziński et al., 2023). For instance, determining myoglobin, creatine kinase, and lactate dehydrogenase serum levels is a golden standard for muscle damage analysis. Further, interleukin (IL) 1, IL-6, C-reactive protein, and tumour necrosis factor α (TNF-α) are considered specific inflammatory state markers (Pyne, 1994; Mieszkowski et al., 2021a; Waldziński et al., 2023). Their measurements are useful for obtaining a holistic overview of body function and muscle activity during competition and assessing an athlete's body adaptation to specific exercise (Pyne, 1994) or training conditions (Ziemann et al., 2014). Every professional sports training event and sport activity is associated with increased inflammation and skeletal muscle tissue damage (Mieszkowski et al., 2021a). In addition to inflammation, oxidative stress markers, such as lipid and protein oxidation, are detected (Sohail et al., 2020). The excessive inflammatory response induced by exercise and driving the secretion of proinflammatory cytokines is considered one of the factors limiting sports performance (Fatouros et al., 2010).

Iron status profoundly influences inflammation, as systemic iron levels and homeostasis alterations affect the inflammatory response. Increased iron stores are associated with oxidative stress and inflammation (Kell, 2009). Interestingly, it has been observed that regular exercise reduces body iron stores and lowers oxidative stress and inflammation (Kortas et al., 2017).

One of the many factors that can influence exercise-induced inflammation may be serum iron and iron stored in human tissues. However, data on this subject are very limited; for example, iron status influences exercise-induced changes in adiponectin and myostatin (Kortas et al., 2020).

Acute exercise can induce a stress response in skeletal muscle and other tissue, which is manifested by the activation of stress-activated protein kinases (SAPK) (Parker et al., 2017). *In vitro*, experimental models demonstrated that activation of SAPK can lead to ferritin degradation, iron-dependent oxidative stress and proinflammatory response (Kell, 2009; Borkowska et al., 2011). Thus, it became reasonable to analyse whether iron status can influence inflammatory response after acute exercise tests.

The post-exercise iron homeostasis is regulated by several factors, but an essential role plays changes in the interleukin-6 (IL-6). This cytokine plays a regulator role in inflammation response and hepcidin secretion (Lee et al., 2005). Hepcidin is an amino acid peptide released by hepatocytes that is the predominant negative regulator of iron absorption in the small intestine and iron release from macrophages (Ganz, 2003). Moreover, its changes contribute to the regulation of inflammation, and many cytokines can stimulate hepcidin biosynthesis, leading to a decrease in serum iron. On the other hand, an increase in the labile iron pool within a cell can augment the activity of NfKB, which can lead to increased expression of proinflammatory cytokines (Kell, 2009).

In many sports disciplines, the physiological and biomechanical involvement of different body parts (e.g., the upper- and lower-body muscles) in physical activity is not the same (Bassa et al., 2002). Unfortunately, data on the associated differences are limited, as are those on the differences in the response to exercise of the upper and lower body (Kochanowicz et al., 2017). In the case of gymnasts, the overwhelming majority of exercise and training routines involve the upper body, e.g., activities involving supports, hanging, pushing, pulling up, or giving momentum to the rest of the body (Jemni et al., 2006; Sawicki et al., 2018; Kochanowicz et al., 2019). It was previously shown (Mieszkowski et al., 2021b) that in gymnasts, the upper-body anaerobic performance output is higher than that of the lower body compared to the untrained population and, thus, different biochemical adaptations in terms of the intensity of the inflammatory response and changes in iron metabolism elicited by the upper and lower body exercise could be expected. Demonstrating such relationships would verify whether the predominant gymnastic training methods, focused on using upper body parts, also affect systemic adaptive changes. Of note, any effort exclusively involving the upper parts of the body is often thought to induce only local adaptations because of the muscle body content.

The aim of the current study was to evaluate the changes in inflammatory response following lower- and upper-body high-intensity exercise in relation to the iron status in gymnasts and non-athletes.

Materials and methods

Experimental overview

In the current study, two study groups, athletes (elite gymnasts) and physically active controls, performed two variants of the maximal anaerobic effort: lower-limb and upper-limb exercises. Before and after exercise, the participants' blood was collected, and inflammatory marker levels were analysed in the context of iron status.

Participants

A group of 14 elite male artistic gymnasts (EAG, 20.12 ± 3.36 years old) and 14 physically active men (PAM, 20.18 ± 1.1 years old) participated in the study. The EAG group consisted of Polish professional gymnasts (training 6 times per week, 5–6 h per session) who compete on a senior level and are ranked in the International Gymnastics Federation classification. The PAM group consisted of volunteers (students) who declared

TABLE 1 Physical characteristics and basal values of iron metabolism markers.

Variable	Physically active men (n = 14)		Elite artistic gymnasts (n = 14)		*p*-value PAM/EAG
	Mean ± SD	(95% CI)	Mean ± SD	(95% CI)	
Body height (cm)	176.62 ± 4.87	174.56–180.10	170.44 ± 3.36*	168.10–172.25	<0.01
Body mass (kg)	72.24 ± 8.80	66.20–77.67	68.21 ± 5.80	64.78–72.12	0.16
BMI (kg × m^{-2})	23.34 ± 3.36	21.85–25.16	22.73 ± 1.76	21.54–24.05	0.54
Percent body fat (%)	10.88 ± 4.81	8.31–13.45	6.48 ± 2.97*	5.12–8.43	<0.01
Iron (μmol/L)	32.51 ± 7.85	27.97–37.05	26.51 ± 10.56	20.41–32.60	0.10
Ferritin (ng/mL)	134.72 ± 20.32	122.99–146.45	147.52 ± 33.96	127.92–167.13	0.23

Note: PAM, physically active men; EAG, elite artistic gymnasts; * significant difference between PAM, and EAG groups at $p < 0.01$.

regular participation in recreational sports, such as running, swimming, and team sports (on average, 2–3 times per week, 45–60 min per session).

All participants were considered healthy 6 months before the beginning of the study. Specifically, no bone or muscle tissue injuries were reported; with negative medical history regarding the cardiovascular, autonomic nervous system, or mental disorders, and any other condition that might have directly or indirectly affected the results. Further, no drugs or any other supplements were taken during the study.

Descriptive physical characteristics and basal (resting) levels of iron metabolism markers are presented in Table 1.

Experimental protocol

Before the experiment, the participants attended an orientation session to ensure they were familiar with the testing equipment and procedures. Their basic anthropometric characteristics were then measured. At least 3 months before the start of the study, all study participants refrain from taking any drugs and supplements that could influence obtained results (including preparations that could improve exercise capacity). Two days before the experiment, all participants were asked to refrain from extensive exercise, stay hydrated, and maintain their regular dietary habits, excluding any drugs and stimulants.

The experimental protocol comprised the measurement of maximal anaerobic effort using the Wingate anaerobic test (WAnT) to assess the adaptation of lower and upper limbs, with the load adjusted individually. All participants began with lower-body WAnT, and after a week's break, they performed upper-limb WAnT. Before and after each WAnT session, blood samples were taken for further analysis. For each participant, the time of day, room temperature and other measurable variables were adequate during both WAnT performances (morning hours from 9 till 12 a.m., room temperature from 20 to 23°C, relative humidity: ≤70%, atmospheric pressure: 86 kPa–106 kPa).

Lower-body and upper-body WAnT

The lower-body WAnT was conducted using a cycle ergometer (Monark 894E, Peak Bike, Sweden) according to the Bar-Or (Bar-Or, 1987). Each participant's saddle height was adjusted individually (with the knee slightly flexed and with the final knee angle of approximately 170°–175°). Before any testing, each individual completed a standardised warm-up on the cycle ergometer (5 min at 60 rpm, 1 W/kg). During the testing, each participant was required to pedal for 30 s with a maximum effort against a fixed resistive load of 75 g/kg of total body mass.

The upper-body WAnT was conducted using a hand cycle ergometer (Monark 891E, Peak Bike) (Sawicki et al., 2018). Participants were seated in a chair, with the seat height and backrest adjusted individually. For the hand grasping the handles, the elbow joint was almost fully extended (140°–155°) (Kochanowicz et al., 2017). Similar to the lower-body WAnT, before any testing, the participants completed a warm-up that involved 5 min of arm cranking using a power output of 1 W/kg and a crank rate of 60 rpm. During the testing, each participant was required to pedal for 30 s with a maximum effort against a standard resistive load equivalent to 50 g/kg of total body mass. In both WAnTs, the procedure started without prior spinning of the flywheel due to the fact that in the specific nature of physical excesses, especially like gymnastics, the generation of maximum force values, regardless of the performed exercises, takes place always from a basic—static position. In a way, this seems to be much more reflected in the specificity of the physical effort than in the continuation of the effort that is already in progress.

During testing, verbal encouragement was given from the beginning until the end of the test to maintain the highest possible cadence throughout both WAnTs. Cycle ergometers were connected to a personal computer running the MCE 5.1 software (Staniak et al., 1994). The following WAnT variables were measured: peak power (W) and relative peak power (W/kg), calculated as the highest single point of power output (recorded at 0.2 s intervals), and mean power (W) and relative mean power (W/kg), calculated as the average power output during the 30 s test.

Sample collection and measurements of inflammatory markers

Blood samples were collected at three time points by a medical diagnostic professional, according to the experimental protocol, i.e., before the test, immediately after (no more than 5 min after the test) and 60 min after the test. The blood was collected into 5 mL BD Vacutainer Clot Activator Tubes (Becton Dickinson and Company, NJ, United States). The serum was separated by

centrifugation at 4,000 *g* for 10 min and aliquoted into 500 μL portions. The samples were frozen and stored (no longer than 6 months) at −80°C until further analysis.

Biochemical analysis of serum ferritin, IL-6, IL-10, and TNF-α levels were performed using high-sensitivity commercially available enzyme-linked immunosorbent assay kits (DRG International, Inc., Springfield, NJ, United States) and Thermo Fisher Scientific Elisa Analyzer (Thermo Fisher Scientific Waltham, MA, United States).

To assess baseline and changes in iron (FE) levels, plasma was collected into the lithium heparin tubes (Becton Dickinson and Company, NJ, United States) and tested using *in vitro* IRON 2 (Roche/Hitachi Cobas c.) systems using a Cobas C analyser 501.

Serum ferritin and iron levels were analysed only at baseline, as their concentrations are stable up to 24 h even after three repetitions of WAnT over a short period (Antosiewicz et al., 2013).

Statistical analysis

Descriptive statistics included mean ± SD for all measured variables. The normality of distribution was checked using the Shapiro–Wilk's test and Levene's test was used to check the homogeneity of variance. As the assumptions of normality and homogeneity of variance were met, the analysis of variance (ANOVA) tests were used. One-way ANOVA was used to determine the difference in WAnT performance characteristics between the EAG and PAM groups.

To evaluate the changes in biochemical markers of inflammation and muscle damage before and after WAnT, two-way (2 × 3) ANOVA of repeated measures was performed, where group (GR) was the between-subject factor (EAG, PAM) and repeated measure (RM) was the within-subject factor (pre-WAnT, 5 min post WAnT, 60 min post WAnT). Pearson's correlation coefficient was calculated between the baseline serum iron and ferritin levels and the changes (5 min vs. baseline; 60 min vs. baseline) in inflammatory marker levels.

The effect size of the participants' characteristics (Cohen's d-value) and biomarkers were determined using eta-squared statistics (η^2). In the analysis, η^2 values equal to or greater than 0.01 (d = 0.2; r = 0.1), 0.06 (d = 0.6; r = 0.3), and 0.14 (d = 0.8; r = 0.5) were the threshold values for a small, moderate, and large effect size, respectively (Cohen, 1988).

Power analysis for the interactions between the effects was performed using GPower ver. 3.1.9.2 to determine the appropriate sample size (Faul et al., 2007). Accordingly, for a medium effect size and test power of 0.80, the minimal required sample size was 28 participants.

All calculations and graphics were generated using GraphPad Prism 6.0 (GraphPad Software, MA, United States). All calculations were done using Statistica 12 (StatSoft, OK, United States). The level of significance was set at $\alpha = 0.05$.

Ethics

The study was approved by the Bioethics Committee for Clinical Research at the Regional Medical Chamber in Gdansk (decision no. KB-24/16) and carried out in accordance with the Declaration of Helsinki. All participants were informed about the purpose and test procedures, as well as the possibility of withdrawing consent at any time and for any reason. All participants gave written informed consent prior to the study.

Results

In the current study, the body height and percent body fat of gymnasts were significantly lower than those of the controls (Table 1). However, body mass and resting iron and ferritin levels were not significantly different between the two groups (Table 1).

The results of one-way ANOVA of the absolute and relative peak power of lower- and upper-body WAnTs are presented in Figure 1. A significantly better performance of EAG was observed only for the relative mean (16.7%, $p < 0.01$) and peak power (15.5%, $p < 0.05$) generated during upper-body WAnT. Lower-body WAnT results for both groups were not statistically different (Figure 1).

Two-way ANOVA with repeated measures of exercise-induced inflammation during lower- and upper-body anaerobic exercise is shown in Table 2. The analysis of lower- and upper-body WAnT data revealed a significant effect of RM on each tested inflammatory marker. The GR effect of the tested markers was also significant for both types of WAnT, except for the effect on changes in IL-10 levels after lower-body WAnT. Of note, IL-6 and TNF-α levels after lower-body WAnT in EAG were significantly lower than those in PAM; on the other hand, upper-body WAnT induced significantly higher levels of IL-6 and TNF-α in EAG than in PAM. Post-hoc analysis of changes in IL-10 levels induced by upper-body WAnT also revealed significantly higher readings in EAG. Considering the interaction of GR and RM factors, while the IL-6 and TNF-α levels in EAG were significantly lower than those in PAM 5 min (IL-6, 29.7%, $p < 0.01$; TNF- α, 37.3%, $p < 0.01$) and 60 min (IL-6, 29.7%, $p < 0.01$; TNF-α, 51.3%, $p < 0.01$) after lower-body WAnT, the IL-10 levels 60 min after exercise were significantly higher in EAG than those in PAM (27.7%, $p < 0.05$) (Figure 2). On the other hand, the IL-6 levels 5 min after upper-body WAnT were significantly higher in EAG than those in PAM (55.17%, $p < 0.01$).

The results of the correlation analysis of changes in the IL-6, IL-10, and TNF-α levels induced by the upper- and lower-body anaerobic exercise with the baseline (resting) serum levels of iron and ferritin are presented in Tables 3, 4, accordingly. The resting iron levels showed a significant positive correlation with changes in the IL-10 levels in PAM (Table 3). Similarly, the correlation analysis of baseline ferritin levels revealed a significant positive correlation with the change in IL-10 levels 60 min after lower-body WAnT in PAM only.

Discussion

The aim of the current study was to evaluate and compare the inflammatory response (i.e., changes in IL-6, IL-10, and TNF-α levels) after lower- and upper-body high-intensity exercise in gymnasts and non-athletes in relation to iron status.

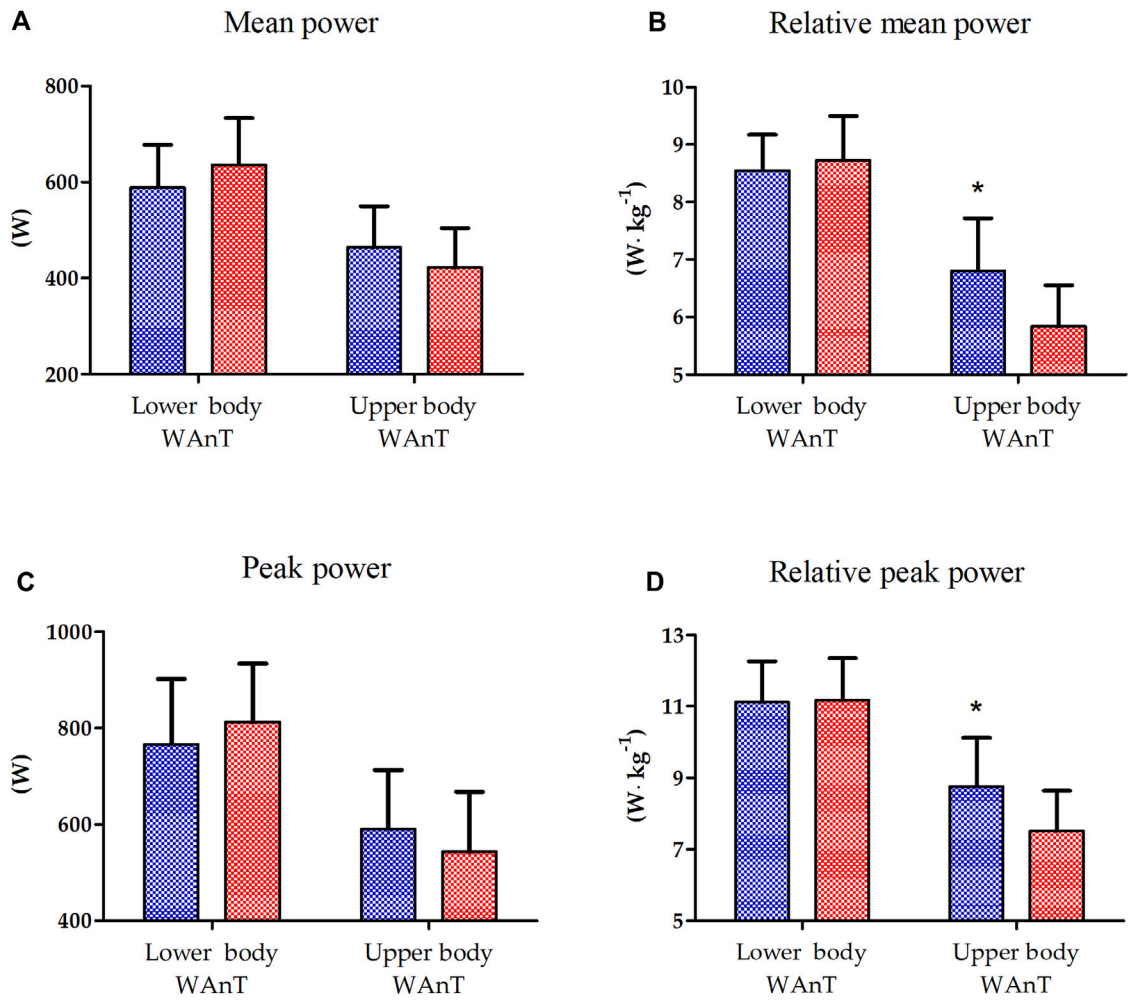

FIGURE 1
Lower and upper body Wingate Anaerobic Test (WAnT) characteristics in elite artistic gymnasts (blue, n = 14) and physically active men (red, n = 14). **(A)** mean power, **(B)** relative mean power, **(C)** peak power, **(D)** relative peak power. The data are presented as the mean and standard deviation; *$p < 0.01$, difference between elite artistic gymnasts and physically active men.

To the best of our knowledge, this is the first study in which the effect of upper- and lower-body anaerobic exercise on the inflammatory state markers was compared in professional athletes and non-athletes in the context of iron status. The main outcome of the study is that the lower- and upper-body maximal exercise in the form of WAnT elicited different responses of inflammatory markers depending on the training status. Specifically, the increase in IL-6 levels was more pronounced in EAG after upper-body WAnT, while it was more pronounced in PAM after lower-body WAnT. The other observed differences, i.e., relatively higher IL-10 levels in EAG and relatively higher TNF-α levels in PAM, were only associated with lower-body WAnT.

The study revealed that the relative peak (15.46%) and mean (16.72%) power of the upper body during WAnT are significantly higher in EAG than those in PAM. That is mainly because of the specific adaptation induced by and observed in professional gymnastic training. Namely, gymnasts mainly engage the upper body muscles to perform most of their exercises during the competition (e.g., floor exercises, parallel bars, horizontal bars, and others), with the lower body mainly engaged in short, explosive efforts (e.g., jumping). Such discrepancy in the upper- and lower-body WAnT performance in gymnasts has been reported before (Jemni et al., 2006). This may help to explain the lack of differences in the relative peak and mean power between EAG and PAM observed for lower-body WAnT and could be a starting point for understanding the differences in the response of inflammatory markers in the two groups.

Exercise initiates a cascade of inflammatory events, which affect human health in the long term. During and after acute exercise of the skeletal muscle, interactions between immune cells, cytokines, and other intracellular components create an inflammatory milieu responsible for the recovery from an adaption to an exercise bout. One of the main cytokines responsible for regulating the inflammatory process is IL-6, essential in initiating and controlling the post-exercise inflammatory process. Typically, physical exercise is accompanied by increased IL-6 levels due to the onset of inflammation (Aaseth and Birketvedt, 2012; Antosiewicz et al., 2013).

In the current study, analysis of the tested inflammatory markers revealed that considering the nature of the maximal anaerobic

TABLE 2 Two-way (two groups × three repeated measurements) ANOVA of the secretion of specific cytokines induced by lower- and upper-body anaerobic exercise in elite artistic gymnasts and physically active men.

Variable	Exercise	Effect	F	Df	p	Effect size (η^2)	Post-hoc outcome
IL-6	Lower body WAnT	GR	6.83	1, 26	0.01*	0.20	EAG < PAM
		RM	402.10	2, 52	0.01**	0.93	III > II > I
		GR × RM	106.05	2, 52	0.01**	0.80	$II^{EAG} < II^{PAM}$; $III^{EAG} < III^{PAM}$
	Upper body WAnT	GR	16.25	1, 26	0.67	0.01	EAG > PAM
		RM	300.97	2, 52	0.01**	0.91	III > II > I
		GR × RM	10.25	2, 52	0.01**	0.27	$II^{EAG} > II^{PAM}$
IL-10	Lower body WAnT	GR	3.67	1, 26	0.07	0.11	
		RM	150.78	2, 52	0.01**	0.85	III > II > I
		GR × RM	8.35	2, 52	0.01**	0.24	$III^{EAG} > III^{PAM}$
	Upper body WAnT	GR	0.83	1, 26	0.36	0.03	EAG > PAM
		RM	75.28	2, 52	0.01**	0.73	III > II > I
		GR × RM	2.45	2, 52	0.09	0.08	
TNF-α	Lower body WAnT	GR	61.96	1, 26	0.01*	0.70	EAG < PAM
		RM	613.68	2, 52	0.01**	0.95	III > II > I
		GR × RM	207.48	2, 52	0.01**	0.88	$II^{EAG} < II^{PAM}$; $III^{EAG} < III^{PAM}$
	Upper body WAnT	GR	8.52	1, 26	0.01**	0.24	EAG > PAM
		RM	112.75	2, 52	0.01**	0.81	III > II > I
		GR × RM	0.72	2, 52	0.48	0.02	

Note: IL-6, interleukin 6; IL-10, interleukin 10; TNF-α, tumour necrosis factor α; Df, degrees of freedom, where a first and second number are variability between and withing groups, respectively; GR, group; RM, repeated measure; PAM, physically active men (n = 14); EAG, elite artistic gymnasts (n = 14); I, resting value; II, 5 min after 30 s upper- or lower-body, as indicated, Wingate anerobic test (WAnT); III, 60 min after 30 s upper- or lower-body, as indicated, WAnT; * significant differences at $p < 0.05$, ** significant differences at $p < 0.01$.

exercise, the IL-6 and TNF-α levels after lower-body WAnT in gymnasts were significantly lower than those in the controls. In comparison, the IL-6 levels induced by upper-body anaerobic exercise were significantly higher in gymnasts than in the controls. Typical physical training-induced adaptation leads to a decrease in basal and acute post-exercise IL-6 production is observed. This is related to the counteractive effects of several potential stimuli of IL-6 (Keller et al., 2001; Pedersen et al., 2001; Fischer, 2006). In the current study, we observed that the resting (before worm up) IL-6 levels, especially in the case of lower-body WAnT in EAG, were increased. This may be associated with two factors. First, the gymnasts are professionals, training 6 times per week, 5–6 h per session. Second, the emotional reaction to the test performance should be considered. As mentioned, gymnasts are very well prepared for upper body testing because of the specificity of their training. However, lower-body WAnT is not the type of physical effort characteristic for their sports training. It may be associated with excessive adrenergic activation, which also increases IL-6 levels (Rodas et al., 2020). The observed differences were not statistically significant in meters of maximal and mean power achievements. Furthermore, the analysis of IL-10 levels induced by upper-body anaerobic exercise revealed significantly higher readings among gymnasts. IL-10 is an anti-inflammatory cytokine whose blood levels mainly increase after exercise (Stankiewicz et al., 2023). Accordingly, while we observed a significant increase in the IL-10 levels after upper- and lower-body WAnT in EAG and PAM, the increase was more pronounced for the former. This may suggest that the anti-inflammatory response in gymnasts is more pronounced than that in non-athletes because of their long-term training (Marciniak et al., 2009; Kajaia et al., 2018). Finally, it has been reported that the IL-6 level increase in response to exercise prevents a subsequent increase in the levels of pro-inflammatory cytokines, such as TNF-α (Petersen and Pedersen, 2005) and induces the production of IL-10 (Steensberg et al., 2003), conferring anti-inflammatory properties to that response (Pedersen et al., 2003). This aligns with the observations in the current study.

Inflammation is profoundly influenced by iron status, as alterations of systemic iron levels and homeostasis affect the inflammatory response. Increased iron stores are correlated with increased secretion of inflammatory response markers (Kell, 2009). However, we are unaware of any study that has studied the role of iron in acute exercise-induced inflammation.

The current study analysed iron status, interleukin (IL-6 and IL-10), and TNF-α secretion revealed differences in PAM and EAG upon lower- and upper-body exercise. Each type of intensive exercise induces physiological stress that can contribute to an increased formation of free radicals. Body iron stores can modulate this process. One of the training adaptations associated with systemic radical formation and iron metabolism is the reduction of ferritin levels (body iron stores) (Lakka et al., 1994; Kortas et al., 2017). This type of adaptation may be related to lower oxidative stress caused by decreased iron-dependent free radical formation (Nemeth et al., 2004; Kortas et al., 2017). Furthermore, it has been shown that oxidative stress (which can be iron-dependent) induced during intensive exercise leads to increased levels of pro-inflammatory cytokines, such as IL-6 and TNF-α (Suzuki, 2018). This may explain why a reduction in body iron stores, which may be

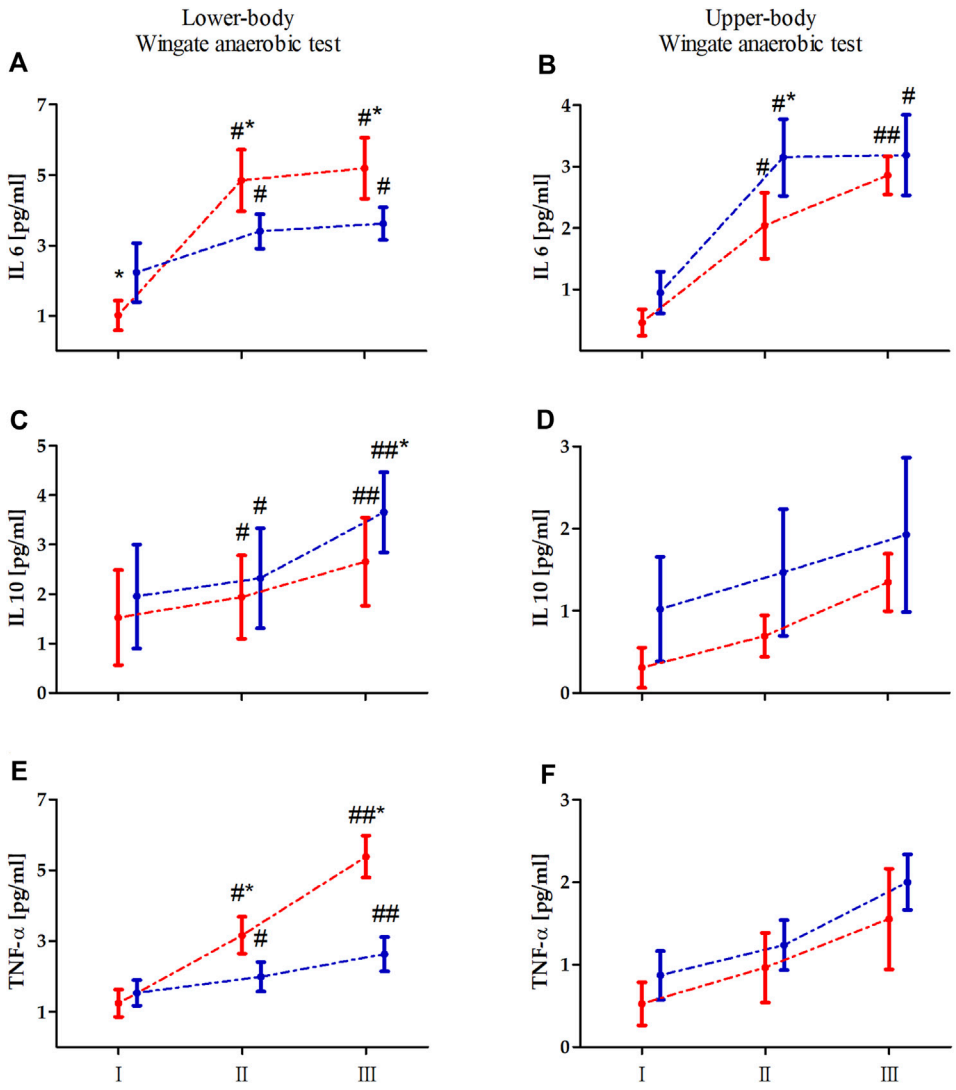

FIGURE 2
Changes in the levels of interleukin (IL) 6, IL-10, and tumor necrosis factor alpha (TNF-α) induced by lower **(A, C, E)** an upper-body **(B, D, F)** Wingate anaerobic test (WAnT) in elite artistic gymnasts (blue, n = 14) and physically active men (red, n = 14). Vertical bars, mean and standard deviation; I, resting value; II, 5 min after WAnT; III, 60 min after WAnT. Statistical analysis: * difference between elite artistic gymnasts and physically active men at particular time point at $p < 0.01$; # significant difference vs. rest value in particular group at $p < 0.01$, ## significant difference vs. rest value and 5 min after the WAnT in particular group at $p < 0.01$.

TABLE 3 Correlation of changes in specific cytokine levels induced by upper- and lower-body Wingate anaerobic test with baseline iron serum levels.

Variable	*Time point (min)*	*Lower-body Wingate anaerobic test*			*Upper-body Wingate anaerobic test*		
		PAM	EAG	All	PAM	EAG	All
IL-6	Delta 5	−0.39	0.01	0.22	0.01	−0.02	−0.19
	Delta 60	−0.50	0.14	0.24	0.09	0.15	0.19
IL-10	Delta 5	0.83*	−0.12	0.06	0.45	0.29	0.27
	Delta 60	0.78*	−0.19	−0.06	0.29	0.17	0.23
TNF-α	Delta 5	0.03	0.14	0.32	0.36	−0.20	0.07
	Delta 60	−0.13	0.51	0.35	0.31	−0.20	0.02

Note: PAM, physically active men (n = 14); EAG, elite artistic gymnasts (n = 14); IL-6, interleukin 6; IL-10, interleukin 10; TNF-α, tumor necrosis factor α; * significant correlation at $p < 0.05$.

TABLE 4 Correlation of changes in specific cytokine levels induced by upper- and lower-body Wingate anaerobic test with baseline ferritin serum levels.

Variable	Time point (min)	Lower-body Wingate anaerobic test			Upper-body Wingate anaerobic test		
		PAM	EAG	All	PAM	EAG	All
IL-6	Delta 5	−0.22	−0.22	−0.30	0.24	0.29	0.35
	Delta 60	−0.17	−0.32	−0.32	−0.08	0.20	0.09
IL-10	Delta 5	0.50	−0.04	0.03	0.19	−0.34	−0.16
	Delta 60	0.76*	0.11	0.36	0.12	−0.24	−0.18
TNF-α	Delta 5	0.47	0.12	−0.14	0.18	−0.04	0.01
	Delta 60	−0.14	−0.16	−0.26	0.30	−0.05	0.12

Note: PAM, physically active men (n = 14); EAG, elite artistic gymnasts (n = 14); IL-6, interleukin 6; IL-10, interleukin 10; TNF-α, tumor necrosis factor α; * significant correlation at $p < 0.05$.

observed as a training adaptation, would contribute to reducing oxidative stress and inflammation caused by physical activity (Kortas et al., 2017).

In the present study, the basal serum-iron levels in EAG were lower than in PAM (26.51 ± 10.56 vs. 32.51 ± 7.85 (μmol/L)). While the difference was not statistically significant, it may be associated with long-term gymnastic training. Further, we observed that in PAM, the baseline serum levels of iron and ferritin were highly correlated with the changes in IL-10 levels induced by lower-body WAnT. In addition to higher IL-6 and TNF-α levels, it indicates a higher post-exercise inflammation in non-athletes and a possible modulatory role of iron in this process (Stankiewicz et al., 2023). Serum iron can have signalling properties as it can enter cells through the transferrin receptor, which can lead to an increase in the labile iron pool (LIP). An increase in LIP can lead to the activation of NFKB, a transcriptional factor that can augment the transcription of genes encoding proinflammatory cytokines like IL-6 and TNF. Conversely, IL-6 has been proposed to induce the expression of antiinflammatory cytokines, including Il-10. Here, we observed that lower-body exercise test-induced changes in IL-10 are strongly correlated with serum iron, confirming its signalling role. Similarly, we observed that ferritin concentration correlates with exercise-induced changes in IL-10. Ferritin iron is considered inert as it does not stimulate free radicals' formation. However, studies on cell culture demonstrated that during stress conditions, part of ferritin undergoes ferritin degradation, which can lead to an increase in LIP (Borkowska et al., 2011). The degradation process depends on c-jun terminal kinase (JNK), which belongs to stress-activated protein kinases (Antosiewicz et al., 2007). If we consider that JNK activation can be blunted by heat shock proteins (HSP), their higher levels can influence the reaction to exercise. Regular exercise has been shown to upregulate HSP (Febbraio and Koukoulas, 2000). Thus, we can speculate that our athletes are much more resistant to exercise-induced activation of JNK. Fewer possibilities can increase LIP in skeletal muscle and other tissue. This can be a likely explanation for why, in EAG, there is no correlation between ferritin and changes in serum cytokines.

The current study has some limitations. Specifically, although we evaluated the acute inflammatory response induced by upper- and lower-body WAnT, we focused on only a few well-known parameters contributing to the inflammatory status. This approach may not fully reflect the complexity of the adaptation process induced by many years of training, especially considering the molecular and physiological aspects of the process. On the other hand, we have previously reported that gymnastic training may induce some adaptations on the molecular level, impacting the expression of inflammatory genes (those encoding IL-6 and IL-10) and genes encoding heat-shock proteins HSPA1A and HSPB1 (Kochanowicz et al., 2017; Zychowska et al., 2017). In the current study, we confirmed the observed molecular adaptations, manifesting as changing serum levels of the related inflammatory markers.

Conclusion

We here showed that gymnastic training significantly affects the post-exercise inflammatory response and that the response is lower- and upper-body WAnT-dependent. This effect is most likely a result of many years of specific training focused on various upper-body muscle groups and the explosive muscle strength of the lower body, which induces physiological and biochemical adaptations to exercise. Further, the presented findings suggest that exercise-induced pro- and anti-inflammatory cytokine production, essential for body homeostasis, may depend on body iron storage and serum iron.

Analysis and evaluation of post-exercise secretion of pro- and anti-inflammatory cytokines in relation to iron status may be a useful indicator of exercise adaptation, and showing the health benefits of sports training and complexity of the body's response to exercises.

Data availability statement

The raw data supporting the conclusions of this article will be made available by the authors, without undue reservation.

Ethics statement

The studies involving humans were approved by the Bioethics Committee for Clinical Research at the Regional Medical Chamber in Gdansk (decision no. KB-24/16). The studies were conducted in accordance with the local legislation and institutional requirements. The participants provided their written informed consent to participate in this study.

Author contributions

AK: Conceptualization, Data curation, Formal Analysis, Funding acquisition, Investigation, Methodology, Project administration, Resources, Software, Supervision, Validation, Visualization, Writing–original draft, Writing–review and editing. TW: Conceptualization, Data curation, Funding acquisition, Investigation, Methodology, Resources, Validation, Writing–original draft. BN: Conceptualization, Data curation, Formal Analysis, Methodology, Validation, Visualization, Writing–review and editing. PB: Methodology, Software, Validation, Visualization, Formal Analysis, Writing–review and editing, Funding acquisition, Investigation. MK: Data curation, Formal Analysis, Investigation, Resources, Software, Writing–original draft. JA: Conceptualization, Funding acquisition, Supervision, Validation, Writing–original draft, Formal Analysis. JM: Conceptualization, Formal Analysis, Funding acquisition, Methodology, Resources, Software, Supervision, Validation, Writing–original draft, Writing–review and editing, Investigation, Project administration.

Funding

The author(s) declare that no financial support was received for the research, authorship, and/or publication of this article.

Conflict of interest

The authors declare that the research was conducted in the absence of any commercial or financial relationships that could be construed as a potential conflict of interest.

Publisher's note

All claims expressed in this article are solely those of the authors and do not necessarily represent those of their affiliated organizations, or those of the publisher, the editors and the reviewers. Any product that may be evaluated in this article, or claim that may be made by its manufacturer, is not guaranteed or endorsed by the publisher.

References

Aaseth, J., and Birketvedt, G. (2012). Hemolysis and rhabdomyolysis after marathon and long distance running. *Immunol. Endocr. Metabolic Agents Med. Chem.* 12, 8–13. doi:10.2174/187152212799857655

Alshammari, E., Shafi, S., Nurmi-Lawton, J., Burut, D. F., Lanham-New, S., and Ferns, G. (2010). Markers of inflammation, endothelial activation and autoimmunity in adolescent female gymnasts. *J. Sports Sci. Med.* 9, 538–546.

Antosiewicz, J., Kaczor, J. J., Kasprowicz, K., Laskowski, R., Kujach, S., Luszczyk, M., et al. (2013). Repeated "all out" interval exercise causes an increase in serum hepcidin concentration in both trained and untrained men. *Cell Immunol.* 283, 12–17. doi:10.1016/j.cellimm.2013.06.006

Antosiewicz, J., Ziolkowski, W., Kaczor, J. J., and Herman-Antosiewicz, A. (2007). Tumor necrosis factor-alpha-induced reactive oxygen species formation is mediated by JNK1-dependent ferritin degradation and elevation of labile iron pool. *Free Radic. Biol. Med.* 43, 265–270. doi:10.1016/j.freeradbiomed.2007.04.023

Bar-Or, O. (1987). The Wingate anaerobic test. An update on methodology, reliability and validity. *Sports Med.* 4, 381–394. doi:10.2165/00007256-198704060-00001

Bassa, H., Kotzamanidis, C., Siatras, T., Mameletzi, D., and Skoufas, D. (2002). Coactivation of knee muscles during isokinetic concentric and eccentric knee extensions and flexions in prepubertal gymnasts. *Isokinet. Exerc. Sci.* 10, 137–144. doi:10.3233/ies-2002-0094

Borkowska, A., Sielicka-Dudzin, A., Herman-Antosiewicz, A., Halon, M., Wozniak, M., and Antosiewicz, J. (2011). P66Shc mediated ferritin degradation--a novel mechanism of ROS formation. *Free Radic. Biol. Med.* 51, 658–663. doi:10.1016/j.freeradbiomed.2011.04.045

Cohen, J. (1988). *Statistical power analysis for the behavioral sciences*. Hillsdale, MI, USA: Lawrence Erlbaum Associates.

Fatouros, I. G., Chatzinikolaou, A., Douroudos, I. I., Nikolaidis, M. G., Kyparos, A., Margonis, K., et al. (2010). Time-course of changes in oxidative stress and antioxidant status responses following a soccer game. *J. Strength Cond. Res.* 24, 3278–3286. doi:10.1519/JSC.0b013e3181b60444

Faul, F., Erdfelder, E., Lang, A. G., and Buchner, A. (2007). G*Power 3: a flexible statistical power analysis program for the social, behavioral, and biomedical sciences. *Behav. Res. Methods* 39, 175–191. doi:10.3758/bf03193146

Febbraio, M. A., and Koukoulas, I. (2000). HSP72 gene expression progressively increases in human skeletal muscle during prolonged, exhaustive exercise. *J. Appl. Physiol.* 89, 1055–1060. doi:10.1152/jappl.2000.89.3.1055

Fischer, C. P. (2006). Interleukin-6 in acute exercise and training: what is the biological relevance? *Exerc Immunol. Rev.* 12, 6–33.

Ganz, T. (2003). Hepcidin, a key regulator of iron metabolism and mediator of anemia of inflammation. *Blood* 102, 783–788. doi:10.1182/blood-2003-03-0672

Jemni, M., Sands, W. A., Friemel, F., Stone, M. H., and Cooke, C. B. (2006). Any effect of gymnastics training on upper-body and lower-body aerobic and power components in national and international male gymnasts? *J. Strength Cond. Res.* 20, 899–907. doi:10.1519/R-18525.1

Kajaia, T., Maskhulia, L., Chelidze, K., Akhalkatsi, V., and McHedlidze, T. (2018). Implication of relationship between oxidative stress and antioxidant status in blood serum. *Georgian Med. News*, 71–76.

Kell, D. B. (2009). Iron behaving badly: inappropriate iron chelation as a major contributor to the aetiology of vascular and other progressive inflammatory and degenerative diseases. *BMC Med. Genomics* 2, 2. doi:10.1186/1755-8794-2-2

Keller, C., Steensberg, A., Pilegaard, H., Osada, T., Saltin, B., Pedersen, B. K., et al. (2001). Transcriptional activation of the IL-6 gene in human contracting skeletal muscle: influence of muscle glycogen content. *FASEB J.* 15, 2748–2750. doi:10.1096/fj.01-0507fje

Kochanowicz, A., Niespodzinski, B., Mieszkowski, J., Marina, M., Kochanowicz, K., and Zasada, M. (2019). Changes in the muscle activity of gymnasts during a handstand on various apparatus. *J. Strength Cond. Res.* 33, 1609–1618. doi:10.1519/JSC.0000000000002124

Kochanowicz, A., Sawczyn, S., Niespodzinski, B., Mieszkowski, J., Kochanowicz, K., and Zychowska, M. (2017). Cellular stress response gene expression during upper and lower body high intensity exercises. *PLoS One* 12, e0171247. doi:10.1371/journal.pone.0171247

Kortas, J., Kuchta, A., Prusik, K., Prusik, K., Ziemann, E., Labudda, S., et al. (2017). Nordic walking training attenuation of oxidative stress in association with a drop in body iron stores in elderly women. *Biogerontology* 18, 517–524. doi:10.1007/s10522-017-9681-0

Kortas, J., Ziemann, E., Juszczak, D., Micielska, K., Kozlowska, M., Prusik, K., et al. (2020). Iron status in elderly women impacts myostatin, adiponectin and osteocalcin levels induced by nordic walking training. *Nutrients* 12, 1129. doi:10.3390/nu12041129

Lakka, T. A., Nyyssonen, K., and Salonen, J. T. (1994). Higher levels of conditioning leisure time physical activity are associated with reduced levels of stored iron in Finnish men. *Am. J. Epidemiol.* 140, 148–160. doi:10.1093/oxfordjournals.aje.a117225

Lee, P., Peng, H., Gelbart, T., Wang, L., and Beutler, E. (2005). Regulation of hepcidin transcription by interleukin-1 and interleukin-6. *Proc. Natl. Acad. Sci. U. S. A.* 102, 1906–1910. doi:10.1073/pnas.0409808102

Marciniak, A., Brzeszczyńska, J., Gwoździński, K., and Jegier, A. (2009). Antioxidant capacity and physical exercise. *Biol. Sport* 26, 197–213. doi:10.5604/20831862.894649

Marqués-Jiménez, D., Calleja-González, J., Arratibel, I., and Terrados, N. (2016). Relevant biochemical markers of recovery process in soccer. *Arch. Med. Deport.* 33, 404–412.

Mieszkowski, J., Borkowska, A., Stankiewicz, B., Kochanowicz, A., Niespodziński, B., Surmiak, M., et al. (2021a). Single high-dose vitamin D supplementation as an approach for reducing ultramarathon-induced inflammation: a double-blind randomized controlled trial. *Nutrients* 13, 1280. doi:10.3390/nu13041280

Mieszkowski, J., Kochanowicz, A., Piskorska, E., Niespodzinski, B., Siodmiak, J., Busko, K., et al. (2021b). Serum levels of bone formation and resorption markers in relation to vitamin D status in professional gymnastics and physically active men during upper and lower body high-intensity exercise. *J. Int. Soc. Sports Nutr.* 18, 29. doi:10.1186/s12970-021-00430-8

Nemeth, E., Rivera, S., Gabayan, V., Keller, C., Taudorf, S., Pedersen, B. K., et al. (2004). IL-6 mediates hypoferremia of inflammation by inducing the synthesis of the iron regulatory hormone hepcidin. *J. Clin. Invest* 113, 1271–1276. doi:10.1172/JCI20945

Parker, L., Trewin, A., Levinger, I., Shaw, C. S., and Stepto, N. K. (2017). The effect of exercise-intensity on skeletal muscle stress kinase and insulin protein signaling. *PLoS One* 12, e0171613. doi:10.1371/journal.pone.0171613

Pedersen, B. K., Steensberg, A., Fischer, C., Keller, C., Keller, P., Plomgaard, P., et al. (2003). Searching for the exercise factor: is IL-6 a candidate? *J. Muscle Res. Cell Motil.* 24, 113–119. doi:10.1023/a:1026070911202

Pedersen, B. K., Steensberg, A., Fischer, C., Keller, C., Ostrowski, K., and Schjerling, P. (2001). Exercise and cytokines with particular focus on muscle-derived IL-6. *Exerc Immunol. Rev.* 7, 18–31.

Petersen, A. M., and Pedersen, B. K. (2005). The anti-inflammatory effect of exercise. *J. Appl. Physiol. (1985)* 98, 1154–1162. doi:10.1152/japplphysiol.00164.2004

Pyne, D. B. (1994). Exercise-induced muscle damage and inflammation: a review. *Aust. J. Sci. Med. Sport* 26, 49–58.

Rodas, L., Martinez, S., Aguilo, A., and Tauler, P. (2020). Caffeine supplementation induces higher IL-6 and IL-10 plasma levels in response to a treadmill exercise test. *J. Int. Soc. Sports Nutr.* 17, 47. doi:10.1186/s12970-020-00375-4

Sawicki, P., Dornowski, M., Grzywacz, T., and Kaczor, J. J. (2018). The effects of gymnastics training on selected parameters of anaerobic capacity in 12-year-old boys. *J. Sports Med. Phys. Fit.* 58, 591–596. doi:10.23736/S0022-4707.17.06778-0

Sohail, M. U., Al-Mansoori, L., Al-Jaber, H., Georgakopoulos, C., Donati, F., Botre, F., et al. (2020). Assessment of serum cytokines and oxidative stress markers in elite athletes reveals unique profiles associated with different sport disciplines. *Front. Physiol.* 11, 600888. doi:10.3389/fphys.2020.600888

Staniak, Z., Nosarzewski, Z., and Karpilowski, B. (1994). Computerized measuring set for rowing ergometry. *Biol. Sport* 11, 271–282.

Stankiewicz, B., Cieslicka, M., Mieszkowski, J., Kochanowicz, A., Niespodzinski, B., Szwarc, A., et al. (2023). Effect of supplementation with black chokeberry (aronia melanocarpa) extract on inflammatory status and selected markers of iron metabolism in young football players: a randomized double-blind trial. *Nutrients* 15, 975. doi:10.3390/nu15040975

Steensberg, A., Fischer, C. P., Keller, C., Moller, K., and Pedersen, B. K. (2003). IL-6 enhances plasma IL-1ra, IL-10, and cortisol in humans. *Am. J. Physiol. Endocrinol. Metab.* 285, E433–E437. doi:10.1152/ajpendo.00074.2003

Suzuki, K. (2018). Cytokine response to exercise and its modulation. *Antioxidants* 7, 17. doi:10.3390/antiox7010017

Waldziński, T., Brzezińska, P., Mieszkowski, J., Durzyńska, A., Kochanowicz, M., Żołądkiewicz, K., et al. (2023). Effect of semi-professional boxing training on selected inflammatory indicators and anaerobic performance. *Arch. Budo* 19, 11–19.

Ziemann, E., Olek, R. A., Grzywacz, T., Kaczor, J. J., Antosiewicz, J., Skrobot, W., et al. (2014). Whole-body cryostimulation as an effective way of reducing exercise-induced inflammation and blood cholesterol in young men. *Eur. Cytokine Netw.* 25, 14–23. doi:10.1684/ecn.2014.0349

Zychowska, M., Kochanowicz, A., Kochanowicz, K., Mieszkowski, J., Niespodzinski, B., and Sawczyn, S. (2017). Effect of lower and upper body high intensity training on genes associated with cellular stress response. *Biomed. Res. Int.* 2017, 2768546. doi:10.1155/2017/2768546

frontiers | Frontiers in Physiology

TYPE Original Research
PUBLISHED 14 November 2024
DOI 10.3389/fphys.2024.1258175

OPEN ACCESS

EDITED BY
Hailin Zhao,
Imperial College London, United Kingdom

REVIEWED BY
Jens Djurhuus,
Aarhus University, Denmark
Linto Thomas,
University of South Florida, United States

*CORRESPONDENCE
Limin Liao,
lmliao@263.net

RECEIVED 13 July 2023
ACCEPTED 29 October 2024
PUBLISHED 14 November 2024

CITATION
Liu X, Li X and Liao L (2024) Animal study on factors influencing anterograde renal pelvis perfusion manometry.
Front. Physiol. 15:1258175.
doi: 10.3389/fphys.2024.1258175

Animal study on factors influencing anterograde renal pelvis perfusion manometry

Xin Liu[1,2,3], Xing Li[1,4] and Limin Liao[1,2,3,4,5]*

[1]Department of Urology, China Rehabilitation Research Center, Beijing Bo'ai Hospital, Beijing, China, [2]Cheeloo College of medicine, Shandong University, Jinan, Shandong, China, [3]University of Health and Rehabilitation Sciences, Qingdao, Shandong, China, [4]School of Rehabilitation, Capital Medical University, Beijing, China, [5]China Rehabilitation Science Institute, Beijing, China

Objects: Anterograde renal pelvis perfusion manometry is an effective method to assist in the diagnosis of upper urinary tract obstruction.

Methods: To established a rat model of partial ureteral obstruction to explore the perfusion rate, renal pelvis volume, obstruction sites, contralateral upper urinary tract, and lower urinary tract functions, which may affect anterograde renal pelvis perfusion manometry. To measure the renal pelvis volume using ultrasound. Depending on whether clamped the contralateral ureter and it continuously emptied the bladder, perfused the renal pelvis at rate of 15, 30, 60, 90, or 120 mL/h to measure the pressure synchronously.

Results: The research showed the renal pelvis volume of UPJ and UVJ at 1, 2, 3, and 4 weeks respectively, significantly increased compared with the control group. Comparison of the renal pelvis volume between the UPJ and UVJ groups was not statistically significant. The renal pelvis pressure of UPJ and UVJ was significantly increased compared with the control group, and the UVJ group was greater than the UPJ group. The renal pelvic pressure increased as the perfusion rate increased. Comparing the renal pelvis pressure measured using synchronous bladder emptying with the renal pelvis pressure measured singly, the difference was statistically significant. Comparing the renal pelvis pressure measured using synchronous bladder emptying with measured with a clamped contralateral ureter, the difference was not statistically significant; however, in some groups, the difference was statistically significant. Measuring the renal pelvis pressure singly and clamping the contralateral ureter, the difference was not statistically significant, except in some groups, the difference was significant.

Conclusion: The study suggested that ureter obstruction sites, perfusion rates, renal pelvis volumes, and synchronous bladder emptying affects the renal pelvis pressure. The function of the contralateral upper urinary tract did not affect renal pelvis pressure in the short term.

KEYWORDS

upper urinary tract urodynamics, partial ureter obstruction, lower urinary tract function, pressure-perfusion study, renal pelvis pressure

1 Introduction

Upper urinary tract urodynamics is a science that studies the physiologic and pathologic mechanisms of urine production and delivery. The measurement of upper urinary pressure is important to the study of upper urinary tract urodynamics. Upper urinary tract obstruction may lead to abnormal changes in urodynamics. Measuring upper urinary tract pressure can provide a reference and basis for the mechanism, auxiliary diagnosis, treatment strategy, and postoperative evaluation of upper urinary tract diseases.

Upper urinary tract obstruction increases the resistance to urine delivery. Researchers have conducted studies to clarify the critical value of renal pelvis pressure caused by obstruction. In 1973, Whitaker was the first to establish percutaneous pyelocentesis by perfusing the renal pelvis at a constant flow rate of 10 mL/min and expressing the renal pelvis pressure minus the intravesical pressure as the pressure through which a bolus could pass through the ureter. Less than 15cmH_2O indicated no obstruction, greater than 22cmH_2O showed obstruction, and 15 to 22cmH_2O revealed ambiguous obstruction (Whitaker, 1973; Whitaker, 1979). This procedure is suitable for patients whose condition cannot be confirmed through imaging and those with poor renal function accompanied by suspected obstruction; a negative diuretic nephrogram and lumbago pain, suspected interstitial obstruction; a positive diuretic nephrogram concomitant with severe dilatation of the upper urinary tract.

The Whitaker test has been used in clinical practice. Lupton reported on 25 years of experience in a single-center clinical application of the Whitaker test on 145 kidneys suspected of upper urinary tract obstruction, among which 61 patients were confirmed to have obstruction, and 17 had probable abnormal pelvis peristalsis. In patients with idiopathic hydronephrosis, the results were consistent with the diuretic nephrogram in 72% of cases (Lupton and George, 2010). Li and colleagues conducted magnetic resonance urography with the Whitaker test for patients with ileal ureter replacement after surgery. They found that the images and pressure changes of upper urinary tract reconstruction under different perfusion loads were different, aiding in the clinical diagnosis of many suspected cases (Li et al., 2021). Johnston found that the Whitaker test has diagnostic value in patients with suspected the uretopelvic junction (UPJ) or the uretovesical junction (UVJ) obstruction and those with primary ureteral dynamic deficiency (Johnston and Porter, 2014).

The Whitaker test has other clinical value as well. Yang performed the modified Whitaker test combined with image-urodynamics examination for postoperative patients with complex upper urinary tract reconstruction to evaluate the urodynamics and to guide removal of the nephrostomy tube (Yang et al., 2021). Grauer confirmed a diagnosis of a renal ptosis patient with recurrent back pain through the modified Whitaker test, the patient was confirmed to have position-dependent obstruction resulting in elevated renal pelvis pressure (Grauer et al., 2020). All of these studies reflect the significant clinical value of the Whitaker test.

Many studies have shown that ureter obstruction can cause different degrees of kidney damage on the affected side, and after a period of time, the renal function tends to be stabilize with no major changes (Wang et al., 2021; Yuvanc et al., 2021). However, there are few studies about variation in contralateral renal function. Ekinciet reported that obstruction can cause compensatory hyperplasia of the contralateral renal tissue, tubular dilatation, glomerular congestion, and other changes (Ekinci et al., 2018). So far, it is not known whether upper urinary tract urodynamic abnormalities can affect contralateral renal pelvis pressure.

We found that the Whitaker test has several shortcomings, including that the perfusion rate and upper urinary tract volume lead to poor repeatability of experimental results and that false-positive outcomes such as abnormal lower urinary tract dynamics may occur. Due to the unique anatomical characteristics of UPJ and UVJ, the measured renal pelvis pressure cannot fully represent the functional status of the ureter (Burgos et al., 1986). We intend to establish a rat model of partial ureter obstruction and study different renal pelvis volumes and perfusion rates, contralateral ureter function, and the influence of an empty bladder to determine whether these factors can meaningfully affect renal pelvis pressure.

2 Materials and methods

2.1 Experimental animals

90 SD rats weighing 200–220 g (Beijing SPF Biotechnology Co., Ltd., China). Rats were kept in an environment of 22°C, 50%–60% humidity, good ventilation, a 12-h light/dark cycle, and free access to food and water. All animal procedures were conducted in compliance with the institutional guidelines for the care and use of laboratory animals and were approved by the Animal Care and Use Committee at China Rehabilitation Research Center. All experimental protocols for this study were approved by the Animal Ethics Committee of the China Rehabilitation Research Center (Beijing, China, ID: AEEI-2022-150).

2.2 Establish the partial ureter obstruction model

The rats were randomly assigned to an experimental group and a control group, and the experimental group was classified into 1-, 2-, 3-, and 4-week groups with UPJ and UVJ partial obstruction, with 10 rats in each group. The rats were anesthetized using an intraperitoneal injection of 3 mL/kg 3% pentobarbital sodium. The UPJ and UVJ were isolated from the ureter along the pounds central through the retroperitoneum. We placed a 1.5 cm-long 3F ureteral catheter parallel to the ureter and tightened the wire knot when the ureteral wall on both sides of the ureteral catheter was closed. Then we extracted the ureteral catheter, established UPJ and UVJ partial obstruction, administered 5 mg/100 g ceftazidime sodium to prevent infection, and offered clean water after operation. The control group did not undergo operation.

2.3 Renal pelvis ultrasonography

The rats were anesthetized using an intraperitoneal injection of 3 mL/kg 3% pentobarbital sodium. We measured the anteroposterior diameter (APD), long diameter (L), and transverse diameter (T) using a Siemens color Doppler ultrasonic

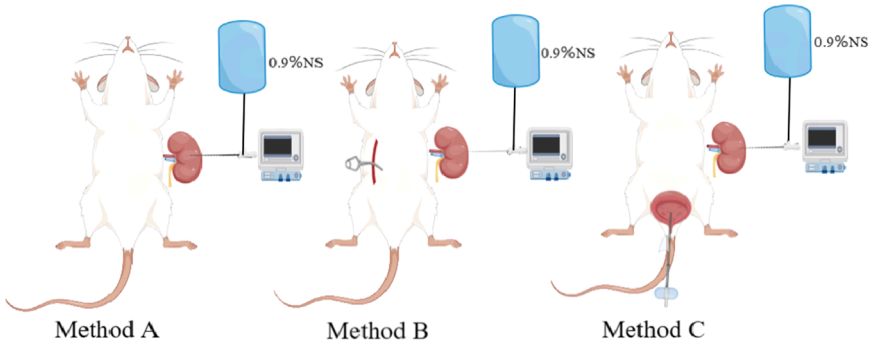

FIGURE 1
Schematic diagram of different pressure measurement methods.Method **(A)** measure the renal pelvis pressure singly; Method **(B)** clamp the contralateral ureter; Method **(C)** emptied bladder synchronously.

diagnostic instrument with a probe frequency of 8 MHz and calculated the renal pelvis volume with the formula V = APD*L*T*π/6 (Janki et al., 2018).

2.4 Perfusion-pressure measurement

Before the experiment, rats were restricted from drinking water for 24 h, the rats were anesthetized using an intraperitoneal injection of 3 mL/kg 3% pentobarbital sodium, give a blanket to keep warm, exposing the affected kidney and the contralateral ureter via a retroperitoneal approach. We used a G18/1.3 × 80 mm intravenous puncture needle to puncture the renal pelvis along the hypovascular area at the back of the kidney. Depending on the measurement method, we decided whether to place an indwelling catheter through the urethra to empty the bladder.

Using an MP150 multi-channel physiological recorder (BIOPAC, United States), we filled the pipes of the manometry and perfusion system with 0.9% normal saline (heat to 38°C), discharged the air, placed the distal end of the tube in the atmosphere, and zeroed at the same horizontal plane as the affected renal pelvis and puncture needle. Subsequently, the pyrheliometer was connected to a three-way tube, and the micro-perfusion pump and pressure sensor were connected. Perfusion was successively performed at 15, 30, 60, 90, and 120 mL/h, and the renal pelvis pressure was measured and recorded according to whether we measured the renal pelvis pressure singly (method A), the contralateral ureter was clamped when the rats began measurements after needle insertion (method B), and the bladder was emptied bladder synchronously (method C). After the adaptive contraction of the renal pelvis, the perfusion measurement was performed, and when the renal pelvis contraction and the curve was stable about 10–15 min, the next cycle of measurement was performed. After recording five datas each time, we took the average value as the final renal pelvis pressure under the corresponding measurement conditions (Figure 1).

2.5 Statistical analysis

Data are presented as mean ± standard deviation ($\bar{X} \pm S$). Statistical analysis was performed using SPSS 26 software (IBM, Armonk, NY, United States). An independent sample t-test was used to compare the two groups. Comparison of renal pelvis pressure at different perfusion rates was performed using a paired t-test or One-way analysis of variance. Multiple linear regression analysis and a regression model were used to explore the efficacy of the correlation between parameters and renal pelvis pressure. $P < 0.05$ was considered statistically significant.

3 Results

3.1 Renal pelvis volume

The renal pelvis volumes at 1, 2, 3, and 4weeks in the UPJ and UVJ groups compared with the control group, the difference was statistically significant. Comparison of the UPJ and UVJ showed a non-significant difference. (Table 1; Figure 2).

3.2 Renal pelvis pressure curve

The images show the Renal pelvis pressure curve under different perfusion rates, groups, obstruction sites and method.(Figure 3).

3.3 Renal pelvis pressure at different groups

The renal pelvis pressure in the UPJ and UVJ groups was higher than the control group. (Figure 4).

3.4 Renal pelvis pressure at different obstruction sites

The renal pelvis pressure in the UVJ group was greater than the corresponding UPJ group. (Figure 5.).

TABLE 1 Volume of renal pelvis: cm.^{3}.

Control	UPJ 1w	UPJ 2w	UPJ 3w	UPJ 4w	UVJ 1w	UVJ 2w	UVJ 3w	UVJ 4w
0.016 ± 0.007	1.64 ± 0.25*	2.43 ± 0.18*	2.79 ± 0.17*	3.07 ± 0.16*	1.65 ± 0.18*#	2.28 ± 0.18*#	2.57 ± 0.14*#	2.98 ± 0.14*#

Note:*$P < 0.05$, #$P > 0.05$.

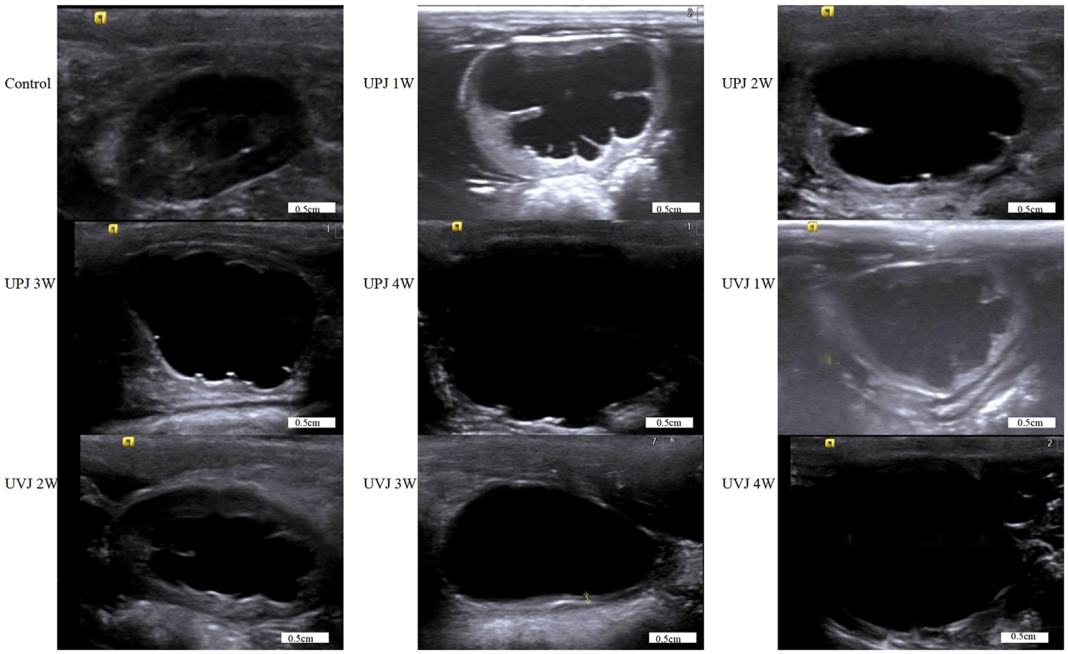

FIGURE 2
Images of renal pelvis in each group were obtained by B-ultrasound.

3.5 Renal pelvis pressure under different perfusion rates

There were significant differences in renal pelvis pressure under different perfusion rates between the UPJ, UVJ, and control groups. (Table 2).

3.6 Renal pelvis pressure under different measurement methods

The renal pelvis pressure measured under the single method was higher than that using the synchronous method, with a statistically significant difference ($P < 0.05$). In most groups between clamped contralateral ureter and single measurement of renal pelvis pressure, the difference was not statistically significant. In some groups, the renal pelvis pressure of clamped contralateral ureter was significantly lower than under the single measurement method. Comparison of the renal pelvis pressure measured with synchronous bladder emptying and clamped contralateral ureter showed no statistical significance, while in some groups, the difference was statistically significant. (Figure 6).

3.7 Multiple linear regression analysis

In this study, obstruction time, obstruction sites, renal pelvis volume, manometry method and perfusion rate were used as independent variables, and the renal plevic pressure is used as dependent variables in the multiple linear regression analysis.Multiple linear regression is used to establish the regression equation: the renal pelvis pressure = 0.805 + 0.052*time + 3.854*site + 0.455*renal pelvis volume + 0.104*perfusion rate-1.006*method ($F = 1{,}438.614$, $P < 0.01$) and the model constant = 0.805 and the independent variable could explain 91.8% of the renal pelvis pressure. (Table 3).

4 Discussion

Different noninvasive imaging examinations can be used to diagnose most abnormal upper urinary tract urodynamics. However, the diagnostic value of upper urinary tract manometry for urodynamic abnormalities cannot be ignored. Whitaker proposed pyelostomy and perfused the renal pelvis at a constant rate of 10 mL/min while recording the pressure in the renal pelvis and bladder to aid the diagnosis of upper urinary tract

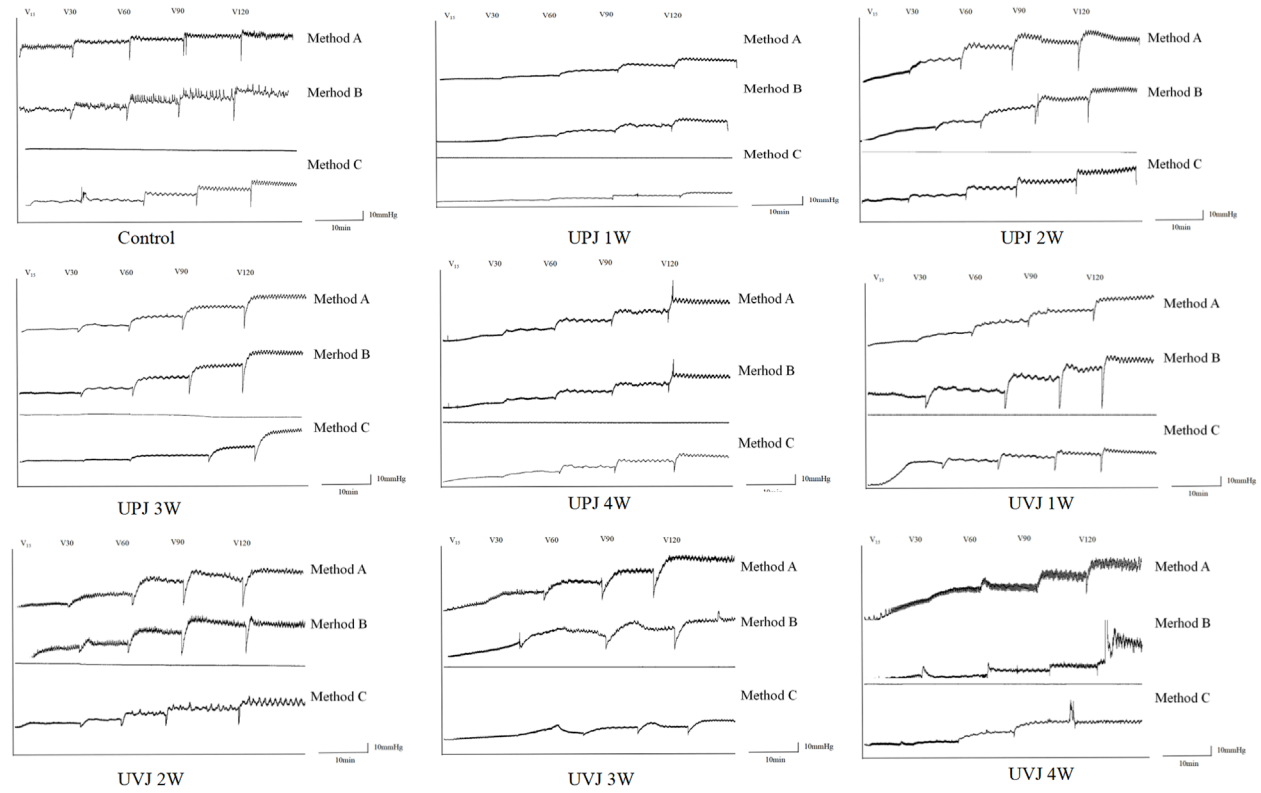

FIGURE 3
Images of the renal pelvis pressure curve under different perfusion rates, groups, obstruction sites and method.

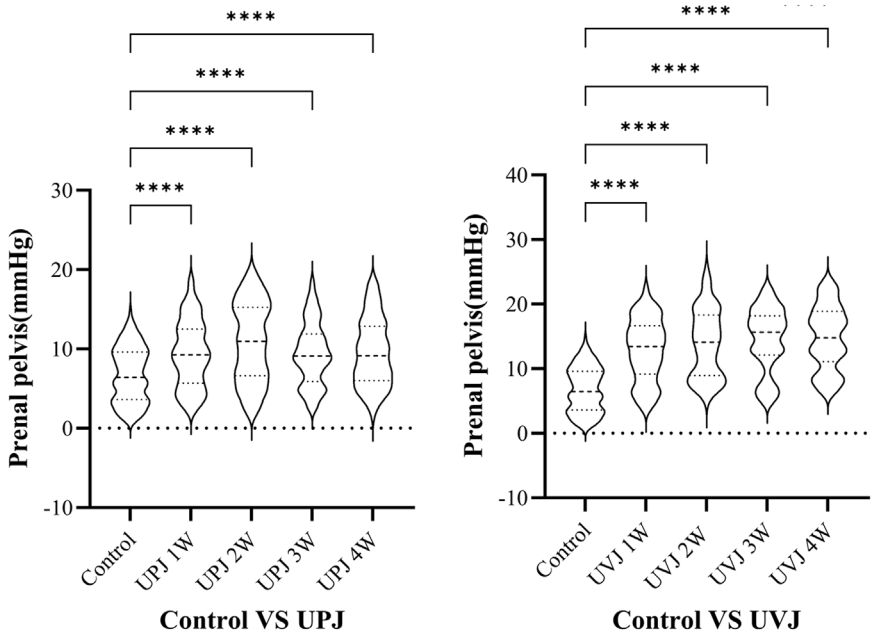

FIGURE 4
Comparison the pressure between control group and upj or uvj group. Note:$^{****}P < 0.0001$.

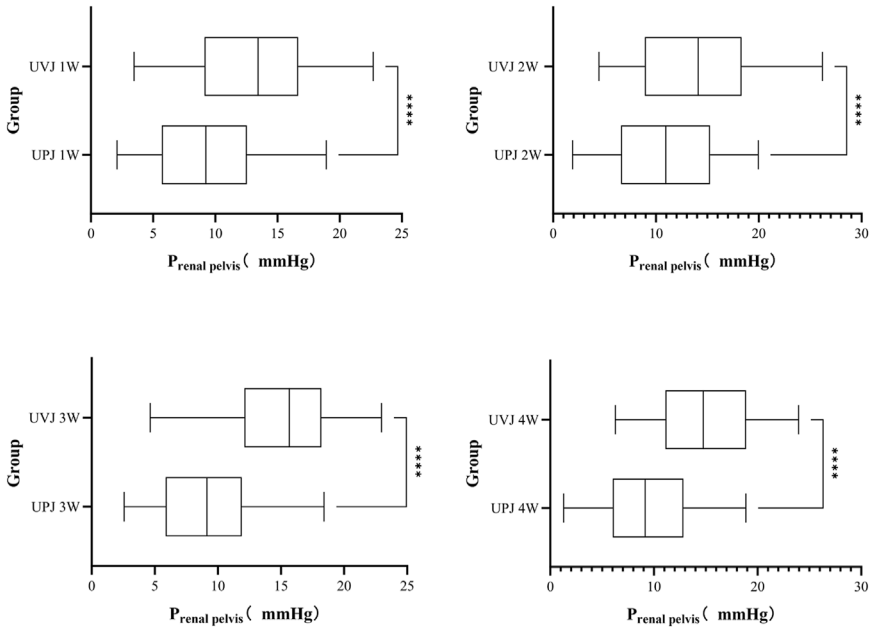

FIGURE 5
Comparison the pressure between UPJ and UVJ group. Note:****$P < 0.0001$.

TABLE 2 Comparison the pressure at different perfusion rates: mmHg.

$Method_{V(mL/h)}$	$\bar{x} \pm s$	P	$Method_{V(mL/h)}$	$\bar{x} \pm s$	P	$Method_{V(mL/h)}$	$\bar{x} \pm s$	P
A15-30	−3.49 ± 1.73	<0.001	B15-30	−3.15 ± 1.89	<0.001	C15-30	−3.44 ± 1.89	<0.001
A15-60	−6.38 ± 1.72	<0.001	B15-60	−6.30 ± 2.43	<0.001	C15-60	−6.17 ± 1.86	<0.001
A15-90	−9.10 ± 2.09	<0.001	B15-90	−8.97 ± 2.65	<0.001	C15-90	−8.83 ± 1.96	<0.001
A15-120	−11.60 ± 2.25	<0.001	B15-120	−11.81 ± 2.72	<0.001	C15-120	−11.14 ± 1.93	<0.001
A30-60	−2.89 ± 1.37	<0.001	B30-60	−3.15 ± 1.15	<0.001	C30-60	−2.72 ± 1.47	<0.001
A30-90	−5.61 ± 1.99	<0.001	B30-90	−5.82 ± 1.78	<0.001	C30-90	−5.38 ± 1.91	<0.001
A30-120	−8.11 ± 2.35	<0.001	B30-120	−8.66 ± 2.01	<0.001	C30-120	−7.70 ± 2.00	<0.001
A60-90	−2.72 ± 1.14	<0.001	B60-90	−2.68 ± 1.10	<0.001	C60-90	−2.66 ± 1.12	<0.001
A60-120	−5.22 ± 1.75	<0.001	B60-120	−5.51 ± 1.48	<0.001	C60-120	−4.98 ± 1.37	<0.001
A90-120	−2.50 ± 1.35	<0.001	B90-120	−2.84 ± 1.00	<0.001	C90-120	−2.32 ± 1.00	<0.001

Note: Methods: A: measured the renal pelvis singly; B: clamped the contralateral ureter; C: Emptied the bladder synchronously. V: Perfusion rate (mL/h).

obstruction. However, many subsequent studies have found that patients with chronic alcohol consumption and interstitial obstruction may have false-negative results when perfused at a rate of 10 mL/min (Farrugia and Whitaker, 2019).

When Djurhuus and colleagues performed the Whitaker test on 28 patients with upper urinary tract obstruction, 9 patients with severe hydronephrosis needed a perfusion rate higher than 10 mL/min to obtain correct obstructive renal pelvis pressure, indicating that different degrees of hydronephrosis may affect the pressure (Djurhuus et al., 1985). Some studies have established acute and chronic ureteral obstruction models and included perfusion rate experiments at 1, 5, and 10 mL/min, finding that perfusion rate and renal pelvis volume may be the key factors affecting the reliability of Whitaker test results (Ryan et al., 1989).

In our study, the renal pelvis volumes at 1, 2, 3, and 4 weeks in the UPJ and UVJ groups increased significantly. There was no significant difference between the UPJ and UVJ groups renal pelvis volume. The renal pelvis pressure in the UPJ and UVJ groups was

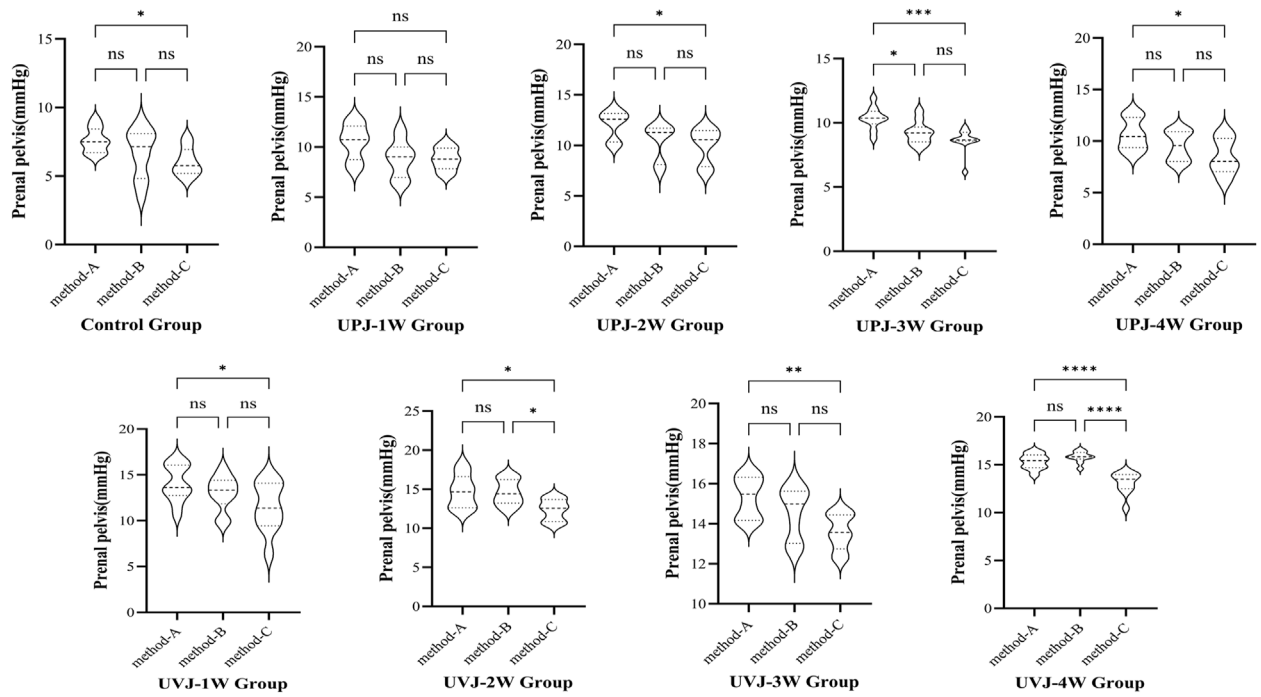

FIGURE 6
Comparison the pressure between different methods.Note:*$P < 0.05$;**$P < 0.01$;***$P < 0.001$;****$P < 0.0001$.

significantly higher than in the control group. The renal pelvis pressure in the UVJ group was higher than the UPJ group. The renal pelvis pressure increased gradually with renal pelvis volume, we speculate that the reason is that the pressure increases with volume during maintenance of upper urinary tract compliance balance. Although the comparison of renal pelvis volume between the UPJ and UVJ groups was not statistically different, actual measurements showed that the pressure in the UVJ group was higher than the UPJ group. Partial ureter obstruction at the UVJ may have led to dilation of the whole ureter, which may have increased the volume of the upper urinary tract and, thus, renal pelvis pressure.

In other studies, the renal pelvis pressure peaked at 2w after ureteral ligation, then gradually decreased and remained constant at 8w (Wen et al., 1998). Koff studied an animal model of chronic ureter partial obstruction, finding that renal pelvis compliance allowed it to adapt to increasing capacity under low pressure (Koff, 2019). As the pelvis volume increases, the pressure increases to a critical point, after which a slight change in the volume of the pelvis causes a significantly increase in pressure. As the renal pelvis volume increases significantly, hydronephrosis increases, the pressure decreases gradually, and the pressure-volume of the partially obstructed renal pelvis reaches equilibrium.

The decrease in renal pelvis pressure is caused by a decrease in glomerular filtration rate and regurgitation of renal pelvis urine to the renal tubules, veins, lymphatics, and renal interstitium (Strobel et al., 2016). In addition, dilation compliance is different across renal pelvis types. The renal parenchyma restricts the intrarenal pelvis and is difficult to dilate, while the extrarenal pelvis is easy to dilate outwardly, and its pressure drops rapidly (Chavez-Iniguez et al., 2020). Our experiment was conducted on rats whose renal pelvis was mainly intrarenal, and the study endpoint was 4w, which was shorter than that of the previously studies. Most of the renal pelvis volume was still in the acute ascending stage; thus, the renal pelvis pressure increased with increasing renal pelvis volume.

The study found that regardless of whether the control or UPJ or UVJ groups were at different perfusion rates, the renal pelvis pressure was significantly different. With an increased perfusion rate, the pressure increased. The flow of perfusion in the upper urinary tract conforms to the hydrodynamics of the Poiseuille formula (Zheng et al., 2021). Therefore, the renal pelvis pressure also increases with the perfusion rate. Hopf conducted the Whitaker test on patients after pyeloplasty and found that the perfusion rate of 10 mL/min can cause a false increase in renal pelvis pressure in some patients (Hopf et al., 2016). Therefore, perfusion rate in the study was questioned, but they did not conduct further study. Lupton measured renal pelvis pressure in patients with upper urinary tract dilatation after useing diuretic and found almost no significant changes in the renal pelvis pressure at a perfusion rate of 10 mL/min. The renal pelvis pressure gradually increased to a stable level when the perfusion rate was increased to 30 mL/min (Lupton et al., 1985). These studies are consistent with the experimental phenomena that we have observed. However, one study measured the renal pressure at the upper, middle, and lower renal calyces and outlet pelvis after 100–150 mL/min perfusion with pig kidneys and found no statistical difference when monitoring pressure among groups under different perfusion rates (Zhu et al., 2016). Jens Mortensen found a renal resting pressure of 0.3–14.7cmH_2O through perfusion of 40 healthy pig kidneys. The renal pelvis pressure difference was only 3.7cmH_2O after perfusion of 8–20 mL/min, with a slight fluctuation range (Mortensen et al., 1982; Mortensen et al., 1983). Because upper

TABLE 3 Multiple Linear Regression Analysis of independent variables vs. the renal pelvis pressure.

Model summary[b]					
Model	R	R^2	R_{adj}^2	Std.Errors of the estimate	Durbin-Watson
	0.918[a]	0.843	0.842	2.08727	1.007

ANOVA[a]					
Model	Sum of squares	Degree of freedom	Mean square	F	Sig
Regression	31,337.887	5	6,267.577	1,438.614	0.000[b]
Residuals	5,855.376	1,344	4.357		
Total	37,193.263	1,349			

Coefficient[a]								
Model	Unstd.Coefficient		Std.Coefficient	t	Sig	95.0% CI for B		Collinear statistics	
	B	Std.Error	Beta			Lower	Upper	Tolerance	VIF
Constant	0.805	0.200		4.028	0.000	0.413	1.197		
Position	3.854	0.104	0.489	36.989	0.000	3.649	4.058	0.669	1.495
Volume	−0.455	0.165	−0.079	−2.758	0.006	−0.779	−0.131	0.142	4.041
Method	−1.006	0.070	−0.157	−14.462	0.000	−1.143	−0.87	1.000	1.000
Rate	0.104	0.001	0.763	70.479	0.000	0.101	0.107	1.000	1.000
Time	0.052	0.015	0.091	3.428	0.001	0.022	0.082	0.166	3.006

[a]Predictive variable: (constant), Time, Rate, Method, Position, Volume.
[b]Dependent variable: Pressure.

urinary compliance is inversely proportional to renal pelvis pressure, false positives may occur when the perfusion rate is too fast or when the patient uses diuretics and drinks excessive water.

In contrast, an inadequate perfusion rate may cause some cases of mild obstruction to be missed. Therefore, when clinically performing the pressure-perfusion test, the perfusion rate should be increased, and the pressure value of the renal pelvis with obstruction should be reduced for severely dilated patients. The pressure value of the renal pelvis with obstruction should be decreased for patients with mild dilated or retroperitoneal adhesion.

Whitaker also suggested that renal pelvis pressure measured by perfusion pressure measurement was the absolute pressure of the whole measuring system. After zero adjustments of the whole system, the intra-abdominal pressure should be subtracted (taking intravesical pressure as the intra-abdominal pressure), and the absolute renal pelvis pressure minus the intravesical pressure is equal to the relative pressure, which is expressed as the pressure required by the bolus passing through the obstruction site (Whitaker, 1973). Therefore, whether intravesical pressure should be measured synchronously at different obstruction sites is still undetermined. The research established obstruction models for specific sites in the UPJ and UVJ and found that the renal pelvis pressure measured by synchronous bladder emptying was significantly lower than that measured singly. This phenomenon is consistent with what Whitaker described in the experiment. Jones conducted the Whitaker test on patients with upper urinary tract obstruction and poor bladder compliance, finding that the degree of bladder filling significantly affected upper urinary tract urodynamics. Subsequently, he conducted a study on patients with normal bladder compliance, finding that the rate and degree of bladder filling also affected upper urinary tract urodynamics (Jones et al., 1988).

Other studies have found that the influence of intravesical pressure and detrusor pressure on upper urinary tract urodynamics can be predicted by measuring intravesical pressure and detrusor pressure during the early, middle, and late bladder-filling periods and that the intravesical pressure and detrusor pressure in the middle and late periods were more sensitive and specific in predicting the urodynamic changes in the upper urinary tract (Lyu et al., 2022). This may be because, under normal circumstances, urine is transported to the bladder as a bolus, and continuous perfusion breaks this physiologic mode of transport. After the perfusion liquid fills the bladder, the antireflux mechanism at the vesicoureteral disappears, resulting in increased pressure in the upper urinary tract. The effect of bladder filling on upper urinary tract urodynamics may be altered if the bladder is emptied continuously and synchronously with an indwelling catheter while the renal pelvis pressure is measured.

Mayo found that when the obstruction was located in the UPJ or upper ureter, simultaneous intravesical pressure measurement may not be necessary after the renal pelvis and bladder are emptied before manometry and after standard and strict *in vitro* zeroing. No significant change in renal pelvis pressure was observed on normal ureter manometry, even when the upper urinary tract was dilated due to bladder filling. However, in cases of suspected UVJ obstruction, renal pelvis hypertension with bladder filling was found (Mayo, 1983). Based on these studies, we recommend that the renal pelvis and bladder be emptied entirely before manometry and standardized using *in vitro* zeroing. Bladder emptying should be synchronized to reduce the influence of atmospheric and intraperitoneal pressure and bladder filling on upper urinary tract urodynamics.

The study also found no statistically significant difference in renal pelvis pressure between the clamped contralateral ureter and the single measurement of renal pelvis pressure in most groups. But in some groups, the clamped contralateral ureter-measured renal pelvis pressure was significantly lower than the single measurement method. The measurement error may have been caused by incomplete air emptying, poor sealing, or other reasons in the pressure measuring system during the experiment. However, the overall trend of experimental results is significant, and such measurement errors are acceptable. Therefore, whether abnormal contralateral upper urinary tract urodynamics have long-term effects on the pther side needs further study.

There are also limitations to our study. Firstly, a partial ureteral obstruction model was established, but due to the limitations of detection techniques and evaluation criteria, the degree of obstruction was not measured. No studies of patients were conducted due to ethical constraints. Our prediction model involves a lot of independent variables.These defects may have led to missing reference values in the clinical research methods and conclusions. However, we found that the obstruction site, perfusion rate, renal pelvis volume, and other factors affected the renal pelvis pressure, suggesting that individual diagnosis should be carried out in the clinical setting.

5 Conclusion

The research suggested that the obstruction site, perfusion rate, renal pelvis volume, and whether the bladder was emptied synchronously during measurement may affect the renal pelvis pressure, while the function of opposite upper urinary tract does not affect the other side renal pelvis pressure in the short term.Our regression model has a good precision and provides a reference for evaluating the renal pelvis pressure. However, our prediction model still needs multi-center and randomized controlled validation. In order to obtain a simple and convenient non-invasive model for predicting renal pelvis pressure.

Data availability statement

The original contributions presented in the study are included in the article/supplementary material, further inquiries can be directed to the corresponding author.

Ethics statement

The animal study was approved by the Animal Care and Use Committee at Capital Medical University. The study was conducted in accordance with the local legislation and institutional requirements.

Author contributions

XnL : Data curation, Writing–original draft. XgL : Methodology, Supervision, Writing–review and editing. LL: Conceptualization, Writing–review and editing.

Funding

The author(s) declare that financial support was received for the research, authorship, and/or publication of this article. This work was supported by the fundamental research funds for central public welfare research institutes (2023CZ-1); The Beijing Natural Science Foundation (No. 7222235); National Key Research and Development Program of China (No.2023YFC3605301).

Conflict of interest

The authors declare that the research was conducted in the absence of any commercial or financial relationships that could be construed as a potential conflict of interest.

Publisher's note

All claims expressed in this article are solely those of the authors and do not necessarily represent those of their affiliated organizations, or those of the publisher, the editors and the reviewers. Any product that may be evaluated in this article, or claim that may be made by its manufacturer, is not guaranteed or endorsed by the publisher.

References

Burgos, F. J., Tallada, M., Perales, L., and Romero, M. J. (1986). The value of the Whitaker test in the diagnosis of the equivocal obstruction of the pyeloureteral junction. *Arch. Esp. Urol.* 39 (2), 83–91.

Chavez-Iniguez, J. S., Navarro-Gallardo, G. J., Medina-Gonzalez, R., Alcantar-Vallin, L., and Garcia-Garcia, G. (2020). Acute kidney injury caused by obstructive nephropathy. *Int. J. Nephrol.* 2020, 8846622. doi:10.1155/2020/8846622

Djurhuus, J. C., Sorensen, S. S., Jorgensen, T. M., and Taagehoj-Jensen, F. (1985). Predictive value of pressure flow studies for the functional outcome of reconstructive surgery for hydronephrosis. *Br. J. Urol.* 57 (1), 6–9. doi:10.1111/j.1464-410x.1985.tb08974.x

Ekinci, C., Karabork, M., Siriopol, D., Dincer, N., Covic, A., and Kanbay, M. (2018). Effects of volume overload and current techniques for the assessment of fluid status in patients with renal disease. *Blood Purif.* 46 (1), 34–47. doi:10.1159/000487702

Farrugia, M. K., and Whitaker, R. H. (2019). The search for the definition, etiology, and effective diagnosis of upper urinary tract obstruction: the Whitaker test then and now. *J. Pediatr. Urol.* 15 (1), 18–26. doi:10.1016/j.jpurol.2018.11.011

Grauer, R., Gray, M., and Schenkman, N. (2020). Modified Whitaker test: a novel diagnostic for nephroptosis. *BMJ Case Rep.* 13 (4), e235108. doi:10.1136/bcr-2020-235108

Hopf, H. L., Bahler, C. D., and Sundaram, C. P. (2016). Long-term outcomes of robot-assisted laparoscopic pyeloplasty for ureteropelvic junction obstruction. *Urology* 90, 106–110. doi:10.1016/j.urology.2015.12.050

Janki, S., Kimenai, H., Dijkshoorn, M. L., Looman, C. W. N., Dwarkasing, R. S., and Ijzermans, J. N. M. (2018). Validation of ultrasonographic kidney volume measurements: a reliable imaging modality. *Exp. Clin. Transpl.* 16 (1), 16–22. doi:10.6002/ect.2016.0272

Johnston, R. B., and Porter, C. (2014). The whitaker test. *Urology J.* 11 (3), 1727–1730.

Jones, D. A., Holden, D., and George, N. J. (1988). Mechanism of upper tract dilatation in patients with thick walled bladders, chronic retention of urine and associated hydroureteronephrosis. *J. Urol.* 140 (2), 326–329. doi:10.1016/s0022-5347(17)41594-1

Koff, S. (2019). The search for the definition and effective diagnosis of upper urinary tract obstruction: the Whitaker test then and now, Whitaker et al. 2018. *J. Pediatr. Urol.* 15 (1), 27–28. doi:10.1016/j.jpurol.2018.10.032

Li, X., Wang, X., Li, T., Zhu, W., Ma, M., Yang, K., et al. (2021). Cine magnetic resonance urography and Whitaker test: dynamic visualized and quantified tools in ileal ureter replacement. *Transl. Androl. Urology* 10 (11), 4110–4119. doi:10.21037/tau-21-507

Lupton, E. W., and George, N. J. (2010). The Whitaker test: 35 years on. *BJU Int.* 105 (1), 94–100. doi:10.1111/j.1464-410X.2009.08609.x

Lupton, E. W., Holden, D., George, N. J., Barnard, R. J., and Rickards, D. (1985). Pressure changes in the dilated upper urinary tract on perfusion at varying flow rates. *Br. J. Urol.* 57 (6), 622–624. doi:10.1111/j.1464-410x.1985.tb07019.x

Lyu, L., Yao, Y. X., Liu, E. P., Zhang, Y. P., Hu, H. J., Ji, F. P., et al. (2022). A study of urodynamic parameters at different bladder filling stages for predicting upper urinary tract dilatation. *Int. Neurourol. J.* 26 (1), 52–59. doi:10.5213/inj.2142244.122

Mayo, M. E. (1983). Clinical experience with upper tract urodynamics. *J. Urol.* 129 (3), 536–538. doi:10.1016/s0022-5347(17)52222-3

Mortensen, J., Bisballe, S., Jorgensen, T. M., Tagehoj-Jensen, F., and Djurhuus, J. C. (1982). The normal pressure-flow relationship of pyeloureter in the pig. *Urol. Int.* 37 (1), 68–72. doi:10.1159/000280799

Mortensen, J., Djurhuus, J. C., Laursen, H., and Bisballe, S. (1983). The relationship between pressure and flow in the normal pig renal pelvis - an experimental-study of the range of normal pressures. *Scand. J. Urology Nephrol.* 17 (3), 369–372. doi:10.3109/00365598309182148

Ryan, P. C., Maher, K., Hurley, G. D., and Fitzpatrick, J. M. (1989). The whitaker test: experimental analysis in a canine model of partial ureteric obstruction. *J. Urol.* 141 (2), 387–390. doi:10.1016/s0022-5347(17)40779-8

Strobel, S., Spitz, L., and Marks, S. D. (2016). "Hospital for sick children (London england)," in *Great ormond street handbook of paediatrics*. Boca Raton: CRC Press, Taylor and Francis Group.

Wang, F., Otsuka, T., Takahashi, K., Narui, C., Colvin, D. C., Harris, R. C., et al. (2021). Renal tubular dilation and fibrosis after unilateral ureter obstruction revealed by relaxometry and spin-lock exchange MRI. *NMR Biomed.* 34 (8), e4539. doi:10.1002/nbm.4539

Wen, J. G., Chen, Y., Frokiaer, J., Jorgensen, T. M., and Djurhuus, J. C. (1998). Experimental partial unilateral ureter obstruction. I. Pressure flow relationship in a rat model with mild and severe acute ureter obstruction. *J. Urol.* 160 (4), 1567–1571. doi:10.1097/00005392-199810000-00116

Whitaker, R. H. (1973). Methods of assessing obstruction in dilated ureters. *Br. J. Urol.* 45 (1), 15–22. doi:10.1111/j.1464-410x.1973.tb07001.x

Whitaker, R. H. (1979). The Whitaker test. *Urologic Clin. N. Am.* 6 (3), 529–539. doi:10.1016/s0094-0143(21)01211-8

Yang, Y., Li, X., Xiao, Y., Li, X., Chen, Y., and Wu, S. (2021). A modified Whitaker test (upper urinary tract videourodynamics) using for evaluating complex upper urinary tract reconstruction surgical effect. *Transl. Androl. Urology* 10 (1), 336–344. doi:10.21037/tau-20-1055

Yuvanc, E., Tuglu, D., Ozan, T., Kisa, U., Balci, M., Batislam, E., et al. (2021). Evaluation of pheniramine maleate and zofenopril in reducing renal damage induced by unilateral ureter obstruction. An experimental study. *Arch. Med. Sci.* 17 (3), 812–817. doi:10.5114/aoms.2019.88320

Zheng, S., Carugo, D., Mosayyebi, A., Turney, B., Burkhard, F., Lange, D., et al. (2021). Fluid mechanical modeling of the upper urinary tract. *WIREs Mech. Dis.* 13 (6), e1523. doi:10.1002/wsbm.1523

Zhu, X., Song, L., Xie, D., Peng, Z., Guo, S., Deng, X., et al. (2016). Animal experimental study to test application of intelligent pressure control device in monitoring and control of renal pelvic pressure during flexible ureteroscopy. *Urology* 91 (242), e211–e15. doi:10.1016/j.urology.2016.02.022

frontiers | Frontiers in Physiology

TYPE Original Research
PUBLISHED 06 January 2025
DOI 10.3389/fphys.2024.1370586

OPEN ACCESS

EDITED BY
Joaquin Garcia-Estañ,
University of Murcia, Spain

REVIEWED BY
Nikos Margaritelis,
Aristotle University of Thessaloniki, Greece
Ricardo Mora-Rodriguez,
University of Castilla-La Mancha, Spain

*CORRESPONDENCE
Ira Jacobs,
ira.jacobs@utoronto.ca

RECEIVED 15 January 2024
ACCEPTED 05 November 2024
PUBLISHED 06 January 2025

CITATION
McLaughlin M, Dizon K and Jacobs I (2025) The effects of aerobic exercise and heat stress on the unbound fraction of caffeine. *Front. Physiol.* 15:1370586. doi: 10.3389/fphys.2024.1370586

The effects of aerobic exercise and heat stress on the unbound fraction of caffeine

Mackenzie McLaughlin[1,2], Kaye Dizon[3] and Ira Jacobs[1,3,4]*

[1]Human Physiology Research Unit, Faculty of Kinesiology and Physical Education, University of Toronto, Toronto, ON, Canada, [2]Department of Clinical Research, Cleveland Clinic Canada, Toronto, ON, Canada, [3]Department of Pharmacology and Toxicology, Faculty of Medicine, University of Toronto, Toronto, ON, Canada, [4]The Tannenbaum Institute for Science in Sport, University of Toronto, Toronto, ON, Canada

Introduction: The fraction of drug circulating in the blood that is not bound to plasma proteins (f_u) is considered pharmacologically active since it readily binds to its receptor. *In vitro* evidence suggests that changes in temperature and pH affect the affinity of drug binding to plasma proteins, resulting in changes in f_u. In light of the well-established effects of exercise on body temperature and blood pH, we investigated whether an increase in blood temperature and decrease in pH facilitated through passive heating and exercise translated to a change in the f_u of caffeine.

Methods: Ten healthy participants (4 females and 6 males; age: 21.9 ± 2.7 years [means ± SD]) ingested 3 mg/kg of anhydrous caffeine on two separate occasions comprised of a control trial involving 105 min of rest, and an experimental trial involving 10 min of passive heating, followed by 20 min of cycling at 55% $\dot{V}O_{2peak}$, and then 10 sprint intervals at 90% $\dot{V}O_{2peak}$. Venous blood was sampled and the plasma was processed via ultrafiltration to quantify the f_u of caffeine and its major metabolite, paraxanthine.

Results: The exercise protocol resulted in maximal increases in core temperature of 1.37°C ± 0.27°C and lactate of 10.34 ± 3.33 mmol/L, and a decrease in blood pH of 0.12 ± 0.051 (all $p < 0.05$), which did not affect the f_u of caffeine (baseline: 0.86 vs post-exercise: 0.75; $p = 0.30$) or paraxanthine (baseline: 0.59 vs. post-exercise: 0.70; $p = 0.11$). Furthermore, the rate of metabolism of caffeine assessed through the metabolic ratio ([paraxanthine]/[caffeine]) did not differ between resting and exercise trials.

Discussion: Therefore, the changes in blood temperature and pH in this study did not affect the f_u of caffeine or paraxanthine.

KEYWORDS

exercise pharmacokinetics, plasma protein binding, metabolic ratio, ultrafiltration, Centrifree®, exercise hemodynamics, Q10 effect

1 Introduction

Evaluating potential interactions when medications are ingested by individuals increasing their physical activity is becoming more important given the rise in drug prescriptions (OECD, 2019) and exercise recommendations (Task Force on Community Preventive, 2002). Previous drug-exercise investigations have focussed on exercise-induced hemodynamic changes on drug pharmacokinetics (PK) (Sweeney, 1981), yet drug binding in blood remains unstudied. This is puzzling since exercise is associated with physicochemical and biochemical changes in the blood, with temperature and acidity being major factors that both affect drug binding and, thus, its efficacy. Therefore, a patient given prescriptions for both exercise and medications may experience unintended drug effects. Examining exercise's effect on drug-plasma protein binding will add to our repository of drug interactions for personalized medicine and provide insight into exercise as a modality to elicit specific physiological changes that can predictably change a medication's effect.

Drugs travel in the blood in two forms—that which is bound to plasma proteins, known as the bound fraction (f_b), and that which is not bound to plasma proteins, known as the free/unbound fraction (f_u). The degree and relative affinity of drug binding to plasma proteins (e.g., albumin, α1-acid glycoprotein [AGP], and lipoprotein) is based on the drug's physicochemical properties, with basic drugs binding well to AGP, and acidic and neutral drugs preferentially binding to albumin (Brown et al., 2010). Since the f_b is bound to proteins, it is not available to bind to its receptor and is, thus, rendered inactive. In contrast, the f_u is free in the circulation and can: 1. bind to its receptor to elicit a pharmacological response; 2. move to extravascular tissues, increasing the drug's volume of distribution (V_d); and 3. interact with enzymes and transporters, increasing the rate of drug metabolism and excretion (Roberts et al., 2013). For example, a 9.7% increase in the %f_u of the antibiotic, ertapenem, resulted in a 112% increase in its clearance (CL) and 160% increase in its V_d (Burkhardt et al., 2007). Thus, drug binding is highly relevant to understanding both drug PK as well as pharmacodynamics (PD).

All drugs have an inherent affinity for plasma proteins which, in exception to pregnancy and aging, remains relatively constant for healthy individuals under normal physiological conditions (Kremer et al., 1988). However, disruption of the drug-protein complex through competitive binding with exogenous substances and conformational changes from physiological perturbations can alter the degree of drug-protein binding. Competitive binding is commonly observed with drug-drug interactions, whereby drug A will competitively bind to a similar binding spot occupied by drug B, effectively disrupting its interaction and increasing drug B's f_u. For example, valproic acid displaces phenytoin from a shared albumin binding spot because of its higher association constant (McElnay and D'Arcy, 1983). Conformational changes to proteins from endogenously-generated perturbations can affect ligand-binding sites, thus, affecting drug-protein affinity. For example, *in vitro* studies give evidence that changes in blood pH and temperature can affect a drug's f_u. In pooled human serum spiked with propranolol (a beta blocker with %f_u < 10%), a decrease in pH from ~7.6 to ~6.6 was associated with an increase in %f_u from 6% to 10.5% (Paxton and Calder, 1983). The same study showed that an increase in temperature from 25°C to 30°C was associated with a ~1.5% increase in propranolol's %f_u (Paxton and Calder, 1983). This effect is rather common. A review of *in vitro* studies investigating >20 compounds revealed that all of the basic drugs investigated experience an increase (e.g., ranging from 3.5% [practolol] to 136% [fentanyl]) in f_u when pH is decreased, while acidic drugs exhibit unpredictable changes in f_u (e.g., ranging from −15% [etopside] to 95% [tenoxicam]) (Hinderling and Hartmann, 2005). The therapeutic significance of alterations in *fu* of these magnitude are maximized in drugs that: 1. are highly protein bound, 2. have a high intrinsic clearance (CL_{int}); or 3. are not titrated to the pharmacological response (Roberts et al., 2013). The first point is exemplified with (R)-warfarin, a commonly prescribed oral anticoagulant that has a plasma protein binding of 99%, which, if decreased to 97%, for example, would result in a 2-fold increase in f_u, which would affect V_d and CL.

Mechanistically, increasing the temperature results in increased enzyme activity, known as the Q_{10} effect, up until a threshold where the enzyme's tertiary (i.e., globular) and secondary structures are denatured (Sinha et al., 2008). Changes in pH will alter the degree of ionization and the resulting charge on amino acid side chains (Baler et al., 2014). In the case of albumin, deviating the pH from 7.4 decreases α-helical and increases β-sheet structures, with alkalinic conditions (e.g., pH = 9) reducing overall charge and promoting the N-B (normal-to-base) transition and acidic conditions resulting in the N-F (normal-to-fast) transition at pH = 4 (Peters and Peters, 1995). These conformational changes are reversible up to the extremes of pH < ~2 and > ~9, beyond which disulfide bonds are cleaved and, in basic conditions, tyrosyl hydroxyl groups are deprotonated (Peters and Peters, 1995). These changes can be further accelerated by fluctuations in calcium content, urea, and temperature (Peters and Peters, 1995), which are all increased in some capacity during exercise (Foran et al., 2003), and, cumulatively, may promote the conformational changes to albumin within the physiological pH range. For example, the N-B transition at higher pH values is augmented with increasing calcium concentration, which, in the case of warfarin, led to higher binding with albumin (Wilting et al., 1980).

The normal blood pH range is 7.38–7.44, yet exercise above the anaerobic threshold results in the formation and immediate dissociation of lactate to its ion (La^-) and H^+, which can decrease blood pH to 6.8 during exhaustive exercise (McArdle et al., 2007). Exercise also increases metabolic heat production, elevating core body temperature (T_c), with values of >41°C being reported in athletes during competition (Byrne et al., 2006). Given that *in vitro* experiments have characterized changes in drug f_u resulting from changes in the pH and temperature of a drug's medium, and exercise is associated with changes in blood pH and increased temperature, it is reasonable to speculate that exercise has the potential to affect a drug's f_u. The current investigation is the first to assess in humans the effects of acute exercise on a drug's f_u. Because of the potential risk for aberrant drug effects, we chose to study these interactions using caffeine, the world's most consumed drug that is toxic at doses ~30-fold higher than the average daily intake (Nawrot et al., 2003). Moreover, any change in its %*fu* is likely to be reflected in its efficacy, which will be of interest to the ~75% of professional athletes who ingest caffeine as an ergogenic aid (Aguilar-Navarro et al., 2019). An increase in the %*fu* may cause a stronger ergogenic effect, which may

engender recommendations for a lower dose while a decreased %*fu* may engender the opposite.

Caffeine is a weak base that has been shown to bind to albumin (Wu et al., 2009); yet, information about its binding to AGP is scant. After being absorbed within 45 min, caffeine distributes throughout well-hydrated tissues with a V_d of 0.5–0.8 L/kg and is primarily (90%) metabolized by the enzyme, CYP1A2, to paraxanthine (84% of CYP1A2 metabolites), which makes caffeine a commonly used probe drug to phenotype 1A2 activity (Nehlig, 2018). Caffeine experiences relatively low protein binding (%f_u = 70–90%) (USIM, 2001) and few studies have evaluated changes in its binding capacity. Comparison of caffeine f_u between young (25–30 years) and elderly (66–78 years) individuals using CF-25 ultrafiltration 'cones' revealed that age is associated with a decrease in plasma albumin concentration (45.9–41.13 g/L) but is not associated with a change in %f_u (Blanchard, 1982a). Another study using fluorescence spectroscopy to evaluate albumin-caffeine interactions found a decrease in the apparent binding constant (K_b) and number of binding sites with increasing temperatures, giving evidence that the albumin-caffeine complex may dissociate at higher temperatures and increase the f_u of caffeine (Wu et al., 2009). Therefore, the purpose of the current study was to clarify if the f_u of caffeine is influenced by exercise-mediated changes in body temperature and blood pH changes in healthy humans. The study was designed to test the hypothesis that increases in body temperature due to passive heating would increase f_u, and that high intensity exercise—but not low intensity exercise—would further increase f_u via decreases in blood pH.

2 Methods

2.1 Participants

A sample size of 10 was selected based on calculations provided by Lammers et al. (2018) who suggest—based on a *post hoc* power analysis of their values—a sample size of 9 participants will have a power ≥98% in detecting a 15% difference with significance at $\alpha < 0.05$ in free fractions of caffeine between control and fasting conditions. Since the current study used similar statistical parameters to calculate sample size (with the exception of a more liberal power of >80%) and considering potential participant attrition and methodological/technical challenges that may result in missing data, we recruited a total of 10 participants (4 females) who were briefed on the study details, completed pre-screening questionnaires, including the CSEP Get Active Questionnaire (CSEP, 2017), and provided written informed consent. This study was approved by the University of Toronto Health Sciences Research Ethics Board (approval # 37008).

2.2 Study design

The study followed a repeated-measures, counterbalanced, cross-over study design that had participants visit the lab on three occasions. The first was to perform baseline testing while the two subsequent visits consisted of resting (Rest), and combined heat-and-exercise (EXS) trials in a random order separated by a minimum of 1 week. The laboratory was set to an ambient temperature of 21–23°C.

2.3 Baseline measurements

In addition to providing basic anthropometric measurements, participants performed sex-specific Åstrand cycle ergometry protocols (Heyward and Gibson, 2014) for determination of peak aerobic power ($\dot{V}O_{2peak}$), with females starting at 50 W and increasing by 25 W every 2 min, and males starting at 100 W and increasing by 50 W every 2 min, until volitional fatigue. Oxygen consumption rates were recorded throughout each test to calculate cycling economy via power-$\dot{V}O_2$ linear regression, which was used to calculate intensities that would elicit steady state oxygen uptake equivalents of 55% and 90% of each participant's $\dot{V}O_{2peak}$ for the subsequent EXS trials. These intensities were confirmed after a 10 min rest following the test by having participants engage in cycling for 3 min while monitoring $\dot{V}O_{2peak}$.

2.4 Heat and exercise trial

An overview of the exercise trial is presented in Figure 1. Participants abstained from caffeine for 48 h before each trial and arrived at the laboratory after a 3-h fast. The trial started with participants ingesting 3 mg/kg of anhydrous caffeine to the closest 25 mg in tablets (Wake Ups, Toronto, Canada)—equivalent in caffeine to a strong cup of coffee—and a Vitalsense® core temperature capsule (Philips Respironics, Pennsylvania, United States) with 1 cup of water 45 min before the start of the trial. Ingestion of caffeine with the core temperature capsule coincided with the timing of maximum drug concentration (T_{max}) of caffeine (45 min post-ingestion), and allowed us to minimize participant time requirements and standardize ingestion of the core temperature capsules pre-intervention. This timing between ingestion and T_c measurement is clearly shorter than the general recommendation of 3–5 h (Goodman et al., 2009); however, previous experiments in our lab had shown that the core temperature capsule stabilized within 30 min and previous reports show that the capsule would likely have been situated in the small intestine (O'Grady et al., 2020).

The exercise trial began with collection of the first blood sample (t = 45 min post-caffeine ingestion) via venipuncture before passive heating in a sauna until T_c increased by 0.5°C or 10 min had elapsed. The participants' T_c was monitored real-time on a laptop within Bluetooth range of the sauna using the companion eqView Professional software (Version 3, Equivital, New York, United States). Participants then returned to the lab and a flexible venous catheter (Nexiva, BD, Franklin Lakes, United States) was inserted in a superficial vein in the antecubital fossa for serial blood sampling and kept patent with saline infusions. Each participant was instrumented with a portable oxygen uptake system (Metamax 3B R1, CORTEX Biophysik Gmbh, Leipzig, Germany), and a heart rate monitor (Polar Electro Oy, Kempele, Finland). Participants then engaged in 20 min of steady-state cycling at 55% $\dot{V}O_{2peak}$, which was selected in order to maintain or slightly increase T_c without affecting blood pH. Immediately after, participants performed 10 bouts of high-intensity intervals (HIIT) cycling at intensities consistent with

10.3389/fphys.2024.1370586

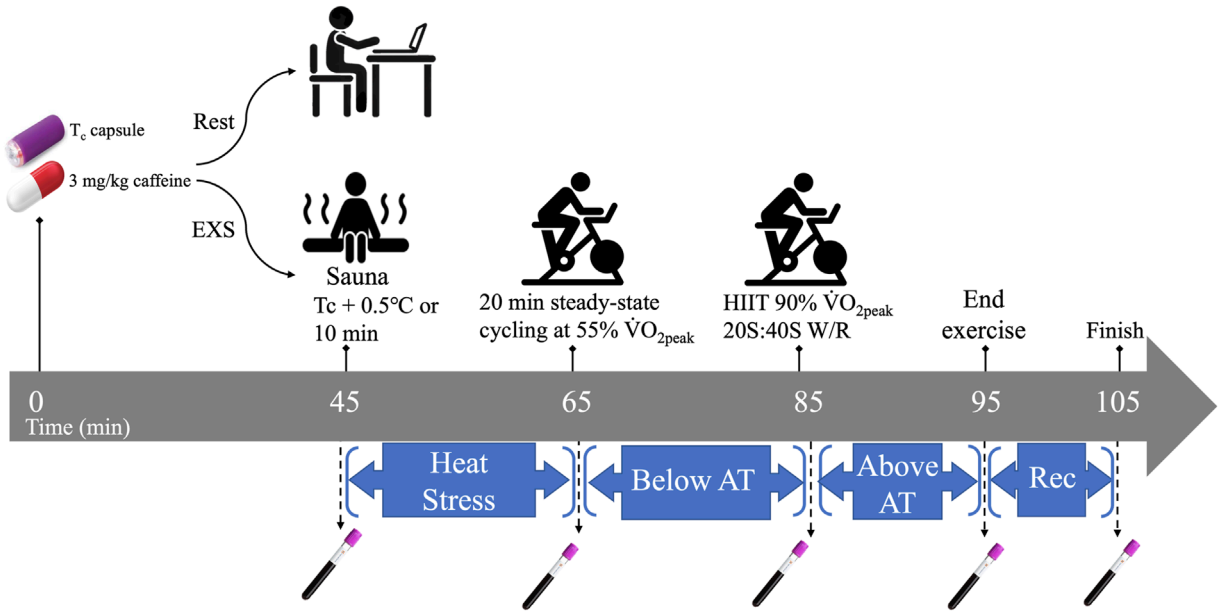

FIGURE 1
Temporal overview of Rest and EXS trials. AT, anaerobic threshold; HIIT, high intensity intervals; Rec. recovery; T_c, core temperature; $\dot{V}O_{2peak}$, peak aerobic power; W/R, work-to-rest intensity ratio.

90% $\dot{V}O_{2peak}$ at work-to-rest ratios of 20 s sprints to 40 s recovery. The HIIT was designed to cause a significant increase in T_c and decrease in blood pH. *Ad libitum* water ingestion was allowed only within the first 15 min of the trial to minimize interference with the T_c capsule readings during the trial. Five blood samples were taken over the trial (t = 45, 65, 85, 95, and 105 min post-caffeine ingestion) corresponding with pre-sauna (BASE), post-sauna (HEAT), post-steady state cycling (SS), post-HIIT cycling (HIIT), and 10 min into recovery after HIIT (REC), respectively.

2.5 Rest trial

The resting trial consisted of 105 min of inactivity (i.e., computer work, reading, etc.) and mimicked the exercise trial in caffeine dose, time of day, blood sampling timeline, and water limitation. Participants remained in the lab during this time.

2.6 Blood processing

Two samples of blood were taken at each timepoint. A small fraction of blood (~1 mL) was collected in a heparinized vacutainer (BD Diagnostics, Franklin Lakes, United States) that was injected into an iSTAT CG4+ cartridge that was inserted into an iSTAT blood analyser (Abbott, Princeton, United States) for determination of blood lactate and pH. Another sample was collected in a 6 mL K_2EDTA blood collection tube (BD Diagnostics, Franklin Lakes, United States) and the temperature was immediately recorded using a Long-stem Traceable®ULTRA™ thermometer (VWR International, Mississauga, Canada) with a precision of ±0.2°C. Hemoglobin was determined via Hemocue Hb 201 cuvettes (Hemocue AB, ÄNGELHOLM, Sweden), and hematocrit was measured in duplicate through microhematocrit tube centrifugation. The remaining blood was then centrifuged for 3 min using a PlasmaPREP (Separation Technology Inc., Sanford, Florida, United States) and designated as the total plasma concentration (C_t). From this, a 1.0 mL aliquot of plasma was carefully transferred into the sample reservoir of a Centrifree® ultrafiltration device (Merck KGaA, Darmstadt, Germany), which was then spun in a fixed-angle rotor (Hettich fixed-angle rotor and Hettich Universal 320R centrifuge, Föhrenstr, Germany) for 10 min at a temperature consistent with the blood temperature recorded at collection to avoid the influence of ambient temperature on caffeine binding. This resulted in separation of C_t into the bound concentration (C_b), which remained in the protein-rich plasma residing in the sample reservoir, and unbound concentration (C_u), which was filtered along with protein-free plasma in the filtrate cup.

2.7 Plasma processing and analysis

Caffeine and paraxanthine were purchased from Sigma-Aldrich (St. Louis, United States) and caffeine-d9 and paraxanthine-d3 (Internal standards) were obtained from Toronto Research Chemicals (Toronto, Canada). All LC-MS/MS grade solvents were purchased from Caledon Laboratories Ltd. (Georgetown, Canada). Auto sampler vials/glass inserts used in the sample extraction were purchased from Chromatographic Specialties Ltd. (Brockville, Canada).

10.3389/fphys.2024.1370586

All samples were stored at −80°C until analysis. After allowing samples to thaw to room temperature, 100 µL (C_u) or 200 µL (C_t and C_b) were mixed with 10 µL of methanol and 10 µL of methanol containing 1 ng of internal standards (caffeine-d9 and paraxanthine-d3), followed by vortexing. Standard curves of caffeine and paraxanthine (10 points from 0.01 ng to 50 ng, 10 µL for each point of the curve) were prepared in the same conditions. Then, 1.2 mL of acetonitrile was added to each assay (standards and samples). After vortexing for 5 min, standards and samples were centrifuged at 20,000 g for 15 min at 4°C and the supernatants were transferred into 15 mL siliconized glass tubes before the addition of 3 mL of acetonitrile and being dried under nitrogen gas at 35°C. Samples were reconstituted in 120 µL of methanol, vortexed, centrifuged at 20,000 g for 20 min at 4°C, transferred to inserts and placed in the autosampler set at 4°C.

Samples were then injected (5 µL) and analytes were separated via high-performance liquid chromatography (HPLC; Agilent 1290, Agilent, Santa Clara, United States) using a Kinetex XB-C18 100 A (50 × 3.0 mm, 2.6 µm particle size) column (Phenomenex, Torrance, United States) with mobile phases consisting of 0.1% formic acid in water (A) and 0.1% formic acid in acetonitrile (B) at a flow rate of 0.7 mL/min, isocratic (15% B). Each run was 2 min.

The HPLC was coupled to a SCIEX QTRAP 5500 triple-quadruple mass spectrometer (SCIEX, Framingham, United States) equipped with a Turbo Ion Spray source. Electrospray ionization (ESI) was performed in the positive mode with multiple reaction monitoring (MRM) to select both parent and characteristic daughter ions specific to each analyte simultaneously from a single injection. The transitions used to quantify cbaseline were calculated using changes iaffeine and paraxanthine were as follows: caffeine (195.1 → 138.1), caffeine-d9 (204.1 → 144.1), paraxanthine (181.1 → 124.0), and paraxanthine-d3 (184.1 → 71.9). Nitrogen was used as the nebulizing, turbo spray, and curtain gas. Each target is then uniquely identified by the parent-to-daughter ion mass transition and the specific retention time. Data was collected and analyzed using Analyst v1.6.2 (SCIEX, Framingham, United States).

2.8 Plasma volume changes

Plasma volume changes (ΔPV) relative to baseline were calculated using changes in [Hb] and Hct, based on the equation by Dill and Costill (1974). Corrections were applied for the F-cell (whole blood vs. sample site) for Hct (x 0.91) and Hb (x 0.92), as well as for trapped plasma in Hct (x 0.96), as described by Novosadova (1977).

2.9 Determination of unbound fraction, metabolic ratio, and plasma volume changes

The $\%f_u$ of caffeine was calculated by dividing the concentration in the ultrafiltrate (C_u) by the concentration in plasma (C_t) and converted to a percentage (Equation 1). Additionally, the metabolic ratio (MR)—an indicator of the enzyme-mediated metabolism of caffeine and the associated production of its primary metabolite, paraxanthine—was determined for CYP1A2 by taking the quotient of C_t of [paraxanthine]/[caffeine] at each time point.

$$Unbound\ fraction\,(fu) = \frac{Unbound\ concentration\,(Cu)}{Total\ plasma\ concentration\,(Ct)} \times 100\% \quad (1)$$

TABLE 1 Participant physical characteristics, aerobic power, and exercise intensities for EXS trial (n = 10).

	Mean ± SD
Age (y)	21.9 ± 2.7
Height (cm)	169.7 ± 6.4
Weight (kg)	67.4 ± 9.8
$\dot{V}O_{2peak}$ (mL·kg^{-1}·min^{-1})	39.5 ± 4.4
Power output at 55% $\dot{V}O_{2peak}$ (W)	78.7 ± 20.4
Power output at 90% $\dot{V}O_{2peak}$ (W)	171.8 ± 36.6

SD, standard deviation; $\dot{V}O_{2peak}$, peak oxygen consumption.

2.10 Statistical analyses

Statistical analyses were performed using Prism (version 8, GraphPad Software Inc., San Diego, United States; RRID:SCR_002798) and an alpha level of .05. Plasma volume changes and drug concentrations were compared using 2-way, repeated measures ANOVA with treatment (Rest and EXS) and blood sampling timepoint (baseline, post-sauna, post-steady state cycling, post-HIIT, and 10 min post-HIIT) as within-subjects variables. In the case of missing values, we analyzed the data by fitting a mixed model as implemented in GraphPad Prism 8. Post-hoc analyses were applied to significant F-ratios yielded by the ANOVA using Dunnett's multiple comparisons test to compare within-trial PV changes relative to baseline values, and Šidák's multiple comparison test comparing isochronous values between Rest and EXS for all other measurements.

3 Results

3.1 Participants

The study was completed by all 10 participants that were recruited (Table 1). There were minor adverse events (i.e., nausea and vomiting) that occurred after the HIIT bout, but these resulted in no withdrawals of study participation. Of the 80 core temperature measurements, five displayed non-physiological readings (i.e., unexpected decreases in T_c) and two were missing due to connection issues, resulting in their omission.

10.3389/fphys.2024.1370586

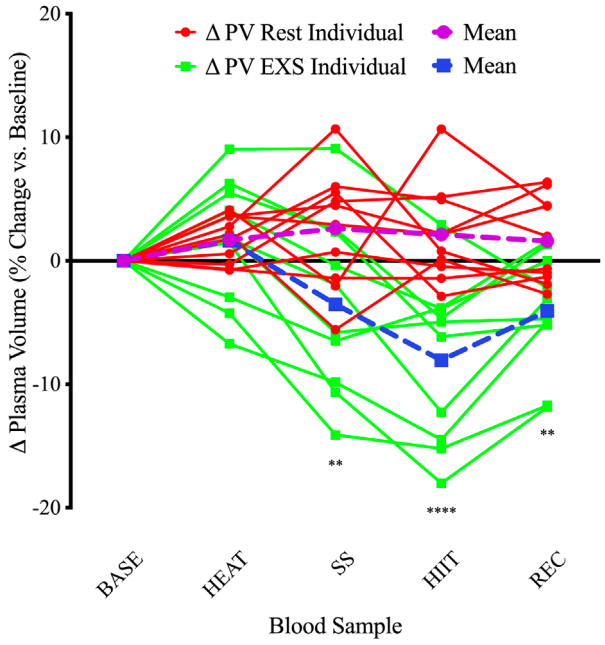

FIGURE 2
Individual changes in plasma volume compared to baseline. ΔPV, change in plasma volume for Rest and EXS trials; BASE, Baseline; HEAT, after passive heating; HIIT, after high-intensity intervals; REC, 10 min into recovery after exercise; SS, after steady-state cycling. $^{**}p < .01$; $^{****}p < .0001$ significant difference compared to baseline.

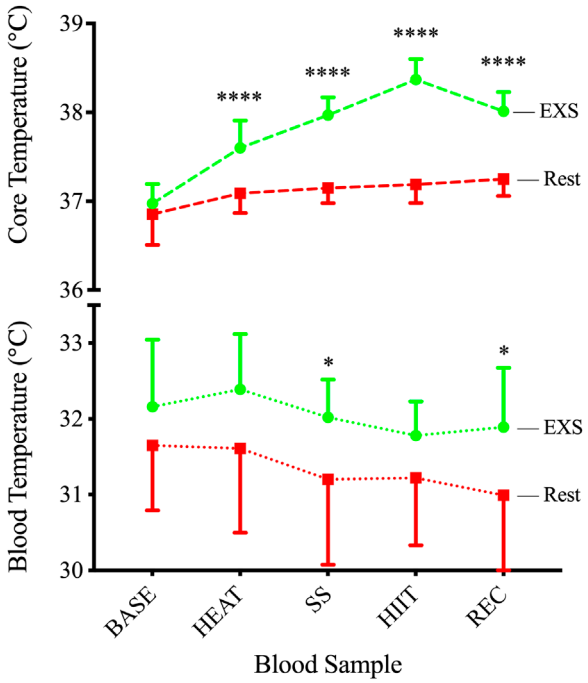

FIGURE 3
Core (TOP) and blood (BOTTOM) temperatures during Rest and EXS trials. $^{*}p < .05$; $^{****}p < .0001$ significant difference between isochronous Rest and EXS values.

3.2 Plasma volume

Changes in plasma volume relative to baseline were determined using changes in [Hb] and Hct. In general, the Rest trial resulted in hemodilution while the EXS trial resulted in hemoconcentration (Figure 2). There were significant Time and Trial differences, and a Time × Trial interaction [$F(4, 36) = 7.58$, $p < .0005$]. Comparing mean changes to baseline using Dunnett's multiple comparisons test, it was revealed that only after HIIT and into REC in the EXS trial were there significant differences ($p < .0001$ and $p < .05$, respectively). Comparing time-paired blood samples between trials with Šidák's multiple comparisons test, significant differences were apparent after exercise was initiated (SS) and remained over the remainder of the trial.

3.3 Core temperature

All participants completed 10 min of passive heating in the sauna, increasing T_c by 0.63°C above baseline before continuing to rise throughout the protocol and peak at 38.37°C ± 0.23°C during HIIT. This resulted in a significant Time × Trial interaction [$F (4,29) = 34.61$, $p < .0001$] via mixed-effects model, with T_c being significantly elevated over resting conditions (Figure 3, Top) at each time point after BASE. This increase in T_c was reflected in measurements of increased blood temperatures only after SS (+1.02°C; $p = .040$) and REC (+.90°C; $p = .020$) when measured immediately after sampling (Figure 3, Bottom).

3.4 Blood lactate and pH

During the EXS trial, there was a significant Time × Trial interaction involving increases in blood [La^+] after the commencement of exercise (i.e., SS, HIIT, and REC; $F (4,36) = 72.88$; $p < .0001$; Figure 4, Left). These increases were associated with a significant Time × Trial interaction for blood pH [$F (4,36) = 12.71$; $p < .0001$]; however, it was only after the high intensity exercise and into the recovery period (i.e., HIIT and REC) that *post hoc* analysis revealed a decrease during EXS (Figure 4, Right).

3.5 Plasma-drug concentrations

ANOVA tests showed a Time × Trial interaction in paraxanthine plasma concentrations [$F (4,36) = 2.662$; $p = .0482$] but not of caffeine [$F (4,36) = 1.038$; $p = .401$] between Rest and EXS. Šidák's post-test revealed no difference in paraxanthine values across time points between Rest and EXS. When blood concentrations were corrected for the relative changes in PV (Figure 5), the ANOVA interaction for paraxanthine was no longer significant. The MR of CYP1A2 (Figure 5, Subfigure) displayed only a Time effect [$F (4, 36) = 15.89$; $p < .0001$] as caffeine was metabolized to paraxanthine equally over the course of both trials. Post-hoc analysis

10.3389/fphys.2024.1370586

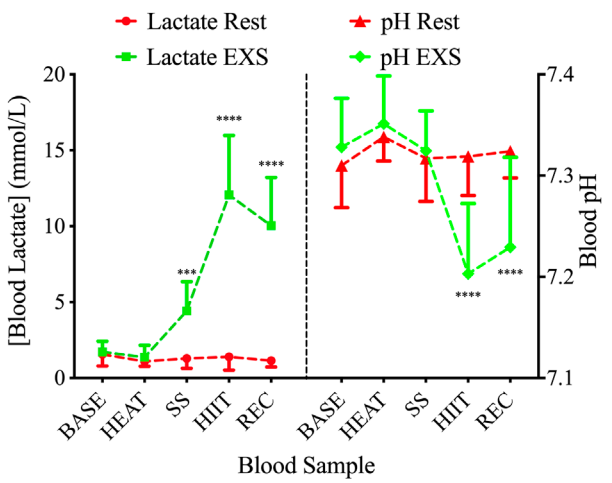

FIGURE 4
Blood lactate (left) and pH (right) during Rest (red lines) and EXS (green lines) trials. ***$p < .001$; ****$p < .0001$ significant difference between isochronous Rest and EXS values.

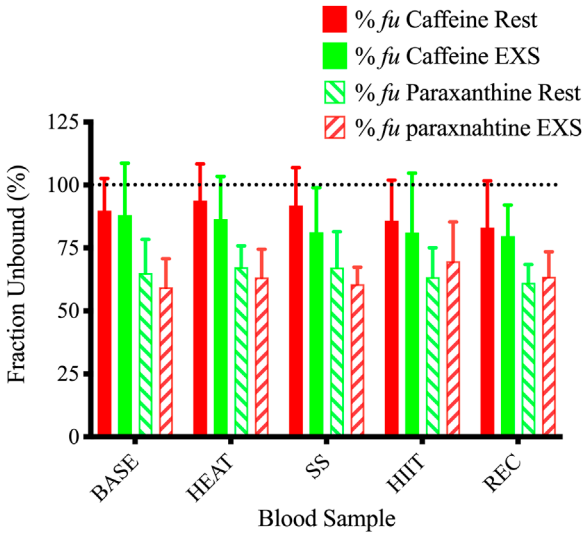

FIGURE 6
Unbound fractions of caffeine and paraxanthine during Rest and EXS trials. Dotted line shows 100% unbound fraction cut-off.

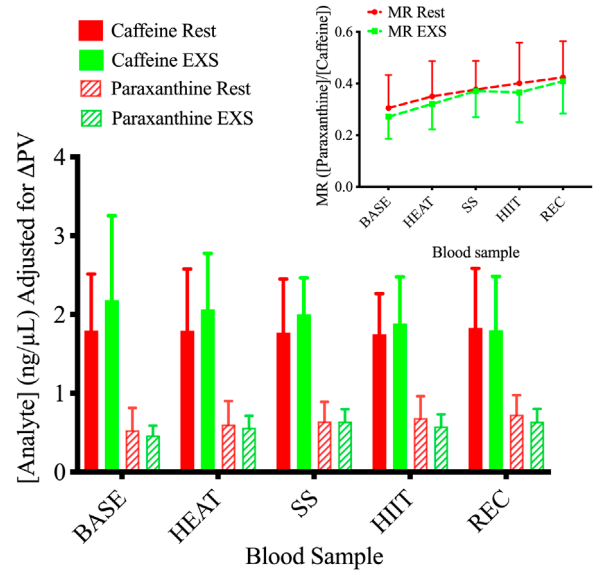

FIGURE 5
Plasma concentrations of caffeine and paraxanthine during Rest and EXS trials. Subfigure. Metabolic ratio (MR) of CYP1A2 measured as the ratio of [paraxanthine]/[caffeine].

was not performed since a Time × Trial interaction was not significant.

The $\%f_u$ of caffeine and paraxanthine did not differ across time points between Rest and EXS trials (Figure 6). The methods we used resulted in 23 of the 100 sampling points having $\%f_u$ values that were above 100%, which is impossible. Regardless, nearly all values were included in the analysis to allow for comparison between Rest and EXS. The values that were omitted were from a single participant that had a $\%f_u$ of >200% during their EXS trial as a result of relatively low caffeine C_t values. These samples were rerun but the new results were even more aberrant; therefore, these values were deemed unreliable, and all of their caffeine values (C_t and C_u) were excluded.

4 Discussion

The f_u of a drug determines many PK and PD properties that can dictate its efficacy and potential for side effects. This is the first study, to our knowledge, to investigate *in vivo* changes in blood temperatures and pH on the f_u of a drug using ultrafiltration. An experimental protocol was designed with the intent of eliciting changes in T_c and blood pH, which are normal physiological responses to acute exercise. The results demonstrate that the intervention protocol was successful in raising T_c and decreasing blood pH compared to a non-exercise, control trial. However, the hypothesis that the intensity and duration of exercise used in the current study would lead to changes in T_c and blood pH that would affect f_u was not supported.

We used a combination of passive heating and various intensities of cycling to induce physiological changes in T_c and blood pH. T_c showed a gradual increase over the course of the interventions in the exercise trial with the greatest relative increase occurring from passive heating and the highest absolute temperature peaking at 38.37°C during HIIT. Even with this profound 1.37°C increase in T_c relative to BASE, and the swiftness of our research personnel to record blood temperature after collection in <1 min, blood temperature changed in the opposite direction to T_c but was still statistically slightly higher than time-matched results during the Rest trial after SS (+0.82°C) and REC (+0.90°C). Steady-state cycling was successful in maintaining a consistent blood pH while increasing T_c, whereas the HIIT protocol effectively decreased blood pH while further increasing T_c compared to the Rest trial. Despite these pronounced changes, the plasma concentrations of caffeine and paraxanthine showed no difference between trials when corrected for PV fluctuations. Accordingly, the

MR of CYP1A2 did not change during exercise, indicating that over the measurement period heat stress and exercise did not change the enzymatic rate of CYP1A2. Similarly, C_u did not differ between trials, resulting in no difference in the $\%f_u$ of caffeine or paraxanthine. Our resting data shows a $\%f_u$ of 89% (SD = 0.04%), which is at the upper end of the reported $\%f_u$ (70%–90%) (USIM, 2001), greater than the 64.55% reported using another ultrafiltration device (Blanchard, 1982b), and comparable to a study using the same ultrafiltration tubes (Lammers et al., 2018). Thus, our mean values appear acceptable; however, the same cannot be said for the variability, which might be masking potential differences. Of similar concern is that some of the $\%f_u$ values in our study were >100%, which is not physiologically possible. This, however, is consistent with other studies have also reported $\%f_u$ values above 100%. A major analysis of 25 epileptic medications showed mean unbound fractions of 102.7% for both gabapentin and pregabalin (Patsalos et al., 2017), which is slightly above their reported $\%f_u$ of 99% and 97%, respectively. This is obviously a smaller margin of error than the current study, yet still highlights the variability that is possible when deriving a value (e.g., $\%f_u$) using multiple mass spectrometry data. Nonetheless, there could be other factors that should be considered. For example, the use of protein precipitation in the sample preparation could be interfering with the caffeine concentration in C_t. Although we did not validate the currently used assay under the full measures of the FDA guidelines (FDA, 2018), a protein precipitation method very similar to the one used in the current investigation has been validated with great % recoveries of caffeine and its metabolites recently (Chen et al., 2017). It is possible that the slight difference in reagents used (acetonitrile vs. formic acid (Chen et al., 2017)) resulted in differences in drug precipitating with protein, leading to the aberrantly low C_t values and resulting in $\%f_u$ >100%. Additionally, a long spin time might also artificially inflate the C_u as previously reported with valproic acid (Liu et al., 1992). This could result from perpetual flux from C_b to C_u according to the law of mass action as C_u is continually being spun through the filter and a true equilibrium is never attained. Findings by Kratzer et al. (2014) contradict this by showing no effect of centrifugation time on vancomycin, which they attribute to the constancy of K_b, and that free protein and drug-bound protein are both concentrated in the sample reservoir at the same rate. Regardless, since all of the samples were processed similarly, a systemic effect on all the samples would have been apparent, which is not the case. This study highlights the need for standardized ultrafiltration methodology.

The cumulative thermal load (+1.37°C over BASE) during EXS in the current study is higher than the +0.9°C increase (36.9 → 37.8°C) reported previously by Kelly and colleagues (Kelly et al., 2016), who employed a similar protocol that had a 3 min warm-up at 60% $\dot{V}O_{2\ max}$, followed by fifteen high-intensity intervals (work:rest) of 30:30 s sprints at 90%:30% $\dot{V}O_{2\ max}$, respectively. Comparing the increases from exercise alone, however, reveals that their protocol elicited a slightly more elevated response in T_c (+0.9 vs. +0.8°C), which is likely a combination of their longer duration (7.5 vs. 3.3 min) of high intensity (i.e., 90% $\dot{V}O_{2\ max}$) cycling and the higher T_c starting point of our participants who had just undergone passive heating (HEAT). Further comparisons show that our values are more in line with rectal temperatures reported by Reeve and colleagues (Reeve et al., 2019) (38.17°C), who performed a similar protocol of 10 min of passive heating, followed by a 6 min warm-up at 50% of work max (W_{max}; watts), and then 12 × 1-min intervals at 100% W_{max} with rests of 1 min. Blood temperature may not mirror this increase because of differences in the measurement site. In our study, T_c was measured by a capsule situated in the GI tract. The temperature gradient has been reported to reach as high as 0.4°C between muscle tissues generating metabolic heat during exercise and the GI tract (Parkin et al., 1999). Therefore, blood flowing through arterial and venous conduits during exercise experiences temperatures ranging from ~39°C at the muscle (Parkin et al., 1999) to ~32°C in a superficial vein, based on our values. This reduction in temperature in mixed venous blood sampled from an arm vein is the result of combined efforts of radiative, convective, and evaporative heat loss, and is a display of our profound capacity to dissipate heat. This was elegantly displayed in exercising horses where temperatures of the gluteal muscle, pulmonary artery (representing T_c), and superficial thoracic vein were 43.9, 42.8, and 39.5°C, respectively, after 10 min of running at 90% $\dot{V}O_{2\ max}$ (Hodgson et al., 1985). This showcases the cascade of heat transfer and the rate at which blood is cooled in the vasculature during exercise. The greater difference between T_c and blood temperature in our study (6.6°C vs. 3.3°C) is likely a result of more efficient cooling in humans through a greater surface area to body weight ratio (Hodgson et al., 1985), better convection through our well-exposed dermis, the delay in measurement time after collecting the blood, and an evaporative response that begun in the sauna and was effective before the start of any exercise in our study.

The maintenance of blood pH over SS cycling can be explained by the increase in mean blood lactate ($[La^-]_b$) to 4.42 (range = 0.97–7.79) mmol/L, indicating that participants were very close to their lactate threshold, which is typically ~4 mmol/L, yet varies inversely with training status (Stegmann et al., 1981). This increase in $[La^-]_b$ is greater than we anticipated since we had participants cycle at 55% of their $\dot{V}O_{2peak}$ with the intent to keep intensity below anaerobic threshold during SS cycling, which was previously reported to be 61.6% $\dot{V}O_{2\ max}$ in untrained participants (Simon et al., 1985). Therefore, although lactate threshold was not determined in the present study, it is likely that SS cycling was performed near the individual lactate anaerobic threshold in the majority of participants. To efficiently lower blood pH, we chose a HIIT protocol with a work:rest ratio derived from work by Nicolo et al. (2014), which showed that "iso-effort" cycling at 20:40 s provided the largest increase in $[La^-]_b$ compared to 30:30 s, 40:20 s, and continuous cycling. In comparison, our participants engaged in 1/3rd of the HIIT volume in sets, yet displayed considerably higher $[La^-]_b$ levels (12.1 vs. 9.5 mmol/L), which is likely from a generally lower level of fitness (i.e., $\dot{V}O_{2peak}$; 40 vs. 67 $mL{\cdot}kg^{-1}{\cdot}min^{-1}$).

The calculated changes in PV were similar until initiation of cycling (i.e., SS, HIIT, and REC) in the EXS trial. Indeed, the %PV change after HEAT was comparable to the time-equivalent at rest (EXS: 1.63 ± 4.97% vs. Rest: 1.68 ± 1.87%); however, the variability was much greater in response to passive heating (Figure 2). This suggests that 10 min of passive heating may not be long enough to facilitate the same ~5% hemodilution expected after 30 min of heating (Fortney and Miescher, 1994), which results from absorption of interstitial fluid into the vasculature in response to peripheral vasodilation and as an early compensatory mechanism for the ensuing sweating response (Bass and Henschel, 1956). This response shifts to hemoconcentration with the addition of exercise as the greater metabolic demands, coupled with an increased systolic arterial pressure, leads to greater vasodilation

and an increased hydrostatic pressure of more capillary beds causing filtration to the extravascular compartments (Harrison, 1986). Additionally, since participants were instructed to abstain from drinking fluids after 15 min from the trial initiation, fluids lost from sweating during HEAT were not replaced and likely magnified the hemoconcentrated state during EXS since hydration status is a determinant of the direction of PV changes during exercise (Sawka et al., 1984). The 3.52% decrease in PV after 20 min of SS cycling at 55% $\dot{V}O_{2peak}$ is almost half of the previously described 6.8% decrease after 15 min of cycling at 67% $\dot{V}O_{2\,max}$ (Novosadova, 1977). The 8.05% decrease at the end of HIIT is also shy of the reported ~19% reduction after various HIIT protocols employed by Bloomer and Farney (Bloomer and Farney, 2013). After our participants stopped cycling, there was a classic PV rebound where they netted a +3.98% PV increase 10 min into REC. This is expected as exercise-induced decreases in PV tend to rebound to pre-exercise levels after a brief recovery period of ≥30 min (Novosadova, 1977).

Applying PV corrections avoids the inaccurate interpretation that total-body solute concentrations increase during hemoconcentration, and typically decreases the magnitude of change elicited by exercise (Berthoin et al., 2002). This is reflected in the current study where the Time × Trial interaction for paraxanthine was no longer significant when PV corrections were applied since variability from PV changes during EXS were accounted for. The results suggesting that caffeine is not sequestered in the intravascular space as fluid is expelled to the extravascular compartments during exercise is supported by previous research showing that $[caffeine]_{pl.}$ was no different after 60 min of walking at 30% $\dot{V}O_{2\,max}$ (Collomp et al., 1991) and appeared slightly lower in lean individuals walking for 90 min at 40% $\dot{V}O_{2\,max}$ (Kamimori et al., 1987). In proportion to the studies evaluating caffeine and exercise, relatively few researchers have compared the MR of caffeine and its metabolites during rest and exercise. One investigation in horses (Aramaki et al., 1995) revealed increases in the enzymatic conversion of caffeine to theophylline—the major metabolite in horses and converted by CYP1A2 and 2E1—in blood samples taken 3 to 71 h after 4,000 m of various intensity exercise. Theobromine, another metabolite, showed elevated conversion after 22 h of exercise, but paraxanthine, which is the only metabolite solely metabolized by CYP1A2, showed no change after exercise. Regardless, the combination of these processes resulted in caffeine's half-life time ($t_{1/2}$) to be hastened during exercise. This is congruent with post-exercise data in humans that showed a similarly faster $t_{1/2}$ after 60 min of walking at 30% $\dot{V}O_{2\,max}$; yet, MR changes cannot be substantiated since paraxanthine was not measured (Collomp et al., 1991). Based on these studies, it is possible that a longer sampling period in the current study would have revealed a change in the MR in the hours following the trial completion, or, simply, that the activity of CYP2E1, and not CYP1A2, increases with heat stress.

Given the complexity and time-dependence of measurements in the current study, there were some limitations that, if replicated, should be accounted for. The sample size met the *a priori* sample size calculation described previously in the Methods, but was relatively small, increasing the risks associated with extrapolation of our results to a larger sample size. At the time of our sample size calculations, very limited data were available to enable an *a priori* determination of the statistical power associated with that sample size; we thus determined power *post factum*. The results of our investigation can hopefully be used by those who will plan future related research, including an *a priori* determination of statistical power. The temperature of the sauna was not controlled by our study personnel since we lacked access to the controls. Controlling the temperature would allow for consistent heating among participants. Dermal and muscle temperatures were not measured. These values could describe the range of temperatures experienced by various drug-protein complexes and provide insight into thermal unloading of blood. Storing the vacutainers at mean venous blood temperature (e.g., 32°C), instead of room temperature, and insulating it upon collection would have minimized heat loss and provided greater confidence in the temperature of the blood sampled. To keep sample processing time to a minimum, the volume of fractions before (C_t) and after separation (C_b and C_u) were not measured, which precludes the possibility of calculating % recovery of C_u through the ultrafiltration method. Lastly, the results are only applicable insofar as they relate to the exercise employed and cannot preclude the possibility of changes in *fu* from greater perturbations in T_c and pH from other forms of exercise.

This is the first report of an *in vivo* study of healthy humans in which the effects on a drug's f_u were assessed after a challenge involving passive heat stress and acute exercise. Passive heating followed by steady state and high-intensity cycling on a cycle ergometer were responsible for increasing T_c and decreasing blood pH 45–105 min after ingestion of caffeine. Despite previous reports on the necessity to control temperature and pH when analyzing drugs *in vitro*, we find no reason to be concerned about the effects of acute whole-body heat stress and exercise on the $\%f_u$ of caffeine. The validity and reproducibility of the methodology used to derive the f_u should be further investigated.

Data availability statement

The raw data supporting the conclusions of this article will be made available by the authors, without undue reservation.

Ethics statement

The studies involving humans were approved by the University of Toronto Health Sciences Research Ethics Board. The studies were conducted in accordance with the local legislation and institutional requirements. The participants provided their written informed consent to participate in this study.

Author contributions

MM: Writing–original draft, Writing–review and editing, Conceptualization, Data curation, Formal Analysis, Investigation, Methodology, Project administration, Supervision, Validation, Visualization. KD: Data curation, Investigation, Methodology, Project administration, Validation, Writing–review and editing. IJ: Conceptualization, Funding acquisition, Methodology, Project administration, Resources, Supervision, Writing–review and editing.

Funding

The author(s) declare that no financial support was received for the research, authorship, and/or publication of this article.

Acknowledgments

This research is part of a doctoral thesis published on the institution's website (McLaughlin, 2022). A stick figure in Figure 1 was generated using OpenAI's DALL·E 3 model, a text-to-image generative AI system (OpenAI, 2024). Retrieved from https://openai.com/dall-e.

Conflict of interest

The authors declare that the research was conducted in the absence of any commercial or financial relationships that could be construed as a potential conflict of interest.

Publisher's note

References

Aguilar-Navarro, M., Munoz, G., Salinero, J. J., Munoz-Guerra, J., Fernandez-Alvarez, M., Plata, M. D. M., et al. (2019). Urine caffeine concentration in doping control samples from 2004 to 2015. *Nutrients* 11 (2), 286. doi:10.3390/nu11020286

Aramaki, S., Suzuki, E., Ishidaka, O., and Momose, A. (1995). Effects of exercise on plasma concentrations of caffeine and its metabolites in horses. *Biol. Pharm. Bull.* 18 (11), 1607–1609. doi:10.1248/bpb.18.1607

Baler, K., Martin, O. A., Carignano, M. A., Ameer, G. A., Vila, J. A., and Szleifer, I. (2014). Electrostatic unfolding and interactions of albumin driven by pH changes: a molecular dynamics study. *J. Phys. Chem. B* 118 (4), 921–930. doi:10.1021/jp409936v

Bass, D. E., and Henschel, A. (1956). Responses of body fluid compartments to heat and cold. *Physiol. Rev.* 36 (1), 128–144. doi:10.1152/physrev.1956.36.1.128

Berthoin, S., Pelayo, P., Baquet, G., Marais, G., Allender, H., and Robin, H. (2002). Plasma lactate recovery from maximal exercise with correction for variations in plasma volume. *J. Sports Med. Phys. Fit.* 42 (1), 26–30.

Blanchard, J. (1982a). Protein binding of caffeine in young and elderly males. *J. Pharm. Sci.* 71 (12), 1415–1418. doi:10.1002/jps.2600711229

Blanchard, J. (1982b). Protein binding of caffeine in young and elderly males. *J. Pharm. Sci.* 71 (12), 1415–1418. doi:10.1002/jps.2600711229

Bloomer, R. J., and Farney, T. M. (2013). Acute plasma volume change with high-intensity sprint exercise. *J. Strength Cond. Res.* 27 (10), 2874–2878. doi:10.1519/JSC.0b013e318282d416

Brown, D., and Tomlin, M. (2010). "Pharmacokinetic principles," in *Pharmacology and pharmacokinetics. IX*. Editor M. Tomlin 1 ed. (London (UK): Springer-Verlag), 13–52.

Burkhardt, O., Kumar, V., Katterwe, D., Majcher-Peszynska, J., Drewelow, B., Derendorf, H., et al. (2007). Ertapenem in critically ill patients with early-onset ventilator-associated pneumonia: pharmacokinetics with special consideration of free-drug concentration. *J. Antimicrob. Chemother.* 59 (2), 277–284. doi:10.1093/jac/dkl485

Byrne, C., Lee, J. K., Chew, S. A., Lim, C. L., and Tan, E. Y. (2006). Continuous thermoregulatory responses to mass-participation distance running in heat. *Med. Sci. Sports Exerc* 38 (5), 803–810. doi:10.1249/01.mss.0000218134.74238.6a

Chen, F., Hu, Z. Y., Parker, R. B., and Laizure, S. C. (2017). Measurement of caffeine and its three primary metabolites in human plasma by HPLC-ESI-MS/MS and clinical application. *Biomed. Chromatogr.* 31 (6). doi:10.1002/bmc.3900

Collomp, K., Anselme, F., Audran, M., Gay, J. P., Chanal, J. L., and Prefaut, C. (1991). Effects of moderate exercise on the pharmacokinetics of caffeine. *Eur. J. Clin. Pharmacol.* 40 (3), 279–282. doi:10.1007/BF00315209

CSEP (2017). Get active questionnaire. Available at: https://www.csep.ca/CMFiles/GAQ_CSEPPATHReadinessForm_2pages.pdf.

Dill, D. B., and Costill, D. L. (1974). Calculation of percentage changes in volumes of blood, plasma, and red cells in dehydration. *J. Appl. Physiol.* 37 (2), 247–248. doi:10.1152/jappl.1974.37.2.247

FDA (2018). "Bioanalytical method validation," in *Guidance for industry*. Silver Spring, MD: U.S. Food and Drug Administration. Available at: https://www.fda.gov/files/drugs/published/Bioanalytical-Method-Validation-Guidance-for-Industry.pdf.

Foran, S. E., Lewandrowski, K. B., and Kratz, A. (2003). Effects of exercise on laboratory test results. *Lab. Med.* 34 (10), 736–742. doi:10.1309/3pdq4ah662atb6hm

Fortney, S., and Miescher, E. (1994). "Changes in plasma volume during heat exposure in young and older men," in *Institute of medicine (US) committee on military nutrition research. Fluid replacement and heat stress. 16*. Washington (DC): National Academies Press (US): Marriott BM.

Goodman, D. A., Kenefick, R. W., Cadarette, B. S., and Cheuvront, S. N. (2009). Influence of sensor ingestion timing on consistency of temperature measures. *Med. Sci. Sports Exerc* 41 (3), 597–602. doi:10.1249/MSS.0b013e31818a0eef

Harrison, M. H. (1986). Heat and exercise. Effects on blood volume. *Sports Med.* 3 (3), 214–223. doi:10.2165/00007256-198603030-00005

Heyward, V. H., and Gibson, A. (2014). *Advanced fitness assessment and exercise prescription*. 7th Edition. Windsor, ON: Human Kinetics.

Hinderling, P. H., and Hartmann, D. (2005). The pH dependency of the binding of drugs to plasma proteins in man. *Ther. Drug Monit.* 27 (1), 71–85. doi:10.1097/00007691-200502000-00014

Hodgson, D. R., McCutcheon, L. J., Byrd, S. K., Brown, W. S., Bayly, W. M., Brengelmann, G. L., et al. (1985)1993). Dissipation of metabolic heat in the horse during exercise. *J. Appl. Physiol.* 74 (3), 1161–1170. doi:10.1152/jappl.1993.74.3.1161

Kamimori, G. H., Somani, S. M., Knowlton, R. G., and Perkins, R. M. (1987). The effects of obesity and exercise on the pharmacokinetics of caffeine in lean and obese volunteers. *Eur. J. Clin. Pharmacol.* 31 (5), 595–600. doi:10.1007/BF00606637

Kelly, M., Gastin, P. B., Dwyer, D. B., Sostaric, S., and Snow, R. J. (2016). Short duration heat acclimation in Australian football players. *J. Sports Sci. Med.* 15 (1), 118–125.

Kratzer, A., Liebchen, U., Schleibinger, M., Kees, M. G., and Kees, F. (2014). Determination of free vancomycin, ceftriaxone, cefazolin and ertapenem in plasma by ultrafiltration: impact of experimental conditions. *J. Chromatogr. B Anal. Technol. Biomed. Life Sci.* 961, 97–102. doi:10.1016/j.jchromb.2014.05.021

Kremer, J. M., Wilting, J., and Janssen, L. H. (1988). Drug binding to human alpha-1-acid glycoprotein in health and disease. *Pharmacol. Rev.* 40 (1), 1–47.

Lammers, L. A., Achterbergh, R., Romijn, J. A., and Mathot, R. A. A. (2018). Short-term fasting alters pharmacokinetics of Cytochrome P450 probe drugs: does protein binding play a role? *Eur. J. Drug Metab. Pharmacokinet.* 43 (2), 251–257. doi:10.1007/s13318-017-0437-7

Liu, H., Montoya, J. L., Forman, L. J., Eggers, C. M., Barham, C. F., and Delgado, M. (1992). Determination of free valproic acid: evaluation of the Centrifree system and comparison between high-performance liquid chromatography and enzyme immunoassay. *Ther. Drug Monit.* 14 (6), 513–521. doi:10.1097/00007691-199212000-00013

McArdle, W., Katch, F., and Katch, V. (2007). "Exercise physiology energy, nutrition, and human performance," in *351 west camden street*. Editor L. Emily (Lippincott WIlliams and Wilkins).

McElnay, J. C., and D'Arcy, P. F. (1983). Protein binding displacement interactions and their clinical importance. *Drugs* 25 (5), 495–513. doi:10.2165/00003495-198325050-00003

McLaughlin, M. (2022). *The effects of aerobic exercise on the distribution and metabolism of select xenobiotics*. Toronto, ON: University of Toronto. Available at: https://hdl.handle.net/1807/123589.

Nawrot, P., Jordan, S., Eastwood, J., Rotstein, J., Hugenholtz, A., and Feeley, M. (2003). Effects of caffeine on human health. *Food Addit. Contam.* 20 (1), 1–30. doi:10.1080/0265203021000007840

Nehlig, A. (2018). Interindividual differences in caffeine metabolism and factors driving caffeine consumption. *Pharmacol. Rev.* 70 (2), 384–411. doi:10.1124/pr.117.014407

Nicolo, A., Bazzucchi, I., Haxhi, J., Felici, F., and Sacchetti, M. (2014). Comparing continuous and intermittent exercise: an "isoeffort" and "isotime" approach. *PLoS One* 9 (4), e94990. doi:10.1371/journal.pone.0094990

Novosadova, J. (1977). The changes in hematocrit, hemoglobin, plasma volume and proteins during and after different types of exercise. *Eur. J. Appl. Physiol. Occup. Physiol.* 36 (3), 223–230. doi:10.1007/BF00421753

OECD (2019). Health expenditure and financing. Available at: https://stats.oecd.org/Index.aspx?DataSetCode=SHA:OECD (Accessed June, 2019).

O'Grady, J., Murphy, C. L., Barry, L., Shanahan, F., and Buckley, M. (2020). Defining gastrointestinal transit time using video capsule endoscopy: a study of healthy subjects. *Endosc. Int. Open* 8 (3), E396–E400. doi:10.1055/a-1073-7653

Parkin, J. M., Carey, M. F., Zhao, S., and Febbraio, M. A. (1999). Effect of ambient temperature on human skeletal muscle metabolism during fatiguing submaximal exercise. *J. Appl. Physiol.* 86 (3), 902–908. doi:10.1152/jappl.1999.86.3.902

Patsalos, P. N., Zugman, M., Lake, C., James, A., Ratnaraj, N., and Sander, J. W. (2017). Serum protein binding of 25 antiepileptic drugs in a routine clinical setting: a comparison of free non-protein-bound concentrations. *Epilepsia* 58 (7), 1234–1243. doi:10.1111/epi.13802

Paxton, J. W., and Calder, R. L. (1983). Propranolol binding in serum: comparison of methods and investigation of effects of drug concentration, pH, and temperature. *J. Pharmacol. Methods* 10 (1), 1–11. doi:10.1016/0160-5402(83)90009-8

Peters, T. (1995). "The albumin molecule," in *All about albumin*. Editor T. Peters (San Diego: Academic Press), 9–II.

Reeve, T., Gordon, R., Laursen, P. B., Lee, J. K. W., and Tyler, C. J. (2019). Impairment of cycling capacity in the heat in well-trained endurance athletes after high-intensity short-term heat acclimation. *Int. J. Sports Physiol. Perform.* 14 (8), 1058–1065. doi:10.1123/ijspp.2018-0537

Roberts, J. A., Pea, F., and Lipman, J. (2013). The clinical relevance of plasma protein binding changes. *Clin. Pharmacokinet.* 52 (1), 1–8. doi:10.1007/s40262-012-0018-5

Sawka, M. N., Francesconi, R. P., Pimental, N. A., and Pandolf, K. B. (1984). Hydration and vascular fluid shifts during exercise in the heat. *J. Appl. Physiol. Respir. Environ. Exerc Physiol.* 56 (1), 91–96. doi:10.1152/jappl.1984.56.1.91

Simon, J., Young, J. L., Blood, D. K., Segal, K. R., Case, R. B., and Gutin, B. (1985)1986). Plasma lactate and ventilation thresholds in trained and untrained cyclists. *J. Appl. Physiol.* 60 (3), 777–781. doi:10.1152/jappl.1986.60.3.777

Sinha, S. S., Mitra, R. K., and Pal, S. K. (2008). Temperature-dependent simultaneous ligand binding in human serum albumin. *J. Phys. Chem. B* 112 (16), 4884–4891. doi:10.1021/jp709809b

Stegmann, H., Kindermann, W., and Schnabel, A. (1981). Lactate kinetics and individual anaerobic threshold. *Int. J. Sports Med.* 2 (3), 160–165. doi:10.1055/s-2008-1034604

Sweeney, G. D. (1981). Drugs–some basic concepts. *Med. Sci. Sports Exerc* 13 (4), 247–251. doi:10.1249/00005768-198104000-00009

Task Force on Community Preventive, S. (2002). Recommendations to increase physical activity in communities. *Am. J. Prev. Med.* 22 (4 Suppl. l), 67–72. doi:10.1016/s0749-3797(02)00433-6

USIM (2001). "Pharmacology of caffeine," in *Caffeine for the sustainment of mental task performance: formulations for military operations*. Editor Comn, R. (Washington (DC): US Institute of Medicine, National Academies Press US).

Wilting, J., van der Giesen, W. F., Janssen, L. H., Weideman, M. M., Otagiri, M., and Perrin, J. H. (1980). The effect of albumin conformation on the binding of warfarin to human serum albumin. The dependence of the binding of warfarin to human serum albumin on the hydrogen, calcium, and chloride ion concentrations as studied by circular dichroism, fluorescence, and equilibrium dialysis. *J. Biol. Chem.* 255 (7), 3032–3037. doi:10.1016/s0021-9258(19)85847-7

Wu, Q., Li, C., Hu, Y., and Liu, Y. (2009). Study of caffeine binding to human serum albumin using optical spectroscopic methods. *Sci. China Ser. B Chem.* 52 (12), 2205–2212. doi:10.1007/s11426-009-0114-z

Glossary

ΔPV	change in plasma volume
ANOVA	analysis of variance
AGP	α1-acid glycoprotein
BASE	baseline/pre-sauna
C_b	bound drug concentration
CL	clearance
C_t	total plasma drug concentration
C_u	unbound drug concentration
CYP#X#	Cytochrome P450 isozyme
EXS	heat-and-exercise trial
f_b	bound fraction
f_u	free/unbound drug fraction
Hb	hemoglobin
Hct	hematocrit
HEAT	passive heating/sauna
HIIT	high intensity intervals
K_b	apparent binding constant
La^-	lactate
MR	metabolic ratio
N-B	normal-to-base
N-F	normal-to-fast
PD	pharmacodynamics
PK	pharmacokinetics
REC	recovery period
Rest	resting drug trial
SD	standard deviation
SS	steady state
$t_{1/2}$	drug half-life
T_c	core body temperature
T_{max}	timing of maximum drug concentration
V_d	volume of distribution
$\dot{V}O_{2peak}$	peak aerobic power
W_{max}	maximal work

Frontiers in Physiology

Understanding how an organism's components work together to maintain a healthy state

The second most-cited physiology journal, promoting a multidisciplinary approach to the physiology of living systems - from the subcellular and molecular domains to the intact organism and its interaction with the environment.

Discover the latest Research Topics

See more →

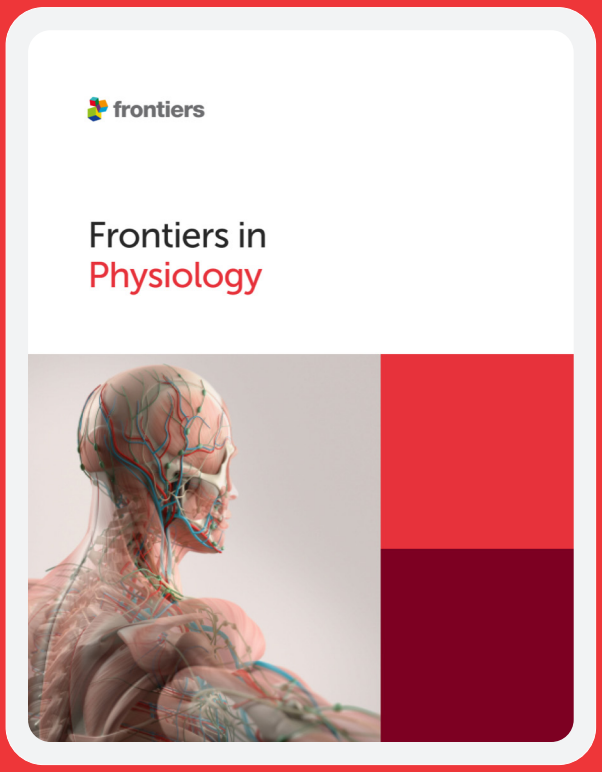

Frontiers

Avenue du Tribunal-Fédéral 34
1005 Lausanne, Switzerland
frontiersin.org

Contact us

+41 (0)21 510 17 00
frontiersin.org/about/contact